

AGARD

ADVISORY GROUP FOR AEROSPACE RESEARCH & DEVELOPMENT

7 RUE ANCELLE 92200 NEUILLY SUR SEINE FRANCE

AGARDograph No. 169

on

Effects of Streamline Curvature on Turbulent Flow

by

P. Bradshaw

ROYAL AIRCRAFT
ESTABLISHMENT

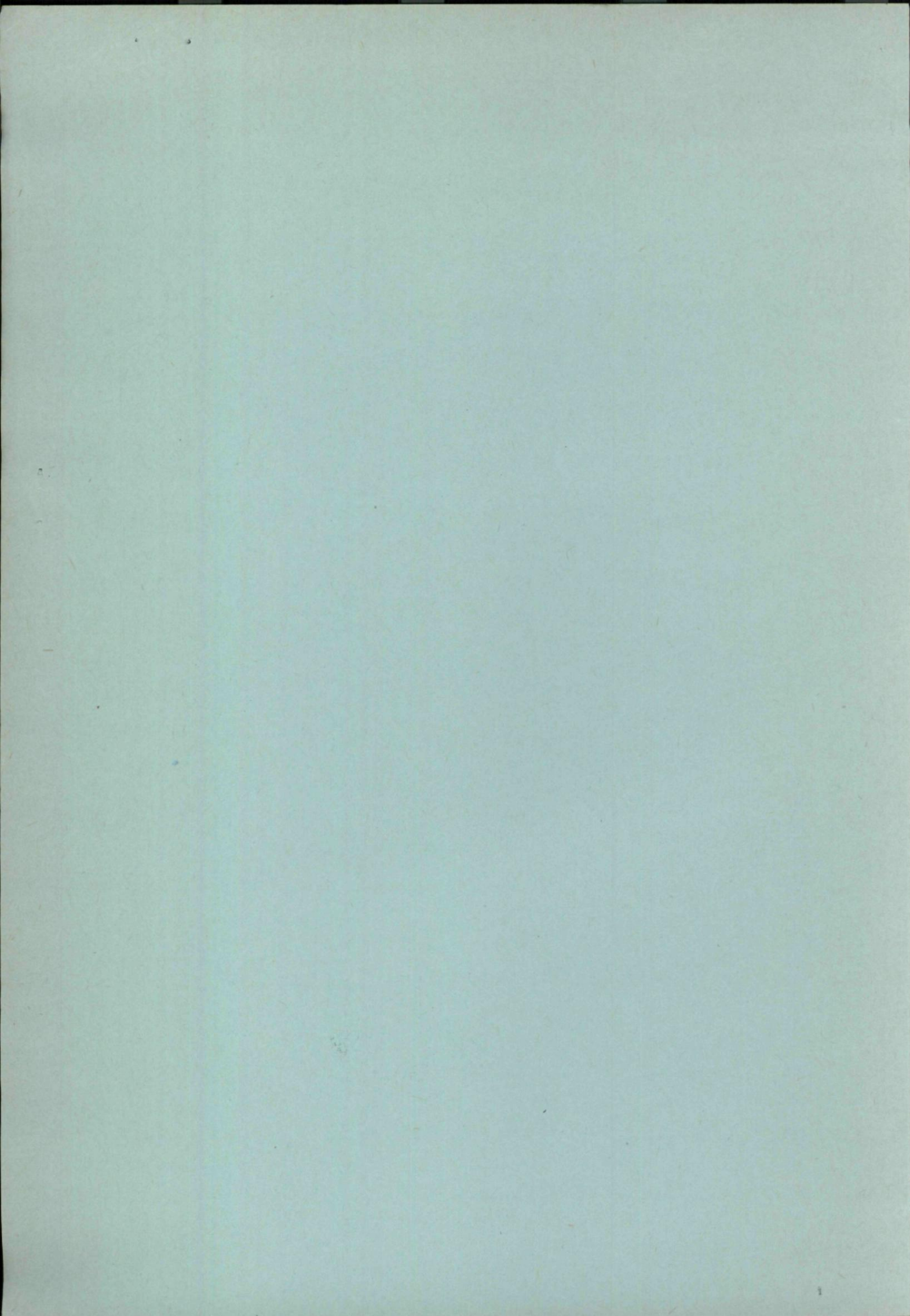
- 8 OCT 1973

LIBRARY

NORTH ATLANTIC TREATY ORGANIZATION



DISTRIBUTION AND AVAILABILITY
ON BACK COVER



NORTH ATLANTIC TREATY ORGANIZATION
ADVISORY GROUP FOR AEROSPACE RESEARCH AND DEVELOPMENT
(ORGANISATION DU TRAITE DE L'ATLANTIQUE NORD)

AGARDograph No.169

EFFECTS OF STREAMLINE CURVATURE ON TURBULENT FLOW

by

P.BRADSHAW

Department of Aeronautics,
Imperial College of Science and Technology,
London, Gt. Britain

Edited by

A.D.YOUNG

Department of Aeronautical Engineering,
Queen Mary College,
London, Gt. Britain.

THE MISSION OF AGARD

The mission of AGARD is to bring together the leading personalities of the NATO nations in the fields of science and technology relating to aerospace for the following purposes:

- Exchanging of scientific and technical information;
- Continuously stimulating advances in the aerospace sciences relevant to strengthening the common defence posture;
- Improving the co-operation among member nations in aerospace research and development;
- Providing scientific and technical advice and assistance to the North Atlantic Military Committee in the field of aerospace research and development;
- Rendering scientific and technical assistance, as requested, to other NATO bodies and to member nations in connection with research and development problems in the aerospace field;
- Providing assistance to member nations for the purpose of increasing their scientific and technical potential;
- Recommending effective ways for the member nations to use their research and development capabilities for the common benefit of the NATO community.

The highest authority within AGARD is the National Delegates Board consisting of officially appointed senior representatives from each member nation. The mission of AGARD is carried out through the Panels which are composed of experts appointed by the National Delegates, the Consultant and Exchange Program and the Aerospace Applications Studies Program. The results of AGARD work are reported to the member nations and the NATO Authorities through the AGARD series of publications of which this is one.

Participation in AGARD activities is by invitation only and is normally limited to citizens of the NATO nations.

The material in this publication has been reproduced directly from copy supplied by AGARD or the author.

Published August 1973

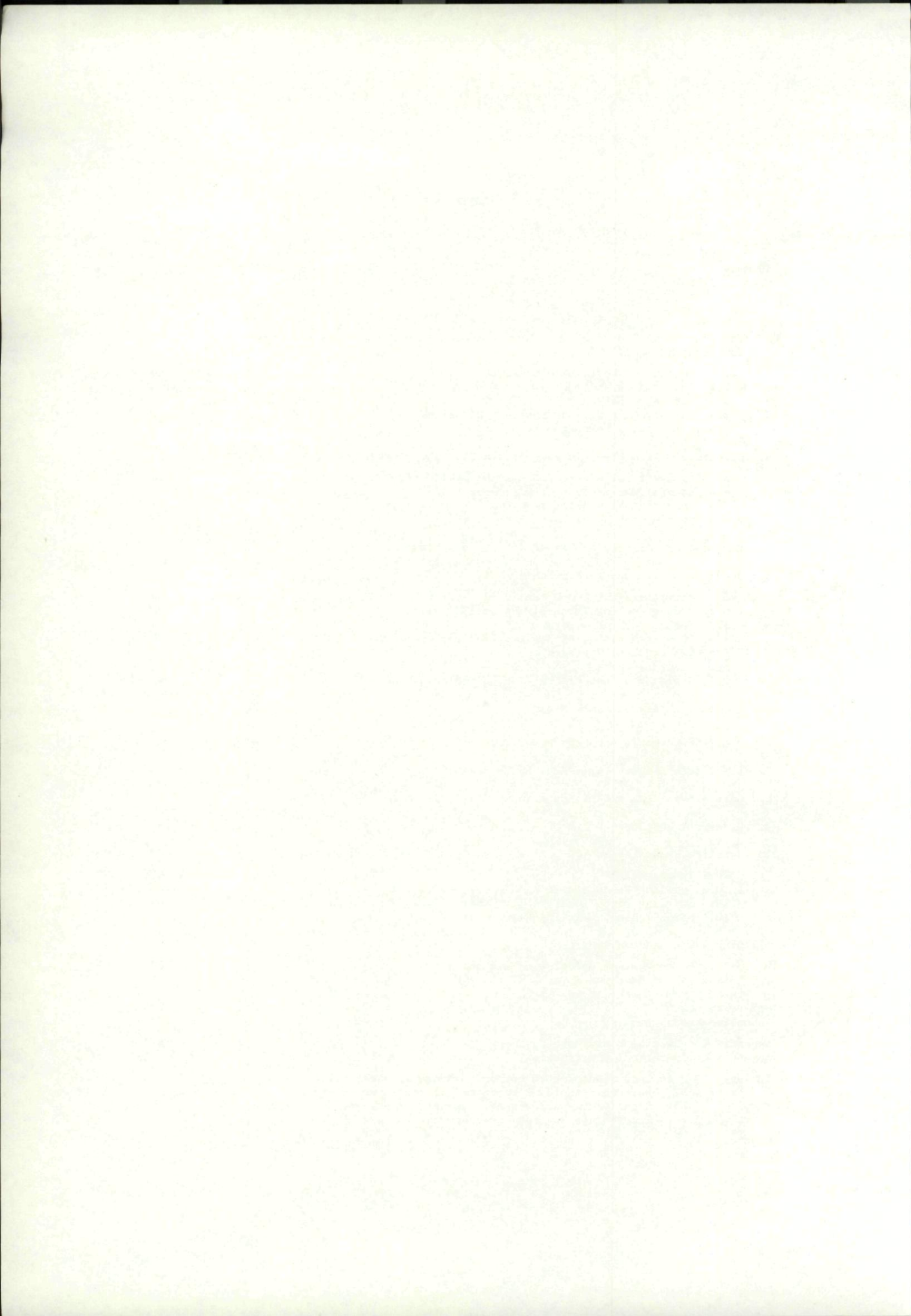
533.6.011:532.517.4



*Printed by Technical Editing and Reproduction Ltd
Harford House, 7-9 Charlotte St. London. W1P 1HD*

CONTENTS

	Page
Summary	1
List of Symbols	1
1. Introduction	1
2. The Equations of Motion: Coordinate Systems, Approximations and Strategy for Solution	
2.1 Choices of Coordinate Systems	6
2.2 The (s,n) System	8
2.3 The (x,r) System	10
2.4 The Reynolds-Stress Transport Equations	12
2.5 Calculation Methods	14
3. Effects of Extra Strain Rates on Turbulent Shear Layers	
3.1 A Simple Correlation Scheme for Small Extra Strain Rates	16
3.2 Lateral Convergence or Divergence	20
3.3 Longitudinal Acceleration	21
3.4 Compression or Dilatation	22
4. Introductory History of Research on Curved Flows	23
5. Description of Curvature Effects	
5.1 Parameters for Two-Dimensional Flows	30
5.2 Parameters for Three-Dimensional Flows	35
5.3 Use of the Parameters	38
5.4 Quantitative Use of Buoyant Flow Data	39
5.5 Longitudinal Vortices	40
5.6 Internal Waves	42
5.7 Collapse of Turbulence in Highly-Stable Flows	45
6. Boundary Layers and Duct Flows	
6.1 Low Speed Flow	46
6.2 Supersonic Boundary Layers	52
7. The Coanda Effect — Wall Jets on Curved Surfaces	53
8. Curved Free Jets and Mixing Layers	56
9. Classical Vortices	57
10. Swirling Shear Layers	
10.1 Introduction	61
10.2 Swirling Wakes and Jets	64
10.3 Swirling Pipe Flows	65
10.4 Miscellaneous Swirling Flows	
11. Discussion and Conclusions	
11.1 Phenomena and Calculation Methods	68
11.2 Future Research Work	71
References	72
Acknowledgements	80
Appendix 1 Special Coordinate Systems	A 1-1
Appendix 2 Numerical Experiments	A 2-1
Tables	
1. Conditions for 10 per cent change in shear stress	
2. Reference table of buoyancy/curvature parameters	
3. Experiments on low-speed boundary layers and duct flows	
4. Experiments on high-speed boundary layers	
Figures	



EFFECTS OF STREAMLINE CURVATURE ON TURBULENT FLOW

by

Peter Bradshaw
 Reader in Fluid Dynamics
 Department of Aeronautics
 Imperial College of Science and Technology
 London SW7 2BY, England

SUMMARY

Streamline curvature in the plane of the mean shear produces surprisingly large changes in the turbulence structure of shear layers. These changes are usually an order of magnitude more important than normal pressure gradients and other explicit terms appearing in the mean-motion equations for curved flows. The effects on momentum and heat transfer in boundary layers are noticeable on typical wing sections and are very important on highly-cambered turbomachine blades: turbulence may be nearly eliminated on highly-convex surfaces, while on highly-concave surfaces momentum transfer by quasi-steady longitudinal vortices dominates the ordinary turbulence processes. The greatly enhanced mixing rates of swirling jets and the characteristic non-turbulent cores of trailing vortices are also consequences of the effects of streamline curvature on the turbulence structure. This AGARDograph is a progress report, comprising a review of current knowledge, a discussion of methods of predicting curvature effects in engineering calculation methods, and a presentation of principles for the guidance of future workers.

LIST OF SYMBOLS

Infrequently-used symbols are defined on use. The overbar ($\bar{\quad}$) denotes an average, usually with respect to time.

a	factor of order unity in Eq(31); speed of sound
C	additive constant in logarithmic law, Eq(43)
c_p	pressure coefficient (defined on use), specific heat at constant pressure
c_f	skin friction coefficient, $\tau_w / \frac{1}{2} \rho U_e^2$
d	diameter
D/Dt	substantial derivative, $\partial/\partial x + \partial/\partial y + \partial/\partial z$
e	extra rate of strain
F	"F-factor", Eq(32,36)
f	"f-factor", Eq(31); function
g	gravitational acceleration; metric tensor (App.1)
h	duct height; scale factor
K	Karman's constant Eq(42)
\vec{k}	wave number vector, components k_1, k_2, k_3 ; thermal conductivity
L	dissipation length parameter, $(-\overline{uv})^{3/2}/\epsilon$
L_{mo}	Monin-Obukhov length Eq(70,81)
ℓ	mixing length, $(-\overline{uv})^{1/2}/(\partial U/\partial y)$
M	Mach number U/a
n	normal coordinate in (s,n) system, Fig.1(b)
P	total pressure
Pr	molecular Prandtl number, $\mu c_p/k$
p	static pressure (mean and fluctuation distinguished by \bar{p}, p')
Q	volume flow rate; heat transfer/unit area/unit time
q^2	$u^2 + v^2 + w^2$
R	surface radius
Ri	gradient Richardson number } Table 2
R_f	flux Richardson number
r	local radius
S	curvature parameter, Eq(86)
s	curvilinear coordinate in (s,n) system, Fig.1(b)
T	mean temperature
U,V,W	mean velocity components in (x,y,z), (s,n,z) and (x,r, θ) coordinate systems (Fig.1)
u,v,w	fluctuating velocity components
u_τ	friction velocity, $\sqrt{(\tau_w/\rho)}$
X	"time constant" of energy-containing eddies, Eq(37)
x,y,z	rectangular cartesian coordinates
x_i	cartesian tensor coordinates, x_1, x_2, x_3
α	factor of order 10 in Eq(32)
β	factor in Monin-Obukhov formula, Eq(119)
Γ	circulation
γ	ratio of specific heats
δ	boundary layer thickness: $y = \delta$ when $U = 0.995U_e$
δ^*	displacement thickness $\int_0^\infty (1 - \rho U / (\rho_e U_e)) dy$
$\delta_{.5}$	wall jet thickness: $y = \delta_{.5}$ when $U = 0.5U_m$
ϵ	turbulent energy dissipation/unit mass/unit time
θ	angular coordinate in (x,r, θ) coordinate system; temperature fluctuation

κ	thermometric conductivity, $k/(\rho c_p)$
λ	microscale, $\sqrt{u^2/(\partial u/\partial x)^2}$
μ	viscosity
ν	kinematic viscosity, μ/ρ
ρ	density (mean and fluctuation distinguished by $\bar{\rho}, \rho'$)
τ	shear stress, $-\rho \bar{u'v'}$ in fully-turbulent part of two-dimensional flow
Ω	angular velocity of rotating duct
ω	circular frequency
ω_{BV}	Brunt-Väisälä frequency, Eq(5)

Suffixes

e	external stream conditions
i, j, l	tensor indices
T	turbulent
w	wall (surface)
o	reference or initial value
1, 2, 3	tensor indices for x, y, z

1. INTRODUCTION

The subject of this AGARDograph is the surprisingly large effect exerted on shear-flow turbulence by curvature of the streamlines in the plane of the mean shear (Fig.1). Significant effects on shear stress and heat transfer can occur even for radii of curvature more than a hundred times the shear layer thickness. The most common example of a turbulent flow influenced by streamline curvature is the boundary layer on a highly-cambered aerofoil or turbomachine blade; its rate of growth, compared with that of a boundary layer in the same pressure gradient on a flat surface, is decreased on the convex upper (suction) surface and increased on the concave lower (pressure) surface. The title is chosen to include other cases, such as deflected jets, vortices and other swirling flows, and flow in various types of rotating duct (Fig.1): there is no connection with the "streamline curvature" method of calculating essentially inviscid flow in turbomachines.

The subject is discussed from the point of view of engineering calculation methods. However, attention to the physics of the curious phenomena involved is even more necessary than usual in turbulent flow, and it is helpful to recognise that streamline curvature is not an isolated pathological case but one of a group of distortions ("extra rates of strain") which produce unexpectedly large effects on turbulent shear layers. By the words "surprisingly" and "unexpectedly" we imply that the effects of extra rates of strain are an order of magnitude larger than would be predicted by straightforward extensions of calculation methods for simple shear layers. This suggests, and the discussion below tends to confirm, that recent progress in calculating simple shear layers does not guarantee the development, in the near future, of a calculation method suitable for all common types of turbulent flow. If this is true, or even if we merely acknowledge that there may be some truth in it, we need to classify the common types of turbulent flow and, without losing sight of possible unifying features, to develop calculation methods for one class at a time. The classification is better made by phenomena than by geometry or engineering applications. We start by distinguishing "simple" shear layers, with monotonic velocity profiles and nearly straight streamlines, from "complex" turbulent flows, comprising all other flows which are significantly affected by turbulent (Reynolds) stresses. We then find (1, 2) that nearly all complex flows are recognisable as perturbations of simple shear layers by interaction with other shear layers (3) or by the imposition of body forces or extra rates of strain (additional, that is, to the simple shear, $\partial U/\partial y$ in Fig.1(a)). Shear-layer interaction seems, at least in the two-dimensional case, to be a fairly innocuous phenomenon which does not result in spectacular changes in turbulence structure, but body forces and extra strain rates merit more respect. Fig.2 is a summary of the suggested classification. Where possible, we shall classify curved or rotating flows under the names of the shear layers of which they are perturbations. The classification of Fig.2 is not unique, and the figure itself may be more reminiscent of genealogy than engineering, but I regard classification of some sort as an essential aid to understanding and a prerequisite of unification, especially in the case of flows with extra rates of strain.

Streamline curvature in the plane of the mean shear is possibly the most common of the extra rates of strain, probably the most important and certainly the best documented. This AGARDograph has been written specifically as a summary of current knowledge of its effects and a discussion of desirable future work. However, it can be read as a general introduction to complex turbulent flows and the effects of extra strain rates and body forces, because the strategy of research described or advocated here should be applicable to other cases: moreover, the simplest way of modifying calculation methods to account for curvature effects is also valid for other types of extra strain rate.

Fig.3, due to Thomann (4), shows the effect of longitudinal surface curvature on the Stanton number (dimensionless surface heat transfer coefficient) in a supersonic turbulent boundary layer. Reading from top to bottom, the curves show results for concave, plane and convex surfaces (see Fig.1 for definitions), each preceded by a plane surface. The ratio of boundary layer thickness to radius of curvature was roughly 0.02. The inset sketch which defines the symbols shows the general arrangement - not to scale - and the deflectors used to maintain a near-constant external Mach number of about 2.5 over the test surface in each case. These, therefore, are boundary layers with negligible longitudinal pressure gradients, and any differences in behaviour between the plane and curved flows can be attributed to the effects of streamline curvature. These effects are clearly very large: the difference in heat transfer increases gradually from the start of the curved section ($x/L = 1$) and is still increasing at the end of the measurement section, where the concave-surface heat transfer is about 20 per cent greater than the plane value and the convex-surface heat transfer is about 20 per cent less. Surface shear stress was not measured in this experiment but other work suggests that it would have changed by about the same percentage as heat transfer: other work also makes it clear that the effects are not confined to supersonic flow, but Thomann's elegant set of measurements gives the clearest and most incontrovertible evidence in one graph.

Now in a laminar boundary layer the fractional change in surface shear stress or heat transfer caused by longitudinal surface curvature is of order δ/R . Van Dyke (5) gives a theoretical result for the skin-friction coefficient c_f in low-speed constant-pressure flow which can be rewritten as

$$c_f = c_{fo} (1 - 1.24 \delta/R) \quad (1)$$

taking δ as $5.0 \sqrt{(\nu x/U_e)}$. Thomann's results show that the effects of curvature in turbulent flow are roughly ten times greater than this. Both in laminar and in turbulent flow, the extra terms that appear in the equations of mean motion for a thin shear layer when streamline curvature is imposed are of order δ/R times the largest existing terms. Evidently, streamline curvature changes the Reynolds stresses of turbulent flow by roughly ten times as much as it changes viscous stresses. However, if we look at the Reynolds-stress transport equations, which are exact equations expressing the conservation of Reynolds stress in the same way that the mean-motion equations express conservation of momentum, we find that the explicit extra terms appearing in curved flows are again only of order δ/R times the largest existing terms in a simple shear layer and therefore cannot explain the large effects observed. There is, of course, no reason to suppose that the instantaneous Navier-Stokes equations or the Reynolds stress transport equations are no longer valid in a curved flow, so we conclude that streamline curvature directly causes large changes in the higher-order parameters of the turbulence structure.

Effects of this size and obscurity would demand attention from engineers and research workers even if they were confined to boundary layers, but numerous other experiments show that similar effects can occur in any shear layer whose streamlines have a component of curvature in the plane of the mean shear, whether the curvature is caused by surface curvature, swirl [helical streamlines: Fig.1(d)] or rotation of the whole flow system. Figure 4 shows the effect of surface curvature on the spreading rate of a two-dimensional wall jet. In two cases (6, 7) logarithmic spiral surfaces were used so that δ/R was independent of distance along the surface, s : in the third case (8) a surface of constant radius was used, and the results have been plotted at a plausible average value of δ/R . In all cases large changes in growth rate occur even when the curvature is small enough for the extra terms in the equations of motion to be negligible to the thin-shear layer ("boundary layer") approximations. In the most extreme case, where the radius of curvature was equal to the distance from the orifice, the spreading rate is four times that on a plane surface. We note that in this case the Reynolds stresses are decreased on a concave surface and increased on a convex one. Since the mean shear $\partial U/\partial y$ is predominantly negative in a wall jet, except for a thin region near the surface, we can provisionally deduce that the effects change sign with the mean shear, and that Reynolds stresses increase when $(\partial V/\partial x)/(\partial U/\partial y)$ - measured in Cartesian coordinates coincident with the local direction of the shear layer, as in Fig.1(a) - is positive. The increase of spreading rate in the wall jet on a convex surface is the phenomenon (strictly one of the phenomena) called the "Coanda effect".

Even more spectacular and unexpected effects can occur. Figure 5 is a photograph of smoke entrained in the trailing vortex behind a C-47 aircraft (9). Despite the fact that this is a flow at high Reynolds number ($\Gamma/\nu \approx 4 \times 10^6$, where Γ is the circulation round the vortex), the inner core of the vortex is laminar, being stabilized by streamline curvature; a noteworthy result is that there is little resistance to axial motion in the core, and this seems to play a large part in the dynamics of the vortex as a whole. Outside the core there is a region of turbulence, but the overall growth rate depends strongly on Reynolds number because of the viscous effects in and near the core. Note that in this swirling flow the plane of the mean shear and the plane of curvature of the streamlines do not necessarily coincide. Figure 6 shows the destabilizing effects of streamline curvature in a straight duct rotating about a spanwise axis (10): see Fig.1(e), and note that the turbulence responds to streamline curvature as seen in an inertial frame of reference. On the side where the angular velocity of rotation is in the opposite sense to the rotational part of the mean shear (corresponding to positive $(\partial V/\partial x)/(\partial U/\partial y)$ in inertial axes) the turbulent motion is strongly augmented and the large eddies develop into longitudinal vortices. In some curved or rotating turbulent flows these vortices have preferred spanwise positions and thus contribute to the mean vorticity, although of course turbulent fluctuations still occur. On the other side of the rotating duct the turbulent motion is almost completely damped out, except for incursions by the longitudinal vortices. Evidently streamline curvature can produce not only quantitative changes in mixing rate but also qualitative changes, leading on the one hand to an apparent instability of the mean flow and on the other to virtual elimination of the turbulence. We notice the difference between this behaviour and the effect of streamline curvature on laminar flow stability: laminar boundary layers become less stable on concave surfaces (the case in which turbulent motion is augmented) but do not become significantly more stable on convex surfaces, because the dominant mode of instability is different in the two cases. In what follows, the words "stable" and "unstable" will be used to describe turbulent flows whose intensity is respectively decreased and increased by the effects of streamline curvature: "stability" does not necessarily imply complete absence of turbulence or its irretrievable decay.

Figure 7 shows another spectacular effect. The turbulent intensity in an impinging jet (11) decreases, because the curvature is in the same sense as in a wall jet on a concave surface: this is to be expected from the foregoing discussion, but, quite unexpectedly, the intensity downstream of the impingement region overshoots the plane-layer value before finally relaxing towards it. Again, modification of the large eddies seems to be responsible.

Figures 3 to 7 are sufficient evidence that many flows of aeronautical or engineering interest will be significantly affected, or even dominated, by the direct effect of streamline curvature on the turbulence. For instance, Thomann's results (4) show that on a circular-arc turbomachine blade with a turning angle of the order of 60 degrees (giving $\delta/R \approx 0.02$ near the trailing edge) heat transfer rates will be decreased by roughly 20 per cent on the top (suction) surface and increased by roughly 20 per cent on the bottom (pressure) surface, as compared with results for flat surfaces. This is a serious matter. Table 1 gives a list of some of the flows in which curvature effects can produce a change in Reynolds stress of 10 per cent or more. Unless some explicit empirical allowance is made, all calculation methods for turbulent shear layers known to me underpredict the effects by a factor of the order of 10, since at best they recognize only the explicit extra terms in the mean-motion equations and Reynolds-stress transport equations (Section 2). For example, thin shear layers are frequently predicted by "eddy viscosity" formulae of the type

$$\text{shear stress} = \mu_T \times (\text{rate of shear strain}) \quad (2)$$

This would predict the effect of adding an extra rate of strain $\partial V/\partial x$ to an existing "simple shear" $\partial U/\partial y$ to be an increase in shear stress by a factor

$$1 + \frac{\partial V/\partial x}{\partial U/\partial y}$$

obviously the same factor of increase as in a laminar flow where the molecular viscosity μ replaces μ_T . Thomann's results suggest that the real factor of increase after a prolonged region of streamline curvature is much larger, of the order of

$$1 + 10 \frac{\partial V/\partial x}{\partial U/\partial y}$$

for small values of the "rate-of-strain ratio" $(\partial V/\partial x)/(\partial U/\partial y)$. However, the evidence of Figs 3 to 7 makes it clear that a linearized empirical formula of this sort will not be reliable for large curvature effects. Also, since we attribute curvature effects to changes in the higher-order structure parameters, we cannot expect the full effects on the local Reynolds stress to appear as soon as the curvature is imposed. We shall, however, use linearized formulae for simple discussions, and at present little can be said about higher-order formulae.

It is evident that streamline curvature has a large effect on the processes by which Reynolds stresses are generated and maintained, and that empirical modifications to calculation methods for simple shear layers are unlikely to be reliable unless they are based on some physical and mathematical understanding of these processes. Therefore Section 2 of this AGARDograph includes a brief introduction to the exact Reynolds stress transport equations, partial differential equations whose terms represent different physical processes contributing to the maintenance of Reynolds stress. This is followed by a discussion of the strategy used to convert these and other exact transport equations into empirical, soluble equations for Reynolds stress. Nearly all existing calculation methods can be explained in terms of this strategy or simplifications of it. It is not necessarily implied that curved flows can be predicted only by calculation methods that use the most advanced form of this strategy, involving the solution of several transport equations: however we should base our initial discussion of these mysterious curvature effects on the most realistic models of turbulence processes and make simplifications later if we can justify them. Cartesian coordinates are not very convenient for a discussion of curved flows, so Section 2 begins with a description of two alternative systems, suitable for two-dimensional curved flow and axisymmetric swirling flow respectively. Extensions of the thin-shear-layer approximation to these systems are also discussed. In other cases of shear layers subjected to curvature or other extra rates of strain, more complicated coordinate systems may be needed for convenience of description or to assure stability and accuracy of numerical solutions, and Appendix 1 is an attempt to treat general, non-orthogonal coordinate systems with more rigour than is sometimes employed.

Recently it has become clear that streamline curvature, $\partial V/\partial x$, is only one of a number of extra rates of strain which, when applied to an initially simple shear layer, produce effects on Reynolds stress which are large compared to the explicit effects of the extra terms that appear in the equations of motion or the effects of the changes in coordinates needed to align the axes with the shear layer. Other examples include lateral divergence and bulk compression (in compressible flow). Pure rotation of the flow system, though not strictly a rate of strain, has much the same effect as streamline curvature, with the angular velocity Ω taking the place of $\partial V/\partial x$. Section 3 is an introduction to these effects: it seems to be almost a universal law that if a small extra rate of strain, e say, is added to a simple shear $\partial U/\partial y$ the Reynolds shear stress eventually changes by a factor of order

$$1 \pm 10 \frac{e}{\partial U/\partial y}$$

The number here written as 10 is most unlikely to be a universal constant, but while our ignorance of the effects of extra strain rates remains so extensive it is helpful to consider the effects together, without necessarily implying a direct qualitative connection between the phenomena or a quantitative connection between the various empirical constants. It is also helpful to regard the flows as perturbations of simple shear layers rather than as completely new flows. We therefore define a "simple shear layer" more precisely as one in which the simple shear $\partial U/\partial y$ is so much larger than any other rate of strain that the direct effect of the latter on the turbulence is negligible. Now the thin-shear-layer approximation is, roughly speaking, that the effect of extra rates of strain on the mean-motion equations is negligible: it follows by inspection of the Reynolds stress factor set out above that the requirement of a simple shear layer is about ten times stronger than the requirement of a thin shear layer. The simple shear layer provides a basis for comparison: it is rather rare in practice. Some curved flows violate even the thin-shear-layer approximation, but it is shown in Section 2 that Reynolds stress gradients are significant only in fairly thin shear layers: and even a region of strong distortion in which pressure gradients greatly exceed Reynolds stress gradients is likely to be preceded or followed by a fairly thin shear layer. The following summary table may be helpful: the sign ">>" can be read as a factor of inequality not much less than 100, and e is any one of the relevant extra strain rates.

simple shear layer	$\partial U/\partial y \gg 10e$	e does not affect turbulence
thin shear layer	$\partial U/\partial y \gg e$	e does not affect mean-flow equations
fairly thin shear layer	$\partial U/\partial y > 10e$	Reynolds-stress gradients still significant
strong distortion	$\partial U/\partial y < 10e$	Reynolds-stress gradients locally insignificant

Classical "rapid distortion" theory requires $\partial U/\partial y \ll e$ ($\partial U/\partial y$ is a fair approximation to the turbulence timescale that appears in the theory).

At intervals over the last 40 years the large effects of streamline curvature on turbulent flow have been demonstrated by experiments on several different types of shear layer, but only in the last few years have these effects been allowed for in engineering calculation methods and even now they are frequently neglected. The history of research on the subject and its curious lack of impact is outlined in Section 4

as an introduction to the phenomena of curvature effects: current knowledge of particular curved flows is reviewed in later sections. In view of the long neglect of the subject by research workers it is interesting to note that the late Henri Coanda not only demonstrated increased mixing in the wall jet on a convex surface in the early 1930s but made use of it in a variety of useful devices (for an affectionate obituary of M. Coanda see Ref.12). In contrast, half the references quoted below date from 1969 or later.

The traditional qualitative explanation of the effect of streamline curvature on a fluid flow is based on the motion of a disturbed element of fluid (Fig.8). The argument first given by Von Karman (13) in 1934 is as follows. Suppose that an element of fluid in an axisymmetric rotating flow is displaced by some externally-applied force in a radial direction, and then released. If the fluid is frictionless we may assume that the displaced element conserves its angular momentum about the centre of curvature of the streamlines, distant r from the point considered. Therefore if the angular momentum of the steady flow, Ur per unit mass, numerically decreases outwards, the displaced element will have a larger circumferential velocity than its surroundings. In consequence, the radial pressure gradient $\rho U^2/r$ that maintains the mean flow in its circular path is too small to keep the displaced element in equilibrium, and it will therefore continue to move outwards. Conversely, if the angular momentum of the mean flow increases outwards, the mean pressure gradient will force the displaced element into a path of radius less than r , returning it towards its original radius, about which it will oscillate.

Quantitatively, for the case of incompressible flow, if the radius and velocity of the fluid element before disturbance are r_0 and U_0 its circumferential speed after displacement to radius $r \equiv r_0 + dr$ is

$$U_0 \left(1 - \frac{dr}{r_0} \right)$$

whereas the mean speed of the fluid, U , is

$$U_0 + \frac{dU}{dr} dr$$

so that the difference between the mean pressure gradient $\rho U^2/r$ and the pressure gradient required to keep the displaced element in a path of radius $r_0 + dr$ is

$$2\rho \frac{U}{r^2} \frac{d}{dr} (Ur) dr \equiv \frac{\rho}{r^3} \frac{d}{dr} (U^2 r^2) \cdot dr \quad (3)$$

Consequently the radial acceleration of the particle is proportional to the displacement dr , and the displaced element executes simple harmonic motion at circular frequency

$$\omega = \left(2 \frac{U}{r^2} \frac{d}{dr} (Ur) \right)^{1/2} \quad (4a)$$

if this number is real, and diverges if it is imaginary. Zero frequency implies neutral stability. Alternative expressions are

$$\omega = \left(\frac{2}{\rho r} \frac{\partial P}{\partial r} \right)^{1/2} \quad (4b)$$

where P is the total pressure $p + \frac{1}{2}\rho U^2$ and we use the equation of radial equilibrium, $dp/dr = \rho U^2/r$, or

$$\omega = \left(2 \frac{U}{r} (\text{mean vorticity}) \right)^{1/2} \quad (4c)$$

These expressions emphasize that the irrotational external stream adjoining a shear layer is neutrally stable. The above analysis applies in full only to flows whose velocity along the axis of rotation is zero.

A closely similar analysis can be done for a displaced element in a stationary, stratified fluid in a gravitational field in the negative y direction: if the displaced element conserves its density (i.e. if we neglect the adiabatic lapse rate) the net buoyancy force after displacement dy produces a restoring force leading to oscillation at the Brunt-Väisälä frequency

$$\omega_{BV} = \left(\frac{-g}{\bar{\rho}} \frac{d\bar{\rho}}{dy} \right)^{1/2} \quad (5)$$

In the meteorological literature the Brunt-Väisälä frequency is usually given symbol N , or sometimes ω_0 : we will use the symbol above as a reminder of the name and of the fact that Eq(5) gives the circular frequency in radians per second. In buoyant flows, the square of the ratio of the Brunt-Väisälä frequency to a typical time scale of the flow defines the well-known meteorological parameter, the Richardson number (see Section 5.1).

Now these analyses totally neglect perturbations to the flow or the pressure gradient caused by the motion of the disturbed element, and therefore leave something to be desired even in a frictionless flow: the buoyancy analysis seems rather more plausible than that for curvature. Proofs based on energy considerations [the proof for curved flow being due to Rayleigh (14)] obscure, but do not entirely remove, the impossibility of the physical situation. If applied to turbulent flow, the arguments are uncomfortably reminiscent of those of classical mixing-length theory, which at best can only reproduce results obtainable by dimensional analysis for the special case of flows in "local equilibrium" (see Section 2.4). However proofs for special cases have been obtained by rigorous use of hydrodynamic stability theory, the only arbitrary feature remaining being the choice of the disturbance mode. Moreover, the qualitative result that the sense of stability depends on the sense of the gradient of angular momentum or density is well established even for real flows, and in buoyant fluid, if not in curved flows, oscillations of a displaced element at very nearly the predicted frequency have actually been observed (15).

Section 5 is based on a discussion of the analogy between buoyancy and curvature effects including further treatment of stability analyses, like that outlined above, which are applicable to both effects.

It is shown that displaced-element arguments lead to dimensionless stability parameters similar to those inferred from the Reynolds-stress transport equations: each has some advantage. The qualitative phenomena of strongly-curved flows, including longitudinal vortices (or other convective instabilities), and possibly internal waves, are also most simply introduced by analogy with buoyant flows in which the phenomena are generally better documented. The quantitative analogy between the effects of buoyancy and of curvature on a given type of shear layer should be nearly as accurate as Reynolds' analogy between momentum transfer and heat transfer, being based on nearly the same arguments. Unfortunately a direct correspondence with meteorological flows is possible only in the inner layer of a turbulent wall layer, and a correspondence with buoyant flows in the laboratory is not likely to be a very useful way of obtaining data because it is generally easier to measure curved flows than buoyant ones. The analogy between buoyancy and curvature can be illustrated by comparing the gravitational body force with the "centrifugal" body force. Rotation of a shear layer, with mean shear $\partial U/\partial y$, about the z axis produces an apparent Coriolis body force in the y direction, very closely analogous to the apparent centrifugal body force: this is an analogy parallel to that between a true angular velocity and the pseudo-angular-velocity $U/r \equiv -\partial v/\partial x$.

Sections 6 to 10 are reviews of the basic flows in which streamline curvature (or bodily rotation of the flow) significantly affects turbulence. Since a quantitative discussion is possible only for fairly small curvature effects, classification under the names of classical thin shear layers begs no questions. Examples include boundary layers and wall jets on curved surfaces, curved duct flows, curved free jets and mixing layers, swirling jets, vortices and swirling flow in ducts. We distinguish between "rotating" ducts, rotating about an axis more or less normal to the plane of the mean shear $\partial U/\partial y$, and "spinning" ducts, rotating about the general direction of the flow: in the first case only two-dimensional flows, and in the second case only axisymmetric ones, will be considered, because flows in rectangular spinning or rotating ducts of small aspect ratio are likely to be dominated by secondary flows driven by pressure gradient, and the direct effects of rotation on the turbulence cannot yet be distinguished. Sections 6 to 10 are not general discussions of the title flows (background references are given) but concentrate on the changes in turbulence structure that result from curvature: where it has been possible to discuss the effect of these changes on the mean flow I have done so. I have concentrated on experiments which seemed to me likely to contribute to the understanding of curvature effects on turbulence: this by no means disqualifies careful mean-flow measurements without turbulence data, but in general I have passed over experiments whose results are insufficiently detailed for inferences to be drawn about turbulence behaviour. Unfortunately very few data are available on three-dimensional curved flows: at present one can only hope that rules derived for two-dimensional or axisymmetric flows can be applied locally; axisymmetric swirling flows are closely related geometrically to flows over developable surfaces such as infinite swept wings. In compressible flow, the picture is rather brighter: a number of experiments on supersonic boundary layers have been done on surfaces curved so as to induce the required pressure distribution. These boundary layers suffer from the effects of two extra strain rates, curvature and bulk compression, but some inferences can be drawn about the Mach-number dependence of curvature effects.

The discontinuity between the general theoretical discussion of Sections 2 to 5 and the miscellaneous experimental results of Sections 6 to 10 is a consequence of the undeveloped nature of the subject. It is hoped that future work will benefit from the general discussion, and I have therefore included material that could be used in future as well as material that can be used at present, even though the foundations for a large structure are necessarily less tidy and less appealing than a small, complete edifice. Section 11 is a list of conclusions useful to design engineers and to experimental and theoretical research workers. It includes both a summary of the existing methods of allowing for curvature effects in calculation methods, principally for thin shear layers, and some suggestions for desirable future work. The main conclusion, foreshadowed above, is that there is no immediate prospect of a calculation method that will naturally predict all the effects of extra rates of strain, even in thin shear layers. Different empirical inputs are necessary for different strain fields: this implies that we are forced to regard each as a perturbation of a simple shear layer and that the reliability of the results will decrease with the strength of the perturbation.

As mentioned above, Appendix 1 is an introduction to general coordinate systems and the need for them. Appendix 2 gives details of suitable test cases for calculation methods, together with a discussion of the performance of allowances for curvature effects in the method of Ref.16, which must now be regarded as a method of average complexity, intermediate between the most modern transport-equation methods and the older procedures still in use in industry.

The purpose of this AGARDograph is to ensure the widest possible realization of the importance of curvature effects on turbulent flow and to point out the necessity — and difficulty — of predicting them. Because the subject has only recently become popular there is no consensus of opinion about it, and because I have been personally involved in its redevelopment I have naturally presented it from my own point of view, which I hope will not be found unduly contentious. (The last sentence may also be applied to the subject of calculation methods for turbulent shear layers in general, which necessarily recurs throughout the monograph.) I have included, with suitable warnings, some small pieces of unpublished original work. I have tried to present the subject in the way that will be found most useful by the developer of calculation methods for the turbulent flows that appear in engineering fluid dynamics. Fortunately, the point of view of the developer is nowadays fairly close to that of the experimental research worker on the one hand and the industrial user of calculation methods on the other, and I hope the review will be useful to them also. Streamline curvature is the only one of the extra rates of strain that is sufficiently well understood for a review monograph to be timely but — because of its recent rise to popularity — our knowledge is increasing so rapidly that any attempt at a definitive treatment would be futile. This is a progress report: I hope it will help to stimulate future progress.

2. THE EQUATIONS OF MOTION: COORDINATE SYSTEMS, APPROXIMATIONS AND STRATEGY FOR SOLUTION

2.1 CHOICES OF COORDINATE SYSTEMS

The Navier-Stokes equations and the exact Reynolds-stress transport equations (Section 2.4) are given in

general tensor notation in Appendix 1 (see the first paragraphs of that Appendix for an explanation of notation) with a summary of the steps needed to deduce the equations in any special coordinate system. This information is not easily accessible in the literature but will be needed in the analysis of three-dimensional curved flows. For normal purposes the equations can be read as if they were written in ordinary tensor suffix notation, and in the main text we normally use (x, y, z) notation or variants thereof. We begin this section by discussing the types of flow in which Reynolds stress gradients are likely to be important, to limit the field of study: we then derive the equations of motion in coordinate systems to suit the most common types of curved flows, and discuss the validity of approximations to them as a generalization of the thin-shear-layer approximation (boundary-layer approximation) in plane flow. Finally we review the strategy of calculation methods for plane flows, with a view to the incorporation of allowances for curvature effects.

It can be shown that the only flows in which Reynolds stress gradients significantly affect the mean motion are those containing fairly thin shear layers. Consider a flow with a typical velocity U_e and a typical length s in the general direction of flow. In general, mean pressure gradients in any direction will be of the order of $\rho U_e^2/s$, while according to experiments Reynolds stresses are at most of order $0.01 \rho U_e^2/s$. Therefore Reynolds stress gradients will be of the same order as pressure gradients only if Reynolds stresses change appreciably over distances of the order of $0.01 s$. Examination of the Reynolds-stress transport equations shows that the Reynolds stresses are unlikely to change so rapidly with distance along a mean streamline, and we conclude that Reynolds stress gradients will significantly affect the mean motion only if they change significantly in a distance of order $0.01 s$ more or less normal to the mean streamline. This requires the existence of thin sheets or slender tubes of high Reynolds stress, and the only general mechanism by which such layers can maintain themselves is extraction of energy from the mean flow by working of a mean rate of strain against the Reynolds stresses. The rate of dissipation of turbulent energy per unit volume in a sheet or tube of width $0.01 s$ carrying Reynolds stresses of order $0.01 U_e^2$ will be of order $(0.01 U_e^2)^{3/2}/0.01 s$, and if a roughly equal rate of turbulent energy production is to be maintained the rate of strain acting on Reynolds stresses of order $0.01 U_e^2$ must be of order $10 U_e/s$. Rates of normal (tensile or compressive) strain cannot for long exceed U_e/s without causing velocity changes of greater order than U_e , so that a rate of shear strain of order $10 U_e/s$ must exist in the sheet or tube, which must therefore be a shear layer, with a velocity change of order U_e in a transverse distance of order $0.1 s$ or a smaller velocity change across an even thinner layer, say of the order of $0.01 s$ as originally required. Note carefully that this argument has nothing to do with the mathematical thin-shear-layer approximation: in particular, it does not prove that the layers with high Reynolds stress gradients are thin enough for any version of that approximation to apply. Nor, of course, does it exclude the presence of some regions in which pressure gradients greatly exceed Reynolds stress gradients. Clearly, the most difficult flows to predict will be those in which a shear layer has its turbulence structure perturbed by a short region of strong pressure gradients and extra rates of strain, and then emerges into a longer region in which its Reynolds stress gradients are significant compared to smaller pressure gradients: an example of such a flow - and of the eccentric behaviour of perturbed turbulence - is the impinging jet of Fig.6. The argument does, however, justify an unrigorous version of the thin-shear-layer approximation, stating that the most important Reynolds stress gradients are almost always the shear stress gradients: the implication is that normal stresses need not be calculated as accurately as shear stresses, except perhaps in non-axisymmetric slender shear layers where normal-stress gradients drive secondary flows. Note that the division of the stress tensor into "shear stresses" and "normal stresses" depends on the axes: however in regions where Reynolds stresses are important the above argument shows that the direction of the shear layer can be located, to sufficient accuracy, and used as a coordinate axis. As pointed out in the discussion of coordinate systems in Appendix 1, it may be not only convenient but necessary to do this, to ensure accuracy and stability of numerical calculations.

Nearly all the experimental information on curved flows refers to slender axisymmetric swirling flows or to thin two-dimensional shear layers: there is some information on non-slender swirling flows and on non-thin shear layers but no significant data on non-axisymmetric or three-dimensional flows. Clearly the latter flows may be more complicated than axisymmetric or two-dimensional flows, but there is no reason to suppose that the effects of curvature as such are much more complicated although some difficulties of interpretation arise. At all events there is no present need to consider the equations of motion for these cases, and we therefore discuss only the equations for two-dimensional curved flows or axisymmetric swirling flows, both in general and with the approximation of thinness or slenderness. Either these or the plane-flow equations can be extended to coordinates rotating at angular velocity Ω by adding the appropriate components of the Coriolis acceleration or body force $2\Omega \times U$: in a constant-density fluid, the centripetal acceleration can be absorbed into the pressure gradient (10). It is important to distinguish between rotating flows (between coaxial rotating cylinders, say) and the rotating axes in which it may or may not be convenient to study them.

The most appropriate coordinate systems for simple curved flows are as follow.

1. Two-dimensional (s, n) coordinates, in which s is measured along a single curved reference line (usually a solid surface or other streamline) and n is measured along straight lines normal to the reference line [Fig.1(b)]. The third coordinate, measured along straight lines normal to the (s, n) plane, will be called z . Note the difference between this system and the more general orthogonal curvilinear system of Fig.1(c) in which the constant - n lines are all arbitrary and the constant - s lines are everywhere orthogonal to them. In our system the radius of curvature of the s -axis, R , may be a function of s , in which case the coordinates become non-unique on the locus of the centre of curvature; if R is constant the locus shrinks to a point and the (s, n) system reduces to polar coordinates (r, θ) with $r \equiv n + R$, $\theta \equiv s/R$, while if n is small compared with R (as in a thin shear layer) it reduces to rectangular Cartesian coordinates $x \equiv s$, $y \equiv n$. We shall use the (s, n) system only for fairly thin shear layers so that the centre of curvature lies outside the region of interest. It will sometimes be convenient to denote $n + R$ by r and dn by dr . An axisymmetric (s, n) system can be used on fat bodies of revolution, and the appropriate modifications to the two-dimensional system will be indicated below. Although the point is not directly relevant to the present topic it is worth noting that the (s, n) system based on a reference streamline is particularly suitable for matching a free-shear-layer calculation to a calculation of the external flow because the s -axis streamline appears explicitly in both calculations.

2. Axisymmetric (x,r) coordinates in which x is measured along, and r normal to, a straight axis [Fig.1(d)]. The third (angular) coordinate will be called θ . The system will be used mainly for flows which are turbulent over most or all of the distance from the axis to radius r : if the turbulent layer is thin compared with r , as in thin boundary layers in pipes or annuli or on bodies of revolution, the system reduces to rectangular Cartesian coordinates with $y \equiv r$, while not-so-thin axisymmetric layers can be analysed in the axisymmetric (s,n) system.

Now we shall see that in the (s,n) system dR/ds appears explicitly only in the second derivatives in the viscous term, and even there it is nearly always negligible in practice, so that, for purposes of deriving the equations, (s,n) coordinates are locally equivalent to (r,θ) coordinates, as when R is truly constant. Thus the equations of motion in our two coordinate systems are special cases of those that appear in cylindrical (x,r,θ) coordinates; in the first case the x derivative, and in the second case the θ derivative, is negligible. The mean-motion and Reynolds-stress transport equations in (x,r,θ) coordinates are given by Rodi (17).

The reduction of (s,n) coordinates and (x,r) coordinates to conventional (x,y) coordinates for small values of (shear layer thickness)/(radius) justifies the common pretence that aeroplane surfaces are flat for the purposes of deriving the boundary layer equations. However, the message of this AGARDograph is that aeroplane surfaces are not flat for the purpose of solving the boundary layer equations in turbulent flow - in other words the effects of streamline curvature on the turbulence are much larger than would be expected from the extra terms introduced into the mean-motion or Reynolds-stress-transport equations. In highly-curved flows (δ/R of order 1) the extra terms become comparable with the existing terms, while the effects on the turbulence are necessarily limited in size by considerations like non-negativity of turbulent energy or energy dissipation rate, so that in these cases the effects on the Reynolds stresses may be of no greater order than the extra terms: see, for example, the results for the impinging jet in Fig.7, where $(\partial V/\partial x)/(\partial U/\partial y)$ - representative of the ratio of "extra terms" to plane-layer terms - reached a maximum numerical value of about 0.2. In such a case all or nearly all of the extra terms introduced by curvature must be retained. In intermediate cases of moderate curvature some of the extra terms may be negligible and it is therefore advisable to put on record not only the exact forms of the equations of motion but also the hierarchy of consistent approximations to them. When we use plane boundary layer equations for curved flows we are using the lowest members of this hierarchy.

2.2 THE (s,n) SYSTEM

As a simple example of the extra terms introduced by the (s,n) system, we derive the continuity equation for incompressible two-dimensional flow, which specifies that the net rate of mass flow out of an elementary control volume, such as that shown in Fig.1(b), is zero. With symbols U, V and W for the mean velocity components in the s, n and z directions respectively, the net outward rate of mass flow through the faces seen in side view as AB and CD , supposed to be of unit depth in the z direction, is

$$\rho \left(U + \frac{\partial U}{\partial s} ds \right) dn - \rho U dn$$

exactly as in rectangular Cartesian coordinates. The net outward rate of mass flow through the faces AD and BC is

$$\rho \left(V + \frac{\partial V}{\partial n} dn \right) \left(1 + \frac{n+dn}{R} \right) ds - \rho V \left(1 + \frac{n}{R} \right) ds$$

(remember that s is measured at height $n = 0$). Neglecting the term in $(dn)^2$, and dividing by $\rho ds dn$ we get

$$\frac{\partial U}{\partial s} + \left(1 + \frac{n}{R} \right) \frac{\partial V}{\partial n} + \frac{V}{R} \equiv \frac{\partial U}{\partial s} + \frac{\partial}{\partial n} \left\{ V \left(1 + \frac{n}{R} \right) \right\} = 0 \quad (6)$$

where the second element implies the definition of a stream function. The term arising from flow in the z direction is $(1 + n/R)\partial W/\partial z$ because the area of the face $ABCD$ is $(1 + n/R)ds dn$. In axisymmetric flow (6) is valid if U and V are multiplied by the radius to the point (s,n) .

The Navier-Stokes equations can be derived by applying to the curvilinear control volume the arguments about conservation of momentum used to derive or explain the equations in rectangular Cartesian coordinates. Van Dyke (5) gives the equations for steady two-dimensional incompressible laminar flow: the mean-motion equations for turbulent flow can be deduced by inspection once the continuity equation, Eq(6), is used to put Van Dyke's equations into "divergence" form with the left hand side composed of pure spatial derivatives. Writing h for $1 + n/R$ in the viscous term for compactness (noting that both $\partial h/\partial s$ and $\partial h/\partial n$ are non-zero in general) and adding U times the continuity equation to the s -component equation and V times the continuity equation to the n -component equation, we get

s -component mean momentum

$$U \frac{\partial U}{\partial s} + \left(1 + \frac{n}{R} \right) V \frac{\partial U}{\partial n} + \frac{UV}{R} \\ \equiv \frac{\partial U^2}{\partial s} + \left(1 + \frac{n}{R} \right) \frac{\partial UV}{\partial n} + 2 \frac{UV}{R} = - \frac{1}{\rho} \frac{\partial \bar{p}}{\partial s} - \frac{\partial \bar{u}^2}{\partial s} - \left(1 + \frac{n}{R} \right) \frac{\partial \bar{uv}}{\partial n} - \frac{2 \bar{uv}}{R} + \nu h \frac{\partial}{\partial n} \left(\frac{\frac{\partial}{\partial n} (hU) - \frac{\partial V}{\partial s}}{h} \right) \quad (7)$$

n -component mean momentum

$$U \frac{\partial V}{\partial s} + \left(1 + \frac{n}{R} \right) V \frac{\partial V}{\partial n} - \frac{U^2}{R} \\ \equiv \frac{\partial UV}{\partial s} + \left(1 + \frac{n}{R} \right) \frac{\partial V^2}{\partial n} + \frac{V^2 - U^2}{R} = - \left(1 + \frac{n}{R} \right) \frac{1}{\rho} \frac{\partial \bar{p}}{\partial n} - \frac{\partial \bar{uv}}{\partial s} - \left(1 + \frac{n}{R} \right) \frac{\partial \bar{v}^2}{\partial n} - \frac{(\bar{v}^2 - \bar{u}^2)}{R} - \nu h \frac{\partial}{\partial s} \left(\frac{\frac{\partial}{\partial n} (hU) - \frac{\partial V}{\partial s}}{h} \right) \quad (8)$$

where the Reynolds-stress terms on the right have the same layout as the divergence forms on the left, the latter being obtained by adding U times the continuity equation to the original left-hand side of Eq(7), and similarly for Eq(8). Note that in Eqs (6) to (8) the n -derivative always appears as $h \partial/\partial n \equiv (1 + n/R) \partial/\partial n$. In axisymmetric (s, n) coordinates the main differences appear in the viscous terms which can almost always be drastically simplified: apart from this, the divergence forms of Eqs (7) and (8) are still valid if all velocity products and the pressure gradients are multiplied by the radius to the point (s, n) .

Van Dyke summarizes previous work and controversy on the application of the boundary-layer approximation (thin shear layer approximation) to the equations for laminar flow. In plane laminar flow ($R \rightarrow \infty$, $h \rightarrow 0$) the ratio of the neglected viscous term in the s -component equation, $v \partial^2 U/\partial s^2$, to the retained term $v \partial^2 U/\partial n^2$ is of order $(\delta/s)^2$, whereas in plane turbulent flow the ratio of the neglected term $\partial u^2/\partial s$ to the retained term $\partial \overline{uv}/\partial n$ is only of order (δ/s) because u^2 and \overline{uv} are of the same order in general. Therefore (i) the thin-shear-layer approximation is less accurate in turbulent flow than in laminar flow, quite apart from the fact that δ/s is generally larger, (ii) we cannot make direct use of the order-of-magnitude arguments developed for laminar curved flows. Furthermore the effect of turbulence on pitot and static tubes introduces uncertainties of order u^2 into measurement of U^2 so that the inaccuracy of measurement of $\partial U^2/\partial s$ is of the same order as the Reynolds-stress gradient $\partial u^2/\partial s$ and attempts to use sets of equations more accurate than the boundary-layer equations may not be realistic. For a careful discussion see the 1951 paper by Newman (18), and for data on corrections to static-tube measurements in shear layers see Bradshaw and Goodman (19). Despite these sources of difficulty or inaccuracy we can still produce consistent approximations to the exact equations for curved turbulent flow: for clarity only the two-dimensional case will be treated.

We consider the case where R/s and dR/ds are both of order unity, say R/δ of the order of 50 in a boundary layer: if the curvature is sharper or changes more rapidly few simplifications can be made with any rigour. In virtually all turbulent flows the viscous term in Eq(8) will be negligible everywhere and the viscous term in Eq(7) will be negligible except in the viscous sublayer, $n < 30\nu\sqrt{(\rho/\tau_w)}$ say. If we take the surface as the s -axis h will be very close to unity in the sublayer and if, as assumed, dR/ds is not of greater order than unity the viscous term in Eq(7) becomes approximately

$$v \left(\frac{\partial^2 U}{\partial n^2} + \frac{\partial^2 U}{\partial s^2} + \frac{1}{R} \frac{\partial U}{\partial n} + \frac{2}{R} \frac{\partial V}{\partial s} - \frac{U}{R^2} \right)$$

Less rigorous, but entirely trustworthy, arguments based on the known properties of the viscous sublayer in plane flow suggest that all terms except the first will be negligible. Therefore the difficulties encountered in approximating the viscous terms in laminar flow do not appear in turbulent wall flows, nor of course in turbulent free shear layers.

The largest of the Reynolds stress gradients in Eq(7) is $\partial \overline{uv}/\partial n$, the others being smaller by factors of δ/s or, equivalently, δ/R , since we have assumed s/R to be of order unity. Since n/R is clearly not much greater than δ/R , and since V is of order $U\delta/s$, the only consistent simplification of Eq(7), neglecting terms of order δ/s or δ/R , is

$$U \frac{\partial U}{\partial s} + V \frac{\partial U}{\partial n} = -\frac{1}{\rho} \frac{\partial \overline{p}}{\partial s} - \frac{\partial \overline{uv}}{\partial n} + v \frac{\partial^2 U}{\partial n^2} \quad (9)$$

identical with the familiar boundary-layer equation for a plane flow except that we have not yet proved that $\partial \overline{p}/\partial s$ is independent of n .

If we neglect the terms in Eq(8) which are of order δ/s or δ/R compared to U^2/R , and also neglect $(n/R)V \partial V/\partial n$ which is of order $(\delta/s)^2$, we get

$$-\frac{U^2}{R} \approx -\frac{U^2}{(n+R)} = -\frac{1}{\rho} \frac{\partial \overline{p}}{\partial n} - \frac{\partial \overline{v^2}}{\partial n} \quad (10)$$

Differentiating with respect to s and rearranging, we get

$$\frac{\partial^2}{\partial s \partial n} (\overline{p} + \rho \overline{v^2}) = \frac{\partial}{\partial s} \left(\frac{U^2}{R} \right) = \frac{2}{R} U \frac{\partial U}{\partial s} - \frac{U^2}{R^2} \frac{dR}{ds} \quad (11)$$

so that

$$\frac{\partial}{\partial s} (\overline{p} + \rho \overline{v^2}) - \frac{\partial \overline{p}_0}{\partial s} = \int_0^n \frac{1}{R} \left(2U \frac{\partial U}{\partial s} - \frac{U^2}{R} \frac{dR}{ds} \right) dn \quad (12)$$

where the operator $\int dn$ is of order δ and where \overline{p}_0 is the pressure at $n = 0$. Now dR/ds is of order unity and U^2/R or U^2/s is in general of the same order as $U \partial U/\partial s$ so that the difference between the longitudinal pressure gradient at $n = 0$ and at $n = \delta$ is of order δ/R times the first term in Eq(9) and we have already neglected terms of this order in deriving Eq(9). Furthermore $\partial \overline{v^2}/\partial s$ is of the same order as $\partial u^2/\partial s$ which has also been neglected in Eq(9). Therefore, for purposes of substitution in Eq(9), Eq(10) reduces to

$$\frac{\partial \overline{p}}{\partial n} = 0 \quad (13)$$

as in plane boundary layers: there is no rigorous approximation intermediate between Eq(7) and Eq(9) in which a higher approximation than Eq(13) could be used. We note that the terms neglected in passing from Eq(7) to Eq(9) (leaving aside the viscous term) are all of order δ/R or δ/s times those retained: there are no terms of order $(\delta/R)^2$ in Eq(7). Now using Eq(10) to substitute for $\partial \overline{p}/\partial s$ in Eq(7) would introduce more terms of order δ/R times the main terms in Eq(7); if, on the other hand, we substituted for $\partial \overline{p}/\partial s$ in Eq(7) by manipulating the full n -component equation, Eq(8), in the same way as we

manipulated Eq(10) to get Eq(12), we should be introducing terms of order $(\delta/R)^2$ into Eq(7). This suggests that a consistent set of equations, including terms of order δ/R but not smaller terms, is the (exact) Eq(7), with the viscous term simplified to taste, and the (approximate) Eq(10). In view of the experimental difficulties mentioned above, use of Eq(8) is probably never justifiable.

It is popularly supposed that in numerical calculations we can substitute Eq(12) into Eq(9) and regard the resulting equation as parabolic, so that it can be solved by a marching method, given $\bar{p}_0(s)$. The integrals in Eq(12) are evaluated by using velocities calculated at the previous step or at the previous iteration. Now the fact remains that Eq(9) and Eqs (10) or (12) are elliptic: only if Eq(12) is replaced by Eq(13) with \bar{p} known does the system become parabolic. Obviously the elliptic system is strongly constrained by the specification of $p_0(s)$, even if $p_0(s)$ is itself calculated in an outer iteration, but the popular procedure may be expected to fail when the pressure difference across the layer is large, or in other difficult cases. Baum (20) was unable to allow in this way for the pressure difference across the subsonic part of a curved compressible shear layer although his explanation of the reasons is mathematical rather than physical: in reality, the effect of small perturbations on a flow near $M = 1$ is to produce a "choking" phenomenon. The well-known non-uniqueness difficulties of the Crocco-Lees series of methods (21) also stem from attempts to march an elliptic problem but for slightly different reasons. There seems to have been no general investigation of the consequences of treating a slightly elliptic problem as parabolic for numerical purposes and so all one can do is to urge people who try it to apply careful checks for accuracy and stability. A useful and entirely acceptable application of Eq(5) is in the analysis of pitot-pressure profiles in curved shear layers. Substituting $2(P-p)/\rho$ for U^2 and ignoring $\partial v^2/\partial n$ as being of the same order as neglected terms in the pitot equation, we get

$$\frac{\partial p}{\partial n} + \frac{2p}{n+R} = \frac{2P}{n+R} \quad (14)$$

solving for p in terms of P , we get

$$p(n+R)^2 - p_0 R^2 = 2 \int_0^n P(n'+R) dn' \quad (15)$$

or, a useful form in boundary layers due to Wilcken (22),

$$p - p_0 = \frac{2}{(n+R)^2} \int_0^n (P - p_0)(n'+R) dn' \quad (16)$$

In the case where dR/ds is of greater order than unity, assuming that the viscous term is not significantly altered, we see that the only explicit alteration to the above analysis is that the last term in Eq(11) is of larger order: in an engineering calculation method it would be easy enough to subtract a term

$$\frac{1}{R} \frac{dR}{ds} \int_0^n U^2 ds$$

from $\partial \bar{p}/\partial s$ in Eq(7) or Eq(9). However if dR/ds remains large s/R becomes of greater or less order than unity and the whole analysis breaks down, as it obviously does if dR/ds becomes infinite (sudden change of surface curvature). It seems almost inevitable that "marching" solutions will fail in such cases. Furthermore, large values of dR/ds are likely to lead, via the integral correction term just derived, to large longitudinal accelerations and to modifications of the turbulence structure additional to those caused directly by the streamline curvature.

We summarize the above analysis by the following table for R/s not much smaller than, and dR/ds not much larger than, unity.

	s-equation	n-equation	
Exact	(7)	(8)	
Terms in δ/s or δ/R retained	(7)	(10)	} viscous term in s-equation simplified to $v \partial^2 U/\partial n^2$, } viscous term in n-equation neglected
Terms in δ/s or δ/R neglected	(9)	(13)	

Now these are rigorous order-of-magnitude approximations valid for any flow: but there is no reason why we should not use our knowledge of a particular flow to do better than an order of magnitude, by ignoring terms which the rigorous analysis requires to be included but which we know are negligible in the flow concerned. For instance, in a shear layer which is sharply-curved but slowly-growing we may be justified in using Eq(5) with the viscous term reduced to $v \partial^2 U/\partial y^2$ and the $\partial u^2/\partial s$ term neglected, and Eq(10) with the factors $(1+n/R)$, present in Eq(8), retained on the right hand side: the term $(v^2 - u^2)/R$ on the right hand side of Eq(8) is likely to be fairly small compared with $(1+n/R)\partial v^2/\partial n$ in practical cases. Then U^2/R in Eqs (10) and (11) is replaced by $U^2/(n+R)$, $(n+R)$ being the local radius of curvature of the streamline, and the resulting set of equations satisfies the thin-shear-layer requirement $\partial/\partial s \ll \partial/\partial n$ but not the requirement $\partial p/\partial n = 0$.

2.3 THE (x,r) SYSTEM

The exact equations for incompressible swirling flow in the axisymmetric (x,r) system, with symbols U , V and W for the mean velocity components in the x , r and θ directions respectively and with $\partial/\partial \theta \equiv 0$, are

x-component mean momentum

$$U \frac{\partial U}{\partial x} + V \frac{\partial U}{\partial r} = -\frac{1}{\rho} \frac{\partial \bar{p}}{\partial x} - \frac{\partial \bar{u}^2}{\partial x} - \frac{\partial \bar{u}v}{\partial r} - \frac{\bar{u}v}{r} + \text{viscous terms} \quad (17)$$

r-component mean momentum

$$U \frac{\partial V}{\partial x} + V \frac{\partial V}{\partial r} - \frac{W^2}{r} = -\frac{1}{\rho} \frac{\partial \bar{p}}{\partial r} - \frac{\partial \bar{u}v}{\partial x} - \frac{\partial \bar{v}^2}{\partial r} - \frac{\bar{v}^2 - \bar{w}^2}{r} + \text{viscous terms} \quad (18)$$

θ -component mean momentum

$$U \frac{\partial W}{\partial x} + V \frac{\partial W}{\partial r} + \frac{VW}{r} = -\frac{\partial \bar{u}w}{\partial x} - \frac{\partial \bar{v}w}{\partial r} - \frac{2\bar{v}w}{r} + \text{viscous terms} \quad (19)$$

continuity

$$\frac{\partial U}{\partial x} + \frac{\partial V}{\partial r} + \frac{V}{r} = 0 \quad (20)$$

The equations can be derived by applying the principles of conservation of mass and momentum to the elementary control volume shown in Fig.1(d). Note that here r is an independent variable: in the (s,n) system n is an independent variable and R is a prescribed function of s . The viscous terms are given by Rodi (17).

The approximations to this system have generated less controversy than approximations to the (s,n) system, partly because the (x,r) system is used for so many different flows that no one set of approximations is generally valid. For instance, in a normally-impinging circular jet (whether swirling or not) we pass from a slender-shear-layer approximation, $\partial/\partial r \gg \partial/\partial x$, before impingement to a thin-shear-layer approximation, $\partial/\partial x \gg \partial/\partial r$, in the radial wall jet after impingement; and the viscous terms are negligible except for $\partial^2 V/\partial x^2$ and $\partial^2 W/\partial x^2$ close to the solid surface. In axisymmetric swirling flows which change rapidly in the x direction, such as the impingement regions of the jet mentioned above, or a bursting vortex or the recirculating region of a swirl burner, the full equations must be used, except for some allowable simplifications in the viscous terms.

The slender-shear-layer approximation applied to swirling jets, wakes, vortices and pipe flows allows us to ignore all x -derivatives in the Reynolds stress and viscous stress terms: generally terms in $1/r$ are of the same order as terms in $\partial/\partial r$. The main difficulty occurs in dealing with the pressure terms: most of the remarks in Section 2.2 are relevant. Finally the special case of cylindrical flow ($\partial/\partial x = 0$) appears in some mathematical analyses: the only curved turbulent flow that qualifies exactly is that in a long spinning pipe.

In a strongly-swirling slender flow (with the maximum value of W of the same order as the maximum value of U) the r -component mean momentum equation is approximately

$$\frac{W^2}{r} = \frac{1}{\rho} \frac{\partial \bar{p}}{\partial r} \quad (21)$$

since $\frac{V}{r}$ and $\sqrt{v^2}$ are both much less than W : we can without prejudice group \bar{v}^2 with \bar{p} and argue that $(\bar{v}^2 - \bar{w}^2)/r$ will in practice be smaller than $\partial \bar{v}^2/\partial r$, but this is not rigorously justifiable. Repeating the argument used to derive Eq(12) from Eq(10) we get

$$\frac{1}{\rho} \frac{\partial (\bar{p} - \bar{p}_0)}{\partial x} = \frac{\partial}{\partial x} \int_{r_0}^r \frac{W^2}{r'} dr' \quad (22)$$

where \bar{p}_0 is the pressure at some reference position $r = r_0$ for substitution in Eq(17). If W is of the same order as U this is not negligible compared to $U \partial U/\partial x$ and we therefore conclude that, almost by definition, the x -component and θ -component equations in a strongly-swirling flow interact via the pressure term in the r -component equation. An exception, of course, is the case where r/r_0 is close to unity in the region of interest - the case of a thin annular shear layer - when the effects of the radial pressure gradient on the axial motion can be neglected and the equations reduce to

$$U \frac{\partial U}{\partial x} + V \frac{\partial U}{\partial r} = -\frac{1}{\rho} \frac{dp}{dx} - \frac{\partial \bar{u}v}{\partial r} + v \frac{\partial^2 U}{\partial r^2} \quad (23)$$

$$U \frac{\partial W}{\partial x} + V \frac{\partial W}{\partial r} = -\frac{\partial \bar{v}w}{\partial r} + v \frac{\partial^2 W}{\partial r^2} \quad (24)$$

$$\frac{\partial U}{\partial x} + \frac{\partial V}{\partial r} = 0 \quad (25)$$

on noting that in a thin annular shear layer $\partial/\partial r \gg 1/r$. These are identical with the boundary layer equations for an infinite swept wing with x measured in the surface, normal to the generators. The x -component equation depends on the r -component equation only via the Reynolds-stress transport equations: in laminar flow the x -component equation would not depend on the r -component equation, according to the "independence principle" (Ref.23, p.468).

In a weakly-swirling slender flow ($W \ll U$) we can neglect the effects of $\partial \bar{p}/\partial r$ on the x -component equation, and therefore ignore the radial-component equation altogether. The equations

therefore become Eqs (23)-(25) again with the addition of the terms in $1/r$ from the original equations Eqs (17), (19) and (20), which are not negligible unless the shear layer is a thin annulus.

In the present context we do not need to consider the equations for a swirling radial thin shear layer such as that on a rotating disc, because moderate streamline curvature in the plane of the layer has not yet been shown to have any significant effect on turbulence structure.

2.4 THE REYNOLDS-STRESS TRANSPORT EQUATIONS

These are exact equations, derived from the Navier Stokes equations (24, 25). They are the simplest equations to give us information about turbulence quantities (we define a "turbulence quantity" as the mean, usually with respect to time, of a function of fluctuating quantities; the mean of any one fluctuating quantity is zero by definition). There are six Reynolds-stress transport equations, one for each of the independent elements of the Reynolds-stress tensor (Appendix 1)

$$\begin{bmatrix} -\rho\overline{u^2} & -\rho\overline{uv} & -\rho\overline{uw} \\ -\rho\overline{vu} & -\rho\overline{v^2} & -\rho\overline{vw} \\ -\rho\overline{wu} & -\rho\overline{wv} & -\rho\overline{w^2} \end{bmatrix}$$

The element in the i -th row and j -th column is denoted by $-\rho\overline{u_i u_j} \equiv -\rho\overline{u_j u_i}$: it represents an apparent stress acting in the x_i -direction (where $x_1 = x$, $x_2 = y$, $x_3 = z$) on a plane normal to the x_j -direction, as a consequence of the mean rate of transfer of u_i -component momentum in the u_j direction by the turbulence. Each Reynolds-stress transport equation can be arranged to give the mean rate at which that Reynolds stress increases along a mean streamline of the flow: the rate operator D/Dt is defined as

$$U \frac{\partial}{\partial x} + V \frac{\partial}{\partial y} + W \frac{\partial}{\partial z}$$

and is the rate of increase with respect to time as seen by an observer following the mean motion of the fluid. Thus the Reynolds-stress transport equation gives $D \overline{u_i u_j} / Dt$ just as the x_1 -component mean momentum equation gives $D U_1 / Dt$. If we rewrite $D \overline{u_i u_j} / Dt$ in "divergence form" by adding $\overline{u_i u_j}$ times the mean continuity equation,

$$\frac{D \overline{u_i u_j}}{Dt} \text{ becomes equal to } \text{div}(\underline{U} \overline{u_i u_j}) \text{ or } \frac{\partial}{\partial x_1} (U_1 \overline{u_i u_j}) + \frac{\partial}{\partial x_2} (U_2 \overline{u_i u_j}) + \frac{\partial}{\partial x_3} (U_3 \overline{u_i u_j})$$

which is recognizable as the net rate at which $\overline{u_i u_j}$ is transported out of a unit control volume by the mean velocity \underline{U} just as the continuity equation $\text{div}(\rho \underline{U}) = 0$ gives the net rate of transport of mass out of a unit control volume by \underline{U} . In the case of $\overline{u_i u_j}$ the net rate of transport by \underline{U} is generally non-zero. As shown in Fig.9(a) it is the sum of contributions from several processes

$$\begin{aligned} & \text{(net rate of transport of } \overline{u_i u_j} \text{ out of control volume by mean flow)} \\ &= \text{(mean rate of generation of } \overline{u_i u_j} \text{ within control volume)} \\ & \quad - \text{(mean rate of destruction of } \overline{u_i u_j} \text{ within control volume)} \\ & \quad - \text{(mean rate of transport of } \overline{u_i u_j} \text{ out of control volume by fluctuating velocity,} \\ & \quad \quad \text{pressure and viscous stresses)} \end{aligned}$$

Reynolds stress is generated by interaction of the existing Reynolds stresses with the mean rates of strain or with body forces (Reynolds stress and vorticity fluctuations can appear in non-turbulent fluid only by the action of viscosity or unusual kinds of body forces). It can be destroyed by fluctuating viscous stresses. Any given component can be augmented or reduced by pressure-fluctuation terms which do not, however, change the sum of the principal stresses: therefore we sometimes call these "redistribution" rather than "destruction" terms.

Minus one-half of the sum of the principal stresses, $\frac{1}{2}\rho(\overline{u^2} + \overline{v^2} + \overline{w^2})$, is called the turbulent kinetic energy. Its transport equation [Fig.9(c)], obtained as half the sum of the separate equations for $\overline{u^2}$, $\overline{v^2}$ and $\overline{w^2}$, is strictly an energy-conservation equation, which the individual equations for $\overline{u_i u_j}$ are not, and is therefore easier to explain in physical terms. The generation term in the turbulent energy equation, called the "production" term, is equal to the rate at which the mean rates of strain do work against the Reynolds stresses, thus transferring mean-flow kinetic energy to turbulent kinetic energy; the destruction (viscous "dissipation") term is equal to the mean rate at which the fluctuating rates of strain in the turbulence do work against fluctuating viscous stresses, thus transferring turbulent kinetic energy to thermal internal energy. It is very important to remember that the eddies directly affected by viscosity are much smaller than those which make the main contribution to the turbulent kinetic energy and the Reynolds stresses. At all but the lowest local Reynolds numbers (based on intensity and eddy length scale) the energy-containing eddies are independent of viscosity: since the rate at which they transfer energy to smaller eddies is equal to the dissipation rate, the viscous dissipation rate is also independent of viscosity. Another consequence is that the viscous terms in the shear-stress equations ($i \neq j$) are negligible except at low local Reynolds number.

The net rate of spatial transport of $\overline{u_i u_j}$ by the fluctuations themselves ("turbulent transport" for short) is best thought of as a further example of the propensity of turbulence to transport or diffuse any quantity it carries, such as mass, momentum or energy. Transport by fluctuating viscous stresses is negligible except very close to a solid surface or in certain flows at low Reynolds number: transport by pressure fluctuations seems to be generally rather smaller than transport by velocity fluctuations, but this may not be the case in stably-stratified or stably-curved flows carrying internal waves. A simple example of transport by velocity fluctuations is the eruption of large eddies near the free edge of a turbulent flow: fluid that moves outwards near the edge is generally more intensely turbulent than the

fluid from beyond the edge that moves in to take its place. We can see that the net rate at which $\overline{u_i u_j}$ is deposited in (or removed from) a given control volume by this process depends on the rate at which the $u_i u_j$ carried by the eddies decreases (or increases) as they move through the control volume. Therefore the turbulent transport terms in the equations, like the mean transport terms, can always be expressed as spatial gradients of turbulence quantities: being rates of transport from one place to another, their integrals over the whole volume of the flow are always zero.

A special case of some importance is "local equilibrium" [Fig.9(b) and Ref.26] in which mean and turbulent transport terms are negligible so that the generation and destruction (or "redistribution") terms are equal. The implication is that the turbulence has adjusted itself so that the rate of increase of $\overline{u_i u_j}$ due to interaction with the mean flow is in equilibrium with the rate of decrease due to the destruction terms, and further that the characteristic velocity and length scales of the turbulence must therefore have adjusted themselves to be proportional to the characteristic velocity and length scales of the mean flow. The only extended region in which transport terms are negligible is the inner layer of a turbulent wall flow, the region within roughly one-tenth of the flow width from the surface where eddy time scales are small enough for adjustment to occur quickly: transport terms do become significant once more in the viscous sublayer, $u_\tau y/\nu < 30$ say, where they supply turbulent energy to the region of finite dissipation but negligible production close to the wall. In the outer layer of a slowly-changing boundary layer, the mean and turbulent transport terms, though not small, are roughly equal and opposite, so that "generation" = "destruction" is a fairly good empirical approximation: therefore local-equilibrium arguments give results acceptable for some engineering purposes although this cannot properly be called a local-equilibrium flow. For similar reasons, local-equilibrium results are usable in duct flows, not too close to the centre line where generation goes to zero and destruction is necessarily balanced by transport. Local equilibrium is not a good approximation in free shear layers: in a mixing layer, for instance, the dissipation of turbulent energy in the region of maximum intensity is only about half the production, the rest being transported to lower-intensity regions by the turbulence. A relative of local equilibrium is self-preservation, [(25), Sections 3.1 and 4.1], in which the length and velocity scales of the mean flow and turbulence have gradually become proportional over a long development length: this requires the free-stream velocity and other boundary conditions to be constant or to vary in certain restricted ways. In a self-preserving shear layer, the ratio of generation to destruction is a function only of y/δ , independent of x but not closely equal to unity except in the inner layer of a wall flow. It can be seen that a local-equilibrium analysis leading to an empirical function of y/δ will apparently apply to all parts of a self-preserving flow if the (variable) ratio of generation to destruction is hidden in the empirical function: this does not imply that the flow is truly in local equilibrium.

The local-equilibrium approximation to the turbulent energy equation in a simple shear layer [which is itself the approximation to Eq(A1.28) in the limit $R \rightarrow \infty$, with $\partial/\partial n \gg \partial/\partial s$] is

$$\text{production} = -\overline{uv} \frac{\partial U}{\partial y} = \text{dissipation} \equiv \epsilon \equiv \frac{(-\overline{uv})^{3/2}}{L} \quad (26)$$

where the last identity sign defines the dissipation length parameter L . Hence

$$\frac{\partial U}{\partial y} = \frac{(-\overline{uv})^{1/2}}{L} \quad (27)$$

Now the "mixing length" ℓ is defined in any simple shear layer by

$$\frac{\partial U}{\partial y} \equiv \frac{(-\overline{uv})^{1/2}}{\ell} \quad (28)$$

and is therefore equal to L in a local-equilibrium region: in non-equilibrium regions L is still a meaningful length scale but ℓ is not (it is somewhere between a length scale of the mean shear and a length scale of the turbulence, and the two are not directly related). The oft-quoted ambiguity of definition of the rate of strain to be used in the mixing length formula for curved flows will be briefly discussed in Section 4: the effects of the ambiguity are small compared to the direct effects of curvature on the turbulence. Formulae like Eq(27) could be derived from local-equilibrium approximations like Eq(26) to the other transport equations: even in the most advanced calculation methods it is assumed that one length scale is enough to specify the turbulence so that the other formulae would not at present be significantly more useful than Eq(27) alone. Conversely, what we say about the dissipation length parameter could equally well be said about other length scales defined by other types of destruction term.

In the present monograph we shall often represent the effects of extra strain rates, particularly streamline curvature, as factors on L . The factors could equally well be applied directly to the destruction terms in the transport equations but using L allows us to apply the well-known local-equilibrium approximation Eq(27) for the purpose of assessing the effects of extra strain rates. As long as the local-equilibrium approximation is fairly accurate the evaluation of the empirical factors on L can be fairly accurate. We can then invoke the fact that L is always a meaningful length scale of the turbulence to justify using the same empirical factors in flows where local equilibrium is no longer even fairly accurate: that is, having used the local equilibrium approximation to establish the correction to L , we use the corrected L in a calculation method which does not invoke local equilibrium. This, like most of the arguments used in treating the Reynolds-stress transport equations, is not exact but is the best way of extrapolating limited data and limited physical understanding.

For the purposes of discussing the Reynolds-stress transport equations in the general, non-equilibrium case, the physical processes summarized in Fig.9(a) are more important than their mathematical representation. The equation for $D \overline{u_i u_j} / Dt$ is obtained by multiplying the u_i -component Navier-Stokes equation (whose first term is $\partial u_i / \partial t$) by u_j , and adding u_i times the u_j -component Navier-Stokes equation to obtain $u_j \partial u_i / \partial t + u_i \partial u_j / \partial t \equiv \partial u_i u_j / \partial t$. This term vanishes on taking the mean with respect to time, but is a simple mnemonic for the derivation of this or any other transport equation; manipulate the Navier-Stokes equations to form the time derivative, $\partial/\partial t$, of the quantity whose substantial derivative,

D/Dt , is required. The equation for $D \overline{u_i u_j} / Dt$ is given in general tensor notation as Eq(A1.24). The Reynolds-stress transport equations in (s,n) and (x,r) coordinates can be deduced as explained in Appendix 1. Since the coordinates are not isotropic each equation must be written out separately: the turbulent energy equation, the \overline{uv} equation and — for (x,r) coordinates only — the \overline{vw} equation, are given as Eqs (A1.28) to (A1.32) of Appendix 1. A qualitative guide to the effects of extra rates of strain in general and of streamline curvature in particular is given by the production terms in the turbulent energy equations, which we equate to the dissipation rate ϵ in the local-equilibrium approximation. These are, roughly in order of importance in typical shear layers,

$$P_n \equiv - \left(1 + \frac{n}{R} \right) \overline{uv} \frac{\partial U}{\partial n} - \left(\overline{uv} \frac{U}{R} - 2 \overline{uv} \frac{U}{R} \right) - \overline{u^2} \frac{\partial U}{\partial s} - \left(1 + \frac{n}{R} \right) \overline{v^2} \frac{\partial V}{\partial n} - \overline{uv} \frac{\partial V}{\partial s} - \overline{u^2} \frac{V}{R} \quad (29)$$

in two-dimensional (s,n,z) coordinates, where the two parts of the second term come from the $\overline{u^2}$ and $\overline{v^2}$ equations respectively, and

$$P_r \equiv - \overline{uv} \frac{\partial U}{\partial r} - \overline{vw} \left(\frac{\partial W}{\partial r} - \frac{W}{r} \right) - \overline{v^2} \frac{\partial V}{\partial r} - \overline{w^2} \frac{V}{r} - \overline{u^2} \frac{\partial U}{\partial x} - \overline{uw} \frac{\partial W}{\partial x} - \overline{uv} \frac{\partial V}{\partial x} \quad (30)$$

in axisymmetric (x,r,θ) coordinates. Note the sign of W/r in the second term of the last expression: turbulent energy is not produced by pure rotation ($\partial W/\partial r = W/r$). In a simple shear layer the only term that remains is $-\overline{uv} \partial U/\partial y$, as in Eq.(26).

The Reynolds-stress transport equations introduce further unknowns and therefore cannot be solved as they stand. We go on to discuss methods of replacing these unknown terms by empirical functions of known quantities.

2.5 CALCULATION METHODS

Many reviews of the strategy of calculating turbulent shear layers — that is, the process of inserting empirical information into a chosen set of exact equations to make them soluble — have been written in recent years. Digital computers enable quite complicated systems of partial differential equations to be solved. Even the earlier computer-oriented methods for thin shear layers, dating from the mid-1960s, performed at least as well as the most highly-developed of the traditional "integral" methods, based on ordinary differential equations for integral parameters and intended for solution on desk calculators. Therefore most of the basic research of the last few years has been devoted to methods based on partial differential equations, mostly recognizable as simulations or simplifications of the exact Reynolds-stress transport equations. Calculation methods developed by 1968 are nearly all described, and their performance analysed, in Ref.27. More recent reviews (25), (28-30) have tended to concentrate on methods based on explicit, term-by-term approximation of the Reynolds-stress transport equations. This reflects the state of current research but also the personal enthusiasms of the reviewers. The application of computers to the older mixing length and eddy viscosity formulae is described in the books by Patankar and Spalding (31) and Cebeci and Smith (32). The book by Nash and Patel (33) concentrates on three-dimensional thin shear layers.

The strategy into which nearly all methods can be fitted is as follows, different types of method terminating in empirical formulae, or complete neglect of some terms, after different numbers of stages.

(i) Take the time mean of the Navier Stokes equations, obtaining the Reynolds equations for the rates of change, along a mean streamline, of the components of mean momentum or velocity. Unknown Reynolds stress gradients, depending on second-order mean products of fluctuating velocities, $\overline{u_i u_j}$, appear on the right hand side.

(ii) Take the time mean of u_j times the u_i -component Navier Stokes equation plus u_i times the u_j -component equation, obtaining the Reynolds stress transport equations for $D \overline{u_i u_j} / Dt$, the rate of change, along a mean streamline, of the Reynolds stresses $\overline{u_i u_j}$. Unknown mean triple products of velocity fluctuations, second-order mean products of fluctuating velocity gradients, and mean products of pressure fluctuations and fluctuating velocity gradients appear on the right hand side.

(iii) Manipulate the Navier Stokes equations to obtain exact differential equations for the unknown quantities on the right hand sides of the Reynolds stress transport equations. A simple mnemonic for the process is that the time derivative in the x_i -component Navier Stokes equation, $\partial u_i / \partial t$, must be factored to give the time derivative of the required "unknown quantity" [e.g. $\partial u_i u_j / \partial t \equiv u_j \partial u_i / \partial t + u_i \partial u_j / \partial t$ in the example in (ii) above]: the time mean then gives the transport equation for the unknown quantity (e.g. $D \overline{u_i u_j} / Dt$). Further unknown quantities appear on the right hand sides of these further transport equations. At any stage, ordinary differential equations can be derived by integrating partial differential equations across the thickness of the shear layer: to obtain a practicable system, several weighted integrations may be required for each partial differential equation.

An infinite number of transport equations would be needed to recover all the information lost by time-averaging the Navier Stokes equations. To solve a large but finite number of transport equations might take longer than solving the time-dependent equations themselves, but the empirical information needed to close the system becomes too difficult to obtain or to handle long before this stage is reached. The "order" of closure is the highest order of equation considered. Mixing-length and eddy viscosity formulae, for insertion after stage 1 above, are examples of first-order closure; approximation of the terms on the right hand sides of the Reynolds stress transport equations constitutes second-order closure; and of the equations of third-order closure, only the transport equations for mean squares of fluctuating velocity gradients, related to the energy dissipation rate, have been treated quantitatively (34, 35). Equations of one order higher than those to be closed may give useful qualitative information about the quantities to be approximated: for example, the mixing-length formula can be justified by taking the local-equilibrium approximation to the Reynolds-stress transport equation; Hanjalic and Launder (34) support their treatment of the triple products in the Reynolds-stress transport equation by reference to

the exact transport equations for triple products; and it is scarcely possible to treat the fluctuating pressure correctly without reference to the exact equation which describes it. In some calculation methods transport equations are used only for the Reynolds stresses whose gradients actually appear in the problem: in more refined methods, some or all of the other Reynolds stresses may be left in exact form in a given transport equation, so that transport equations must be solved for these as well.

Some work has been done on empirical transport equations for mixing length or eddy viscosity. However we have just seen that the mixing length formula can be justified, in the sense of relating the apparent "mixing length" to a true length scale of the turbulence, only by making the local equilibrium approximation: the same is true of eddy viscosity (whose relation to a definable turbulence property is even more distant). The use of second-order closure concepts on quantities which are physically meaningful only to first order is clearly not rigorous, even for simple shear layers. In complex flows it becomes necessary to admit that the eddy viscosity is anisotropic, so that separate equations are needed for its separate components. Also, the argument that the eddy viscosity generally varies less than the Reynolds stresses, and is therefore easier to correlate, fails in cases where the mean velocity gradient goes to zero while the shear stress does not, for the eddy viscosity then becomes infinite. Therefore my own opinion, disputed by some, is that wholly-empirical transport equations for eddy viscosity or mixing length are not to be preferred above term-by-term empirical approximation of the exact Reynolds-stress transport equations.

At all levels of closure, some assumptions must be made about turbulence length scales or the equivalent. The mixing length is obviously a length scale, if not a physically meaningful one. All the terms in the Reynolds-stress transport equations have the dimensions of (velocity)³/(length) so that those which are pure turbulence quantities (i.e. not spatial gradients of mean properties or turbulence quantities) must each be represented as the cube of a typical turbulent velocity scale, such as $(-uv)^{3/2}$, divided by a turbulence length scale. An example is the replacement of the dissipation rate ϵ in Eq(26) by $(-\overline{uv})^{3/2}/L$. It is of course possible to make empirical assumptions about the dissipation itself, rather than about the dissipation length parameter L , and then deduce a length scale for use in modelling other terms. In simple eddy-viscosity and mixing length treatments, and in some second-order closures, the length scale is related to the mean flow length scales and perhaps the details of the Reynolds-stress distribution. This is, at best, reasonable only for thin shear layers, perhaps with small extra rates of strain, where it can be argued that the largest eddies necessarily have a length scale nearly equal to the width of the shear layer: it is clearly not true if the shear layer is perturbed by large extra rates of strain. In methods intended for such complex flows, differential "transport" equations are needed for length scales as well as for the Reynolds stresses. We note in passing that the local-equilibrium approximation to a length-scale transport equation may never be acceptably accurate, even in a thin shear layer: the boundaries have a large influence on the flow, and turbulent transport of length scale normal to the boundaries is likely to be appreciable. It may, however, be permissible to neglect the mean transport terms in slowly-changing flows. Once the length scale is defined, an exact transport equation can be deduced from the Navier-Stokes equation. For instance, a transport equation for $\epsilon \approx v(\partial u_i/\partial x_j)^2$ can be obtained by differentiating the x_i -component Navier-Stokes equation with respect to x_j , multiplying by $2(\partial u_i/\partial x_j)$ so that the leading term becomes $\partial(\partial u_i/\partial x_j)^2/\partial t$ and the time mean gives $D(\partial u_i/\partial x_j)^2/Dt$. The transport equation for $L \equiv (-\overline{uv})^{3/2}/\epsilon$ follows from the transport equations for ϵ and for $-\overline{uv}$: the terms on its right hand side can in principle be expressed as empirical functions of the Reynolds stresses and of L itself. The transport equation for the integral scale of the two-point space correlation

$$\frac{1}{\overline{u_i u_j}(\underline{x})} \int_0^\infty \overline{u_i(\underline{x}) u_j(\underline{x} + \underline{r}_\ell)} d\tau_\ell$$

(where \underline{r} is the separation vector, not a radius of curvature) is a more complicated form of the Karman-Howarth equation for isotropic turbulence (where $u^2 = v^2 = w^2$, etc.): in isotropic turbulence all correlations are related by symmetry and other conditions, so one integral scale defines all, but in shear-flow turbulence the 27 choices for the integral scale (3 choices each for i, j and ℓ) are not simply related to each other, to the dissipation length parameter L or to any other length scale. At present it is assumed, even in the most advanced calculation methods, that all relevant length scales are proportional, so that - say - L is used as a length scale in modelling the pressure-fluctuation "redistribution" terms as well as in modelling the dissipation term itself. Probably the errors or uncertainties introduced in thin or fairly thin shear layers are no worse than those already present in the modelling process, but one feels intuitively that more than one length scale will be needed to describe turbulence subjected to several roughly equal rate of strain components (36). Also, a solid boundary forces the turbulence to become anisotropic at distances from the boundary less than one or two eddy wavelengths, whatever its state elsewhere. Allowance for this effect in a single length-scale equation is necessarily somewhat arbitrary.

Cebeci (private communication, February 1972) and Rotta (30) have both suggested that a distinction should be drawn between methods whose empirical content has to be adjusted for each species of shear layer (jets, boundary layers, ducts, etc.) and methods which are nominally capable of application to any shear layer without alteration, except to the boundary conditions. Rotta calls these "incomplete" and "complete" methods. The distinction is indeed a useful one, but it must be emphasized very strongly, especially to design engineers, that a calculation method which is nominally capable of treating a given case (in the sense that it will accept the required boundary conditions and complete the run without error messages from the computer) may not be actually capable of producing acceptably accurate results. Naturally the results are likely to be most inaccurate in complex cases where few data are available to test their acceptability! We shall see that in order to predict even the effects of small extra rates of strain on thin shear layers we have to abandon one of the necessary features of a "complete" method, namely invariance with respect to rotation of the coordinate axes. For example, the effects of streamline curvature on a shear layer flowing in the x direction can be represented by factors like $1 + 10(\partial V/\partial x)/(\partial U/\partial y)$; but if the flow were in the y direction the factor would become $1 + 10(\partial U/\partial y)/(\partial V/\partial x)$. For such reasons and for more important physical reasons, it is important to distinguish between "nominally complete" and "actually complete" methods, and to admit that at present no methods are "actually complete" (although some are more complete than others).

Analogous to the well-known procedure for (x,y) coordinates, weighted integrals — with respect to n — of the s -component momentum equation in (s,n) coordinates can be used to generate ordinary differential equations, expressing conservation of momentum, energy, etc., for the shear layer as a whole, for use in "integral" calculation methods. As well as the difficulties caused by the extra terms as such there are also conceptual difficulties, introduced by the presence of a finite velocity gradient $\partial U/\partial n$ even in the free stream and by ambiguities in definition of the displacement thickness and momentum-deficit thickness: for instance if $\partial U/\partial n$ is non-zero outside the shear layer the displacement of the external streamlines by the shear layer — the displacement thickness — varies with n and any unique definition must therefore be an arbitrary one. The problems have been discussed by Patel (37), Myring (38) and others. However, it seems unlikely, to this author at least, that the simpler types of "integral" method, in which empirical information is introduced directly into ordinary differential equations, will be able to deal with turbulent shear layers so highly curved that quasi-rectangular coordinates are unacceptably inaccurate. The assumptions made about the turbulence in these methods are necessarily crude, since they refer only to weighted integrals of turbulence properties and do not consider conditions at each point across the shear layer. Therefore even the representation of the effects of small curvature on the turbulence may be difficult because the importance of these effects varies significantly across the shear layer, and larger curvature effects would probably cause even greater difficulties. These comments do not apply to the use of the generalized Galerkin method or "method of weighted residuals" (27, p.16) to convert partial differential equations with empirical information already inserted — such as closed versions of the mean-motion equations and the turbulent transport equations — into ordinary differential equations. As its use in the analysis of complex structures shows, the Galerkin method is easily applicable to complicated boundary conditions, and it is not necessary for each weighted integral equation to represent conservation of a physical property such as the momentum or energy integrals, because the method is simply a mathematical technique. Therefore the problem of generating physically-meaningful ordinary differential equations for curved shear layers does not seem to merit further attention.

3. EFFECTS OF EXTRA STRAIN RATES ON TURBULENT SHEAR LAYERS

3.1 A SIMPLE CORRELATION SCHEME FOR SMALL EXTRA STRAIN RATES

We define an "extra" strain rate as any rate-of-strain component* other than a simple shear $\partial U/\partial y$: in general we denote it by symbol e . In a thin curved shear layer the extra rate of strain is $e = \partial V/\partial x$ in x,y coordinates, or $e = -U/(n+R)$ in (s,n) coordinates. Other examples (with the signs of e chosen for later convenience) are

- lateral divergence: $e = \partial W/\partial z$
- longitudinal extension } $e = -\partial U/\partial x$
- or normal divergence } or $\partial V/\partial y$
- bulk compression: $e = -\text{div } \underline{U} \equiv -(\partial U/\partial x + \partial V/\partial y + \partial W/\partial z)$
- rotation of whole flow system about z axis: $e = \Omega$

We do not regard $\partial W/\partial y$ as an extra rate of strain: with respect to axes in the direction of the resultant of $\partial U/\partial y$ and $\partial W/\partial y$ the fluid experiences a simple shear equal to that resultant. Moderate values of $\partial W/\partial x$, or moderate spatial gradients of $(\partial W/\partial y)/(\partial U/\partial y)$ in either the x or y directions, do not seem to have a significant effect on turbulence structure beyond that predicted by conventional calculation methods.

If an extra strain rate is applied to a flow initially in simple shear, extra "generation" terms (see Section 2.4) appear in the Reynolds stress transport equations. For example, if $e = \partial V/\partial x$ (streamline curvature) the generation terms in the \overline{uv} transport equation in (x,y) coordinates change from the simple-shear contribution $\overline{v^2}\partial U/\partial y$ to $\overline{v^2}\partial U/\partial y + \overline{u^2}\partial V/\partial x$: the exact change depends on the coordinate axes used and it is simplest to keep to (x,y) axes for this discussion. Results for other extra strain rates are similar: in general the total generation terms are greater than the simple-shear terms by a factor

$$f = 1 + a \frac{e}{\partial U/\partial y} \quad (31)$$

where a is numerically of order 1, its sign being immaterial at this stage. (The expression "of order x " means "between about $x/\sqrt{10}$ and $x\sqrt{10}$ ".) Since none of the other terms in the exact transport equation explicitly contains the rate of strain, only the generation terms change their algebraic form. It follows that the change in Reynolds stress following the prolonged application of an extra rate of strain, as predicted by any of the empirical turbulence models discussed in Section 2.5, will again be a factor like f with roughly the same value of a . For instance, Eq(2) shows that a simple eddy viscosity formula applied to a curved shear layer predicts an increase in shear stress by a factor f with $a = 1$ exactly.

In fact, as mentioned in Section 1, the Reynolds stresses are observed to change, after prolonged application of a small extra rate of strain, by a factor much larger than f . The change is what would be predicted by a typical turbulence model if the generation terms had changed, not by a factor f but by a factor

$$F = 1 + \alpha \frac{e}{\partial U/\partial y} \quad (32)$$

where α varies from case to case but is always of the order of \underline{ten} . The factor F can be regarded either as an empirical extension of f or as a simple, linear, dimensionally-correct correlating factor which defines an empirical coefficient α . The rate-of-strain ratio $e/(\partial U/\partial y)$ is a general case of the curved-flow analogue of the Richardson number (Section 5): strictly, $\partial U/\partial y$ represents the reciprocal of a typical time scale of the turbulence and it is sometimes better to use the latter explicitly in regions

*For the qualitative part of the present discussion we ignore the separate contributions of deformation and rotation and refer to any departure from simple shear (even a pure rotation!) as an "extra rate of strain" for compactness of terminology.

which are far from local equilibrium, especially regions where $\partial U/\partial y \rightarrow 0$. α is positive for the signs of e chosen in the first paragraph of this section: usually α has the same sign as a but even this is not always the case.

Now of course the generation terms change only by a factor f , not F : the reason why the Reynolds stresses change so much is that the extra strain rate has a large direct effect on terms in the exact Reynolds-stress transport equations which do not explicitly contain the mean rate of strain. By a "direct effect" we mean that the changes are not simply those that result, according to conventional turbulence models, from changes in Reynolds stress: they are changes in the higher-order structural parameters, which cause the Reynolds stress to change*. We therefore need to insert empirical factors of the order of F in conventional turbulence models before they can predict the large effects of even small extra rates of strain. That is, F -factors are required in calculation methods developed for thin shear layers even if $e/(\partial U/\partial y)$ is still small enough for the thin-shear-layer approximation to be valid — see the table on p.4. This conclusion seems to be valid for all turbulence models from the simplest local-equilibrium formulae for eddy viscosity and mixing length up to the most advanced transport-equation methods. In the case of transport-equation models, we must expect changes of order F both in the destruction (and redistribution) terms and in the turbulent transport terms, in addition of course to the changes of order f in the generation terms. However a fair first approximation is to apply the correction for the effect of extra rate of strain to the destruction terms alone. This amounts to making the local-equilibrium approximation (Section 2.4) solely for the purpose of analysing the effects of extra strain rate, and should be acceptable if the basic flow is not too far from local equilibrium and if the effects of the extra strain rate are themselves not too large. It has the advantage of applicability to local-equilibrium methods as well as transport equations. However large extra rates of strain are likely to lead to gross modification of the large-eddy structure, which is responsible for most of the turbulent transport, and, particularly in "unstable" flows, it may be essential to use a transport-equation method, with empirical modifications to the transport terms, to represent this effect.

Body forces, like extra strain rates, can produce unexpectedly large changes in Reynolds stresses. The consequence of uniform rotation of a complete flow system at angular velocity Ω [Fig.1(e)] can be regarded either as an extra mean rate of strain, equal to the component of Ω normal to the plane of the shear, the (x,y) plane say, or as a mean Coriolis body force $2\Omega \times U$ whose relevant component is in the y direction and therefore again depends on the component of Ω normal to the plane of the shear. The effects of buoyancy forces on turbulence in a gravitational field are well known: we shall draw an approximate analogy between the effects of buoyancy forces and the effects of "centrifugal force" in a curved shear layer, where the consequence of curvature can again be regarded either as an extra mean rate of strain or — at least for semi-quantitative purposes — as a body force. There is no evidence at present about the effect of the $J \times B$ force in magnetohydrodynamic turbulence: the situation is obscured by the use of the word "turbulence" as a derogatory term for all types of plasma instabilities. For an Orr-Sommerfeld analysis showing that in certain special cases of inviscid MHD flow the stability is governed by the analogue of a Richardson number and that the Richardson number analogues for MHD body force and for curvature are additive, see Howard and Gupta (39). We shall see in Section 5 that this is a general property of Richardson number analogues derived from displaced-element analyses or from Reynolds-stress transport equations.

There is unlikely to be a common explanation for the surprisingly large effects of extra strain rates and body forces, although in addition to the buoyancy/curvature analogy, whose application to turbulence is due to Prandtl, we can draw an analogy between lateral divergence and bulk compression. If the effects of extra strain rate were always to decrease the Reynolds shear stress we could plausibly argue that a simple shear is bound to be the most efficient means of producing shear stress, but Figs 3 and 4 show that extra strain rates can produce large increases in shear stress and other turbulent transfer rates. The qualitative effects of body forces can be "explained" by the displaced-element arguments of Section 1, but if displaced-element or mixing-length arguments are taken far enough to deduce quantitative correction factors for body forces or extra strain rates these factors are invariably of the order of f and not F . Lateral divergence or bulk compression reduce the cross sections of fluid elements in the (x,y) plane and thus increase their z -component vorticity: again the factor predicted is of order f , not F , although z -component vorticity fluctuations play an important part in large-eddy dynamics and small changes may produce large effects. It seems wisest to admit that we do not yet know enough about turbulence to explain away an unexpected coefficient of order 10 in any of the cases mentioned, let alone produce a unified explanation. However, the phenomena are unified on the empirical level by the unexpected coefficient of order 10 itself, leading to the need to insert extra factors like F in our turbulence models, and in our present state of ignorance this justifies a common discussion and a common empirical treatment. In the study of non-Newtonian fluids, where analogous effects occur, it is common to correlate the response of the fluid in terms of the ratio of one component of the viscosity or elasticity tensor to another: for instance the ratio of the extensional viscosity to the shear viscosity μ is called the Trouton ratio, which may or may not be a property of the fluid in the thermodynamic sense. Similarly, "eddy viscosity anisotropy factors" have sometimes been used in turbulent flow. They are certainly not properties of the fluid and we do not use the concept here: the F -factor analysis is related, but more flexible.

The discussion below will be restricted mainly to the effects of small extra rates of strain on thin shear layers. We will arbitrarily define a rate of strain e as being "small" if $e/(\partial U/\partial y)$ is numerically less than 0.05 so that, if $\alpha = 10$, F is between 0.5 and 1.5 which are likely to be the largest departures from unity at which a linear correction factor like F can be trusted. We will call the explicit changes introduced into the equations of motion by extra strain rates the " f -factor effects" and the much larger direct effects of extra strain rate on turbulence structure the " F -factor effects", and note that in many previous discussions only the relatively small " f -factor effects" have been considered. The effects of a large extra rate of strain depend very much on the axes of the rate of strain and do not

*In some turbulence models, the mean rate of strain appears in the empirical version of the pressure-strain "redistribution" terms (see Section 5.2 of Ref.25): however the effect of applying an extra rate of strain is to multiply these terms by a factor like f , not F .

throw much light on other cases: we discuss the effects of large streamline curvature in later Sections. We do not discuss the traditional shear-layer problem of response to changes in $\partial U/\partial y$, nor the response of initially isotropic turbulence to any rate of strain, because these are described fairly well by existing models (40, 41): since the response is of the same order as the change in the generation terms, we can call these "little-f problems" as distinct from the "big-F problem" of response to extra strain rates. We note that the unsymmetrical response of a simple shear layer to changes in the two elements of the rate of shear strain $\partial U/\partial y + \partial V/\partial x$ implies that experiments (42-44) on the (symmetrical) response of isotropic turbulence to an irrotational plane strain may not be as relevant to shear layers as is normally assumed: in an irrotational plane strain the mean vorticity is zero by definition, while in a simple shear layer the rate of plane strain $\partial U/\partial y + \partial V/\partial x$ and the vorticity $\partial V/\partial x - \partial U/\partial y$ are numerically equal, and small departures from equality [small values of $(\partial V/\partial x)/(\partial U/\partial y)$] have large effects.

For a simplified discussion of the behaviour of the Reynolds-stress transport equations in a shear layer subjected to a small extra rate of strain we will use the local-equilibrium approximation to the turbulent energy equation, as in Section 2.4. The local-equilibrium approximation to any other transport equation merely defines another length scale and it is at present customary to assume that all such length scales are proportional. However it may become necessary to consider more than one independent length scale in flows subjected to large extra rates of strain. Combining Eq(27) and Eq(31) we have

$$\text{production} = -\overline{uv} \frac{\partial U}{\partial y} \left(1 + \alpha \frac{e}{\partial U/\partial y} \right) \equiv -\overline{uv} \frac{\partial U}{\partial y} f = \text{dissipation} \equiv \frac{(-\overline{uv})^{3/2}}{L} \quad (33)$$

In a typical turbulence model for a simple shear layer the dissipation length parameter L is given by an equation or formula which at most contains a factor f : denote this value of L by L_0 . Then observations of the effects of extra strain rate imply

$$-\overline{uv} \frac{\partial U}{\partial y} F = \frac{(-\overline{uv})^{3/2}}{L_0} \quad (34)$$

— that is, "the change is what would be predicted by a typical turbulence model if the generation terms had changed not by a factor f but by a factor F ". Simultaneous validity of the exact equation, Eq(33), and the empirical observation Eq(34) requires

$$\frac{L}{L_0} = \frac{F}{f} \quad (35)$$

Since the coefficient α in F is empirical and an order of magnitude larger than the coefficient α in f , we can absorb f into F and represent the effect of extra rates of strain on the turbulence structure by

$$\frac{L}{L_0} \approx F = 1 + \alpha \frac{e}{\partial U/\partial y} \quad (36)$$

where L_0 is the value of L at the same point in the corresponding simple shear layer. In cases of small extra rate of strain the thin-shear-layer approximation itself requires us to ignore the factor f . Formally, Eq(36) defines a dimensionless quantity α : it is a useful definition only if α varies less, or is easier to correlate empirically, than L itself.

Having chosen to apply the F -factor to the dissipation length parameter or other eddy length scale rather than the mixing length ℓ , we need no longer make the local-equilibrium approximation: we can apply the F -factor to L_0 or any other length scale appearing in a transport-equation calculation method. Nominally we correct only the destruction/redistribution terms, although in some calculation methods the length scale also appears in the modelling of the turbulent transport terms so that correcting the length scale also changes the transport terms (probably in the right direction!). In order to find the F -factor in the first place we must either measure the terms in the transport equations in flows subjected to extra rates of strain or, more feasibly, adjust the coefficient α in the F -factor by trial and error, to optimise agreement between experiment and predictions by a calculation method whose unmodified version gives good results in simple shear layers. Examples of this procedure are given in the later parts of this Section and in Appendix 2: in later sections we shall refer to it as "numerical experiment". Note that using the procedure in this way simply gives the F -factor in the case considered: there is not necessarily any implication that the same calculation method with the same F -factor will give good results in other cases.

We cannot expect α to be an absolute constant.

- (i) F will in general vary linearly with e only for very small rates of strain.
- (ii) The response of the shear layer is bound to depend on the axes of the extra rate of strain.
- (iii) The response to an extra rate of strain, like the response to the simple shear $\partial U/\partial y$, will depend on the history of the rate of strain.

In fact a linear correction factor applied to the eddy length scale is sufficient to correlate most of the rather small amount of accurate experimental information on extra strain rates, except that the analogy between buoyancy and curvature may be precise enough to authorize the use of non-linear factors developed by meteorologists. Furthermore, the data for prolonged extra rates of strain can be correlated almost to within their likely accuracy by a universal value of α of exactly 10: we review the data for each type of extra strain rate — other than curvature — in Sections 3.2 to 3.4. However even the available data clearly show that if e changes suddenly from zero to a constant value the value of α required to optimise agreement with experiment rises rather slowly to its asymptotic value of order 10. Sudden changes in e (i.e. in surface curvature, pressure gradient or sidewall angle) are likely to be frequent in engineering situations and a full discussion of this lag effect is warranted. We note that there is no analogous effect in the response to the primary rate of strain $\partial U/\partial y$ because there is no F -factor effect in the first place: "history" effects in simple shear layers are tolerably well predicted by existing calculation methods.

Now of the terms in the exact Reynolds-stress transport equations only the generation terms and the

terms involving the pressure fluctuation p' can change immediately the mean rate of strain changes (the pressure fluctuation can change because the mean rate of strain appears in the Poisson equation for p'). However, we have seen that the change in the generation terms is only of order f . It has been rigorously proved for initially isotropic turbulence (41) that the initial change in the pressure fluctuation "redistribution" terms is smaller than, and opposes, the change in the generation terms. It seems highly unlikely that the extra redistribution terms in a shear layer subjected to an extra rate of strain will initially augment, and be much larger than, the extra generation terms, so as immediately to produce the full value of α . Therefore even the shear stress, whose "destruction" term is in fact a pressure "redistribution" term, will not immediately experience the full value of α : the turbulent energy equation used in the discussion above has no pressure "redistribution" terms and the energy dissipation rate is highly unlikely to change immediately the mean rate of strain changes. Therefore, the effect of a suddenly-applied extra strain rate will be a small, sudden increase (say) in the generation terms, probably opposed by the "redistribution" terms and followed by an initially linear, but large, decrease in the "destruction" terms (including the redistribution terms), as shown in Fig.10. In the context of a calculation method in which the destruction terms are modelled as (velocity scale)³/(length scale) this implies an initially linear, but large, increase in length scale: this is the behaviour that results if the length scale itself is obtained from a transport equation with the full F-factor (with α of the order of 10) applied to the destruction terms of that equation. It therefore appears that in order to deal with rapid changes in e some form of transport equation for length scale is essential, perhaps even if the basic calculation method for simple shear layers invokes local equilibrium throughout. Figure 11 shows calculations for a case of sudden change of e : the three curves represent the basic method with no allowance for e , the method with a full F-factor applied, and the method with a simplified length-scale equation, and each improvement is significant.

I do not know of any application of an F-factor to an existing length-scale transport equation. The demonstration calculation of Fig.11 and the further calculations to be described below were done with an empirical ordinary differential equation for the effective value of α , which could be inserted in any type of calculation method. Since some sort of length-scale equation seems to be necessary to deal with rapidly-changing extra strain rates and no alternative has been suggested, a short description of this simple equation will be given. The equation is

$$X \frac{d}{dx} (\alpha e)_{\text{eff}} = \alpha_0 e - (\alpha e)_{\text{eff}} \quad (37)$$

where the length X is a "time constant" representing the memory of the stress-containing eddies, $(\alpha e)_{\text{eff}}$ is the effective value of αe for insertion into the F-factor and α_0 is the full value of α (of order 10). The equation can be solved for $(\alpha e)_{\text{eff}}$ for a given streamwise distribution of e : if e rises suddenly from zero to some constant value, $(\alpha e)_{\text{eff}}$ rises proportional to $1 - \exp(-x/X)$. Now the obvious objection that e is in general a function of y can be dealt with in the cases of curvature, lateral divergence and bulk compression, where $e \propto U$, simply by writing Eq(37) in terms of e/U . A further objection, that X will in general be a function of y , is not so serious as might be supposed: X varies strongly only in the inner layer, and if e is small enough for the F-factor analysis to be plausible in the outer layer $e/(\partial U/\partial y)$ is very small in the inner layer, so that we need not use an accurate value of X in the inner layer; it is simplest to use the outer-layer value but zero is a better estimate. A suitable estimate of the memory time of the stress-containing eddies is the ratio of the turbulent energy $\frac{1}{2}q^2$ to the rate of production of turbulent energy (if the production were suddenly shut off the turbulent energy would initially decay exponentially with this time constant). The length X can be taken as U times this memory time, namely

$$X = \frac{\frac{1}{2} q^2 U}{-\bar{u}v \partial U/\partial y} \quad (38)$$

where we include only the mean-shear production rate for simplicity. In a boundary layer $\frac{1}{2}q^2$ is about $3\bar{u}v$ and a typical average value of $U/(\partial U/\partial y)$ in the outer layer ($y > 0.2\delta$ say) is 36, giving

$$X \approx 10\delta \quad (39)$$

In a jet or free mixing layer $U/(\partial U/\partial y)$ is rather less than δ so

$$X \approx 2\delta \quad (40)$$

is a reasonable value to take: in a wake, $U/(\partial U/\partial y)$ can be many times δ . However the local-equilibrium ideas implicit in this derivation of X are not good in free shear layers: Castro's attempt (11) to apply an equation like Eq (37) to his strongly-curved shear layer was not successful, although this was partly the result of the unique reversal of curvature effects in this experiment.

An obvious property of the linear, first-order equation Eq(37) is that if the distance in the x direction over which e is non-zero is much smaller than X , the value of $(\alpha e)_{\text{eff}}$ at the end of the region of extra strain rate is

$$(\alpha e)_{\text{eff}} = \frac{\alpha_0}{X} \int e dx \quad (41)$$

independent of the distribution of e . $\int e dx$ is closely related to the total extra strain on a fluid element, $\int e dt$, where the latter integral is evaluated following the motion of the fluid and is therefore near to $\int Ue dx$. If Eq(37) is at all realistic it implies that the response to a short region of extra strain rate (a "strain impulse") depends more on the total strain than the distribution of strain rate, and gives us some confidence in using the F-factor analysis, with Eq(37), in short regions of large strain rate such as sharp bends or Prandtl-Meyer expansions. Clearly $(\alpha e)_{\text{eff}}/(\partial U/\partial y)$ must not exceed the maximum value permissible after a long region of small extra strain rate, which we arbitrarily took as 0.05 to give $0.5 < F < 1.5$.

Figure 12 shows, qualitatively, the response to extra strain rate predicted by the F-factor, Eq(36) and the "lag equation", Eq(37). Eq(37) is not suggested as a permanent substitute for incorporation of extra-strain effects in a true transport equation for length scale, but merely as a vehicle for the present

sparse data. Discussion of possible refinements to a length-scale transport equation, by inclusion of an F-factor or otherwise, merely exposes our ignorance: are only the destruction terms affected or are the (rather large) turbulent transport terms altered enough to cause a significant change in the distribution of length scale across the shear layer as well as in its magnitude? Do the destruction terms in the length-scale equation change to the full extent of the F-factor as soon as the extra strain rate is applied or (more probably) do we need a wholly-empirical lag equation to modify the F-factor?

In the inner layer of a simple shear layer — but outside the viscous sublayer — we have $L_0 = Ky$ where $K \approx 0.41$. Since the response time is short we do not need the "lag equation" for α and can apply the full F-factor directly to Eq(36): we get

$$\frac{\partial U}{\partial y} + \alpha e = \frac{(-\overline{uv})^{1/2}}{Ky} \quad (42)$$

which can be integrated to give U if the variation of \overline{uv} and e with y is known. In the simplest case of a constant-stress layer with $-\overline{uv} = u_\tau^2$, and with e independent of y, we get

$$\frac{U}{u_\tau} = \frac{1}{K} \log \frac{u_\tau y}{\nu} + C - \alpha \frac{ey}{u_\tau} \quad (43)$$

which is the familiar logarithmic law with one extra term: in principle, the constant of integration C, representing the change in velocity across the viscous sublayer, is a function of the dimensionless quantity $\alpha e \nu / u_\tau^2$, but it seems likely that the F-factor analysis will break down before e is so large as to change C significantly. In cases where e is proportional to U, taking $e = -U/R$ without necessarily defining R as the radius of curvature, we get

$$\frac{U}{u_\tau} = \frac{1}{K\alpha} \left[C_1 \left(\frac{y}{R} \right)^\alpha - 1 \right] \quad (44)$$

and compatibility with the logarithmic law for small α (equivalent to large R since $\alpha U/R$ appears as one group) requires

$$C_1 = 1 + K\alpha \left[\frac{1}{K} \log \frac{u_\tau R}{\nu} + C \right] + f \left(\alpha, \frac{u_\tau R}{\nu} \right) \quad (45)$$

where the last term again represents the effect of e on the viscous sublayer. In simple cases it is probably sufficient to use a rough representation of U as a function of y in the term αe in Eq(42), and integrate directly: if we take $e = -U/R$ with U proportional to $y^{1/5}$, say, the extra term in Eq(43) changes to $+5\alpha U y / (6u_\tau R)$ which can be grouped with U/u_τ on the left hand side.

The demonstration calculations in the following Sections were done using the calculation method of Bradshaw et al. (16: see Ref.45 for the free-shear-layer version). In this method a transport equation for shear stress — $\rho \overline{uv}$ is used, the destruction term being proportional to $(-\overline{uv})^{3/2}/L$: in a simple shear layer, L is defined by an algebraic function, $L_0(y/\delta)$. In flows with extra rates of strain we use Eqs (36) and (37) to modify L, leaving the modelling of the turbulent transport terms unaltered. The solution of the partial differential equations for U and $-\overline{uv}$ is matched to Eq(43), using the approximation to U in the e term mentioned above. This calculation method was used solely for convenience: exactly the same technique could be used with any other field method involving a length scale, whether it is a structure parameter like L, a mixing length or a factor in an eddy viscosity. Green, Weeks and Brooman (46) have used F-factors in an integral method, albeit not a typical one because it depends on the solution, at one value of y only, of the shear-stress transport equation of Ref.16. Practical details of allowances for extra rates of strain will be discussed in Section 11.

We now discuss the different cases of extra rates of strain, omitting the case of curvature which is treated in detail in later sections. In cases for which detailed calculations are not available the behaviour of F will be inferred from published measurements of eddy viscosity or entrainment rate, using sample calculations by the method of Ref(16) to relate changes in L to changes in eddy viscosity or entrainment rate: the assumption that entrainment rate is proportional to maximum shear stress is built into the calculation method. We do not assume that a given percentage change in eddy viscosity implies half that percentage change in mixing length: this is true only if the velocity profile remains unchanged.

3.2 LATERAL CONVERGENCE OR DIVERGENCE ($e = \partial W / \partial z$)

Keffer (47, 48) studied the response of a cylindrical wake to lateral divergence (extension) and convergence (compression): he found that lateral divergence greatly changed the turbulence structure, accentuating the large eddies and suppressing the smaller-scale motion. He compared the mechanism to the lateral stretching of line vortices with axes in the z direction, and presented photographs showing the strong circulation of the large-eddy motions in the x,y plane. The lateral velocity fluctuations were reduced and after the wake span had been increased by a factor of 4 it was found that $\overline{w^2}$ was less than a third of $\overline{v^2}$. The net rate of production of turbulent energy by the lateral rate of strain, $(\overline{v^2} - \overline{w^2}) \partial W / \partial z$, was about as large as the shear production $-\overline{uv} \partial U / \partial y$, so that this is a very strongly-diverging flow indeed by boundary layer standards. In the case of an equally strong lateral convergence the processes of normal wake growth and geometrical distortion appeared to be additive, but no turbulence measurements were made: the mean velocity profile developed large regions of near-constant velocity near the centre line, implying near-zero shear production of turbulent energy, which one would expect to lead to significant changes in turbulence structure.

Crabbe (49) performed an experiment on the boundary layer on the floor of a duct arranged to give $U_e = \text{constant}$, $\partial W_e / \partial z = \text{constant} \approx 0.02 U_e / \delta$. He found that the entrainment rate on the centre line was increased by about $0.5(\delta - \delta^*) \partial W / \partial z$, the entrainment rate in a two-dimensional flow at the same Re_θ being about $0.010 U_e$. If we take $\delta - \delta^* = 6\delta/7$, and $\partial U / \partial y = 0.3 U_e / \delta$ as a typical value in the outer part of the boundary layer, we see that divergence increases the entrainment by a factor of about $1 + 13 (\partial W / \partial z) / (\partial U / \partial y)$ so that the typical shear stress within the layer increases by about the same

factor. This implies Eq(36) with $\alpha \approx 6.5$. Crabbe shows that the increased entrainment rate is quite well predicted by assuming that the turbulence structure depends on the effective total strain in the plane of the mean shear, following Townsend's (50) discussion of two-dimensional flows: of course positive $\partial W/\partial z$ means negative $\partial V/\partial y$ but the structural changes observed by Keffer seem attributable to $\partial W/\partial z$ directly rather than to alterations in the shear strain rate. Crabbe states that the change of entrainment rate in the attachment line boundary layer on a swept-back wing is between 1.0 and 1.2 times that in the diverging duct flow. Note that both types of boundary layer have zero crossflow but that the flow a short distance from the plane of symmetry has a crossflow angle that varies through the layer: these are not collateral flows.

Cham and Head (51) used Head's entrainment method to calculate the vortex diffuser flow of Gardow (52): the entrainment rate required for agreement with experiment was about twice that in a two-dimensional flow with the same profile shape. Attributing the increase entirely to divergence and not to crossflow, and carrying out an approximate analysis like that for Crabbe's flow, we find $\alpha \approx 10$. Head and Patel (53) later allowed for the effect of convergence or divergence on the entrainment in nominally two-dimensional flows and reported very much better agreement. Strictly, the allowance is for perturbations in growth rate, whether caused by convergence/divergence or by longitudinal acceleration. As a correction for convergence/divergence it can be seen to imply $\alpha \approx 10$ for a boundary layer in zero pressure gradient and $\alpha \approx 5$ for a strongly-retarded self-preserving boundary layer (using plausible values for $\partial U/\partial y$ in each case).

Winter, Rotta and Smith (54) studied the collaterally-diverging turbulent boundary layer on a slender waisted body in subsonic and supersonic flow: recent calculations by Green, Weeks and Brooman (46), using the lag-entrainment method but without further allowance for the lag in the F-factor, show that agreement with experiment in subsonic flow is greatly improved by an F-factor allowance for lateral divergence with $\alpha = 7$ (longitudinal curvature also has some effect). It is noteworthy that the F-factor produced improved agreement with experiment over the converging part of the body as well as the diverging part, contradicting Keffer's provisional and dubious conclusion drawn from the strongly-converging wake.

Patel, Nakayama and Damian (55) have recently studied the boundary layer over the rear of a body of revolution with a maximum diameter of one-sixth of its length and an included angle of about 46 deg. at the trailing edge. In this converging flow the shear stress falls very rapidly towards the trailing edge, and the mixing length ℓ increases much more slowly than δ : because of the uncertainty about the effects of the convex streamline curvature and of large ratios of boundary layer thickness to cross-sectional radius of curvature a reliable value of α in the F-factor cannot be inferred but the results can be taken as further evidence that convergence and divergence produce effects of the same order.

Young (57) is studying a slightly simplified body of revolution consisting of a cylinder ahead of a cone: the fairing between the two has a small radius of curvature and therefore provides a curvature "impulse" whereas the subsequent divergence is prolonged with an equivalent value of $\partial W/\partial z$ of at least $0.05 U_e/\delta$. Making the best possible allowance for curvature effects a significant residual effect of divergence is found: a value of α of about 10 is indicated.

McMillan and Johnston (56) present measurements in a laterally-diverging duct, with a virtual origin 55 duct heights upstream of the start of the divergence. Taking a typical value of $\partial U/\partial y$ as $0.3U/(\frac{1}{2}h)$ the maximum value of $(\partial W/\partial z)/(\partial U/\partial y)$ is about 0.03: calculations by an extension (3) of the method of Ref(16) without any allowance for divergence showed no consistent disagreement with experiment.

As shown by several experimenters, a radial wall jet grows at about the same rate as a plane wall jet. This implies that its entrainment rate — and therefore a typical value of shear stress — is double that of the plane flow. $(\partial W/\partial z)/(\partial U/\partial y)$ is typically about 0.1 which leads to a nominal value of α of about 5. Heskestad's results (58, 59) for a free radial jet and a free plane jet again indicate equal growth rates which again leads nominally to $\alpha = 5$. However, the energy production in the high-intensity regions of a jet is about twice the dissipation so that if the turbulent transport terms are altered by divergence a value of α is difficult to evaluate: certainly 5 is a minimum estimate. Heskestad measured the shear stress in both flows but, especially for the radial jet, the values are much lower than those calculated from the mean-motion equations; the calculated maximum shear stress in the radial jet is about 1.7 times as large as in the plane jet which would imply $\alpha = 3.5$, but Heskestad pointed out that the radial jet was not fully developed although full development was assumed in the shear stress calculations. Heskestad's measurements of turbulence intensity show comparatively little difference between the two flows (similar techniques were used in the two cases) but it is difficult to reconcile these results with the above deductions from mean-flow measurements: Heskestad felt that a better experimental arrangement was needed for the radial flow but unfortunately neither he nor any other worker seems to have produced any further data for this simple example of a diverging flow. It appears that values of α deduced indirectly from entrainment or growth rates in diverging flows are at least 5; direct use of α in Eq(36) suggests $\alpha = 7$, and other experience suggests that if the lag in α were allowed for the asymptotic value would be close to 10.

3.3 LONGITUDINAL ACCELERATION ($e = \partial U/\partial x$ or $-\partial V/\partial y$)

The continuity equation requires finite values of $\partial U/\partial x$ to be associated with finite values of $\partial W/\partial z$ or $\partial V/\partial y$: here we consider only the latter case, that of two-dimensional flow. Townsend (Ref.26, p.188) explained differences between jet and wake flows in terms of the negative values of $\partial V/\partial y$ found in the former, which, he suggested, would tend to flatten the large eddies and reduce their contribution to the Reynolds stress. It is implied by Townsend's discussion that positive $\partial V/\partial y$ — found in retarded flows and significant in boundary layers near separation — should tend to increase the Reynolds stress, but Gartshore (60) has suggested that either sign of $\partial V/\partial y$ disturbs the large eddies from their preferred orientation and thus reduces the Reynolds stress. Gartshore's analysis is not rigorous, and his suggestion is certainly not valid for other types of extra strain rate, but it is supported by his experiments in retarded self-preserving wakes ($\partial V/\partial y > 0$) whose eddy viscosity, made dimensionless by the velocity deficit and the wake width, is significantly less than in a wake in a uniform stream. Gartshore correlated

the reciprocal of the eddy viscosity with — logically enough — the square of $(\partial V/\partial y)/(\partial U/\partial y)$ but the results he presents are fitted quite well by

$$\frac{v_T}{v_{T0}} = 1 - 8.5 \left| \frac{\partial V/\partial y}{\partial U/\partial y} \right| \quad (46)$$

implying $|\alpha| \approx 4$. Morel's (45, 61) correlation of the differences in the optimum dissipation length parameter required to calculate jets and wakes implies $|\alpha| = 3.5$ (for $\partial V/\partial y < 0$). Neither author has really proved that the effects observed are directly attributable to $\partial V/\partial y$: in Gartshore's case no account is taken of changes in advection in the retarded flows, and Morel's calculations were intended as a test of the superposition principle in interacting free shear layers. Morel's correlation of changes in optimum dissipation length parameter in mixing layers of differing stream velocity ratios (and therefore differing rates of growth) indicates a much smaller value of α than the jet-wake correlation, although in this case Morel made significant changes in the other terms in his empirical Reynolds-stress transport equation and a direct comparison with our standard F-factor is dubious. Gartshore himself points out that boundary layers appear to be little affected by longitudinal acceleration, even for a rate of strain ratio as large as 0.05.

Reverse transition in strongly-accelerated boundary layers is unlikely to have any necessary connection with the results discussed above: obviously the ratio of root-mean-square intensity to mean velocity will decrease in any strongly-accelerated flow, except near a solid surface where $\partial U/\partial y$ is necessarily very large, and "reverse transition" is deemed to have started when the shear-stress gradient near the surface becomes so large that inner-layer similarity relations begin to break down.

Strongly-retarded wall layers separate, and even retarded wakes can develop a region of reversed flow: these gross effects are likely to mask any direct effects of the retardation on the turbulence, particularly since a rapid increase in $\partial V/\partial y$ implies large $\partial V/\partial x$ — i.e. large streamline curvature.

We must regard the influence of $\partial U/\partial x$ or $\partial V/\partial y$ on turbulent shear layers in general as not proven although physical reasoning strongly suggests that it is mainly responsible for the differences between jets and wakes. The "direct" deductions of α for the latter case suggest $\alpha \approx 4$.

3.4 COMPRESSION OR DILATATION ($e = -\text{div } \underline{U}$)

I mention this effect with some diffidence because it was discovered (a) very recently (b) by me. Nevertheless it seems very important in practice at Mach numbers above the transonic range, and grossly affects the behaviour of boundary layers at quite moderate values of the pressure-gradient parameter $(\delta^*/\tau_w) dp/dx$. For example, in three recent experiments on boundary layers decelerating from $M_e = 4$ the skin friction coefficient, far from decreasing sharply as expected in low-speed flow, actually rose above the value found in constant-pressure flow at the same Mach number and Reynolds number. Now the principle that justifies the extension of low-speed calculation methods to compressible flow is Morkovin's hypothesis that turbulence is unaffected by random fluctuations in pressure or density as long as they are small compared to the mean pressure or density, a condition satisfied at all non-hypersonic speeds. The Reynolds stress transport equations for compressible flow, like those for incompressible flow, do not contain the mean pressure gradient: some of the equations contain components of the mean dilatation, expressing the interaction of Reynolds stresses with normal rates of strain, but as the boundary layer approximation requires $\text{div } \underline{U}$ to be small compared to $\partial U/\partial y$ these terms would normally be neglected.

Until recently the only reliable experiments on strong but distributed pressure gradients (as opposed to flow through shocks, which most people would expect to produce strong effects on turbulence) had been done using curved surfaces to produce the pressure gradient. Many experiments done in the 1960s were therefore unusable as test cases for plane-flow calculation methods, or contained a built-in excuse for the manifest disagreements that existed between calculation and experiment. The good predictions of constant-pressure supersonic flows by extensions of low-speed methods, and the general assurance offered by Morkovin's hypothesis, led most people, including the present writer, to be cautiously optimistic about the performance of these methods in pressure gradients uncomplicated by the effects of curvature: the one clear case of disagreement available at the time of writing of Ref.62 was the experiment of Zwarts (63) on a boundary layer decelerating from $M_e = 4$ to $M_e = 3$, in which the measured skin friction coefficient was markedly higher than predicted. However, Zwarts' flow suffered from fairly severe three-dimensional effects, possibly including secondary flows which could have produced anomalous results. Bushnell and Alston (64) later summarized possible reasons for disagreement between theory and experiment, tentatively concluding that curvature might not be wholly responsible.

In 1971 Peake et al. (65) carried out experiments on a boundary layer decelerating from $M_e = 4$ to $M_e = 2$, with results similar to those found by Zwarts. In this case three-dimensional effects were small but the results appeared to have suffered considerably from probe interference so that they were again not above suspicion. However a set of experiments by Lewis et al. (66), on a boundary layer decelerating from $M_e = 4$ to $M_e = 2.5$ and then accelerating again to $M_e = 3.5$, appeared to be above reproach, and for a third time showed a much larger c_f in adverse pressure gradient than would have been expected from experience in low-speed flow (Fig.11).

The most probable explanation is that dilatation or compression, like other extra rates of strain, produce a large direct effect on the turbulence, with compression increasing, and dilatation decreasing, the Reynolds stress. Insertion of an F-factor with $\alpha = 10$, and $e = -\text{div } \underline{U} (U/\gamma p)(dp/dx)$ in the method of Ref(62) gave improved agreement with the above-mentioned experiments: when a lag equation for α , with a "time constant" of 10δ , was used in the calculations, excellent agreement was obtained in all three retarded flows (67). The friction coefficient in the mildly accelerating flow of Pasiuk et al. (68) seems unnaturally low, and an empirical factor in the calculation method of Wilcox and Alber (69) (which with hindsight can be seen to be an unwitting allowance for dilatation) was chosen to have the same value in accelerating and retarded flow, although the accelerating flow on which they relied most was a highly-curved flow through a Prandtl-Meyer expansion. It is therefore probable that the optimum α is of the same order in retarded and accelerated flow.

After the F factor had been shown to improve agreement between calculation and experiment, Dr. J.E. Green of RAE Bedford realised that the most plausible physical mechanism of the dilatation effect is closely analogous to the effects of lateral divergence or convergence. Both positive $\partial W/\partial z$ and negative $\text{div } \underline{U}$ reduce the cross-sectional area of a fluid element in the (x,y) plane (note that in an accelerating supersonic flow $\partial V/\partial y$ is larger than $\partial U/\partial x$ by a factor M^2) and thus increase the z-component vorticity: the z-component vorticity fluctuations in the larger eddies seem to play an important part in the entrainment process, and so it is plausible that enhancing them should increase the entrainment rate and the turbulence intensity, as in Keffer's diverging wake.

Green has incorporated the F-factor into his own lag-entrainment method (46) and, using $\alpha = 7$ without allowance for lag in α , found improved agreement with the above-mentioned test cases and with the waisted-body experiment of Winter et al. (54): at $M \approx 2$ the effects of dilatation and of lateral divergence on the waisted body are opposite, but so large that their resultant is quite significant. Ignoring the lag effect reduces the value of α required to optimise agreement.

There is practically no direct evidence about the behaviour of turbulence in flows with dilatation or compression, but there seems little doubt that this is yet another example of the large effect of small extra rates of strain. It seems probable that dilatation effects are very important in hypersonic flow and in at least some cases of combustion, internal or external. The best guess for α is 10.

4. INTRODUCTORY HISTORY OF RESEARCH ON CURVED TURBULENT FLOWS

This Section is intended to introduce the phenomena of curved flows rather than to allot credit for advances in understanding them. It covers the period up to the revival of serious work on the subject in the mid-1960s: the more recent work and the present state of knowledge are discussed in Sections 6-11.

Studies of the effect of streamline curvature on stability of laminar flow up to about 1962 are reviewed by Stuart (23, Chapter 9); for more recent work see Ref.70. In 1916 Rayleigh (14) proved by energy considerations that a steady inviscid, axisymmetric curved flow is unstable to infinitesimal axisymmetric disturbances if the angular momentum decreases with increasing distance from the centre of curvature, and vice versa. Use of this or Von Karman's alternative argument (Section 1) for any purpose other than the determination of the stability boundary for this inviscid flow requires careful consideration of the mode of disturbance and of the restoring forces set up by viscous or Reynolds stresses. As Coles (71) comments, it "throws only a very dim light" on the behaviour of real fluids. In 1923 Taylor (72) carried out a theoretical analysis of, and an experiment on, the stability of circumferential laminar flow between two coaxial rotating cylinders. The analysis showed that the equations governing the growth of small axisymmetric disturbances contained a parameter since called the Taylor number. For the simplest case, in which a cylinder of radius R rotates with angular velocity Ω within a fixed cylinder of radius $R + h$ with $h \ll R$, the Taylor number can be written as

$$Ta \equiv \frac{(\Omega R)^2 h^3}{R \nu^2} \equiv \frac{h}{R} \left(\frac{h\Omega R}{\nu} \right)^2 \quad (47)$$

where $(\Omega R)^2/R$ is a typical "centrifugal" force per unit mass and $h\Omega R/\nu$ is a typical Reynolds number. Now according to Rayleigh's arguments for inviscid flow, this flow would be unconditionally unstable, but Taylor found instability only for $Ta > 1700$ approximately: for given h/R , the Reynolds number $h\Omega R/\nu$ must exceed a certain value before disturbances can grow in the presence of viscous restoring forces. The mode of instability is a set of contra-rotating toroidal vortices (Fig.8: for a photograph see Fig IX.1 of Ref.23, following p.496). As the Taylor number is increased above 1700 the disturbances become more complicated - a fascinating account of their complexity and non-uniqueness is given by Coles (71, 73) - but turbulence does not occur until a Taylor number of the order of ten times the critical is reached. Nagib (74) has shown that if an axial flow is superimposed on the fluid between rotating cylinders, two concentric sets of spiral vortices with equal and opposite pitch angles can appear: the sense of rotation is determined by the radial gradient of axial velocity, which changes sign part way across the gap.

Rayleigh's 1916 paper (14) draws a qualitative analogy between the effects of buoyancy forces and of streamline curvature ("centrifugal" force). Taylor and A.R. Low suggested to Jeffreys that the analogy should be quantitatively correct as between buoyant convection between a pair of infinite parallel horizontal plates at different fixed temperatures and the rotating-cylinder flow described above (with $h \ll R$ so that the centripetal acceleration, like the gravitational acceleration, should be constant across the flow). In 1928 Jeffreys (75) proved that the stability equations for these two cases were identical, the analogue of the Taylor number being the Rayleigh number

$$Ra \equiv g \frac{\Delta \rho}{\rho} \cdot \frac{h^3}{\kappa \nu} \quad (48)$$

where $\Delta \rho$ is the density difference between the plates and κ is the thermometric conductivity $k/(\rho c_p) \equiv \nu/Pr$. Taking the Prandtl number Pr to be unity for simplicity we see that Eq(48) is Eq(47) with the typical centrifugal force replaced by a typical buoyancy force. Recently Lezius and Johnston (76) have extended the analogy to plane flows analysed in rotating axes: an additional factor appears in Eq(47) because the Coriolis body force depends on the absolute, not relative, acceleration. In this type of buoyant convection with no mean horizontal flow there is no preferred direction in the horizontal plane and the mode of instability is a pattern of polygonal convection cells (see Fig.IX.5 of Ref.23, following p.512) rather than a row of parallel vortices: the latter are theoretically possible and sometimes appear when a horizontal flow is subjected to buoyancy effects.

In 1940 Görtler (77) investigated the stability of a laminar boundary layer on a curved surface (a horizontal flow subjected to centrifugal effects) and predicted that the basic mode of instability on a concave surface was a row of parallel vortices with axes in the stream direction, since called Taylor-Görtler vortices. These vortices were not actually observed until 1950 (78). The stability parameter is the Görtler number

$$Go = \frac{2}{R} \left(\frac{U_e \theta}{\nu} \right)^2 \quad (49)$$

or the square root of this, where θ , the momentum-deficit thickness, plays the role played by the gap h in the second form of the Taylor number in Eq(47) and the external-stream velocity U_e plays the same role as the circumferential velocity of the rotating cylinder, ΩR . The critical value of Go in a constant-pressure boundary layer is about 0.6 (it would be rather nearer the critical value of the Taylor number if δ , rather than θ , were used as the length scale). In the boundary layer, the ordinary Tollmien-Schlichting instability (Ref.23, Ch.IX), in which disturbances of the spanwise component of vorticity are driven by viscous forces, can also occur, at $U_e \theta / \nu \approx 160$: if δ/R is small enough for the boundary layer approximation to be good, this instability is unaffected by surface curvature of either sign; in particular it is not damped by convex curvature, so that the stability characteristics of laminar boundary layers on plane and convex walls are identical. On a concave wall of constant radius, Görtler instability occurs before Tollmien-Schlichting instability if the Reynolds number $U_e R / \nu$ is less than 1.4×10^7 . Once the disturbances attain finite amplitude, non-linear interaction between the two modes could occur and once the Tollmien-Schlichting disturbances have become three-dimensional, with a streamwise component of vorticity, they will be affected by surface curvature. Johnston (79) discusses the instabilities in the case of plane rotating flow.

The history of research on the effects of streamline curvature on turbulence is an object lesson in the effects of poor communication. In 1929 Prandtl (Ref.80, p.775) extended the analogy between buoyancy and curvature effects to turbulent flow, suggested that either effect could be represented by multiplying the mixing length by a function of a dimensionless buoyancy or curvature parameter, and used pure mixing-length arguments to estimate the behaviour of the function in each case. It must be emphasized that the useful part of Prandtl's results could be derived by dimensional analysis. As usual, pure mixing-length arguments got the dimensional analysis right, but underestimated the importance of the effects by an order of magnitude: in the next few years four experiments (see table) in Prandtl's own laboratory in Göttingen showed that streamline curvature could produce large effects on various kinds of turbulent shear flow. These experiments will be discussed below.

Author	Ref.	Date	Geometry
Wilcken	22	1930	Concave (also convex) boundary layer
Wendt	81	1933	Coaxial rotating cylinders (stable and unstable)
Wattendorf	82	1935	Curved duct (also rotating cylinder)
Schmidbauer	83	1936	Convex boundary layer

Wilcken and Schmidbauer say that their experiments were suggested by Prandtl's colleague Betz rather than by Prandtl himself, and neither explicitly evaluated the F-factor although Wilcken showed that large changes in mixing length occurred. Wendt acknowledges neither Prandtl nor Betz and gives his address as Clausthal (a university town in the hills about 20 miles from Göttingen) but Wattendorf says that Wendt's work was in fact done at Göttingen: Wendt evaluated the F-factor for stably-curved flow and showed much larger effects than predicted by Prandtl. Wattendorf began his experiments at Göttingen with an adaptation of Wilcken's apparatus and finished them in a new test rig with Von Karman at Caltech: he showed that large changes in mixing length occurred but did not evaluate the F-factor. Wattendorf published his paper in Proc. Roy. Soc., thus providing a link to the Göttingen work in the English literature. Also, Karman (13), in a congress held in Cambridge (England) in 1934 discussed several aspects of curvature and buoyancy effects as part of a general review of transition and turbulence and quoted Wattendorf's results. In 1935 Taylor (84) used the unstable flow between rotating cylinders as an experimentum crucis to distinguish between Prandtl's momentum-transport version of the mixing-length theory and his own "modified vorticity transport" version. Taylor's conclusion was that neither performed well but he did not quantify the errors nor discuss the physics of curvature effects on turbulence. He referred to Wattendorf's paper and to Prandtl's work. Schmidbauer (1936) in the last of the series of Göttingen papers, discussed the (large) modifications needed to Gruschwitz's integral boundary-layer calculation method to produce agreement with his own experiments on convex surfaces.

The position in about 1936, therefore, was that well-known English and German publications, including engineering journals, contained evidence of the very large effects of streamline curvature and of the large modifications needed if the mixing length formula or practical integral calculation methods were to be used to predict these effects. Even if one makes allowance for the political distractions of the next few years it is surprising that all this work virtually sank without trace (meteorologists were of course aware of the importance of buoyancy effects before Prandtl's paper: moreover the earliest meteorological version of the F-factor, the Monin-Obukhov formula, was apparently derived, in about 1950, without knowledge of Prandtl's work and I have never seen Prandtl's paper quoted in the meteorological literature). MacPhail (1941) quoted by Townsend (26), and Pai in 1943 (85) inspired respectively by Taylor and by Von Karman, made some further measurements in rotating-cylinder flows, but apart from these two experiments practically no attention was paid to the problem of curvature effects for nearly twenty years, and the subject was completely ignored by developers of boundary layer calculation methods in the 1940's and 1950's. An exception, of course, is the work of Coanda, whose 1932 patent (86) on improvements to various turbulent mixing devices relies on the increase in turbulence level in a wall jet on a convex surface. It was partly the relevance of the flow-deflection aspect of Coanda's work to schemes for boundary layer control by blowing, which became popular in the 1950's as jet-propelled aircraft were developed, that led to a revival of interest in the effects of curvature on turbulence structure. It is not very profitable to speculate on the reasons for the long neglect of the subject after the early Göttingen work had advanced it so far: perhaps an explanation, if not an excuse, for the lack of impact on boundary layer calculation methods is that solutions using the mixing length formula in non-self-preserving flows are practically impossible without a computer, while the integral methods of the 1940s and earlier 1950s, intended for solution by mechanical desk calculators, were so calamitously inaccurate that further discrepancies caused by curvature effects would not have been noticed. However, there is little excuse for forgetting the phenomenon, particularly since it is mentioned, with references to the early Göttingen work, in Prandtl's well-known student textbook "Essentials of Fluid Dynamics" (87) (p.132 of the 1952

edition). I confess that, though I acquired this book in my undergraduate days, I found the discussion only while writing this review. Moreover I rediscovered Prandtl's buoyancy-curvature analogy in complete ignorance of his 1929 paper, so that I have personally paid a penalty for ignoring the early literature.

We now proceed to a detailed review of the early work, starting with Prandtl's buoyancy-curvature analogy of 1929.

Prandtl considered the effect of buoyant or "centrifugal" body forces on the lumps of fluid hypothesized by the mixing-length theory, which in the absence of body forces are supposed to conserve their momentum or angular momentum between collisions. The argument is close to that of Karman quoted in Section 1, and shows that the mixing length in the buoyant case will be a function of a dimensionless parameter

$$\theta \equiv -\frac{g}{\rho} \frac{\partial \rho}{\partial y} / 2 \left(\frac{\partial U}{\partial y} \right)^2 \quad (50)$$

which is half the parameter now called the "gradient Richardson number" Ri [Prandtl refers to Richardson's work of 1920 (88)]. The factor of two arises from an apparently fallacious argument about the variation of buoyancy force on a displaced element of fluid (Ri , or the corresponding curved-flow parameter, is proportional to the square of the frequency of oscillation of a displaced element). Another difference in notation is that Prandtl represents the change in mixing length by

$$\left(\frac{\ell}{\ell_0} \right)^2 = f(\theta) \quad (51)$$

— it is not clear whether he contemplated the possibility of f becoming negative — so that his function equals the square of the local-equilibrium approximation to the factor F defined by Eq(36). Prandtl argued that turbulence could maintain itself only if the rate of production of turbulent energy by the mean shear, $-\overline{uv} \partial U / \partial y$ per unit mass, was greater than the rate of reduction of turbulent energy by buoyancy forces (i.e. minus one times the buoyant production $g \rho' v / \rho$). The turbulent energy extracted by a stable density gradient ($\partial \bar{\rho} / \partial y < 0$) eventually goes into potential energy by reducing the numerical value of $\partial \bar{\rho} / \partial y$ and thus raising the centre of gravity of the fluid: however the initial exchange may be largely from turbulent energy to internal gravity waves (15). Prandtl's argument, rephrased in modern terms, implies that the "flux Richardson number"

$$R_f = \frac{-(\text{buoyant production})}{(\text{shear production})} = -g \frac{\rho' v}{\rho} / \overline{uv} \frac{\partial U}{\partial y} \quad (52)$$

must be less than unity if the turbulence is not to decay. It can be seen that, if we replace density by temperature and change the sign accordingly, Ri/R_f is equal to the ratio of the turbulent diffusivity of heat to the turbulent diffusivity of momentum, called the turbulent Prandtl number Pr_t by engineers and K_M/K_H by meteorologists. The turbulent Prandtl number is near unity in neutrally-stable conditions, increasing in stable conditions ($Ri > 0$) and decreasing in unstable conditions (89). Classical mixing-length arguments lead to $Pr_t = 1$ and therefore to $Ri = R_f$, just as simple kinetic theory leads to a molecular Prandtl number Pr of unity. Therefore Prandtl's argument should lead to a critical Ri or R_f of 1 and a critical θ of 1/2: however the factor 2 is introduced in part of the argument only and Prandtl actually arrives at $\theta_{crit} = 1$. In practice $R_{f,crit}$ must certainly be less than unity in a local-equilibrium flow because energy production by the mean shear must supply viscous dissipation as well as a negative rate of buoyant production, and figures between 0.1 and 0.25 have been quoted in various theories and laboratory experiments. As it happens the critical values of Ri are much closer to unity but $Ri = 1$ has no particular physical significance. Karman (13) commented that the attempts of Richardson and Prandtl to establish stability limits for stratified turbulent flow from energy considerations evidently shared the defects of energy methods for laminar-flow stability problems, where they are well known to give far too low a critical Reynolds number (i.e. to overestimate the ability of disturbances to grow in the presence of restoring forces). We can now agree entirely with Karman's remark that the real merit of the work was to have brought out the significance of the Richardson number as the main parameter controlling turbulence in stratified flows. Prandtl chooses the variation of his mixing length correction factor $f(\theta)$ between the extreme points $\theta = 0, f = 1$ and $\theta = 1, f = 0$ to be

$$f(\theta) = (1 - \theta)^{1/2} \quad (53)$$

rather than a linear variation. This leads to

$$F = (1 - \frac{1}{2} Ri)^{1/4} \quad (54)$$

or, in the linear approximation valid for small Ri

$$F \approx 1 - \frac{1}{8} Ri \approx 1 - \frac{1}{8} R_f \quad (55)$$

More recent meteorological data suggest $F \sim 1 - 7R_f$ for small positive R_f in the inner layer of the Earth's boundary layer. Therefore the cumulative effect of the factor 2 in θ , the choice of a correction factor for ℓ^2 rather than ℓ and the choice of Eq(53) rather than a linear variation with R_f lead to an eightfold underestimation of the effects of small stable buoyancy on top of the customary factor of the order of 10 (7 here) by which mixing length theory underpredicts the effects of extra body forces or rates of strain.

Prandtl carried out an analogous mixing-length analysis for two-dimensional curved flows. In this case the dimensionless parameter that emerges is

$$\theta_1 \equiv \frac{U/r}{\partial U / \partial r - U/r} \quad (56)$$

which, as we shall see in Section 5, is half the curved-flow analogue of R_f rather than Ri . Prandtl again suggested

$$f(\theta_1) = (1 - \theta_1)^{1/2} \quad (57)$$

so for small θ_1 we get

$$F \approx 1 - \frac{1}{4} \frac{U/r}{\partial U/\partial r} \quad (58)$$

roughly a 40-fold underestimate of the effects of curvature.

Clearly, Prandtl's estimates of curvature effects would imply that they could be ignored in all but the most highly-curved shear layers, but, as mentioned above, experiments were started at Göttingen, presumably with the object of checking the theory. Wilcken's report (22) on measurements of boundary layers on the walls of a curved duct is still a pleasure to read: the experimental techniques, the discussion of errors and the analysis of results are surprisingly modern, and the results seem reliable. The boundary layer on the convex wall was so thin that detailed measurements were difficult, but the unstable boundary layer on the concave wall grew rapidly and the velocity profiles were accurate enough for the shear-stress profile to be estimated from the mean-momentum equation. Wilcken carefully discussed three-dimensional effects in the duct corners, leading to possible crossflow and imbalance of the two-dimensional momentum equation, but found no evidence of the spanwise periodicity that might be caused by steady longitudinal vortices. The mixing-length profiles deduced from the calculated shear stress seem trustworthy at least for qualitative purposes. As Wilcken comments, the effects of curvature were large, but although he must have been aware of Prandtl's 1929 analysis (his paper is dated 24 March 1930) he did not deduce a specific form for the mixing length correction factor. The mixing length in the mid-part of the layer was roughly quadrupled: the corresponding value of θ_1 was about 0.4 so that Prandtl's formula Eq(58) would have predicted only about ten per cent increase in mixing length.

In 1933 Wendt (81) made measurements in stable and unstable rotating-cylinder flow, using water or a water/glycerine mixture with a free (and therefore paraboloidal) surface. He measured velocity profiles at one axial position, for a large number of combinations of radius ratio, inner cylinder speed and outer cylinder speed. Possibly because he covered a large number of cases rather than exploring one in depth, he did not notice the probe-interference difficulties which appeared in the later work of Taylor (84) or the random changes in profile shape caused by changes in toroidal vortex patterns that later gave so much trouble to Pai (85). Wendt deduced surface shear stress from the torque on the cylinder, derived the internal shear-stress profile from the mean-momentum equation and plotted values of the mixing length correction factor $f(\theta_1)$, assuming that the mixing length in the absence of dynamic effects of curvature would vary as $Ky(1 - y/h)$, which slightly overestimates the mixing length near the centre of a plane duct. Wendt's estimates of the stabilizing effect of curvature vary somewhat with position: the largest values of F (i.e. the smallest curvature effects) are fitted quite well by his curve

$$f(\theta_1) = \frac{1}{(1 + 16.5\theta_1)^3} \quad (59)$$

giving

$$F \approx 1 - 25\theta_1 \approx 1 - 25 \frac{U/r}{\partial U/\partial r} \quad (60)$$

for small curvature effects. Wendt's values of f are for stable rotation only: he comments that Eq(59) will give impossible results for strongly unstable cases (large negative θ_1). Prandtl presumably had Wilcken and Wendt's results in mind when he commented in later papers (e.g. Ref.80, p.1084) that experimental and other theoretical values of critical Ri for buoyant flow were much smaller than his predicted value of 2. Also Schlichting (90: 1935) in a paper describing his work at Göttingen on buoyant flows refers to the work of Taylor and others on the critical Richardson number, leading to much smaller values than suggested by Prandtl. Therefore the defects of his analysis for curved and buoyant flows must have been clear to Prandtl in the early 1930s: however, in spite of retaining an interest in the problem at least up to 1944 (Ref.80, p.1166), he did not publish any further original work on it.

Wattendorf (82: 1934) presents measurements in another rotating cylinder rig (it is not clear whether these were made in Göttingen or at Caltech): he found, and commented on, the phenomenon of near-constant angular momentum over a large part of the gap between the cylinders. The main part of Wattendorf's paper describes his measurements in a curved duct. He refers to an early analysis of Prandtl's, implying $F \approx 1 - \theta_1$ for small θ_1 , but his own results show much larger effects. Because the shear stress and $\partial U/\partial y$ change sign, the sense of curvature effect also changes sign from one side of the duct to the other, in contrast to the case of one fixed and one rotating cylinder. Wattendorf measured the surface shear stress with a small surface pitot tube, calibrated in turbulent flow in a plane duct: at this time, many users of small surface tubes assumed that the same calibration would hold in laminar and turbulent flow, which is unfortunately not true for practical sizes of tube. Wattendorf's duct had a plane initial section and his measurements show the gradual change from fully-developed plane flow to fully-developed curved flow, but he calculated the shear stress within the fluid only in the fully-developed curved flow. His mixing-length results near the duct walls are shown in Fig.13, the multiplying "constant" α in the F -factor being plotted at the top of the figure. There is a significant difference in the values of α on the two sides, in the same sense as the difference found between stable and unstable buoyant flows (Section 5.4). As in the rotating-cylinder flow, the angular momentum is almost constant over the central part of the duct. The position of zero shear stress did not coincide with the position of zero velocity gradient $\partial U/\partial y$ or the position of zero rate of strain $\partial U/\partial y + \partial V/\partial x \equiv \partial U/\partial r - U/r$, or of course with the - indefinite - position of zero angular momentum gradient $\partial(Ur)/\partial r = \partial U/\partial r + U/r$. Wattendorf comments that it is not clear which of these three quantities should be used in the mixing length formula: the velocity gradient is used in plane flow but 'eddy viscosity' concepts suggest that the shear stress should depend on the rate of strain because it does so in laminar flow, while Prandtl argued that the mixing length concept of conservation of momentum of a fluid element between collisions indicates that angular momentum should be conserved in curved flows so that the shear stress should depend on the angular-momentum gradient. The same difficulties have since been encountered by many other authors who have tried to apply the older phenomenological theories to curved flows, but Wattendorf's discussion is one of the clearest. Today we can see that the ambiguity can account only for a factor of order $f \equiv 1 + e/(\partial U/\partial y)$ whereas direct effects of curvature on turbulence structure introduce a factor of order $F \equiv 1 + 10e/(\partial U/\partial y)$: however the more bizarre consequences of the ambiguity are avoided by relating shear stress to rate of strain. Wattendorf's

rejection of Prandtl's analysis of curved flows seems to be based more on the failure of the point of zero shear stress to coincide with the point of zero anything else than on any comparison between Prandtl's predictions for curvature effects and the measurement nearer the walls of the duct. Wattendorf did not seek or find any evidence of longitudinal vortices in his duct flow: Karman (13) comments that the curious result of negligible angular momentum gradient may be caused by secondary motions but, since he goes on to say that secondary motions would not be expected to be important in a duct with an aspect ratio of 18, he evidently had in mind corner flows rather than Taylor vortices.

Taylor (84: 1935) in the rotating-cylinder experiments mentioned above, discussed the question of whether the fluid lumps hypothesized by the mixing length theory should conserve angular momentum, as Prandtl's original analysis implied, or the z-component of vorticity, as in Taylor's modified vorticity transport theory. The presence of finite shear stress with a negligible angular momentum gradient was held to disprove the first, but while the vorticity transport theory was in principle compatible with constant angular momentum in the central part of the flow it could not explain the results nearer the walls. The temperature distribution when one cylinder was heated was also incompatible with the predictions of mixing-length theory. The demonstration by Wattendorf and Taylor of this qualitative implausibility of classical mixing-length theory was no more heeded by later workers than the demonstration of its quantitative underestimate of curvature effects, although Karman (1934) had pointed out one physical reason why the mixing length hypothesis could be no better than a first approximation (because the apparent mixing length is not small compared with the flow width).

The experiments mentioned above all revolved about the behaviour of the mixing length. Schmidbauer (83: 1936) measured a number of boundary layers on convex surfaces (the one most frequently quoted in the recent literature being the retarded-accelerated flow in Fig.6 of his paper) and discussed the behaviour of the integral parameters used in Gruschwitz's boundary-layer calculation method, the prototype of the integral methods of the 1940's and 1950's based on an empirical ordinary differential equation for some shape parameter of the velocity profile. Schmidbauer presented a plot of skin friction coefficient against θ/R , where θ is the momentum-deficit thickness and R the surface radius of curvature: variation with Reynolds number was ignored but was probably negligible compared to the effects of curvature. The ratio of skin friction at given θ/R to that on a flat surface can be approximated by $1 - 250\theta/R$ for $\theta/R < 0.002$: taking a representative value of $\partial U/\partial y$ to be $0.3 U_e/\delta \approx 0.03 U_e/\theta$, and assuming the fractional change in surface shear stress to be about one-third of the fractional change in L in the outer layer (as found in typical calculations by the method of Ref.16) we find that Schmidbauer's results imply

$$F \approx 1 - \frac{22 U/R}{\partial U/\partial y} \quad (61)$$

but more detailed calculations originally published by Bradshaw (91) show that the skin friction in the boundary layer of Schmidbauer's Fig.6 is well predicted by taking the numerical factor to be 14 (Fig.14). Schmidbauer also produced a correction factor involving θ/R for Gruschwitz's shape-parameter equation: as far as I am aware this factor has never been used in boundary layer calculations or adapted to other shape-parameter equations although Thompson (92: 1965), who was aware of Schmidbauer's work, produced his own empirical modification of Head's entrainment equation to account for curvature effects, again using θ/R as a parameter.

After Schmidbauer's paper little more work appeared. Clauser and Clauser (93: 1937) investigated the effects of surface curvature on transition to turbulence in a boundary layer, finding that transition was delayed by convex curvature. Since, to the thin-shear-layer approximation, convex curvature does not affect two-dimensional Tollmien-Schlichting waves, the most obvious explanation is the effect of curvature on the three-dimensional disturbances occurring in the later stages of transition. However the pressure gradients in the experiment were not accurately zero and may have been at least partly responsible. The main interest in the experiment is that it was the first to include direct measurements of turbulence on curved surfaces by hot wire anemometers, showing that the intensity was greater on a concave surface than on a convex one (this does seem to be a valid conclusion despite the uncertainties about the transition behaviour). No quantitative deductions can be made. The work was done under Von Karman's guidance: however the only direct connection with the previous research was that the Clausers considered using Wattendorf's duct for their experiment but finally decided to build a larger rig.

MacPhail (see Ref.24), working with Taylor, made what appear to have been rather unsatisfactory hot-wire measurements of turbulence in unstable rotating-cylinder flow: the experimental difficulties are of course considerable. Pai (85: report dated 1939, issued 1943) working with Von Karman, used hot wires to measure the mean velocity in unstable rotating-cylinder flow: Karman suggested that small hot-wire probes might be less sensitive than pitot probes to the interference effects found in Taylor's experiment. Pai says "At first it was thought that the flow.... would be two-dimensional except at the ends". However he found that two different velocity profiles could appear at a given axial position, depending on the starting sequence, and further investigation inferred, for the first time, the presence of patterns of streamwise (annular) vortices superimposed on the turbulent flow. It is still not entirely clear whether the existence of two alternative patterns of vortices was a fluke or whether the fully-turbulent cylinder flow invariably exhibits the multiple-state behaviour found in the laminar flow (71). Since the number of vortices is necessarily an integer, the flow between cylinders whose length is nearly $(n + \frac{1}{2})$ times the preferred width of a vortex may develop n vortices on one run and $n + 1$ on another. Pai also measured the root-mean-square intensity of the circumferential velocity fluctuations at different axial positions and the results help to confirm the presence of fixed large-scale circulations which transfer highly turbulent fluid from near the surfaces to the central part of the annulus. Pai did not analyse his results in sufficient detail to extract mixing-length behaviour or other quantitative information about the effect of curvature on the turbulence, and this work seems to be the end of the series of investigations inspired by Prandtl's 1929 paper.

Darkness now descends, and the next explicit consideration of curvature effects that I have been able to find is Kreith's paper (94) of 1955 (following preliminary work reported at a conference in 1953) in which Wattendorf's results are used to estimate heat transfer in curved ducts. Kreith extracts the apparent eddy viscosity from Wattendorf's measurements and deduces the apparent eddy conductivity of heat

by using Reynolds' analogy, assuming that the turbulent Prandtl number is unaffected by curvature. Kreith extends Wattendorf's discussion of the choice of conserved quantity in the mixing length process and provisionally concludes that the "forced vortex parameter" U/R should be chosen. Authors still continued to engage in this discussion as late as 1969, but as it is now generally agreed that mixing length arguments are not quantitatively trustworthy I shall not reference the more recent discussions unless the paper has something else to offer. Kreith's measurements on a small duct with a height-to-radius ratio of 1/12 show that the heat transfer through the concave wall was 1.4 times that through the convex wall, a slightly smaller factor than one would expect on the basis of Wattendorf's surface shear stress measurements, although it is unsafe to make a direct comparison of wall flux rates in a case like this.

In the early 1950's interest in vortex flows arose. Einstein and Li (95: 1951) discussed vortex flows in general and Mabey (96: 1953) working with H.B. Squire, made measurements in a simulated trailing vortex in the prototype of the vortex tube used by many subsequent investigators: the swirl is introduced by vanes in a radial inlet followed by an axisymmetric flare with a short conical centrebody from which the vortex trails. The early work on vortices did not fully consider the direct effects of streamline curvature on turbulence and it was many years before a quantitative explanation for the observed Reynolds-number dependence of this free turbulent flow was found, in terms of stabilization of a vortex core in solid-body rotation. The early work on confined vortex flows is briefly surveyed by Keyes (97) who performed some experiments at Oak Ridge National Laboratory, evidently with application to gas separation in nuclear fuel production. He produced an empirical correlation for eddy viscosity (assumed constant over the cross section) but again there was no consideration of curvature effects. Of course in such strongly rotating flows it is very difficult quantitatively to distinguish the stabilizing or destabilizing effects of curvature because there is no experimentally realizable comparison flow with the same rate of strain field but zero rotation. Therefore the early work on swirling flows will not be discussed in this section.

In 1952 Wislicenus and Yeh of Johns Hopkins University proposed to the US Office of Naval Research a programme of work on flow in ducts and turbomachinery [I have not seen the contract proposal; it is referred to in Refs (98) and (99)]. The results included three of the first recognizably modern papers on curvature effects, based on hot-wire measurements and discussions of the Reynolds-stress transport equations — but none of the papers refers to Prandtl's work (although Eskinazi and Yeh compare Wattendorf's duct results with their own) and none yields any explicit formula for the change in Reynolds stress as a function of a curvature parameter. In an appendix to Traugott's paper (100) Yeh discusses the oscillation of a displaced element in a body of fluid in solid-body rotation and shows that its frequency is twice the rotational frequency (a result which we would now interpret as a value of 4 for the analogue of the gradient Richardson number): he refers to several previous papers on rotating flows but does not mention the connection with the Brunt-Väisälä frequency of a displaced element of fluid in a stratified field which is implicit in Prandtl's work. One can only speculate on the consequences if the Johns Hopkins group had made full use of the early work, especially the boundary-layer measurements of Wilcken and Schmidbauer: at the very least it would have become clear to them that the separating boundary layer measured in the late 1940s by Schubauer and Klebanoff (101) at the nearby National Bureau of Standards was greatly influenced by curvature effects, and in view of the popularity of this experiment as a foundation for calculation methods it is almost certain that the importance of curvature effects in typical boundary layers would have re-emerged at least ten years earlier than was in fact the case.

Eskinazi and Yeh's measurements (98) were made in fully-developed flow in a duct with a straight entry section followed by a curved duct with a height of one-tenth of the outer radius. Intensities, spectra and microscales were measured. As in previous experiments on ducts and rotating cylinders the angular momentum was nearly constant over the central part of the flow, an infallible sign of vigorous mixing either by large eddies or by steady streamwise vortices. Eskinazi and Yeh, like Wattendorf (82) and Taylor (84) found no evidence of steady vortices, but their checks for three-dimensionality consisted simply of mean velocity traverses at three (unspecified) spanwise positions. It is of course inherently less likely that steady vortices will form in duct or boundary layer flow than in the rotating cylinder flow where any streamwise vorticity is fed back round the circumference, but the recent work of Johnston's group (10, 76, 79) has found near-steady vortices in a straight rotating duct at about the same curvature parameter as in Eskinazi and Yeh's experiment. We return to the question of longitudinal vortices in Section 5. Eskinazi and Yeh refer briefly to a possible collapse of their inner-layer velocity profiles on similarity axes and comment that "It is therefore to be expected that U/u_τ is a function not only of $u_\tau y/\nu$ but also of y/R or perhaps of some combinations of the two. Such functional relations are not however obvious at present." In fact, if inner layer similarity considerations are still valid in the presence of curvature the only possible form is

$$\frac{U}{u_\tau} = f\left(\frac{u_\tau y}{\nu}, \frac{u_\tau R}{\nu}\right), \quad (62)$$

and either Prandtl's mixing-length analysis or an alternative derivation of the curvature parameter would suggest that outside the viscous sublayer

$$\frac{\partial U}{\partial y} = \frac{u_\tau}{Ky} / F\left(\frac{U/R}{\partial U/\partial y}\right). \quad (63)$$

The values of the function F (equal to ℓ/Ky) derived from Eskinazi and Yeh's measurements by the present writer are plotted with Wattendorf's in Fig.13. Eskinazi and Yeh discuss the explicit extra terms in the Reynolds-stress transport equations. Unfortunately, as shown in Section 3, consideration only of the explicit extra terms leads to the same order-of-magnitude underestimate of curvature effects as classical mixing length theory. Traugott (100: 1958; unpublished report dated 1956) performed an interesting experiment on turbulence generated by a series of rotating grids. The grids, preceded by an impeller, also imposed solid-body rotation on the mean flow, confined in an annular duct whose walls also rotated (there is of course still a gradient of axial velocity near the walls). The radial component of velocity fluctuations in the central part of the annulus was significantly reduced by rotation, while the circumferential component was increased. Traugott discussed the extra 'Coriolis' production terms in the Reynolds-stress transport equations and measured the production and dissipation terms. The dissipation was

deduced from measurements of the mean-square time derivatives of the three velocity components but the resulting values are too low by a factor of 2, presumably because of the usual deficiencies in spatial resolution or frequency response of the hot wire anemometer: Traugott blames the assumption of local isotropy — the microscale Reynolds number $\sqrt{u^2} \lambda/\nu$ was about 40 — but it seems unlikely that his limited use of the assumption could produce such large errors. The dissipation values were multiplied by the correction factor required to balance the turbulent energy equation in the non-rotating flow. It is probable that Eskinazi and Yeh's measured microscales were also in error but they did not deduce dissipation from them. In the rotating flow, the production terms act to reduce the difference between the radial and circumferential intensities u_r^2 and u_θ^2 in Traugott's notation so that the observed maintenance of a difference must be attributed to the effects of rotation on the pressure-strain terms or, less probably, on the anisotropy of the dissipating eddies. Traugott was not, of course, able to measure the pressure strain terms and he lumps them with the turbulent transport terms (also unmeasured, but probably small except near the walls) in his energy balances for each component. Traugott pointed out that the transport equations show that a shear stress in the plane of rotation, $\overline{u_r u_\theta}$, is produced if $u_r^2 \neq u_\theta^2$. This is unexpected a priori, but simply results from rotation of the axes: if axes are rotated 45 deg, $\overline{u_r u_\theta}$ becomes $(u_r^2 - u_\theta^2)/2$.

In the third of the Johns Hopkins experiments, Yeh (99: 1958) made measurements of the boundary layers on the walls of a stationary annular duct, fed with an axial "free-vortex" flow (negligible gradient of angular momentum outside the boundary layer) from a radial inlet like that used in Mabey's vortex tube. The helix angle near the outer wall was about 20 deg. Hot-wire measurements of turbulence intensity were made, and Yeh discussed the effect of the extra terms appearing in the Reynolds-stress transport equations in curvilinear coordinates. Yeh's turbulence measurements conclusively show an increase in intensity on the concave wall — twenty years after the Clausers' slightly dubious results — but changes in the Reynolds stress were not evaluated in terms of any curvature parameter. Yeh did not report any evidence for the presence of streamwise vortices. Longitudinal vortices were first found in boundary-layer flow by Tani (102) in 1962.

Apparently the first attempt since Schmidbauer's to correct a complete shear-layer calculation method for the effects of curvature on the turbulence was the work of Thompson (92: 1965) mentioned above. The application was to aircraft wing sections so that only convex curvature was considered. Thompson reported improved agreement with experiments but at that date there were few suitable test cases in low-speed flow.

In the same year, a Euromech colloquium on the Coanda effect (103) considered not only the various Coanda phenomena but many other examples of laminar or turbulent curved shear layers. However, little mention was made of the direct effects of curvature on turbulence and no quantitative results were presented. There could be no better demonstration of the general unawareness of the importance of these effects.

Another such demonstration, which this time caused considerable damage, was the series of experiments in the 1960's on supersonic boundary layers with a longitudinal pressure gradient induced by surface curvature. Neglecting the boundary layer displacement thickness we get

$$\frac{dp}{dx} = -\frac{\rho U_e^2}{R} \cdot \frac{1}{(M_e^2 - 1)^{1/2}} \quad (64)$$

$$\text{or } \frac{\delta^*}{\tau_w} \frac{dp}{dx} = \frac{2}{c_f} \cdot \frac{\delta^*}{R} \cdot \frac{1}{(M_e^2 - 1)^{1/2}} \approx 50 \frac{\delta}{R} \quad (65)$$

where the last approximation is based on typical values for a constant-pressure boundary layer at a free stream Mach number of 3. We can see that a pressure-gradient parameter of order unity implies a value of δ/R of the order of 50, leading to changes in apparent mixing length of the order of 50 per cent in the outer layer. Clearly there will be large differences in the behaviour of a boundary layer with a pressure gradient induced by surface curvature and one with an equal pressure gradient induced by incoming Mach waves. Because it was generally more convenient, especially in small wind tunnels, to measure the boundary layer on a curved centrebody or on a curved ramp on the sidewall rather than insert a body in the tunnel to induce a pressure gradient on the sidewall, experiments were done in the former fashion and used, or intended for use, in development of calculation methods to be applied indiscriminately on curved or plane surfaces. It is of course true that most external flows occurring in aeronautics have pressure gradients induced by curvature but this is certainly not true of internal flows in intakes and turbomachines and in any case one ought to distinguish the two. However the main result of the experiments of the 1960s was to create confusion, which can now be seen to have been worse confounded by the direct effects of dilatation on the turbulence mentioned in Section 3 (which in the case of boundary layers with pressure gradients induced mainly by curvature tend to reinforce the direct effects of curvature). Supersonic boundary layers on curved surfaces will be discussed in Section 6.

The "Coanda effect" [Coanda (1932) quoted by Newman (104) and Fernholz (105), but see also Reynolds (1870) quoted by Newman, and others quoted by Wille and Fernholz] is defined in different ways by different people (see Section 7). Here our interest is in the increased mixing rate in turbulent wall jets on convex surfaces. Most of M. Coanda's devices rely on this phenomenon, but he was an engineer rather than a research worker and therefore made use of it without expending his time on establishing its fundamental causes. It is interesting to note that the first basic research work on wall jets on plane surfaces by Förthmann (106) did not appear until 1934: evidently neither Coanda's invention nor Prandtl's analysis prompted Förthmann to extend his work to curved surfaces. Newman (104) and Bradshaw and Gee (107), reporting their own measurements on curved wall jets, found no earlier work to quote. Von Glahn (108) reporting applications to blown-flap schemes, refers only to a paper by Metral, which I have not seen but which appears to be a discussion of the principle of operation of Coanda's devices. Another paper by Metral (109) discusses the inviscid aspects, and a general discussion of the several Coanda phenomena and of the early work is given by Metral and Zerner (86). It is fair to say that practical applications and

basic research remained separate until aeronautical interest in blown flaps led to applications in a research-oriented industry.

Bradshaw and Gee (107) briefly discussed the possibility of centrifugal instability of the turbulence leading to (supposedly unsteady) longitudinal vortex eddies in the convex wall jet, but measurements of spanwise correlations of the radial velocity fluctuation showed no trace of vortex eddies: it was not seriously supposed that steady longitudinal vortices would exist in such a highly-turbulent flow and indeed they have never yet been observed in jet flows.

Sawyer (110) described work on curved free jets: here the practical applications are to jet-flap schemes and to various jet-reattachment situations, and of course the shear-layer curvature is not directly specified by a solid boundary. The convex side of a curved jet is unstable and the concave side stable: any net influence of curvature or growth rate is therefore the result of non-linear effects: Sawyer indeed observed a net increase in growth rate. In his analysis, Sawyer followed Prandtl's 1929 mixing length arguments — to which he refers — in spirit, but used $2(U/r)/(\partial U/\partial y)$ as a curvature parameter: to first order this is twice Prandtl's θ_1 and therefore the correct analogue of the Richardson number. Sawyer's final correction formula applies to the eddy viscosity rather than the mixing length but to first order it is equal to an F-factor correction to the mixing length

$$F = 1 - \alpha(U/r)/(\partial U/\partial y) \quad (66)$$

with α an empirical constant, chosen to fit experiments rather than derived from mixing length arguments. Giles, Hays and Sawyer (111: 1966) extended Sawyer's work to wall jets on concave and convex logarithmic spiral surfaces, chosen to obtain a constant value of δ/R and thus a closely self-preserving flow: most other investigators have used circular-arc surfaces from which the wall jet separates after a turning angle of the order of 180 deg. Very large decreases or increases in growth rate were observed, though increases in growth rate for very large positive δ/R may not be attributable solely to direct effects of curvature because the thin-shear-layer approximation is no longer valid and pressure gradients and normal-stress gradients may have some effect (Section 2.2). Giles et al. reported limited turbulence measurements but did not discuss the turbulence structure in detail.

Stratford, Jawor and Golesworthy (112: 1962) also discussed curvature effects on mixing layers and independently derived the first-order analogue of the Richardson number by classical mixing length arguments. Insertion of plausible data for the velocity profile leads them to

$$F = \frac{\ell}{\ell_0} = \frac{1}{1 - \frac{2}{3} \frac{b}{R}} \quad (67)$$

where b is the width of the mixing layer. They comment that mixing length arguments cannot be trusted to predict curvature effects quantitatively so that the above formula "should really contain a coefficient of ignorance". However they found it to be in fair agreement with a number of experiments for b/R of the order of 0.25 (though the effects predicted are very much smaller than those found in wall jets by Giles et al. and other workers). In a later paper, Stratford, Jawor and Smith (113: 1964) extend the analysis to the mixing of streams of different density and obtain the Richardson number analogue with the total-pressure gradient in the numerator, a form which applies (Section 5.1) to compressible or incompressible flows. They discuss mechanisms by which curvature could affect spreading rate even if the two streams had the same total pressure (but different density and velocity) but the arguments are not conclusive and even today there are no data on such flows.

It is convenient to terminate this historical survey before the revival of widespread interest in curvature effects, so that most of the work that contributes to our current knowledge can be discussed separately for each type of shear layer. I have therefore omitted, or mentioned only briefly, the work done by the research groups that led the revival, notably at McGill and Cambridge.

5. DESCRIPTION OF CURVATURE EFFECTS

5.1 PARAMETERS FOR TWO-DIMENSIONAL FLOWS

At least in simple cases, the rate-of-strain ratio, $(\partial V/\partial x)/(\partial U/\partial y)$ in (x,y) coordinates, is an adequate parameter to describe curvature effects on the turbulence. However, it is restricted, in the form given here, to two-dimensional flow; like any parameter based solely on the mean strain field, it implies local equilibrium between the mean strain field and the turbulence; and the choice of the denominator, like the choice of the rate of strain to be used in the mixing length formula, is not unique. A discussion of alternative parameters, following the treatment by Prandtl mentioned in Section 4, is helpful in illuminating the phenomena, the behaviour of the extra terms in the Reynolds-stress transport equations, and the analogy between curvature and buoyancy effects. Much of the discussion is based on the analogy, which allows us to make use of half a century of meteorological experience (114, 115) and even to use meteorological data for quantitative prediction of curvature effects. We shall see that the various parameters defined by analogy with those used in meteorology become equal to twice the rate-of-strain ratio in the case of small curvature effects and approximate local equilibrium (the factor of two is a consequence of arbitrary definition and not an "analogy factor"). For purposes of deriving F-factors (Section 3) for flows with small curvature effects any parameter can therefore be used; the most convenient choice may differ between different flows and between different calculation methods. In cases of large curvature effects the more realistic parameters are linked by the Reynolds-stress transport equations so that if information about the terms in these equations is generated by the calculation method the choice of parameter is still arbitrary, although a comparison is instructive. Certain difficulties arise in three-dimensional flows and we postpone consideration of these until Section 5.2.

Before discussing the parameters we must justify the analogy between the physical processes. As mentioned in Section 4 there is an exact correspondence between the equations of motion and stability for certain buoyant laminar flows and curved laminar flows, but this is no guarantee of a general correspondence

for turbulent flows. However, a more acceptable justification comes from considering the fluctuating body forces in the two cases. (i) An element of fluid in a buoyant flow which has a density higher by an amount ρ' than the mean density $\bar{\rho}$ experiences a force of $-\rho'g/\bar{\rho}$ per unit mass in the vertical direction. (ii) An element of fluid in a curved flow which has a velocity higher by u than the mean velocity U experiences an apparent "centrifugal" force (in excess of the mean "centrifugal" force balanced by the mean radial pressure gradient) of $((U+u)^2 - U^2)/R \approx 2Uu/R$ in the outward direction. (iii) In a density-stratified shear layer (whether in a gravitational field or not) the coefficient of correlation between the density fluctuation and the velocity fluctuation, $\overline{\rho'u}/(\overline{\rho'^2 u^2})^{1/2}$, is numerically as high as 0.9 (116, 117). Statement (iii) justifies the Reynolds analogy between momentum transfer and heat transfer (density and temperature fluctuations being perfectly anticorrelated in a low-speed flow and very highly anticorrelated even in high-speed flow): the "Reynolds analogy factor" is not exactly unity, partly because the correlation coefficient in (iii) is not exactly unity. Statements (i)-(iii) together justify the analogy between curvature and buoyancy effects replacing the fluctuating gravitational force proportional to ρ' by a fluctuating centrifugal force proportional to u . Clearly we must again expect an "analogy factor" slightly different from unity although the accuracy of data for buoyant or curved flows is not high enough for the difference to appear at present. Note that the "mixing length" concepts implicit in the above analysis are used symmetrically for buoyancy and for curvature and their shortcomings should not seriously affect the argument.

The dimensionless parameters used to describe buoyancy effects are of two types. One type uses the easy concept of oscillation of an element of fluid displaced in the direction of the buoyancy force and the other is based on the extra buoyancy terms in the Reynolds-stress transport equations. Analogies to both can be constructed in curved flows and in addition we have the rate-of-strain ratio, which has no exact equivalent in buoyant flows.

The three common buoyancy parameters, appropriate to a simple shear layer in the x, y plane with the gravitational acceleration in the negative y direction, are

the gradient Richardson number

$$Ri = \left(\frac{\text{Brunt-Väisälä frequency}}{\text{typical turbulence frequency}} \right)^2 \quad (68)$$

$$= (\text{typical body force})/(\text{typical inertia force})$$

where the Brunt-Väisälä frequency ω_{BV} , the circular frequency of oscillation of a displaced element of fluid, was given in Eq(5),

the flux Richardson number

$$R_f = - \left(\frac{\text{v-component energy production due to body force}}{\text{u-component energy production}} \right) \quad (69)$$

and the ratio of L/K to the Monin-Obukhov length L_{mo}

$$\frac{L/K}{L_{mo}} = - \left(\frac{\text{v-component energy production due to body force}}{\text{viscous dissipation}} \right) \quad (70)$$

where L is the dissipation length parameter, $(-\overline{uv})^{3/2}/(\text{viscous dissipation})$, K is the von Karman constant, 0.41 approximately, and L_{mo} is a length defined by Eq(70) itself.

The definitions have been written in a form applicable to curved flows as well as buoyancy. They are to some extent arbitrary (we could have chosen total production for the denominator of R_f , and the factor of K in Eq(70) was introduced so that the parameter reduces, in the inner layer of a wall flow, to the familiar parameter y/L_{mo} used in studies of the atmospheric surface layer). We now derive each parameter, with its analogue for curved flow enclosed in quotation marks to prevent confusion. A suitable choice for a typical frequency of the turbulence in Eq(51) is the mean velocity gradient $\partial U/\partial y$, equal in the local-equilibrium approximation for a non-buoyant thin shear layer to $(-\overline{uv})^{1/2}/L$ where L is the dissipation length parameter a typical length scale of the energy-containing eddies. $(-\overline{uv})^{1/2}/L$ is certainly a typical frequency of the turbulence, and also a typical root-mean-square fluctuating strain rate: it is to be preferred to $\partial U/\partial y$ if the two are different. The gradient Richardson number is

$$Ri = \frac{\omega_{BV}^2}{(\partial U/\partial y)^2} = - \frac{g}{\bar{\rho}} \frac{\partial \bar{\rho}}{\partial y} / \left(\frac{\partial U}{\partial y} \right)^2 \quad (71)$$

This, like all the other parameters mentioned here, is positive in a stable flow, negative in an unstable flow. $Ri = 0$ implies neutral conditions.

In curved flow the analogue of the Brunt-Väisälä frequency was derived in Eq(4), and the analogue of the gradient Richardson number, using (s, n) coordinates with $n + R \equiv r$, is

$$"Ri" = \frac{2}{r^2} \frac{\partial}{\partial r} (Ur) / \left(\frac{\partial U}{\partial r} \right)^2 \quad (72)$$

which for large radii of curvature becomes

$$Ri = \frac{2}{r} \frac{\partial U}{\partial r} \quad (73)$$

or $-2(\partial V/\partial x)/(\partial U/\partial y)$ in rectangular Cartesian coordinates, and is therefore just twice the rate of strain ratio: the difference can be absorbed in any empirical constant. Note that, just as Wattendorf (Section 4) was uncertain whether to choose $\partial U/\partial r$, $\partial U/\partial r + U/r$ or $\partial U/\partial r - U/r$ as the velocity gradient in the definition of mixing length ℓ , there is a similar uncertainty in the choice of the denominator for the

gradient Richardson number, as can be seen if we equate it to $(-\overline{uv})/\ell^2$ as authorized by the local-equilibrium approximation. Since the effects of curvature on the turbulence are large, the local-equilibrium approach embodied in the derivation of Richardson number is likely to be valid only for fairly small Richardson number — that is, for $U/r \ll \partial U/\partial r$ — so that the differences between the three choices for the denominator is negligible. We need to be more careful about the numerator, whose sign indicates the sense of stability.

The gradient Richardson number was historically the first parameter used to describe buoyant flow (88): a less obvious parameter, but one whose derivation is more relevant to the present approach based on the Reynolds-stress transport equations, and which is more convenient in three-dimensional flows where the evaluation of ω_{BY} becomes complicated, is the flux Richardson number R_f . It is so called because it is based on the "buoyancy flux" $g \rho' \bar{v}$ instead of the buoyancy gradient $g \partial \bar{\rho}/\partial y$. From Eq(69) we derive

$$R_f = (-g \overline{\rho' v / \rho}) / (\overline{uv} \partial U / \partial y) \quad (74)$$

R_i and R_f become almost equal in local equilibrium and for small buoyancy effect, where we can use almost the same mixing length to describe $\rho' \bar{v}$ and \overline{uv} . The curved-flow analogue of R_f requires a little thought because, as mentioned in Section 2.4, the extra rate of strain U/r contributes to the production terms in the equations for Du^2/Dt and Dv^2/Dt in (s,n) coordinates though in rectangular Cartesian coordinates it contributes only to Dv^2/Dt : the difference comes from the rotation of axes seen by an observer moving with the mean flow. In (x,y) coordinates

$$\frac{D\frac{1}{2}\overline{u^2}}{Dt} = -\overline{uv} \frac{\partial U}{\partial y} + \dots \quad (75)$$

$$\begin{aligned} \frac{D\frac{1}{2}\overline{v^2}}{Dt} &= -\overline{uv} \frac{\partial V}{\partial x} + \dots \quad (76) \\ &= +\overline{uv} \frac{U}{r} \end{aligned}$$

while in (s,n) coordinates, writing $dn = dr$ as well as $r = n + R$

$$\frac{D\frac{1}{2}\overline{u^2}}{Dt} = -\overline{uv} \frac{\partial U}{\partial r} - \overline{uv} \frac{U}{r} \quad (77)$$

$$\frac{D\frac{1}{2}\overline{v^2}}{Dt} = +2 \overline{uv} \frac{U}{r} \quad (78)$$

The ambiguity in the denominator of Eq(69), like the ambiguity in the denominator of "Ri", will simply introduce a factor of order f into the dimensionless parameter and can be disregarded. Likewise we disregard any higher-order production terms like $\overline{v^2} \partial V/\partial y$: local parameters such as these will be valid only in fairly thin shear layers. However we must decide whether to class as "production" the rotation-of-axis term $-\overline{uv} U/r$ which appears, with opposite signs, in Eq(77) and Eq(78), or to define "R_f" with reference to rectilinear (x,y) coordinates. We choose (s,n) coordinates, giving the form first suggested by Wyngaard (118)

$$"R_f" = \frac{2 \frac{U}{r}}{\frac{\partial U}{\partial r} + \frac{U}{r}} = \frac{2 U}{\frac{\partial}{\partial r} (Ur)} \quad (79)$$

which has the advantages of reducing to "Ri" if $U/r \ll \partial U/\partial r$ and of referring to a system of coordinates in which a thin shear layer remains thin (this does not of course commit us to using (s,n) coordinates in a numerical calculation: we are discussing systems of axes only as an aid to deriving a physically meaningful parameter). Note that the alternative choice, $(\partial V/\partial x)/(\partial U/\partial y)$, is just the rate-of-strain ratio, and that if we had chosen the denominator of "Ri" as $(\partial U/\partial r + U/r)^2$, "Ri" and "R_f" would always be equal. With the present definitions R_i goes to zero and R_f goes to infinity if the angular momentum is constant or the mean vorticity is zero. If this condition occurs at the edge of a turbulent flow it presumably implies neutral stability, whereas if it occurs within the turbulence it implies vigorous large-scale mixing, so that the different behaviour of the parameters is at least mnemonic for these two different situations: analogous situations occur in meteorology: $R_i = 0$ in "free convection". Note that confusion exists in the literature (119, 120) about the phenomenon of "vorticity expulsion" — that is, the tendency to constant angular momentum: it certainly occurs in strongly unstable flows such as highly-curved ducts (82, 98) but published discussions appear to refer to stable flows, to confuse the radial and axial components of vorticity, and to draw no distinction between suppression of turbulence and expulsion of mean vorticity. Lezius and Johnston (76) suggest that the denominator of the Richardson numbers should be chosen as some average value of velocity gradient, rather than the local value, so as to avoid difficulties at velocity extrema within duct or wall jet flows. However, if one regards internal velocity extrema as associated with two interacting — and approximately superposable — shear layers it becomes clear that the free-edge problem and the internal-extremum problem are related, and that what is wanted is a better choice of "typical turbulence frequency" than $\partial U/\partial r$.

To the local-equilibrium approximation the turbulent energy equation for buoyant or curved flows can be written as

$$(\overline{u^2} \text{ production})(1 - R_f) = \text{dissipation} = \epsilon \quad (80)$$

so that $1 - R_f$ plays the role of an f -factor. Other types of Richardson number could be defined by reference to, say, the shear-stress transport equation (91): like the alternative definitions of length scale L mentioned in Section 2, they differ only by ratios of Reynolds stresses and add little to the definition based on the turbulent energy equation.

In buoyant flows the Monin-Obukhov length, sometimes called the "Lettau-Monin-Obukhov" length, can be seen from Eqs (69), (70) and (74) to be

$$L_{mo} = \frac{(-\overline{uv})^{3/2}}{K} \bigg/ g \frac{\rho' v}{\bar{\rho}} \quad (81)$$

and if the flow is in local equilibrium so that total production equals dissipation, Eqs (70) and (80) show that

$$\frac{L/K}{L_{mo}} = \frac{R_f}{1 - R_f} \quad (82)$$

so that in local equilibrium and with small curvature effects the three buoyancy parameters R_i , R_f and $(L/K)/L_{mo}$ become equal. The curved-flow analogue of L_{mo} is

$$"L_{mo}" = \frac{(-\overline{uv})^{3/2}}{K} \quad (v^2\text{-production}) = \frac{r}{2K} \frac{(-\overline{uv})^{1/2}}{U} \quad (83)$$

(which is of the order of $0.05r$ in the central part of a typical boundary layer) so that

$$\frac{L/K}{"L_{mo}"} = \frac{2U}{r} \bigg/ \frac{(-\overline{uv})^{1/2}}{L} \quad (84)$$

which once more becomes equal to " R_i " and " R_f " in local equilibrium and with small curvature effects because we can equate $(-\overline{uv})^{1/2}/L$ and $\partial U/\partial r$ by the mixing length formula Eq(27). It is not immediately obvious how $(-\overline{uv})^{1/2}/L$ behaves at the edge of a shear layer where the angular momentum gradient goes to zero so that $R_i \rightarrow 0$ and $R_f \rightarrow \infty$. Since the flow is intermittently turbulent the most realistic measure of turbulence frequency is based on averages within the turbulent fluid only, but it turns out that the intermittency factor cancels out of $(-\overline{uv})^{1/2}/L$ so that its conventional average is the same as the average within the turbulent fluid. Arguments can be produced in favour of constancy near the edge of a shear layer or tendency to zero, but not for tendency to infinity. Therefore it seems that $(L/K)/L_{mo}$ will probably not tend to zero.

Now in a curved layer the local-equilibrium version of the turbulent energy equation, divided by $-\overline{uv}$, is

$$\left(\frac{\partial U}{\partial r} + \frac{U}{r} \right) = \frac{(-\overline{uv})^{1/2}}{L} \quad (85)$$

To the local-equilibrium approximation we can therefore write all the curved-flow parameters in terms of the simple parameter

$$- \left(\frac{\partial v/\partial x}{\partial U/\partial y} \right) = \frac{U/r}{\partial U/\partial r} = S = \frac{U/r}{(-\overline{uv})^{1/2}/L} \quad (86)$$

as

$$R_i = 2S(1 + S) \quad (87)$$

$$R_f = \frac{L/K}{L_{mo}} = 2S/(1 + S) \quad (88)$$

so to first order all the parameters are equal to $2S$. In a curved flow which is not in local equilibrium the error involved in using local-equilibrium formulae for curvature corrections is probably minimised by using Eq(84), in which the extra rate of strain is divided by a typical root-mean-square fluctuating rate of strain. Near the free edge of a shear layer none of these local-equilibrium parameters is completely satisfactory: this is a reminder, if not a consequence, of the fact that the flow in this region is controlled by turbulent transport from the interior rather than by local generation or destruction of Reynolds stress.

The z -component mean vorticity, $Z \equiv -(\partial U/\partial r + U/r)$, and the total rate of shear strain in the (s,n) plane, $A \equiv (\partial U/\partial r - U/r)$, are equal and opposite in a simple shear layer. Therefore $1 + A/Z$ is a *prima facie* plausible curvature parameter: it is of course equal to R_f . Again, a plausible curvature parameter is the ratio of the static pressure gradient in the radial direction to the total pressure gradient in the radial direction: this is

$$\frac{U^2/r}{U^2/r + U \partial U/\partial r}$$

which is equal to $R_f/2$. Slightly different but equally plausible definitions would have given parameters equal to $2S$ and S respectively. These different derivations of essentially the same parameter are something more than an academic exercise: the different physical concepts may be separately useful and it is helpful to establish the mathematical relation between them.

In flows analysed in rectangular Cartesian coordinates rotating at angular velocity Ω , the equations of motion contain an apparent body force, the Coriolis force $2 \underline{U} \times \underline{\Omega}$. Note that we use the usual sign convention that positive Ω means anticlockwise rotation (the positive x axis follows the positive y axis): the opposite convention, adopted in the simple cases discussed in Ref.(91) so that Ω should have the same sign as U^2/r , is confusing in more complicated cases. In the present convention, positive Ω destabilizes a shear layer with positive $\partial U/\partial y$. Note also that the stability of the flow is not affected by the axes used to analyse it: it is merely a convenience to choose axes in which the flow is statistically steady or has one or more velocity components zero. The above analysis can be repeated with the following results, where $\hat{\Omega}$ is the component of $\underline{\Omega}$ normal to the (x,y) plane.

$$\left. \begin{aligned}
 \text{Brunt-Väisälä frequency } \omega_{BV}^2 &= -2\Omega \left(\frac{\partial U}{\partial y} - 2\Omega \right) \\
 \text{Gradient Richardson number } Ri &= -2\Omega \left(\frac{\partial U}{\partial y} - 2\Omega \right) / \left(\frac{\partial U}{\partial y} \right)^2 \\
 \text{u-component production term} &= -\overline{uv} (\partial U / \partial y - 2\Omega) \\
 \text{v-component production term} &= \overline{uv} \cdot 2\Omega \\
 \text{Flux Richardson number} &= -2\overline{uv}\Omega / \overline{uv} \left(\frac{\partial U}{\partial y} - 2\Omega \right) \\
 \text{Monin Obukhov length } L_{mo} &= -(-\overline{uv})^{1/2} / 2\Omega K \\
 (L/K) / L_{mo} &= -2\Omega / \frac{(-\overline{uv})^{1/2}}{L}
 \end{aligned} \right\} \quad (89)$$

The three dimensionless parameters become equal to $-2\Omega / (\partial U / \partial y)$ or $-2\Omega / ((-\overline{uv})^{1/2} / L)$ in the local-equilibrium approximation when the speed of rotation is small. The analogue of buoyant convection occurs when the absolute vorticity $\partial U / \partial y - 2\Omega$ is zero and $R_f \rightarrow \infty$. Clearly there is a close relation between the parameters for curved flow analysed in fixed axes and rotating flows which are plane in rotating axes: to first order, 2Ω replaces $2U/r$, and the higher-order differences are all extra terms with coefficients of order unity, not, for once, of order 10.

In curved flow with radial density gradients the Brunt-Väisälä frequency becomes more complicated. The general form can be deduced from the displaced-element arguments of Thomann (4): the motion of the displaced element is assumed to be adiabatic which adds a further implausibility to the original Von Karman analysis. We find

$$\omega_{BV}^2 = 2 \frac{U}{r} \frac{\partial U}{\partial r} + 2 \frac{U^2}{r^2} \left(1 + \frac{\gamma-1}{2} M^2 \right) - \frac{U^2}{r} \frac{1}{T} \frac{\partial T}{\partial r} \quad (90)$$

where M is the Mach number, U /(speed of sound) $\equiv U / \sqrt{(\gamma-1)c_p T}$, which is obviously negligible in low speed flow. Our sign convention for r is opposite to Thomann's. Eq(90) can be rearranged in terms of the density gradient using the gas law and the radial-equilibrium equation $\partial p / \partial r = \rho U^2 / r$, to give

$$\omega_{BV}^2 = 2 \frac{U}{r} \frac{\partial U}{\partial r} + 2 \frac{U^2}{r^2} \left(1 - \frac{M^2}{2} \right) + \frac{U^2}{r} \cdot \frac{1}{\rho} \frac{\partial \rho}{\partial r} \quad (91)$$

If the Mach number is low, we get

$$\omega_{BV}^2 = \frac{1}{\rho r^3} \frac{\partial}{\partial r} (\rho U^2 r^2) \quad (92)$$

The stability criterion for inviscid variable-density flow originally due to Synge (121) is that this form of ω_{BV}^2 shall be positive: we note that this criterion is valid only at low Mach numbers because density changes due to pressure changes are neglected. If the total temperature of the flow, $T + U^2 / (2c_p) \equiv T(1 + (\gamma-1)M^2/2)$, is constant, which is a good approximation in boundary layers on adiabatic walls, we get

$$\omega_{BV}^2 = 2 \frac{U}{r^2} \left(1 + \frac{\gamma-1}{2} M^2 \right) \frac{\partial}{\partial r} (Ur) \quad (93)$$

the form given by Bradshaw (91). An equivalent expression is

$$\omega_{BV}^2 = \left(\frac{2}{\rho r} \frac{\partial P}{\partial r} \right) \quad (94)$$

where P is the total pressure, $p(1 + (\gamma-1)M^2/2)^{\gamma/(\gamma-1)}$: compare Eq(4b). The gradient Richardson number can again be defined as $\omega_{BV}^2 / (\partial U / \partial r)^2$. The flux Richardson number can be deduced from the transport equations for u^2 and v^2 for compressible flow given by Rotta. A new production term $\rho' \overline{v} U^2 / r$ appears, where ρ' is the density fluctuation: it can be explained as the product of the radial turbulent mass flux and the mean radial acceleration, which is a rate of doing work. We obtain

$$\begin{aligned}
 R_f &= \frac{-(\text{extra } v^2 \text{ -production})}{\text{total } u^2 \text{ -production}} \\
 &= 2 \frac{U}{r} \left(1 + \frac{1}{2} \frac{\rho' \overline{v} U}{\rho \overline{uv}} \right) / \frac{\partial}{\partial r} (Ur) \quad (95)
 \end{aligned}$$

and the "strong Reynolds analogy" of Morkovin (122) allows us to write, approximately, for flows with constant total temperature (adiabatic flows)

$$\frac{\rho'}{\rho} = (\gamma-1)M^2 \frac{u}{U} \quad (96)$$

where M is the local Mach number, so that to a good approximation the compressibility factor in Eq(95) can be written as $1 + (\gamma-1)M^2/2$ in agreement with Eq(93). Rotta's factor $1 + (\gamma-1)M^2$, which he did not specifically apply to a curvature parameter, is derived from the total production terms in the turbulent energy equation rather than from the separate contribution to $\overline{v^2}$. The present analysis seems preferable if only for reasons of consistency with the foregoing treatment in general and Eq(90) in particular, but one has to conclude that the effects of compressibility are not certain and must be elucidated by

experiment, even in adiabatic flows. In boundary layers with heat transfer the strong Reynolds analogy gives

$$\begin{aligned} \frac{\rho'}{\rho} &= (\gamma-1)M^2 \frac{u}{U} \left(1 + \frac{\text{Pr} Q_w}{U \tau_w} \right) = -(\gamma-1)M^2 \frac{u}{U} \cdot \frac{c_p \partial T / \partial r}{U \partial U / \partial r} \\ &= -\frac{u}{T} \frac{\partial T / \partial r}{\partial U / \partial r} \end{aligned} \quad (97)$$

where Q_w is the rate of heat transfer from the surface to the fluid and Pr is the molecular Prandtl number, and for want of more reliable data this could be used in the compressibility factor in Eq(95). However the Crocco temperature profile, another consequence of Eq(96), is apparently not reliable for flows with heat transfer. It is interesting to note that $\partial U / \partial r$ times the numerator of R_f [using the last element of Eq(97)] is equal to ω_{BV}^2 in Eq(90) without the term in U^2/r^2 . Once more, therefore, the gradient and flux Richardson numbers, obtained by different arguments, agree to the first order in curvature effects, being equal, to this order, to

$$2 \frac{U}{r} \left(1 - \frac{1}{2} \frac{U \partial T / \partial r}{T \partial U / \partial r} \right) / \frac{\partial U}{\partial r} .$$

In compressible flow, the parameter $(L/K)/L_{mo}$ becomes

$$\begin{aligned} \frac{L/K}{L_{mo}} &= \frac{\text{extra } \sqrt{v^2} \text{ -production}}{\text{dissipation}} \\ &= \frac{2}{R} \frac{U}{r} \left(1 + \frac{1}{2} \frac{\rho' v U}{\rho \bar{u} v} \right) / \frac{(-\bar{u}v)^{1/2}}{L} \end{aligned} \quad (98)$$

where any of the elements of Eq(97) can be used to evaluate the compressibility factor in parentheses: it becomes $(1 + (\gamma-1)M^2/2)$ on an adiabatic wall. $(L/K)/L_{mo}$ is again probably the most meaningful parameter if the local-equilibrium approximation fails.

It is interesting to note that the contribution of the density gradient to ω_{BV}^2 in Eq(91) is equal to ω_{BV}^2 in a buoyant flow with the gravitational acceleration g replaced by the centripetal acceleration U^2/R (note change of sign). Beer et al. (123) used this as the only term in the numerator of a "Richardson number" for analysing the stability of swirling flames, but - taking the case of low-speed flow in solid-body rotation ($U \propto r$) for the sake of example - we find that its ratio to the sum of the other contributions to the Brunt-Väisälä frequency in Eq(91) is

$$\frac{1}{4} \frac{r}{\rho} \frac{\partial \bar{\rho}}{\partial r}$$

which will be less than unity unless ρ varies more rapidly than $r^{\pm 4}$. Fahlbusch (124), discussing curved flows with density (temperature) differences, also uses a "Richardson number" based solely on the density gradient with g replaced by U^2/r . We note the useful property of the displaced-element analysis: different contributions to the force on the element in the direction of its displacement can simply be summed, so that contributions to ω_{BV}^2 can also be summed. Correspondingly, of course, different contributions to the $\sqrt{v^2}$ production in the numerator of R_f , Eq(69), can also be summed. A common example of multiple contributions to the numerators of R_i or R_f is curved flow in rotating axes. If the mean shear, curvature and rotation lie in the same plane, as in the case of flow over the curved rotating blades of a radial-flow turbomachine, no difficulties arise, and we get, for example,

$$\omega_{BV}^2 = 2 \frac{U}{r} \frac{\partial}{\partial r} (Ur) - 2\Omega \left(\frac{\partial U}{\partial r} - 2\Omega \right) \quad (99)$$

and to first order all the parameters become

$$R_i = R_f = \frac{L/K}{L_{mo}} = \frac{2 \left(\frac{U}{r} - \Omega \right)}{\partial U / \partial r} \quad (100)$$

5.2 PARAMETERS FOR THREE-DIMENSIONAL FLOWS

Flows in which the plane of the mean shear, the plane of curvature of the streamline and the plane of rotation of the axes (if any) do not all coincide present greater difficulties. As a general rule the displaced-element analysis is more complicated in such cases than the analysis based on Reynolds-stress transport equations, and its physical meaning is not always clear. For instance, if the plane of the mean shear does not coincide with the plane of curvature of the streamlines (which is also the nominal plane of oscillation of a displaced element) it is not immediately obvious whether the gradient Richardson number should be based entirely on velocity and curvature in the plane of curvature or whether the denominator should still contain the resultant mean shear. In cases such as linearly-growing axisymmetric swirling shear layers the plane of curvature of the streamline is still normal to the surfaces containing the shear layer [Fig.15(a)] so that the motion of a displaced element is still relevant to the transfer of momentum normal to the shear layer, but in more general three-dimensional flows such as those on swept wings the streamline curvature may have a component in the surfaces containing the shear layer and it is not obvious how the "centrifugal force" should be resolved.

Therefore we will abandon the gradient Richardson number and analyse three-dimensional flows in terms of the flux Richardson number

$$R_f = - \left(\frac{\text{extra } \overline{v^2} \text{ production}}{\text{sum of } \overline{u^2} \text{ and } \overline{w^2} \text{ production}} \right) \quad (101)$$

where in all our systems of axes the v component is normal to the plane of the shear layer and the main Reynolds-stress gradients are the gradients of \overline{uv} and \overline{vw} in the direction of v . There remains the problem of partitioning the effects of curvature between \overline{uv} and \overline{vw} : virtually the only simple and plausible hypothesis (an echo of displaced-element ideas) is that the effect of curvature is to alter the mean product of v with the velocity component along the streamline, so that the effect on \overline{vw} is to the effect on \overline{uv} as W is to U . Bradshaw (125) implied that the effect of curvature was a change in magnitude of the shear stress without change in direction, which is less plausible. The present hypothesis may provide a partial explanation of the measurements of Johnston (126) in the unstably-curved flow up a swept step: he found that the shear stress vector skewed in the same direction as the velocity, rather than in the same direction as the velocity gradient as would normally be expected. There are virtually no other data suitable for checking this hypothesis: note that the "effect on shear stress" may be an alteration to a term in the transport equation rather than a factor on the shear stress itself, depending on what calculation method is being used.

In (x, r, θ) coordinates (without the restriction of axisymmetry) the transport equations given by Rodi (17) lead to

$$R_f = \frac{2 \frac{W}{r} \overline{vw} - \overline{u_i v} \frac{\partial v}{\partial x_i}}{\overline{u_i u} \frac{\partial u}{\partial x_i} + \overline{u_i w} \frac{\partial w}{\partial x_i} + \overline{w^2} \frac{v}{r} + \overline{vw} \frac{W}{r}} \quad (102)$$

where the terms in u_i are summed over all three values of i , and where as in two dimensions we have counted the "rotation-of-axis" terms as production. To the axisymmetric slender-shear-layer approximation, implying $\partial/\partial r \gg \partial/\partial x$ and $\partial/\partial \theta = 0$, this becomes

$$R_f = \frac{2 \frac{W}{r} \overline{vw}}{\overline{uv} \frac{\partial u}{\partial r} + \overline{vw} \frac{\partial w}{\partial r} + \overline{vw} \frac{W}{r}} = \frac{2 \frac{W}{r} \overline{vw}}{\overline{uv} \frac{\partial u}{\partial r} + \frac{\overline{vw}}{r} \frac{\partial}{\partial r} (Wr)} \quad (103)$$

In local equilibrium $\overline{vw}/\overline{uv} = (\partial w/\partial r)/(\partial u/\partial r)$, and for small curvature effects $W/r \ll \partial w/\partial r$, so that to this approximation

$$R_f = \frac{2 \frac{W}{r} \frac{\partial w}{\partial r}}{\left(\frac{\partial u}{\partial r} \right)^2 + \left(\frac{\partial w}{\partial r} \right)^2} \quad (104)$$

which is the first approximation to

the gradient Richardson number

$$Ri = \frac{2 \frac{W}{r^2} \frac{\partial}{\partial r} (Wr)}{\left(\frac{\partial u}{\partial r} \right)^2 + \left(\frac{\partial w}{\partial r} \right)^2} \quad (105)$$

with ω_{BV}^2 evaluated from the circumferential motion only and with the denominator put equal to the square of the resultant (not only circumferential) mean shear. This can be regarded as a justification for deriving Ri from a displaced-element analysis in the manner indicated, a derivation used on the basis of intuition by Bradshaw (125) for the boundary layer on an infinite swept wing and by Bradshaw (91) and Cham and Head (127) for the boundary layer on a rotating cylinder in an axial non-rotating stream. Another, less satisfactory, justification is that uniform translation in the axial direction obviously leaves the two-dimensional result for ω_{BV} unaltered since there is no component of curvature in the axial direction, and that radial variation of the axial velocity ought not to have much effect. Howard and Gupta (39) derive Ri for swirling flows from a rigorous consideration of the inviscid instability equations: for the case of axisymmetric disturbances the denominator of their version of Ri is $(\partial w/\partial r)^2$ only, but it does not of course have the significance of the square of a turbulence frequency.

The "three-dimensional" form of the mixing length formula [actually Eq(27) rewritten in oblique axes] is

$$\left. \begin{aligned} \frac{\partial u}{\partial r} &= \frac{-\overline{uv}}{|\tau|^{1/2} L} \\ \frac{\partial w}{\partial r} &= \frac{-\overline{vw}}{|\tau|^{1/2} L} \end{aligned} \right\} \quad (106)$$

where

$$|\tau|^2 = (\overline{uv})^2 + (\overline{vw})^2 \quad (107)$$

and the magnitude sign on τ will be omitted henceforth. Using this we can rewrite Eq(104) as

$$R_f = \frac{-2 \frac{W}{r} \overline{vw}}{\tau^{3/2} L} \quad (108)$$

which is probably the most convenient form for axisymmetric swirling flows. For flow over infinite swept wings and other cases in which the shear layer lies in a cylindrical surface [Fig.15(b)] we can rewrite Eq(108) in (s, n, z) coordinates with z measured along the straight generators and $r \equiv n + R$;

$$R_f = \frac{-2 \frac{U}{r} \overline{uv}}{\tau^{3/2}/L} \quad (109)$$

Note that the formula does not contain dR/ds and is therefore nominally valid even when dR/ds is non-zero. Note also that the denominator of Eq(108) (the energy dissipation) is probably a more meaningful quantity than the denominator of Eq(103) (the u^2 and w^2 production) if the two differ greatly because of large departures from local equilibrium: in effect, Eq(108) is $(L/K)/L_{mo}$ [compare Eq(84)]. The "exact" form of R_i for a cylindrical surface is given on p.437 of Ref.125: it reduces to Eq(109) on using Eq(106); the approximation to R_i given in Ref.125 results from using Eq(27) directly and is accurate only when τ is nearly normal to the generators.

The case of a shear layer with compound curvature such as a boundary layer on a surface of general curvature [Fig.15(c)] presents a further difficulty of principle already encountered in two dimensions: what axes should we choose for evaluating R_f ? Note that we cannot simply choose arbitrary orthogonal coordinates in the surface, s and z say, and generalize the numerator of (109) to

$$-2 \left(\frac{U}{n+R_s} \overline{uv} + \frac{W}{n+R_z} \overline{vw} \right)$$

where R_s and R_z are the "radii of curvature" of the s and z axes, because these radii are normal to the surface only if the surface is developable. The normal to the surface that passes through the streamline will clearly have different directions at different positions along the streamline: it will rotate in the plane containing itself and the streamline because of the curvature of the streamline, just as the n -axis rotates in two-dimensional (s,n) coordinates, but it will also rotate normal to this plane. We will call this the "torsion" effect: note that it is not exactly the torsion of the streamline. If the production term in the numerator of R_f refers to the fluctuating velocity component along the normal to the surface, the torsion will give rise to extra rotation-of-axis contributions of the type which we have hitherto grouped with the true production. These are not mere geometrical difficulties but reflect a real gap in our knowledge of turbulence: does streamline torsion, as well as streamline curvature, produce effects of order F on the turbulence? The problem can be disguised in the case of axisymmetric swirling flows and other shear layers lying in developable surfaces, because a system of axes in which the torsion is zero can be set up, as was done in the analysis leading to Eqs (108) and (109). However the torsion in the streamline axes discussed above is still finite, so that although R_f can be satisfactorily defined for developable flows it is not certain that F -factors derived from experiments on the corresponding two-dimensional flows can be immediately applied. Most of the aeronautical flows whose response to streamline curvature we can reasonably hope to predict are nearly developable, so that a simple rule which has the advantage of consistency with the above analysis for developable flows is to evaluate R_f by using Eq(109) with s in the direction that makes U/R (strictly, U/r) a maximum, where R is the radius of curvature of the intersection of the surface and a plane normal to the surface and tangent to the streamline. In effect, since we seek a parameter to describe the effect of an extra rate of strain we choose the larger principal value of the extra rate of strain, at least in dealing with flows in which the smaller principal value is small. If x and z are arbitrary orthogonal coordinates in a developable surface, R_x and R_z the radii of curvature in these directions and U' and W' the mean velocity components, then the radius of curvature R and mean velocity U in any chosen s direction are related by

$$\frac{U^2}{R} = \frac{U'^2}{R_x} + \frac{W'^2}{R_z} \quad (110)$$

and if $R_z \gg R_x$ the maximum value of U/R will usually occur when s is close to x unless U' happens to be small. Finally we note that if the directions of the shear stress, velocity and velocity gradient coincide any system of coordinates gives the same result in the simple formulae like Eq(104) and Eq(109), by virtue of Eq(110), so that in mildly three-dimensional flows the uncertainties discussed above are unimportant.

In compressible flows, we can multiply the simple three-dimensional formulae by the compressibility factors used in two dimensions (e.g. Eq 95). Fresh agonies of indecision arise over the choice of axes but it is again unimportant in mildly three-dimensional flows so that the axes used for the main part of R_f may be retained. Note that Eq(96) becomes

$$\frac{\rho'}{\rho} = \frac{(\gamma-1)}{a^2} (Uu + Ww) \quad (111)$$

so that the final result for a three-dimensional, compressible, adiabatic flow, with the axes chosen to maximise U/R , is

$$R_f = \frac{-2 \frac{U}{r} \overline{uv} \left(1 + \frac{\gamma-1}{2} \left(\frac{U^2}{a^2} + \frac{UW}{a^2} \frac{\overline{vw}}{\overline{uv}} \right) \right)}{\tau^{3/2}/L} \quad (112)$$

where a is the local speed of sound and $\tau^2 = (\overline{uv})^2 + (\overline{vw})^2$. Clearly, if the velocity and shear stress vectors are in the same direction the compressibility factor becomes $1 + (\gamma-1)M^2/2$, where M is the resultant Mach number, as in two dimensions: this form will usually be accurate enough.

A case of some practical importance in which the velocity, velocity gradient and shear stress directions unexpectedly coincide is the boundary layer between a circular cylinder of radius r_0 , rotating about its axis at angular velocity Ω , and a non-rotating axial stream of speed U_e . The following analysis applies either to external flow (flow over the rotating hub of an axial-flow turbo-machine) or to internal flow (in a rotating machine casing). The boundary layer seen in coordinates rotating with the cylinder is found to be collinear: not only do the above-mentioned directions coincide but they are the same at all distances from the surface (to the approximation that the boundary layer thickness δ is small compared to r_0). In (x,r,θ) coordinates rotating with the cylinder, and denoting $\Omega r_0/U_e$ (the tangent of the constant helix angle of the streamlines) by λ , the gradient Richardson number is

$$R_f = \frac{2 \frac{W}{r_0} \overline{vw} - 2 \overline{vw} \Omega}{\overline{uv} \frac{\partial U}{\partial r} + \overline{vw} \left(\frac{\partial W}{\partial r} + \frac{W}{r_0} - 2\Omega \right)} = \frac{-2 \lambda \Omega \left(1 - \frac{U}{U_e} \right)}{(1 + \lambda^2) \frac{\partial U}{\partial r} - \left(2 - \frac{U}{U_e} \right) \Omega} \quad (113)$$

where the first term in the final numerator is the rotation contribution and the second the curvature contribution: here we have added the terms in the numerators and denominators of the versions of R_f Eq(103) (changing U to \overline{W}) and Eq(89). A gradient Richardson number can be derived [a displaced element oscillates radially and $\omega_{\theta V}$ can be evaluated by considering only the circumferential curvature, as outlined following Eq(104)]. We get

$$Ri = \frac{2 \frac{W}{r_0^2} \frac{\partial}{\partial r} (W r) - 2\Omega \left(\frac{\partial W}{\partial r} - 2\Omega \right)}{\left(\frac{\partial U}{\partial r} \right)^2 + \left(\frac{\partial W}{\partial r} \right)^2} \quad (114)$$

given in more compact form by Cham and Head (127) and for $\partial W/\partial r$ large compared to W/r or Ω (requiring δ/r_0 , but not necessarily λ , to be small) we get

$$Ri = R_f = \frac{-2 \lambda \Omega (1 - U/U_e)}{(1 + \lambda^2) \partial U/\partial r} = \frac{-2 U_e}{r} \frac{\lambda^2 (1 - U/U_e)}{(1 + \lambda^2) \partial U/\partial r} \quad (115)$$

identical with the form given by Bradshaw (91) except for the incorrect sign of Ri in the latter.

Now the above analyses, both for two-dimensional and for three-dimensional flow, simply define Richardson number analogues for the different cases: we cannot expect the quantitative effect of streamline curvature to be exactly the same function of Richardson number in all cases. In particular we cannot expect a universal critical Richardson number above which turbulence is suppressed. It is possible to evaluate sufficient (though perhaps not necessary) conditions for stability of complicated inviscid curved or buoyant flows against infinitesimal disturbances: these take the form $Ri > n$ where the number n is frequently $1/4$ as in the analysis of Howard and Gupta (39) who give a useful introduction to analyses for cylindrical swirling flows, including the early work of Ludwig. In view of the marginal relevance of these analyses to turbulent flow a general review will not be given here. One of the latest studies, which will serve to indicate the state of the art, is that of Kurzweg (128). In an extension of Howard and Gupta's analysis for arbitrary disturbances (itself a development of Rayleigh's energy analysis and related to Ludwig's less rigorous work) Kurzweg has obtained a sufficient condition for stability of variable-density low-speed cylindrical swirling flows, although it is not entirely clear how Kurzweg has overcome the limitations in Howard and Gupta's analysis pointed out by them. Kurzweg's sufficient condition is, in our notation with U, V, W the velocity components in the x, r, θ directions

$$\left. \begin{aligned} & \left[\frac{1}{\rho r^3} \frac{d}{dr} (\rho W^2 r^2) - \frac{1}{4} \left(\frac{dU}{dr} \right)^2 \right] \left[\frac{W^2}{r} \cdot \frac{1}{\rho} \frac{d\rho}{dr} - \frac{1}{4} r^2 \left(\frac{d}{dr} \left(\frac{W}{r} \right) \right)^2 \right] \\ & \geq \left(\frac{dU}{dr} \right)^2 \left[\frac{W}{r} + \frac{r}{4} \frac{d}{dr} \left(\frac{W}{r} \right) \right]^2 \end{aligned} \right\} \quad (116)$$

and

$$\left(\frac{W^2}{r^3} \frac{1}{\rho} \frac{d\rho}{dr} \right) \left(\frac{d}{dr} \left(\frac{W}{r} \right) \right)^2 \geq \frac{1}{4}$$

The second clause of the condition is simply a requirement that the second factor in the first clause be positive: unfortunately it restricts the analysis to flows with significant stabilizing density gradients (such as swirling flames or jets of light gas) and no comparison can be made with stability conditions for constant-density flows except to note that the ratio of the two terms in the first factor of the first clause is four times a Richardson number based on the axial shear, corresponding to $Ri > 1/4$ for stability. Kurzweg's criterion, like Synge's, is restricted to low-Mach-number flows. Chigier (129) has given a graphical representation of the first clause of Kurzweg's condition but appears to have ignored the second clause. In addition to noting the particular limitations of Kurzweg's criterion (the most general of those proposed to date) we must remember that all criteria of this type refer to the stability of inviscid flows to infinitesimal wavelike disturbances and no rigorous deductions can be made about turbulent flow. We have already seen, for instance, that Howard and Gupta's Richardson number, whose denominator contains only the circumferential shear, disagrees with the flux Richardson number derived from the turbulent energy equations. At best, inviscid-flow criteria indicate dimensionless parameters of which the turbulent intensity is likely to be a (unique? monotonically-decreasing?) function. The value of such a parameter at which the intensity falls to zero may not be unique and will almost certainly be different from any critical value derived for inviscid flow, even if that critical value is necessary as well as sufficient. In view of the uncertainties outlined in the derivation of R_f for three-dimensional flow it would be unrealistic to use any very elaborate analysis for this case: we conclude that the quasi-two-dimensional parameter Eq(112) is likely to suffice until our experimental knowledge of three-dimensional curved flows improves.

A guide to the parameters derived in Sections 5.1 and 5.2, with recommended approximations for use in cases of small curvature effects, is given in Table 2.

5.3 USE OF THE PARAMETERS

To use the parameters such as Richardson number derived for turbulent flow we define an F -factor by

$$F = 1 - \frac{\alpha}{2} Ri \quad (117)$$

[for Ri read R_f or $(L/K)/L_{m0}$] which in the simplest form becomes

$$F = 1 - \frac{\alpha U/r}{\partial U/\partial r} \quad (118)$$

or $1 + \alpha(\partial V/\partial x)/(\partial U/\partial y)$ in rectangular Cartesian coordinates, a special case of Eq(32). In the present state of development of the subject it would be unwise to be dogmatic about the validity of non-linear F -factors or the full, large-curvature versions of the parameters. One can be certain that in most cases the effects of flow history will be more important than these refinements to local formulae, which should therefore be made only in calculation methods based on transport equations, including a transport equation for length scale or at least a lag equation like Eq(37). One cannot expect α to be an absolute constant: it will vary to some extent from one part of a shear layer to another as well as from one type of shear layer to another, and, since the F -factor approach involves assumptions of local equilibrium for predicting the size of the F -factor, the variation of α will be greatest in flows far from local equilibrium. The effect of mean transport on the F -factor can be allowed for empirically by a lag equation, but the effect of turbulent transport on the F -factor is difficult to assess. Conversely the effect of the F -factor (i.e. the extra strain rate) on the turbulent transport is likely to be large in strongly-unstable flows.

Both Prandtl (80, p.775) and Bradshaw (91) implied that meteorological data could be used to find α . A brief review of quantitative results for buoyant flows is given in the next sub-section, but we already know enough about curvature effects for the simpler meteorological formulae of the F -factor type to be of no further use, and the more refined meteorological results for the atmospheric inner layer are unlikely to be reliable quantitative guides to more refined formulae for curved flows in general. Qualitatively, there is still much to learn from buoyant flows and the next section consists mainly of a comparison of the phenomena of curved and buoyant flows.

Quantitative results, for α and otherwise, obtained in curved shear layers are discussed in later Sections. Practical details of the incorporation of formulae like (117) in calculation methods are treated in Section 11.

5.4 QUANTITATIVE USE OF BUOYANT-FLOW DATA

There are few laboratory data on buoyant shear layers, as opposed to free convection, and we therefore turn to meteorological data (89, 114, 115). These, while large in number, are limited in application because they nearly all refer to the traditional area of meteorological turbulence studies, the inner layer of the Earth's boundary layer. Strictly an "inner layer" must have a shear stress which is constant in magnitude and direction, and the Earth's inner layer, so defined, is only a few tens of metres thick. However, to the necessarily low standards of accuracy of atmospheric turbulence measurement the flow in the first few hundred metres often has a sufficiently small shear-stress gradient and crossflow angle to be analysed by using inner-layer variables. The actual height up to which inner-layer analysis is valid depends greatly on the stability [as defined by the Richardson number or by $(L/K)/L_{m0} \equiv y/L_{m0}$], and on the age of the inner layer. The age depends on the length of time for which the mean wind speed and direction have been constant at the point of observation and also on the upstream distance or "fetch" for which the surface is homogeneous. Usually, measurements are made — or trusted — only if the surface is homogeneous for an upstream distance of the order of 100 times the maximum height of observation, and if the wind has been constant for the time needed to cover this distance. In these conditions, and excluding cases of extreme stability or instability (very light winds), the inner layer is a local equilibrium region: horizontal transport of turbulent energy by the mean flow and vertical transport by the turbulence are found to be negligible. In strongly-stable flow transport by internal waves may be appreciable and in strongly unstable flow vertical transport by convection cells is observed.

In nearly-neutral conditions the total thickness of the Earth's boundary layer (i.e. the region of significant Reynolds stress) is limited by the effects of the Earth's rotation (the flow is called the Ekman spiral). The external stream of this strongly three-dimensional boundary layer is called the geostrophic wind which — according to the equations of frictionless flow — blows along the isobars. In stable conditions the Richardson number increases with height, so that the turbulence dies out: on top of the turbulent region is a thin region of very strong stability, called the inversion layer. In unstable conditions the Richardson number becomes more negative with increasing height, in the absence of condensation of water vapour, and eventually convection cells become important: in extreme conditions cumulus clouds can reach heights near 20 km but these and the other spectacular atmospheric phenomena are greatly influenced by condensation of water vapour and are not relevant to the analogy with curvature. However there is already evidence that convection cells (longitudinal vortices) occur in unstable curved flows and that the boundary of the turbulent region in a stable curved flow can be rather sharp. There do not seem to be any useful data on the interaction of buoyancy and three-dimensionality in the Ekman spiral. This is particularly unfortunate because of the lack of information on three-dimensional boundary layers on curved surfaces. The paper by Tennekes (130) discusses free convection above the surface layer but three-dimensional effects are barely mentioned.

The standard method of correlating data for the atmospheric inner layer (89) is to plot quantities made dimensionless by the usual inner layer variables $u_\tau \equiv (\tau_w/\rho)^{1/2}$ and y against y/L_{m0} or R_f . If the assumption of local equilibrium is valid the plot should be universal. The dimensionless velocity gradient $(Ky/u_\tau)\partial U/\partial y$, usually given symbol ϕ , is the ratio of the mixing length in neutral conditions ($l_0 \equiv Ky$) to its value in buoyant conditions, l . Fig.16 shows a consensus of recent experimental results, favouring the measurements presented in (89). The scatter of the latter measurements is very small by meteorological standards, but the apparent value of K was 0.36, rather than the accepted laboratory value of 0.41. The simplest of the correlation formulae, the Monin-Obukhov formula (114) is

$$\frac{Ky}{\ell} \equiv \phi = 1 + \beta \frac{y}{L_{mo}} \quad (119)$$

where β is about 4.5 for negative y/L_{mo} (unstable conditions) and about 7 in stable conditions. This piecewise-linear formula is plotted on Fig.16: clearly it is at best a rough approximation for small buoyancy effects. The curved-flow version [retaining the standard definition of ℓ , $\partial U/\partial y = (-\overline{uv})^{1/2}/\ell$] can be rewritten to a first approximation as

$$\frac{\ell}{\ell_0} = 1 - 2\beta \frac{U}{R} \frac{(-\overline{uv})^{1/2}}{L} \quad (120)$$

where in the inner layer the denominator of the right hand side is u_τ/Ky which is equal to $\partial U/\partial y$ in near-neutral conditions. Thus the analogue of the Monin-Obukhov formula for curved flow is an example of the linear F-factor correction formula for the effect of extra rate of strain, Eq(36): the use of different values of $2\beta \equiv \alpha$ according to the sign of rate of strain is a refinement which may be usable in other situations but cannot strictly be described as a linear correction formula.

Results such as those in Fig.16 justify more refined analytical formulae in the Earth's inner layer. The two reasons why it is probably not worth relating them quantitatively to curved flows are that the buoyancy/curvature analogy is not exact and that inner-layer formulae are not enough. We are of course entitled to use meteorological data to suggest the general form of second-order correction formulae for curvature.

We note that in buoyant flow and rotating flow L_{mo} is independent of y so that the Monin-Obukhov correction to the mixing length formula integrates to give, in the usual engineering form of the logarithmic law for the inner layer,

$$\frac{U}{u_\tau} = \frac{1}{K} \log \frac{u_\tau y}{\nu} + C + \beta \frac{y}{L_{mo}} \quad (121)$$

In curved flow $L_{mo} \propto U$ and the integral is of the form Eq(44), although the simplification suggested after Eq(44) is probably adequate.

This is not the place for a general review of buoyancy effects. Refs 114 and 115 are general treatments and Ref.1 has a comprehensive list of references on complex turbulent flows, including buoyant flows with special reference to the atmospheric surface layer. For evidence of spectacular collapse of turbulence in a strongly-stable laboratory boundary layer see Ref.131 and for a general review of laboratory simulation of the atmospheric boundary layer see Ref.132. We pass on to qualitative consideration of curvature effects: the analogy with buoyancy will continue to be qualitatively helpful.

5.5 LONGITUDINAL VORTICES

One of the most striking phenomena of unstable curved or buoyant shear layers is the appearance of longitudinal (streamwise) vortices. They were found in unstable laminar flow between rotating cylinders by Taylor (72), and Tani (102) attributes their discovery in buoyant flows to Idrac, in a 1921 PhD thesis which I have not seen. Görtler (77) predicted their appearance in laminar boundary layers on curved surfaces in 1940 but they were not found until 1950 (78). The earlier workers on curved or rotating turbulent flows seem not to have expected to find steady vortices (i.e. spanwise periodicity of the mean flow) although it must have been fairly clear from Taylor's experiments that streamline curvature would favour unsteady longitudinal-roll eddies. Karman (13) suggests that Wattendorf's duct measurements may have been influenced by conventional secondary flows in the corners but did not consider the possibility of longitudinal vortices in the central part of the span. Even Pai (85: 1943) working under Karman on rotating cylinders, clearly took some time to realise that the anomalies in his velocity profiles were caused by vortices similar to those found by Taylor in laminar flow. Tani (102: 1962) who first found vortices in a curved boundary layer, seems to have argued from analogy with Görtler's treatment of laminar flow that vortices would be expected in turbulent flow. Johnston and his collaborators (10) found vortices in fully-developed flow in a rotating duct, whereas they were not noticed in the older curved duct experiments. (Johnston's elegant use of flow visualization was instrumental in the discovery.) Vortices have still not been observed in curved free jets or wall jets.

Confusion can arise over the definition of a longitudinal vortex in turbulent flow: there is always some fluctuating longitudinal vorticity, even in a plane flow, while Johnston et al. (10) found that there was always some unsteadiness in the vortices visualized by dye. Their remarks bear quoting. "In the range of $Ro_Q [\equiv \Omega \times \text{duct height}/\bar{U}]$ where cells are first seen ($0.02 < Ro_Q \leq 0.04$) the flow is very unsteady and sometimes cells form, decay, wash-out and wave about in a very unsteady manner. Only at higher rates of rotation are 'steady' cell patterns observed. We call them 'steady' in the sense that the time period over which a given pattern persists is long relative to the turbulence time scales." Now even such "steady" vortices will contribute to the longitudinal mean vorticity only if their lateral positions are constrained within a range rather smaller than one spanwise wavelength. To take a simple case, if the pattern shown in Fig.6 alternated between the configuration shown and one shifted spanwise by half a wavelength the mean longitudinal vorticity would be zero. Let us call vortices that are sufficiently constrained to produce longitudinal mean vorticity (i.e. spanwise periodicity) steady (without quotation marks) reserving Johnston's term "steady" (with quotation marks) for vortices which are not necessarily weaker than steady ones but which happen not to be sufficiently constrained. The possibilities of constraint are

1. The influence of lateral boundaries. The number of vortices must be an integer, so that lateral displacement implies distortion of the cross-section of one or more vortices, which one would expect to be resisted. This mechanism probably acts only if there is some strong tendency for vortices not to disappear, as in the case of the flow between rotating cylinders where the same fluid recirculates. However we know from Coles' experiments (71) that the number of vortices in laminar flow between rotating cylinders can change in quite a complicated way. Another case where disappearance is unlikely is a low-aspect-ratio flow where the number of vortices is so small that disappearance of one would change the wavelength by a large

fraction: the preferred wavelength of near-circular rolls occupying most of the shear layer is bound to be close to two shear-layer widths (wavelength is twice vortex diameter).

2. The influence of upstream disturbances. Test-rig shear layers always have small spanwise inhomogeneities of the mean flow caused by imperfections in the upstream flow (notably disturbances, apparently longitudinal vortices, introduced by the anti-turbulence screens). These inhomogeneities will probably have some influence on the mean spanwise positions of vortices arising in unstable curved flows: as usual in flows unstable to infinitesimal disturbances the instability pattern can be locked to the initial disturbances. However the amplitude of, say, the spanwise variation of mean velocity in the initial shear layer is likely to be quite small compared to the turbulent velocity fluctuations, so that the initial disturbances may locate only regions of higher-than-average probability of the occurrence of a 'steady' vortex of given sign. It is significant that the most intense vortices (i.e. the largest spanwise variations in mean velocity) are those observed by Mackrodt (133) in the boundary layers in an annular duct, with swirling flow introduced by a row of blades like an axial turbomachine stator. Although the wakes of the blades were undetectable in the free stream or the stable hub boundary layer far downstream, it seems very likely that they located the position of the vortices. Notice that the vortices themselves act as upstream disturbances to the flow further downstream: as Tani showed, the number of vortices in a boundary layer can remain constant while the boundary layer thickness changes by a factor of 2:1 or more. The number of vortices must eventually change if the wavelength is not to become a small fraction of the boundary layer thickness: we do not yet know whether vortices would disappear one by one or whether there are intervals in x in which large changes occur before the vortex pattern settles down again. Indeed this question has not been answered even for laminar flow (mainly because transition occurs shortly after the vortices become distinguishable).

If neither of these influences constrains the vortex position sufficiently, no spanwise periodicity will be found in the mean flow. However it is clear that the behaviour of flow properties averaged both in time and in spanwise distance will be virtually the same for a given strength of vortex whether the vortices are constrained or not: the distinction is man-made. We should therefore measure vortex 'strength' in a way that will give the same answer whether the vortices are constrained or not: that is, we should measure fluctuations with respect to mean values averaged both in time and in spanwise distance, and ignore the distinction between spatial and temporal fluctuations. Therefore we define the mean of a quantity Q as

$$\bar{Q} = \lim_{(b \rightarrow \infty, T \rightarrow \infty)} \frac{Lt}{bT} \int_0^b \int_0^T Q(z, t) dz dt \quad (122)$$

the order of the limits being immaterial if the process is statistically stationary in z and t . Experimentally this could be done by traversing the measuring instruments slowly spanwise while taking time averages (the lower frequency limit being chosen much smaller than the apparent passing frequency of the vortices). Favre (134: 1960) has discussed double-averaging schemes with reference to boundary layers with steady spanwise periodicity: Gupta, Laufer and Kaplan (135) have discussed variable-time averaging with reference to flows with longitudinal streaks that are "steady" only in Johnston's sense. Vortex 'strength' could be defined in terms of the mean-square circulation around — say — a square contour of side δ in the yz plane (see Ref.26, §6.4 for a general discussion). It may be necessary to consider the structure of the vortices in detail for some practical purposes such as estimating the behaviour of separation lines, as well as for basic research purposes.

Johnston's description makes it clear that there is a continuous sequence of events with increasing curvature parameter, corresponding to increasing vortex 'strength' as defined above. It seems very likely that there is no critical Richardson number or bulk rotation parameter at which vortices suddenly appear: our whole experience of turbulent flow suggests that unsteadiness of the flow ensures gradual changes, since if any velocity profile corresponds to the steady velocity profile assumed in hydrodynamic stability calculations it is the instantaneous profile and not the mean. However the change from the ordinary case of momentum transfer by conventional Reynolds stresses to momentum transfer principally by "steady" vortices may take place over a relatively small range of rotation number. In the atmospheric inner layer, data [see Zilitinkevich(136:1972)] suggest that the change from forced convection to free convection (corresponding roughly to the change from Reynolds stress dominance to "steady" vortex dominance) can occur within the range $0.02 < -Ri < 0.05$, where Ri is evaluated at a representative height. If we take $Ri = 2\Omega/(\partial U/\partial y)$ and $\partial U/\partial y = 0.3U/(\frac{1}{2}h)$, h = duct height, in Johnston's experiments, this corresponds to $0.007 < Ro_Q < 0.017$, rather lower than the value of Ro_Q at which vortices first appeared in Johnston's flow patterns and considerably less than the value of about 0.07 at which a significant region of constant angular momentum (the analogue of free convection) appeared in the duct. Let us merely register the possibility — not thoroughly explored in Johnston's experiments — that the change from conventional turbulence to vortex domination may take place fairly rapidly, but probably at a Richardson number or rotation parameter several times that at which the vortices are first seen in flow patterns.

Tani (102) suggested that an estimate of the critical curvature parameter for the appearance of vortices (by which he meant spanwise periodicity of the mean flow) could be obtained by substituting an eddy viscosity for the molecular viscosity in the critical value of the Gortler number for a laminar boundary layer. Direct use of the value for a Blasius profile is not realistic but detailed analyses of the stability of curved turbulent flows to longitudinal vortex disturbances have been made by Sandmayr (137) and by Lezius and Johnston (76). In both cases an assumed distribution of eddy viscosity and an assumed shape of disturbance was used to convert the problem into a classical solution for the eigenvalues of the Orr-Sommerfeld stability equation for the turbulent mean velocity profile. Sandmayr used the eddy viscosity for a plane flow and deduced a preferred spanwise wavelength for the most unstable disturbance — the one that, according to the Orr-Sommerfeld equation, appears first as the curvature parameter increases. The results agree well with Tani's measurements although Smith (138) has pointed out the extreme difficulty of calculating accurate values for the wavelength of Taylor-Gortler vortices in laminar flow: these purely mathematical difficulties are additional to the practical difficulty that the wavelength may be constrained by the need for an integral number of vortices. Lezius and Johnston use an eddy viscosity for rotating duct flow that varies as an empirical F -function of the gradient Richardson number and a wall stress that varies as an empirical function of the bulk rotation number $Ro_Q \equiv \Omega h/\bar{U}$. In fact, the "critical" rotation number is little altered by this refinement, falling from about 0.03 to 0.022,

and the "critical" wavelength is almost constant at 1.4 times the duct height. The word "critical" is enclosed in quotation marks because it is rather difficult to be sure exactly what the values mean. There is obviously some change in turbulence structure, specifically in the longitudinal vorticity fluctuations, even for very small streamline curvature; and there is still some unsteadiness in the observed longitudinal vortices even for very large curvature. Despite the good agreement between the calculated critical rotation number and the value at which distinct longitudinal vortices were first seen in the flow-visualization experiments of Lezius and Johnston it seems to the present author that the stability analysis and the assumed eddy viscosity together introduce a spurious "trigger level", a rather arbitrary value of curvature parameter at which the tendency to spanwise periodicity becomes mathematically distinguishable from the spanwise-invariant turbulence model. Since the "trigger level" is not too sensitive to the turbulence model (i.e. the details of the eddy viscosity assumptions) the analysis may be very useful for comparative purposes, providing a quantitative measure of the likelihood of occurrence of longitudinal vortices (unsteady, "steady" or steady) in different flows.

The remaining questions concern the presence of spanwise periodicity in curved duct flows — as opposed to rotating ones — and in free jets and wall jets. It seems very likely that "steady" vortex patterns may not exist in jets because the growth rate is so large that frequent readjustment of the spanwise wavelength would be needed to keep it near the preferred multiple of the shear-layer thickness. High-aspect ratio, fully-developed duct flows will not be significantly constrained by lateral boundaries, and the effect of disturbances in the intake flow will disappear at large distances downstream, so that there may be very little tendency for the vortex pattern to become "steady": however this argument applies almost as well to Johnston's rotating duct (aspect ratio 7) as to the curved ducts of Wattendorf (aspect ratio 18) and of Eskinazi and Yeh (aspect ratio 15.5) and is not a very convincing explanation of the presence of "steady" vortices in the first flow and their absence from the others, because the values of the curvature parameter in the curved ducts correspond to rotation numbers Ro_0 of between 0.1 and 0.2. More work is clearly needed; careful searches for longitudinal vortices should be made in any experiments on unstable curved flows, and it would be interesting to have theoretical "critical" values of Ro or Ri for flows other than Sandmayr's boundary layer and Lezius and Johnston's rotating duct.

The latest information about longitudinal vortices or "rolls" in the atmospheric boundary layer is given in Refs 139 and 140. There is as yet no evidence that vortices resulting from unstable stratification or curvature develop stable non-turbulent cores.....

5.6 INTERNAL WAVES

Stably-stratified buoyant flows can support internal waves. These are "transverse" waves with particle velocities substantially normal to the phase velocity, whose direction is that in which the crests and troughs propagate. "Longitudinal" waves, with particle velocities in the same direction as the phase velocity, necessarily involve compression and expansion of the fluid which we neglect. The propagation of energy, described by the terms in the Reynolds-stress transport equations which we have so far called the "turbulent transport" terms, may occur in a different direction to the propagation of crests and troughs.

There is still some controversy about coexistent waves and turbulence, even in stratified flows. For instance Pao (141) speaking at a colloquium whose proceedings form an excellent introduction to meteorological turbulence, says "(i) internal waves and turbulence coexist in turbulent stratified flows with internal waves at the large scales [wavelengths] and turbulence at the small scales; (ii) turbulence decays [in a stratified wake] much more rapidly than internal waves; and (iii) the turbulent-nonturbulent interfaces are not necessarily sharp, and the transition region may consist of mostly internal waves". At the same colloquium, Stewart (142) takes the more cautious view that "I think it is extremely important to be aware that there is probably no really clear-cut distinction between turbulence and waves..... when energy is constantly flowing between the two kinds of motion by non-linear effects, the energy cannot be clearly identified as belonging to either kind." After this cautionary remark, he advises that experiments in stratified flows "should incorporate plans to try to distinguish between the waves and the turbulence" in cases where the two are reasonably distinct: clearly one would like to know whether what one is observing, or trying to predict, is waves or turbulence.

Little evidence is available for the presence of waves in stably-curved flows but a casual application of the analogy between buoyancy and curvature strongly suggests that they do exist. The phenomena that constitute vortex breakdown are perhaps too controversial to cite as evidence for waves; about the only experiments on curved shear layers that could be expected to show up internal waves are Cannon and Kays' (143) measurements in a spinning pipe with fully-developed axial flow at entry, and Castro's experiment (11) on a highly-curved free shear layer, and both suggest wave-like effects. The experiments are described in Section 10 and Section 8 respectively. In the pipe experiment, helical instability waves appeared at the interface between the turbulent core and the outer, curvature-stabilized flow: this is a region of large velocity gradient, and the experimenters' description leads one to suspect that the mechanism could be the curved-flow analogue of the Kelvin-Helmholtz instability of a density interface in a gravitational field (144). Castro found a significant increase in the intensity of the irrotational fluctuations near the high-velocity side of his strongly-stabilized mixing layer, and the energy balance suggested that transport by pressure-velocity correlations (not measured) became significant whereas it was negligibly small in a plane mixing layer.

At present, therefore, the presence of waves is little more than a plausible hypothesis. Moreover, it is likely that waves in curved shear layers are more complicated than those in buoyant shear layers because the body force varies in a more complicated way. However a short review of what is known about waves in buoyant flows should be of some help to workers seeking them in curved flows. Where possible the account is written in language and symbols that apply equally to buoyant flows and curved flows: this is not to be construed as a claim that the analogy between the two is exact.

Waves can transfer momentum (though not heat): generally they do so less efficiently than turbulence so that in many cases we might be able to neglect their contribution to the Reynolds-stress

gradients, rather than try to model the wave behaviour as well as that of the true turbulence. However even if we adopt this view we are still faced with a problem in interpreting experimental results: if we seek empirical information to be inserted into transport equations for mean products of the truly turbulent velocity fluctuations (hereafter referred to as the vorticity-fluctuation mode) we have to distinguish between contribution to measured quantities from the vorticity-fluctuation mode and the internal-wave mode. Before discussing ways of making this distinction we consider the curious properties of two-dimensional internal waves in the simplest case of a stratified fluid: of waves in rotating fluids, we merely comment that their properties are even more curious (145). For a short general review of gravity waves in the atmosphere, see Ref.146: they may be rotational if density changes are significant (115).

Let the wave-number vector, whose direction is the direction of propagation of the wave crests and whose magnitude is $2\pi/(\text{wavelength})$, be \underline{k} , with component k_1 in the x direction and k_2 in the y (vertical) direction: k_3 is zero if the disturbance is confined to the x, y plane. Let the frequency seen by a stationary observer be ω . Suppose to begin with that the Brunt-Väisälä frequency ω_{BV} is effectively constant (and positive) over the range of y that interests us, and — an equally strong assumption in practice — that the wavelength is small compared to the "scale height" $\bar{\rho}/(\partial\bar{\rho}/\partial y)$. Then Mowbray and Rarity (147) and other previous and subsequent authors have shown that the "dispersion relation" between frequency ω and wave number \underline{k} is

$$\omega_i = \omega_{BV} \frac{k_1}{(k_1^2 + k_2^2)^{1/2}} \quad (123)$$

where ω_i is the intrinsic circular frequency, $\omega - \underline{U} \cdot \underline{k} \equiv \omega - U_1 k_1 - U_2 k_2$. The difference between ω and ω_i simply represents convection of waves by the mean flow. Writing the scale height as $\omega_{BV}^2/(\text{body force per unit mass})$ we obtain its analogue for a slightly-curved flow as $U/(2\partial U/\partial y)$, whose average value in a shear layer will be at most one or two times the shear-layer thickness so that the condition for validity of Eq(123) is that the wavelength shall be rather smaller than the shear-layer thickness. Waves whose wave number lies in the energy-containing range of the turbulence spectrum will at best barely qualify. The behaviour of these short internal waves can now be summarized as follows (Fig.17)

- (i) The wavelength is determined by the length of the source region (e.g. the diameter of an oscillating-cylinder wave-maker or the wavelength of an eddy) and is usually almost equal to that length.
- (ii) The frequency seen by an observer moving at the same speed as the source is equal to the frequency of the source.
- (iii) The direction of propagation of the wave crests relative to the fluid (the direction of \underline{k} or of the relative phase velocity $\omega_i/|\underline{k}|$) is by definition at $\tan^{-1}(k_2/k_1)$ to the horizontal and Eq(123) shows that this angle is

$$\sin^{-1} \frac{\omega_i}{\omega_{BV}}$$

so that while the wavelength is not determined by the frequency the wave direction is. If $\omega_i > \omega_{BV}$ waves do not propagate, and the disturbance is confined to the neighbourhood of the source.

- (iv) The relative group velocity, which as always has components $\partial\omega_i/\partial k_1$ and $\partial\omega_i/\partial k_2$ in the x and y direction, has a magnitude

$$\frac{\omega_{BV} k_2}{k_1^2 + k_2^2}$$

and a direction $\tan^{-1}(-k_1/k_2)$ to the horizontal: that is, the direction of propagation of the energy of the wave motion is perpendicular to \underline{k} , the direction of propagation of the wave crests. The particle velocities, being necessarily transverse to \underline{k} , are in the direction of the group velocity. Note that the motion is oscillatory and that the energy does not radiate laterally away from the wave train, whose width remains of the order of the width of the source.

Figure 17 shows the wave configuration found in the experiments of Mowbray and Rarity in a stationary, stably-stratified fluid: the wave-maker was a horizontally-oscillating cylinder. In these experiments ω_{BV} was nearly independent of y and the waves propagated in straight lines. If ω_{BV} varies with y the theory becomes more complicated but it is qualitatively clear that if ω_{BV} decreases the direction of propagation of the wave crests becomes more nearly vertical, and vice versa. If ω_{BV} decreases below the (constant) value of ω , the waves are reflected as shown in Fig.17. Waves are reflected as usual from a solid surface without the formation of a cusp in the envelope of the wave vector. Waves are as usual refracted by a velocity gradient: if $V = 0$, then replacing ω_i by $\omega - Uk_1$ in Eq(123) and differentiating gives

$$\frac{\partial k_1}{\partial y} = \frac{-k_1 \partial U/\partial y}{U + (\omega_{BV}/k)(1 - k_1^2/k^2)} \quad (124)$$

assuming for simplicity that ω_{BV} remains constant and remembering that ω and, in this case, k_2 , will remain constant. Therefore k_1 decreases if U increases, but rather more slowly than if the waves were non-dispersive and $k_1 U$ were constant.

The behaviour of waves propagating from an impulsive source is discussed by Mowbray and Rarity: two families of waves appear. Possibly a more realistic situation, in view of our reliance on displaced-element arguments, is that investigated experimentally by McLaren, Pierce, Fohl and Murphy (15), in which a displaced element of a large body of stably-stratified fluid is set free to execute decaying oscillations (the initial potential energy being converted into turbulent energy, thermal internal energy and radiated wave energy). About two complete oscillations are executed, after which the motion of the displaced element can no longer be distinguished from that of the shallow layer either side of it, which oscillates vertically at approximately the Brunt-Väisälä frequency. In the experiments of McLaren et al. both high-frequency waves (propagating almost horizontally, with frequency up to $4\omega_{BV}$) and non-periodic horizontal "displacement" motions were also observed.

In a curved turbulent shear layer the energy-containing eddies, which will presumably be the strongest generators of waves, are not all small compared with the layer thickness or the "scale height", or its analogue $(U^2/r)/\omega_{BV}^2$, equal to $U/(2\partial U/\partial y)$ in the limit of small curvature. The effect described by Eq(124) also tends to increase the lengths of waves propagating towards the high-velocity edge of a shear layer. These medium-length waves ($k\delta \sim 1$) are treated by Bretherton (148) by a "normal mode" analysis, using the wave propagation equation due to Scorer (149, 150) for the case of negligibly small V-component mean velocity. The analysis becomes easy to interpret if $(\partial^2 U/\partial y^2)/(Uk_1^2 - \omega k_1)$ is small. In the inner layer of a turbulent boundary layer $\partial^2 U/\partial y^2 = -u_\tau/(Ky^2)$ and the intrinsic frequency $\omega - Uk_1$ will be of order $u_\tau k_1$ so that the above-mentioned parameter is of order $-1/(Kk_1^2 y^2)$ which is small for wavelengths of order y or greater, so that its neglect is permissible for all wavelengths likely to be important in practice. Then the wave motion can be regarded as propagating in the positive y direction with a y -component wave number given by Eq(123) (with $V = 0$). If ω_{BV} becomes small (as it always does near the free-stream edge of a stable shear layer whether buoyant or curved) the waves are reflected downwards again. Note that prolonged distortion of a train of short waves by a mean shear leads [Eq(124)] to waves with large k_1 which will then behave like normal-mode waves: however an order-of-magnitude change in U is not likely in practice except perhaps for propagation of waves across the thickness of a free shear layer. In the case of a stable boundary layer, the waves are trapped between the surface and the region where ω_{BV} decreases to the most important range of values of ω . Bretherton points out that this happens in the case of lee waves downstream of a range of mountains: it is known that extremely strong waves can occur in this case. This "waveguide" situation is probably the one that actually occurs in boundary layers on convex walls although it must be repeated that no experimental evidence exists. In curved duct or jet flows ω_{BV} falls to zero at the boundary between the stable and unstable regions and the waveguide phenomenon should occur again: it would, however, be rather difficult to distinguish wave motion on the stable side from the irrotational fluctuations generated by the turbulence on the unstable side.

Bretherton (148) also discusses the possibility of "critical layer absorption". Since both k_1 and the frequency seen by a fixed observer, ω , are constant, the intrinsic frequency $\omega - Uk$ (the frequency seen by an observer moving with the fluid) can fall to zero: roughly speaking this will occur when the velocity becomes double that at the value of y at which the waves were generated, since $\omega \approx Uk_1$ there if this happens the wave effectively ceases to propagate relative to the fluid and energy accumulates at this "critical layer". The phenomenon appears to be the converse of that occurring in hydrodynamically unstable (neutrally buoyant) flows in which disturbances are generated near the critical layer: Phillips (151) suggests that critical layers may play an important part in the maintenance of turbulence in neutrally buoyant turbulence. Phillips' theory is not uncontroversial but it is at least possible that strong interactions between waves and turbulence may occur at Bretherton's critical layer.

* In curved mixing layers ω_{BV} falls to zero at both edges, presumably again resulting in trapping of waves. However the normal mode analysis is valid only for wavelengths which are not too large compared with the stable layer thickness. Long two-dimensional waves ($k_1\delta \ll 1$) propagate as interfacial waves along the layer, with an amplitude that decays exponentially on either side, as would be the case for two-dimensional irrotational motion generated by the turbulence in a non-stratified layer. The dispersion relation in this case depends, for buoyant flows, on the density difference across the layer:

$$\omega = U_1 k_1 + \left\{ -g \frac{\Delta \rho}{2\bar{\rho}} \right\}^{1/2} \quad (125)$$

where we can rewrite $-g \Delta \rho / \bar{\rho}$ as $\int \omega_{BV}^2 dy$ to apply the analogy between buoyancy and curvature. The phase velocity relative to the fluid, $\omega/k_1 - U$, is proportional to $k_1^{-1/2}$ and the relative group velocity is half the relative phase velocity: in principle very long waves can propagate upstream. "Breaking" of interfacial waves [Kelvin-Helmholtz instability (144)] occurs only for small Richardson numbers (necessarily less than 1/4) but the Richardson number of a mixing layer of roughly constant curvature is roughly proportional to x so that a catastrophe could occur near the start of the mixing layer if upstream propagation did occur. Very long waves ($k_1\delta \ll 1$) generated by the turbulence will be rare since most eddies have $k_1\delta \not\ll 1$; Pao's (152) shadowgraph pictures of wakes in a fluid with overall stable stratification do show a tendency for long waves to predominate but his situation is closer to that of McLaren et al. than to interfacial waves near a stable layer in an otherwise neutral fluid.

These analyses of internal waves all neglect the scattering or dissipation of wave energy by turbulence. Scattering of waves by turbulence, studied mainly in the context of sound propagation, occurs because the random velocity fluctuations cause random refraction of the waves by the same mechanism that causes refraction by mean velocity gradients. If, as for example in Eq(125),

$$\omega = U \cdot K + \dots = \text{constant} \quad (126)$$

then fluctuations in U cause fluctuations of K in magnitude and direction, and, although the time-mean of the velocity fluctuation at a point is zero by definition, successive wave fronts moving through the turbulence will emerge in slightly different directions so that there is a finite root-mean-square scatter of the direction of the phase velocity (and in general the group velocity) of the emerging waves. To a first (linearized) approximation the total wave energy is unchanged. Dissipation of wave energy by turbulence is essentially a non-linear process, in which the interaction between the turbulence and the fluctuating rate of strain imposed by the wave transfers energy from the waves to the turbulence, after which the energy is transferred by the ordinary vortex-stretching process to smaller wave-lengths and finally to the dissipating eddies. High rates of transfer from waves to turbulence occur when waves "break" but this is likely to be a rare phenomenon in curved flows.

In practice scattering and dissipation take place simultaneously. Eq(123) shows that to first order the scatter in direction of the wave vector K is independent of its magnitude, while the root-mean-square fluctuating rate of strain in a wave system of given energy flux — and therefore the fraction of that energy transferred to the turbulence — is inversely proportional to the wavelength. Scattering of transverse waves will differ only in detail from scattering of longitudinal waves so that discussions and reviews by acousticians are relevant. The papers by W.C. Reynolds and Hussain (153) are a recent comprehensive account

of the behaviour of transverse (rotational) waves in turbulence, biased towards wavelengths of the order of the wavelengths of the energy-containing eddies. This is the range of wavelengths called the "buoyant subrange" in meteorology: energy is extracted from the turbulence by buoyancy effects; part of that energy goes into permanently raising the centre of gravity of the fluid and part into internal waves; the latter part is then returned gradually to the turbulence. The buoyant subrange is still a subject of controversy: the papers by Pao (141) and Stewart (142) summarize current views. Pao suggests that most of the internal wave energy in stable atmospheric layers is concentrated at wavelengths longer than the energy-containing range of the turbulence: this will certainly be the case for a given wave-packet after propagating through a large field of turbulence, but it is not obviously true of waves generated by the turbulence in a restricted shear layer because a given wave is created by an eddy of the same wavelength. However there seem to be no experiments in laboratory buoyant flows to prove the point.

Four possible methods of distinguishing transverse internal waves from turbulence are

flow visualization
spectrum shape
phase velocity
heat-flux or vorticity spectra

None can positively distinguish between waves and the irrotational (but non-propagating) fluctuations that exist even in neutrally-stratified flows as a result of pressure fluctuations produced by the turbulence. In a shear layer the irrotational fluctuations move not at the local speed of the fluid but at the speed of the eddies which generate them: the difference is of the order of (mean velocity gradient) \times (large eddy size), which is itself the ratio of a typical turbulence frequency to a typical turbulence wave number and therefore a typical phase velocity of internal waves. It may scarcely be logical to seek a difference between irrotational fluctuations and waves propagating parallel or nearly parallel to the shear layer.

Flow visualization relies on an observer who thinks he knows the difference between waves and turbulence on sight, and is therefore not universally applicable. It has been applied in elegant dye-trace experiments by Woods (144) and others in the surface layer of the ocean: the shadowgraph technique has been used in buoyant turbulent flows in the laboratory by Pao (152) and radar back-scatter has been used by Browning, Starr and Whyman (154) and others to plot cross-sections of cloud patterns in the atmosphere. In all these cases obvious wave patterns were observed only between, or at the edge of, turbulent regions, so it is not clear whether the technique is useful in the more difficult search for waves actually within the turbulence.

Spectrum shape measurements are useful if the shape of the turbulence spectrum in the absence of waves is known, but since it cannot be known very accurately it is difficult to make quantitative deductions with any accuracy. Caldwell and Van Atta (155) discuss the extraction of the intensity of narrow-band viscous instability waves from background turbulence by spectrum measurements: this is a relatively easy case and one anticipates that waves interacting with intense turbulence will have broader spectrum peaks.

Phase velocity measurements involve space-time correlations or frequency-filtered space correlations, from which wave-number/frequency or wave-number/phase-velocity spectra can be deduced by two-dimensional or one-dimensional Fourier transformation respectively. Stegen and Van Atta (156) describe a simpler technique based on a frequency-filtered space correlation with a fixed spatial separation small compared to the size of the smallest eddies, but it is evidently not very accurate for wavelengths large compared to the spatial separation. The wave number direction is that of the spatial separation between the sensors so that in principle any component can be extracted.

Waves — even short ones — have negligible vorticity. To distinguish waves from turbulence we need a criterion of comparison, such as the ratio of the vorticity spectrum to k^2 times the velocity spectrum. This ratio is unity for the three-dimensional spectra in isotropic turbulence but not necessarily for the one-dimensional spectra measured in shear layers: we need data for turbulence without waves before we can identify waves by divergence from the norm. If only long waves are expected it is not necessary to build a vorticity probe (Ref.157, p.128) small enough to resolve the main, high-wave-number contributions to the mean-square vorticity: a larger probe would be adequate. Since waves and other irrotational fluctuations will not transfer heat, Stewart (142) and Pao (141) suggest isolating the irrotational contribution by measuring the "co-spectrum" and "quadrature spectrum" of the temperature fluctuations θ and the vertical-component velocity fluctuation v . The co-spectrum indicates contributions to the mean product $\overline{\theta v}$ which is the rate of transfer of temperature in the y direction by the turbulence. In the quadrature spectrum, one of the signals has its phase changed by 90 deg. before processing in the same way as for the co-spectrum. Therefore if θ and v are nearly uncorrelated — as in pure waves — the quadrature spectral density is much larger than the co-spectral density, whereas if they are well correlated — as in turbulence — the co-spectral density is the higher. The technique will not work in a curved flow unless it happens to be heated (note that temperature is used as a tracer and not as a measure of buoyancy so that we do not have to invoke any analogy between buoyancy and curvature) but it may be worth heating the flow slightly just to check for the presence of waves. Failure to benefit from meteorological experience and recognise that "turbulence" in a stably-curved flow is very likely to include contributions from transverse, propagating waves would lead to great possibilities of confusion.

5.7 COLLAPSE OF TURBULENCE IN HIGHLY-STABLE FLOWS

This is a common phenomenon in buoyant flows, well-known geophysical examples being the flow of a "wall jet" of salt water along the bed of a fresh-water lake or river and the night-time stabilization of the atmospheric inner layer (115): for a laboratory investigation see Ref.131.

Coles and Van Atta (73) have described the mixed laminar-turbulent flow found between concentric rotating cylinders with a stable gradient of angular momentum, turbulence being confined to a rotating spiral region which continually exchanges fluid with the laminar region. The phenomena are probably more

closely allied to those occurring in the thermocline region of the oceanic surface layer, where thin laminar and thick turbulent layers coexist (144), than to the phenomena occurring in more conventional curved shear layers.

Johnston (158) described in detail the results obtained in a rotating duct (Fig.6) where the flow was stable on one side and unstable on the other. Flow-visualization photographs showed that the characteristic "streaky" structure and "bursting" phenomena found in the viscous sublayer could be almost completely suppressed at rotation numbers $Ro \equiv \Omega h/\bar{U}$ greater than about 0.15, despite the presence of vigorous vortex motions (Section 5.5) on the unstable side of the duct. Mean velocity profiles in the inner layer showed gross departures from the logarithmic law for $Ro > 0.1$, reaching the parabolic shape of laminar Poiseuille flow for $Ro > 0.15$. It is noteworthy that when the ratio of the apparent mixing length ℓ to the mixing length at the same point in a non-rotating duct ℓ_0 was plotted against local Richardson number (in the spirit of the F-factor analysis) a unique curve was not obtained. The ratio ℓ/ℓ_0 at given Ri decreased with increasing Ro. The plots at each rotation number could be fitted quite well by

$$\frac{\ell}{\ell_0} = \frac{1}{1 + \beta Ri} \quad (127)$$

with values of β ranging from 4 to 10 for $0.027 < Ro < 0.081$. This 'Monin-Obukhov' form is a significantly better fit for Ri up to 0.25 than the F-factor form which is its first binomial approximation, although this might not be true if $L/K/L_{mo}$, rather than Ri, was used as a parameter. Clearly the bulk rotation number is an important parameter, implying large effects of rotation on the turbulent transport of Reynolds stress and consequent failure of local-equilibrium analyses. The duct, with adjacent stable and unstable regions, is probably more susceptible to domination by transport effects than a shear layer with the same sense of stability throughout. Johnston refers to the presence, at moderately high Ro, of "highly damped patches, or spots, of turbulence" in the inner layer on the stable side, and it seems probable that they were excursions from the unstable side rather than locally-produced turbulence. Johnston applied a local Reynolds-number criterion for transition from turbulent to laminar flow (159) and obtained quite successful results, but the use of a local Reynolds number for correlating reverse transition must clearly be suspect if a local Richardson number is not an adequate parameter for correlating curvature effects in general.

So and Mellor (160) measured a turbulent boundary layer which developed over a flat surface and then passed to a convex surface whose radius of curvature was about 12 times the boundary layer thickness. The turbulence in the outer layer virtually disappeared [see Fig.18(a): here "station 1" was in the straight entry section and stations 7, 9 and 11 were respectively about 12, 15 and 22 boundary layer thicknesses downstream of the start of the curved region]. As a result the boundary layer thickness changed very little over the curved region. Fig.18(b) shows velocity profiles near the start of the curvature and far downstream: the outer regions are almost identical while the inner region of the profile at the downstream station is effectively a sub-boundary-layer with its edge constrained by the stabilizing effects of curvature. The skin friction coefficient at station 11 was about 0.0024, compared with about 0.0035 at the same Reynolds number on a flat plate, and a significant part of this decrease is due to the smaller free stream velocity seen by the sub-boundary-layer. The parameter $(U/r)/(\partial U/\partial r)$, called S in Eq(86), was about 0.25 or 0.4 at the edge of the turbulent region, depending on whether $\partial U/\partial r$ is evaluated just inside, or just outside, the turbulent region. Ri is rather more than, and R_f or $(L/K)/L_{mo}$ rather less than, twice these values, but since the turbulence near the edge is presumably maintained at least partly by turbulent transport from below local-equilibrium parameters are again of doubtful quantitative validity for discussing the collapse of the turbulence.

In So and Mellor's boundary layer the flow near the surface is still decelerating under the influence of the shear stress gradient, and the edge of the turbulent region is still spreading outwards towards the original edge $y = \delta$. This seems paradoxical: the explanation appears to be as follows. In the boundary layer at the start of the curved region, $\partial U/\partial y$ is small — and the Richardson number or any other curvature parameter therefore large — except near the surface. Therefore the turbulence dies out, except near the surface. The Reynolds stress gradients near the surface continue to decelerate the flow (more rapidly, since $\partial \bar{u}\bar{v}/\partial y$ becomes numerically larger), $\partial U/\partial y$ becomes more nearly constant near the surface [Fig.18(b)], and the region of large $\partial U/\partial y$ gradually increases in thickness. If the surface curvature continued for a long enough distance downstream turbulence could spread beyond the original edge of the boundary layer. The velocity profile would probably still have a rapid decrease in gradient near the edge so that, except near the edge, generation of Reynolds stress by the mean shear would be as important as transport from below: the large-eddy structure in a layer that is stable everywhere is likely to be weaker than in neutral conditions, leading to a relative decrease in turbulent transport terms, so that the turbulence must be maintained largely by local generation. The eventual state of the boundary layer after δ had increased significantly beyond its original value is a matter for speculation: possibly turbulence could gradually die out again throughout the layer, leaving a purely laminar flow, but this would require $\delta \sim R$ and turning angles exceeding 360° and is not likely to be encountered in practice.

In the intermediate stage of recovery, the turbulence structure of the sub-boundary layer will be affected both by the curvature and by the presence of a rotational outer stream, the remains of the initial boundary layer. The problem of a boundary layer in a sheared stream appears in the "superposition" approach to the study of interacting shear layers (3) and it appears that the effects on the turbulence structure may be small. The problem appears in real life in the interaction of a sheared entropy layer with the boundary layer on a body carrying a detached shock wave, but few studies have been made in the turbulent case.

6. BOUNDARY LAYERS AND DUCT FLOWS

6.1 LOW-SPEED FLOW

The boundary layer below an irrotational stream is probably the most important shear layer in aeronautical or mechanical engineering, and the most common examples of flows affected by streamline curvature are

aerofoil, blade or intake boundary layers with R/δ not much less than 100. We have already seen from Thomann's experiment with $R/\delta \approx 50$ (4; Fig.3) that fairly large effects occur even at these moderate curvatures, but the F-factor approach using Eq(36), with Eq(37) if the curvature changes rapidly, should suffice for engineering calculations.

Unfortunately most of the experimental data available at present were obtained in highly-curved flows. Table 3 lists the more detailed of the low-speed experiments on curved or rotating boundary layers and duct flows reported to date, while Table 4 lists the supersonic experiments. The low-speed experimenters deliberately chose large curvatures with the praiseworthy object of obtaining large and easily-measurable curvature effects, while the high-speed experimenters were mostly unaware of possible curvature effects on the turbulence and chose large curvatures to induce strong pressure gradients. It can now be seen that most of the stably-curved boundary-layer flows experienced collapse or incipient collapse of the turbulence in the outer layer, while the unstable flows contained strong longitudinal vortices. Unfortunately these gross non-linear effects generally went unnoticed because of the absence of turbulence measurements on the one hand and the absence of careful checks for three-dimensionality on the other (although, as mentioned in Section 5, it is still not certain whether even strong vortices are always "steady" enough to contribute to the mean vorticity so as to be detectable by mean-flow measurements). Almost the only experiment with R/δ of the order of 100 is the current investigation by Meroney at Imperial College. Even at these large values of R/δ difficulties in the definition of integral thicknesses and of the shape parameter H are apparent, while at the higher curvatures used by some of the other experimenters these difficulties have tended to overshadow the effects of curvature on turbulence structure and to frustrate comparisons between calculation and experiment. In this chapter we review the experimental evidence in a semi-quantitative way: detailed comparisons with typical calculation methods are presented in Appendix 2 to which occasional reference will be made. A rough estimate of the importance of curvature effects can be obtained by taking $0.3 U_e/\delta$ as a typical value of $\partial U/\partial y$ or $(-\bar{u}\bar{v})^{1/2}/L$ in the middle part of a boundary layer. Eq(36) with $\alpha = 10$ then gives $F \approx 1 \pm 30\delta/R$ so that the self-imposed limits $-0.5 < F < 1.5$ for plausibility of the F-factor concepts imply $|\delta/R| < 0.015$. We shall see that quite good agreement is found between calculations using F-factors and experiments on boundary layers with $|\delta/R| > 0.015$, partly because in highly stabilized regions the shear stress is so small that it need not be predicted to good percentage accuracy while in a highly-unstable region the same argument applies to the velocity gradient instead.

The early boundary-layer measurements by Wilcken (22), Schmidbauer (83) and Yeh (99) were mentioned in Section 4. Wilcken's mixing-length distributions on a concave (unstable) surface are reproduced in Fig.19. While one can never have complete confidence in shear stresses deduced from the mean-momentum equation, Wilcken's experimental techniques seem to have been good and the results are acceptable, with some reservations about the presence of longitudinal vortices leading to undetected spanwise variations of mean properties. We note again that vortices which are sufficiently unsteady not to produce spanwise variation of the mean flow simply contribute to the Reynolds stresses, and the flow can legitimately be regarded as two-dimensional. Values of α in the F-factor, Eq(26), applied to the apparent mixing lengths and ignoring lag effects, are shown on Fig.19. As remarked before, we expect the apparent value of α in the linear F-factor to be smaller for large values of $e/(\partial U/\partial y)$: if $e/(\partial U/\partial y)$ were very large so that e were the dominant strain rate α would necessarily be of order unity. This limiting effect is also noticeable on a convex surface, in Schmidbauer's (83) correlation (Fig.20) of skin friction coefficient c_f with θ/R where θ is the momentum thickness (apparently defined with reference to the maximum velocity, ignoring the decrease of free stream velocity with distance from the surface). Schmidbauer realized that c_f also depended on Reynolds number and shape parameter but argued, not very convincingly, that their effects could be neglected in his case. Schmidbauer's results can now be qualitatively explained by the collapse of turbulence in the outer layer at large θ/R (say $\delta/R > 0.03$) leaving a thin inner turbulent boundary layer with a smaller effective free stream velocity (Fig.18) and of course with smaller Richardson number so that the local Richardson number is not very large except near the edge. The quantitative effects shown in Fig.20 seem too large. For $\delta/R \approx 0.01$ (i.e. $\theta/R \approx 0.001$) one expects a reduction in c_f of roughly 10 per cent while Schmidbauer's curve through his points implies 25 per cent. Fig.14 shows comparisons between the boundary layer in Schmidbauer's Fig.6 [using the data as re-analysed by Thompson (161)] and the calculation method of Ref.16, using an F-factor with the "meteorological" value of 14 for α and neglecting lag effects on this constant-radius surface: in this case δ/R was no more than 0.025 (i.e. $\theta/R \approx 0.0025$) and the reduction in c_f due to direct effects of curvature was not more than 15 per cent compared to over 50 per cent from Schmidbauer's correlation.

Yeh's measurements (99) in the boundary layer on the wall of a circular tube carrying a swirling flow are not detailed enough for convenient use as a quantitative test case but show qualitative evidence of curvature effects. The same remarks apply to the more recent measurements of Mackrodt (133) in a similar flow, although the latter may be usable as a test case for theories of "steady" vortex development and show undeniable qualitative evidence of "steady" vortices.

Tani's pioneering study of longitudinal vortices (102) was followed independently by Patel's much more detailed measurements (37, 162). Patel used a rectangular tunnel (we reserve the word "duct" for flows turbulent throughout the cross section) which was 12 in. high and 48 in. wide between false walls, with a centre-line radius of curvature of 30 in.: the boundary layer thickness at entry to the curved portion was about 1.8 in. In Ref.37 Patel reduces his boundary layer profiles to quasi-plane form by plotting $Ur/(Ur)_e$, the circulation ratio, rather than the velocity ratio. As noted in the derivation of Eq(4), Ur and the total pressure P are related by

$$\frac{dP}{dr} = \frac{U}{r} \frac{\partial}{\partial r} (Ur) = \frac{1}{2r^2} \frac{\partial}{\partial r} (U^2 r^2) \quad (128)$$

so that P and $U^2 r^2$ are equivalent over a small range of r . The circulation, for which Patel uses the unfortunate symbol ω , seems to have no real advantage over the total pressure (referred to p_w) for plotting data, and the total pressure is directly measurable. In Ref.162 Patel presents measurements in terms of velocity components made dimensionless by the maximum mean velocity at a given cross-section of the tunnel: this is actually the velocity just inside the boundary layer on the convex side of the tunnel. Even after fitting false walls to remove the end-wall boundary layers at the start of the curved portion, Patel found large secondary flows in the corners of the tunnel. The slow-moving fluid in the sidewall boundary layers is forced by the pressure gradient into a curved path of smaller radius than the path of

the external flow so that fluid migrates from the concave surface to the end walls and from the end walls to the convex surface. Consequently low-velocity regions appear near the corners of the convex surface, extending over a distance of about four times the end-wall boundary-layer thickness. The central part of the convex-wall boundary layer was fairly uniform in thickness although the spanwise variation of skin-friction coefficient was almost as large as on the concave surface and the rate of growth of δ suggests significant lateral convergence. Patel's detailed mapping of the longitudinal and crossflow velocities on the concave surface show the development of "steady" longitudinal vortices whose spanwise wavelength is about 10 in. or 3-4 boundary-layer thicknesses. It is noteworthy that the spanwise wavelength is the same at the two measurement cross-sections, after 135 deg. and 173.5 deg. turning respectively, the distance between the two stations measured around the concave surface being 24 in. or 8-10 boundary-layer thicknesses. The peak-to-peak amplitude of the spanwise c_f variation was nearly 30 per cent, the regions of low c_f being narrower than the regions of high c_f so that the graph of c_f against z looks rather like a rectified sine wave. Bearing in mind that the surface shear stress will be low beneath the outgoing parts of the vortex system and high beneath the ingoing parts, one can see that this is consistent with the flow patterns in Fig.6.

Patel (37) also presented measurements in the very thin and highly-accelerated boundary layer on a circular cylinder. The ratio δ/R is 0.032 at the minimum pressure point, 80 deg. from the leading edge, and rises rapidly thereafter. Interpretation of the effects of convex curvature is complicated by the probable effects of low Reynolds number ($U_e \theta / \nu = 800$ at 80 deg.): the data analysis for plane-wall boundary layers by Coles (163) suggests significant increases in entrainment rate and skin-friction coefficient at such low Reynolds numbers, opposing the stabilizing effects of convex curvature. In addition, the streamline curvature in the outer part of the boundary layer near separation is likely to be greatly different from that of the surface. That some net curvature effects remained is implied by calculations by the method of Ref.16, using the surface curvature and pressure distribution, an F-factor with $\alpha = 14$ and no allowance for lag: separation was predicted at about 105 deg, compared with the experimental value of 110 deg., whereas a calculation with $\alpha = 0$ (still using the measured pressure distribution) showed no separation at all (Fig.21). The experimental values of c_f shown in Fig.22 were obtained from semi-logarithmic plots of Patel's profiles taken from the published graphs and their generally closer correspondence with the $\alpha = 0$ calculations is probably not significant. The c_f calculations would have been almost unaffected by allowances for changes in pressure or streamline curvature across the layer although there would have been some reduction in H because of curvature effects.

So and Mellor's (160) exploration of longitudinal vortices in a concave-surface boundary layer with $\delta/R \approx 0.1$ was less satisfactory than that of Patel in the sense that the measured changes in mean-flow properties were smaller, and indeed of no greater order than the spanwise variations commonly induced by non-uniformity of the entry flow due to irregularities in the screens or elsewhere. This is not necessarily a criticism of So and Mellor's experiment: the more uniform the entry flow, the less likely the vortices are to lock themselves into a "steady" position and thus produce effects on mean vorticity. A criticism that can be levelled is that their hypothesized co-rotating double vortex system is kinematically impossible: also, So and Mellor suffered, like Patel, from pronounced secondary flow in their tunnel, and this may have disturbed the natural vortex system despite attempts to re-energise the sidewall boundary layers by air jets. One fortunate consequence of the lack of strong spanwise variations is that the mean flow may be taken as two-dimensional for calculation purposes (except for the customary allowances for slight lateral convergence or divergence caused by excursions of the sidewall boundary layers). Naturally this highly unstable flow is expected to be beyond the range of validity of linear F-factors since unsteady longitudinal vortex motions were undoubtedly present, with consequent large effects on the turbulent transport terms (unfortunately not measured in this or any other boundary layer experiment). Comparisons between calculation and experiment for the convex and concave sides are shown in Fig.22 and discussed in Appendix 2. The F-factor approach gives tolerably good results, even when applied to the method of Ref.16 using an algebraic length scale, provided that the boundary layer thickness used as a scaling length for L is taken as the thickness of the shear stress profile (Fig.18) rather than the velocity profile: the latter has no relevance to the eddy scale of the sub-boundary layer on a convex surface beneath a stabilized outer layer.

So and Mellor's measurements in adverse pressure gradient (on a convex surface only) do not add any new qualitative features to the data from the constant-pressure runs although the additional test data are useful: essentially one does not expect the mean pressure gradient to have great effects on the turbulence structure, except for the ill-documented effects of $\partial U/\partial x$ or $\partial V/\partial y$ (Section 3), and one does not expect curvature effects to be very important in the inner layer so that large changes in separation phenomena are unlikely. Any experiments on curved boundary layers planned in the near future should be done in nominally zero pressure gradient for simplicity, and So and Mellor's efforts to reduce the strong pressure gradients that necessarily occur where the curvature changes sharply were not really necessary. The only valid reason for applying a pressure gradient would be to increase the turbulence intensity in the outer layer so that turbulent transport became larger and its modifications by streamline curvature easier to study: here a self-preserving ("equilibrium") retarded boundary layer would be most suitable.

So and Mellor measured the Reynolds shear stress (both the "two-dimensional" component $-\overline{uv}$ and the lateral transport of longitudinal momentum $-\overline{uw}$, which will be non-zero if "steady" vortices appear) and the components of turbulent intensity: all components changed in the expected sense and it is their ratios, rather than their absolute values, that provide useful evidence about detailed changes in turbulence structure. The ratio \overline{uv}/q^2 , where $q^2 = u^2 + v^2 + w^2$, is a simple measure of the efficiency of the turbulence in producing shear stress: it is close to 0.15 over most of a plane boundary layer, falling near the surface and near the outer edge where "inactive" motion and irrotational fluctuations are significant. On the convex side, \overline{uv}/q^2 is small in the outer region of the boundary layer and $\overline{v^2}/q^2$ is also somewhat reduced, indicating that stable curvature preferentially suppresses radial motion. Velocity fluctuations in the stable outer layer may arise from several causes, not necessarily distinguishable in practice:

- (i) turbulence generated locally by interaction with the mean shear
- (ii) mean transport from the neutrally-stable boundary layer upstream

- (iii) turbulent transport from the less-stable regions nearer the surface
- (iv) irrotational fluctuations arising as part of (ii) or (iii)
- (v) propagating waves (as opposed to irrotational fluctuations convected with their source) also arising as part of (ii) or (iii).

In strongly-stable flow (i) is negligible and turbulent transport of rotational fluid by the large eddies is probably small also. The relative size of (iv) and (v) in So and Mellor's experiment cannot be deduced from the intensity measurements, but the Richardson number in the outer region was of the same order as in Castro's experiment (11), where oscilloscope traces showed very strong low-frequency fluctuations which were either waves or irrotational fluctuations of a strength not found in plane flows.

Young (57) is making measurements on the flat surfaces of a 30 in. \times 5 in. tunnel downstream of a 30 deg. bend, whose radius is 10 in. on the concave side and 5 in. on the convex side, the boundary layer thickness at entry to the bend being about 1 in. in each case. The discussion of the lag equation, Eq(37), suggests that sharp bends can be regarded as "curvature impulses", the state of the turbulence at exit from the bend depending primarily on the total turning angle and only secondarily on δ/R . Young's measurements do not explicitly support this suggestion because they are restricted to one turning angle and one value of δ/R , but implicit support is provided by the fair agreement between experiment and calculations using Eq(3b) and the linear lag equation Eq(37) — see Fig.23 — although F-factors would not normally be expected to give realistic results with δ/R in the range 0.1 to 0.2, which is even higher than in So and Mellor's experiments. Spanwise periodicity suggests the presence of longitudinal vortices in the boundary layer downstream of the concave side of the bend, but perhaps the most interesting qualitative feature of the concave side is the variation of turbulent intensity with y (Fig.24). The explanation of the relatively greater rise in turbulence intensity in the outer layer, resulting in the trough near the surface, is that the Richardson number is numerically larger in the outer layer and the effects of curvature therefore more pronounced. Note that lag effects do not necessarily play a part, for one would expect the turbulence in the outer layer to respond more slowly than that near the wall. Fig.24 is a satisfying confirmation of the physical ideas behind the local F-factor analysis, and reproduces a phenomenon often found in calculations using F-factors.

Because the direct effects of curvature on the turbulence near the wall are fairly small, the evidence of Young's measurements about the lag-effect "time constant" X (Eq.37) is confined to the outer layer: the discrepancies between experiment and predictions using a linear lag equation are probably to be taken as evidence of the crudity of a linear F-factor and a linear lag equation rather than of a significant departure of the "time constant" of the outer layer from the value of 10δ quoted for many years as typical of constant-pressure boundary layers.

Meroney (164) is making measurements, with the same initial conditions as Young, in a prolonged bend whose radius of curvature is 100 in. on the concave side and 95 in. on the convex side, giving $\delta/R \approx 0.01$ at entry. Even with so small a value the growth of δ over the 48 in. long convex side is almost halved and the skin friction coefficient falls to about 0.9 of the value expected on a plane surface, while the mixing rate on the concave side is increased, c_f is about 1.1 times the plane surface value, and the customary evidence for longitudinal vortices appears. As seen in Fig.25 calculations, using an F-factor with $\alpha = 14$ on the convex side and 8 on the concave side, give fairly good agreement for c_f and δ : sample profiles are also shown in Fig.25. The experiment is still in progress and further details will be given in a forthcoming Imperial College report: it is hoped that values of α derived from this experiment can be taken as standard for calculations in boundary layers with moderate surface curvature. Another piece of work in progress at Imperial College (Mech. Engng. Dept.) is a study by Priddin of boundary layers on curved transpired surfaces of fairly large curvature: various methods of reducing migration of the side wall boundary layers on to the test surfaces are being explored.

The characteristic problems of axial-flow turbomachines are boundary layers on highly-cambered blades (the "centrifugal force" if any being spanwise and therefore not responsible for any curvature effects) and boundary layers on the hub or casing, with a swirling free stream. If the total-pressure rise is independent of radius (the usual nominal design condition) the free stream is irrotational except for the blade wakes: therefore the boundary conditions on the boundary layer are similar to those in the ideal swirling flow studied by Yeh (99). Mackrodt's experiment (133), whose demonstration of the presence of streamwise (spiral) vortices was mentioned in Section 5, was carried out behind a swirl generator like a turbomachine stator. We note that in the absence of longitudinal pressure gradients these flows should approximate to unskewed two-dimensional boundary layers: the change of flow angle through the boundary layer is of order δ/R radians, which is small. Viewed in axes along the local flow direction a longitudinal pressure gradient has a cross-stream component and crossflow therefore results, although the simplification of axisymmetry is retained and the flow now approximates to a boundary layer on an infinite yawed wing. It should therefore be possible to use the same curvature corrections in hub or casing boundary layers as in the corresponding non-swirling curved flows. No quantitative data for curvature effects have been extracted from the (concave, unstable) "casing" boundary layers, but Hughes (165) has analysed his measurements of the boundary layer on a cylindrical non-rotating hub beneath a swirling flow (maximum swirl angle ≈ 10 deg., maximum $\delta/R_{eff} \approx 0.007$) and deduced an optimum α of 13 for the F-factor applied to the mixing length (the usual tendency to decrease with increasing Ri was found). This compares with a value of 14 from the buoyancy analogy and compensates for the value of 15 found at small positive Ri in the above analysis of Eskinazi and Yeh's experiment (98). It need hardly be said that a difference of ± 1 in α is not significant at present, and a reasonable conclusion from the data of Meroney and of Hughes is that a value of 14 [corresponding to $\beta = 7$ in the Monin-Obukhov law, Eq(119)] is adequate for small curvature effects ($Ri < 0.1$, say, giving $1 < F < 1.7$).

The thin boundary layer on a spinning cylinder in a purely axial stream is also effectively two-dimensional, as found experimentally by Parr (166) and Furuya et al. (167) and proved by Cham and Head (127). Cham and Head analysed Parr's results by the indirect but legitimate method of comparing them with calculations by Head's entrainment method and inferred the behaviour of α in the F-factor applied to the mixing length [replacing $e/(\partial U/\partial y)$ by $\frac{1}{2}Ri$ from Eq(115)]. They found that α rose monotonically from values of order unity near the surface to approximately 60 near the edge of the boundary layer. While some departures from normal behaviour may be expected, because Ri itself behaves in an unusual way (being

small near the outer edge as well as near the surface), it is difficult to accept that such a large variation is real. Parr did not measure shear stress, and derivation of shear stress from the mean velocity profiles would not be demonstrably more reliable than Cham and Head's own analysis invoking a well-trying empirical family of velocity profiles.

Dean (168) has reviewed the general problems of boundary layers in centrifugal turbomachines. Pessimistic conclusions are drawn about the utility of current boundary layer methods in dealing with problems that, in the case of the impeller, "include boundary layer separation and free shear flow under the influence of Coriolis forces, separated flow in a rotating coordinate system, transonic flow over the blades, tip leakage and secondary flow" while the fixed radial diffuser suffers from shock/boundary-layer interaction, secondary flow in low-aspect-ratio passages, and sometimes significant curvature effects. The pessimism may well be justified, but a number of experiments have recently been made on rotating ducts or boundary layers with particular application to centrifugal turbomachines, and our knowledge of Coriolis effects rivals, and in some measure outstrips, our knowledge of the effects of streamline curvature in a stationary frame of reference.

Johnston (79) reviews the earlier work on Coriolis (streamline curvature) effects in boundary layers and in ducts of large or small aspect ratio: he gives a full discussion of the problem of laminar flow stability as well as that of turbulent flow, and apart from references to a few recent measurements, notably Johnston's own, little need be added to his account. The work by J. Moore in the Gas Turbine Lab. at MIT, referred to in report form by Johnston, has now appeared as "A wake and an eddy in a rotating, radial-flow passage", parts 1 and 2, ASME papers 73-GT-57 and 73-GT-58, with the possibility of publication in *J. Engg. for Power*. It deals with experiments and calculations on the flow in short rotating ducts of low or moderate aspect ratio. Moore emphasizes the effects of secondary flow in the corners of his rectangular ducts but Johnston comments that the flow in the duct of highest aspect ratio (74) was probably dominated by Coriolis effects on the turbulence structure, which Moore does not explicitly discuss.

Anders (169) made mean-flow measurements on the curved blades of a rotating centrifugal impeller: both circular-arc and logarithmic-spiral blades were tested. The experimental techniques included a hot-wire pressure transducer which measured the velocity in a capillary tube induced by the pressure difference. Velocity measurements were made with conventional hot wires, and surface shear stress was deduced from a surface pitot-static tube, again using the hot-wire pressure transducer. The china-clay (Kaolin) method was used to indicate the flow direction by observing the wakes of small obstacles on the surface. Anders uses $(\delta/U_e)(\partial U/\partial y)_{y=\delta}$ as a stability parameter: since this is equal to δ/R the reason for the more complicated form is not apparent. Anders suggests that near the surface the mixing-length ratio l/Ky should be a function of this stability parameter but does not extract the function from his results. Judging from the development of the boundary layer thickness very large cross-flow must have occurred near the end walls of the low-aspect-ratio blade passage, so that the results are of doubtful quantitative value and it is not possible to assess the net effects of curvature and rotation in this very interesting flow.

Litvai (170) has presented measurements and analysis of the boundary layers in a rotating rig simulating a centrifugal turbomachine. Unfortunately the results are not presented in sufficient detail for use as a test case, while the analysis is not conducted in terms of dimensionless parameters and is therefore inapplicable to other data. It is to be hoped that a more detailed presentation will appear.

A number of experiments has been done on flow in curved (171-173) or radial rotating (174) circular pipes. The effects of secondary flow driven by pressure gradients (171) obscure any direct effects of streamline curvature on the turbulence: all that can be said at present is that the effects of curvature should not be forgotten when calculation methods capable of predicting the details of the secondary flow are being developed.

Tillman (175) has studied transition to turbulence in the "spin-up" boundary layer on the inside of a cylinder impulsively set into rotation about its own axis. The transition process as viewed with increasing time is similar to the "transition by spectral evolution" (71) in steady flow between concentric cylinders as viewed with increasing Reynolds number. The Taylor-Görtler instability vortices that precede transition are still present at a late stage and it seems probable that, in some Reynolds number or curvature ranges at least, they would merge into the vortices found in fully-turbulent flow. Tillman makes the point that the necessarily discontinuous changes in number of vortices cause excursions in the ratio of spanwise wavelength to shear-layer thickness.

Little work on fully-turbulent flow between rotating cylinders has been reported in recent years. The elegant experiments of Coles and Van Atta (73) on the partly-laminar, partly-turbulent flow that occurs in the stable case have been mentioned above: at present we cannot draw any quantitative inferences from this experiment about other types of partly-stabilized flow. Ustimenko and colleagues have published several papers on rotating cylinders and similar flows, of which Ref.176 is the most accessible.

The rotating-duct experiments of Johnston and his collaborators (10, 76, 79, 158) have been discussed in Section 5 with reference to the gross effects of rotation, namely longitudinal vortices on the side where the relative mean vorticity is in the opposite sense to the bulk rotation and suppression of turbulence on the other side. Johnston refers to the unstable side as the "leading" side and the stable one as the "trailing" side, but these names apply only to his own apparatus. Bradshaw (91) found that departures from the logarithmic law in these experiments were quite well correlated by Eq(44) with $\alpha = 8$ on the stable side and $\alpha = 4$ on the unstable side, for $u_{\tau}y/\nu < 500$. Such a correlation neglects the variation of shear stress with y : Johnston's more rigorous correlation of mixing length ratio l/l_0 with the local gradient Richardson number from Eq(89) was less successful, confirming the suspicions aroused by the surprisingly low values of α in the crude correlation. Johnston's correlation on the unstable side was moderately acceptable, most of the data indicating values of α between 8 and 12, with a roughly linear trend up to $(-Ri) \approx 0.25$ and with a significant decrease of α with increase in $(-Ri)$: on the stable side, however, l/l_0 attains constant values for $Ri > 0.08$, while both these constant values and the apparent values of α at lower Ri depend on the bulk rotation parameter $\Omega h/\bar{U}$. A fair, though not necessarily general, correlation for large Ri (large y) on the stable side is

$$\frac{\ell}{\ell_0} = 1 - 6.5 \Omega h / \bar{U} \quad (129)$$

for $0.03 < \Omega h / \bar{U} < 0.09$. This may be regarded as an F-factor of sorts, but, as the local Reynolds numbers involved are rather low, viscous effects as well as curvature effects may be involved.

The rotating duct experiments are a useful extension of the work done on curved ducts by Wattendorf (82) and by Eskinazi and Yeh (98). Eskinazi and Yeh's duct experiment is still the only one to include turbulence measurements, and they appear to be reliable except for the probable undetected presence of "steady" or unsteady longitudinal vortices. The flow at entry to the curved section was a fully-developed duct flow, and the results include mean velocity and u-component intensity profiles at several stations during the re-establishment of self-preservation in the curved flow: unfortunately shear stress measurements were not made in this region. In the fully-developed curved flow, surface shear stress values were obtained by assuming that the logarithmic law held near the surface: in these experiments, as in Wattendorf's, significant deviations from the logarithmic law are found at larger distances from the surface and the apparent mixing length is much larger on the concave side than the convex side. Although mean transport terms are zero in fully-developed flow, turbulent transport normal to the surface is important (especially in the presence of destabilizing curvature effects) leading to displacement of the point of zero shear stress from the point of zero rate of shear strain and thus to eccentric behaviour of the apparent mixing length. Large rates of turbulent transport — or the suspected longitudinal vortices — are probably responsible for the large differences in low-frequency spectrum shape between the two sides of the duct, although it could be argued that all turbulent length scales should increase when the mixing length or dissipation length parameter increase. Eskinazi and Yeh find that the longitudinal integral scale of the radial-component velocity fluctuation was about 5 times larger at 0.1 duct heights from the outer wall than at the same distance from the inner wall and comment that the effects of curvature on the integral scales is about the same as that on the microscales. Fig.13 shows the apparent mixing length, using the definition $\ell = |\overline{uv}|^{1/2} / |\partial U / \partial y|$, and the effective value of α in Eq(36), writing the latter as $\ell / Ky \equiv \ell / 0.41 y = 1 + \alpha (\partial V / \partial x) / (\partial U / \partial y)$. The effect of using second-order definitions of ℓ or of the Richardson-number analogue $2(\partial V / \partial x) / (\partial U / \partial y)$ would be fairly small at the smallest distances from the wall, and at larger distances from the wall the failure of the inner-layer local-equilibrium approximations would be at least as important. Values of ℓ / Ky extrapolate plausibly to unity at the walls and the values of α at small y are quite close to the values of 14 and 8 or 9 deduced from the buoyancy analogy for stable and unstable flows respectively. As in the case of the integral length scale, the mixing length (roughly equal to the dissipation length parameter) at 0.1 duct heights from a wall is about five times larger on the unstable side than on the stable side. Values of mixing length derived by Wattendorf from his data, strictly, the mean of Wattendorf's two sets of values based on $\partial U / \partial y + U/R$ and $\partial U / \partial y - U/R$, are also shown in Fig.13 and agree very well with Eskinazi and Yeh's results except at the larger distances from the "unstable" wall where $\partial U / \partial y$ is difficult to measure from Eskinazi and Yeh's rather sparse profile. The apparent limiting value of ℓ / ℓ_0 at large r on the stable side agrees as well as one could ask with the prediction of Eq(129) derived from Johnston's rotating duct experiments, with $\Omega h / \bar{U}$ replaced by h/r : however the Richardson number at which the limiting value is attained [$(r - r_1)/h = 0.15$, say] is about 0.16 as opposed to 0.08 in Johnston's experiment. On the unstable side the trend of α is similar to that in the rotating duct but the actual values of α are up to 20 per cent lower. The general similarity between the results for the curved and rotating ducts is a fair demonstration of the similarity of the two phenomena and the empirical validity of exchanging U/r and Ω even when curvature or rotation effects are fairly large.

The remaining boundary layer measurements in Table 2 are either fragmentary, done without consideration of curvature effects or mentioned elsewhere in this review. The most important of these studies is Schubauer and Klebanoff's carefully-planned experiment (101) on the separating boundary layer on an aerofoil-shaped body whose rear upper surface had a constant radius of curvature of 31 ft. from about $x = 18$ ft. (where $\delta \approx 2.5$ in.) to the separation point at $x \approx 26$ ft. (where $\delta \approx 8$ in.). Near the separation point $d\delta/dx$ increases rapidly and the streamlines in the outer layer are concave, but over most of the flow curvature has a stabilizing effect. The authors did not anticipate or discuss curvature effects, and the importance of the latter in this experiment did not appear until some years later. In the interval, the results were used for determination of empirical constants in calculation methods intended for surfaces of small curvature: this is not an explanation of the poor performance of calculation methods of that vintage because Head's method is also based on the Schubauer and Klebanoff data and performs significantly better than the other 1950-1960 methods reviewed by Thompson (161). Schubauer and Klebanoff's boundary layer also suffers from strong lateral convergence and — naturally — large $\partial V / \partial y$ near the separation point, but the cumulative dynamic effects of these extra rates of strain do not seem to be as important as those of the relatively prolonged surface curvature. Allowing for $\partial W / \partial z$ only in the continuity equation and neglecting secondary strain effects other than curvature, the calculation method of Ref.16 using Eq(36) with $\alpha = 14$ (from the buoyancy analogue), gives much improved predictions of c_f (Fig.26). The predictions of H are less improved but this is probably because of significant pressure differences across the layer, which are not allowed for even in the mean-flow equations. The conclusion is that the first-order F-factor correction is sufficiently accurate in view of the other uncertainties in the experiment, a conclusion which is likely to apply to other "dirty" flows, although the inclusion of a lag equation like Eq(37) may sometimes be justified.

Most of the recent theoretical work on curved boundary layers has been on F-factor concepts or related empirical correlations for local properties or profile parameters. Examples include Refs 46, 50, 79, 91, 92, 127, 160 and 177-181. The superiority of other linear analyses to the simple F-factor approach, and the justification for postulating non-linear correlations of local quantities in the present state of knowledge are not apparent to the present author. For example, the analysis given by So and Mellor (160) is to first order equal to an F-factor analysis, and their preferred empirical constant $\ell_1 / \lambda = 0.0417$ (Ref.160, p.86) corresponds to $\alpha = 8$. Similar analyses applied to other shear layers are referenced below. It is of course rather difficult to compare correlations for different types of integral parameters without doing calculations by each of the methods for which the correlations are intended, and no attempt will be made to do this here. Green et al. (46) avoid the problem of converting a local F-factor into an integral correlation by applying a transport equation at one point on the profile rather than as a weighted integral over the profile (strictly, it is an integral weighted by a delta function).

The most comprehensive curvature correction for an integral method is that developed by Papailiou et al. (181), adding to the mean kinetic energy dissipation coefficient a quadratic function of $(U_e R/\nu)^{-1}$ whose coefficients are functions of H and Re_θ . Naturally the data available for establishing the functions are limited. The recent paper by Dvorak (182) includes a discussion of the extra (f -factor) terms in the equations of motion in (s, n) coordinates but makes virtually no mention of F -factor effects.

Some apology is necessary for the neglect of heat transfer in this review. Quite simply, the uncertainty of the behaviour of the Reynolds analogy factor and the turbulent Prandtl number is so great even in plane flows that a discussion of the effect of streamline curvature on these quantities would be premature. Application of meteorological data for the variation of the diffusivity ratio K_H/K_M ($\equiv 1/Pr_t$) with stability parameter in buoyant flows would put rather too large a strain on the buoyancy/curvature analogy. At present the best advice is to apply the same F -factor analysis to the heat transfer equations as to the momentum transfer equations; this implies the assumption that the Reynolds analogy factor, the turbulent Prandtl number and the coefficient of correlation between velocity fluctuations and temperature fluctuation are unaltered by streamline curvature.

6.2 SUPERSONIC BOUNDARY LAYERS

It is fair to say that the measurements of supersonic boundary layers in pressure gradients induced by surface curvature (Table 4) have not yet given value for money. According to the arguments of Section 3, a boundary layer on a curved compression surface suffers from the F -factor effects of compression and of curvature, which have the same sign and appear to increase rapidly with Mach number. This obscures the Mach-number independence of turbulence structure, hypothesized by Morkovin and apparent in constant-pressure flows at all non-hypersonic Mach numbers. Even if one accepts the quantitative reliability of the F -factor analysis for small extra strain rates and the accuracy of the rather mechanical arguments used to derive the Mach-number dependence of R_f in Eq(95), much of the supersonic curved-surface data is still indigestible because of the large ratios of δ/R involved (recall that $F \approx 1 \pm 30\delta/R$ in the central part of the boundary layer at low speeds). Experiments like those of Kepler and O'Brien (183), McLafferty and Barber (184) and Clutter and Kaups (185) are little different from shock-boundary layer interaction or sharp corner expansions as far as effects on the turbulence structure are concerned, and the total compressive strain rates involved are too large for the "strain impulse" extension of the F -factor analysis to be trustworthy: the static pressure in Kepler and O'Brien's experiment at $M \approx 3$, for instance, increased by a factor of 6 in a streamwise distance of ten initial boundary-layer thicknesses. The curvature effects as such ($\delta/R \approx 0.05$, turning angle ≈ 24 deg.) would in this case be small enough for the strain impulse analysis to be moderately trustworthy despite the threefold increase in Richardson number predicted by the Mach-number factor in Eq(95) but, as seen in Section 3, the effects of compression are greater, at supersonic Mach numbers, than the effects of curvature of the surface producing the compression. A further difficulty in most supersonic experiments is the lack of skin friction measurements and the consequent inability to check the two-dimensionality of the flow. The only exception is the experiment of Winter, Rotta and Smith (54) on a waisted body of revolution at $0.6 < M_\infty < 2.8$, and here the presence of skin friction measurements is counterbalanced by the presence of lateral convergence and divergence as well as streamline curvature and compression. As mentioned in Section 3, Green et al. (46) have secured good agreement between the waisted body results and unlagged F -factor allowances for the three extra strain effects with $\alpha = 7$ in each case. At the higher Mach numbers the maximum value of δ/R was only about 0.025 and even this was reached only over a very short region, so that, as shown by Green, curvature was much the least important of the three effects. At $M_\infty = 0.6$ the effects of curvature and lateral divergence were roughly equal and opposite and it is more logical to assume the curvature effects to be known and to infer the behaviour of the divergence effects — which are much less well documented — than the reverse.

If one were concerned only with the extreme cases of a flat surface with an externally-induced pressure gradient and a curved surface generating the whole of the pressure gradient itself, one could treat them as distinct types of flow governed by distinct sets of empirical rules. However there are many intermediate cases in which the flow field of, say, a wing influences flow on a neighbouring curved surface (say an intake ramp) so that a unified treatment is desirable.

Some demonstration calculations for supersonic boundary layers over curved surfaces are shown in Fig.27. They seem to be consistent with the proposition that α is independent of Mach number if the rate-of-strain ratio in Eq(36) is replaced by $\frac{1}{2}Ri$ defined by Eq(95), but it must be remembered that the two-dimensionality of the experiments is doubly under suspicion because of the lack of checks on spanwise convergence and the probable presence of longitudinal vortices. Moreover, with the exception of Thomann's constant-pressure flow (4), the ill-documented effects of bulk compression are considerable and could account for, or obscure, any error. The only data available for hypersonic flows refer to shock interactions in sharp corners or bends of very small radius, and no useful attempts at calculation can be made at present. Extrapolation of the trends at lower Mach numbers would suggest that almost any hypersonic boundary layer on a convex surface should be laminar, particularly if the surface generated a favourable pressure gradient, while boundary layers on concave surfaces should consist largely of longitudinal vortices. Refs 186 and 187, for instance, tend to support these suggestions. Doubtless, limiting effects occur: in particular, Green's analogy between the effects of compression and of lateral divergence suggests that the large eddies in a boundary layer under strong compression may degenerate into spanwise vortices like those observed by Keffer (47), with the probability of strong interaction with the supposed longitudinal vortices on a concave compression surface. The truth or falsity of these academic speculations corresponds to large changes in heat transfer to hypersonic vehicles, and a series of experiments deliberately intended to investigate the undoubted effects of curvature and the postulated effects of compression is badly needed. Simple but carefully-controlled experiments in the style of Thomann (4) would be as useful, at least in the short term, as large-scale data-collection exercises.

7. THE COANDA EFFECT - WALL JETS ON CURVED SURFACES

Three entirely different phenomena commemorate the name of Henri Coanda, who died last year at the age of 86 (12), and this is perhaps a suitable opportunity to classify them.

1. The effect originally publicised by Coanda is the tendency of a fluid jet, initially tangential to a curved surface, to remain attached to the surface. This is indeed an unusual effect but requires no unusual explanation. As shown by Lighthill (188) for instance, the effect occurs in an inviscid irrotational fluid: even the well-known experiment with a teapot or with a spoon and a water tap shows fairly conclusively that the jet does not suck itself on by entrainment since a water jet in air accomplishes no entrainment. However one still finds statements like that in a recent report "The physical effect is well known..."; followed by an explanation involving viscous effects. Fernholz (private communication) quotes unpublished work which shows that surface tension helps to promote attachment of a liquid jet in air.

2. The effect whereby a jet whose initial axis does not intersect a solid surface can nevertheless attach itself to the surface (because of the low pressure region resulting from the acceleration of the fluid that supplies the entrainment) is called by Metral and Zerner (86) the "Chilowsky effect". Obviously this is a real-fluid phenomenon and easy to understand in principle; special effects of streamline curvature on turbulent mixing need not be involved. Young (1800) as quoted by Wille and Fernholz (103) observed - but confused - (i) and (ii).

3. The effect whereby a jet attached to a convex surface grows more rapidly than the wall jet on a plane surface is much more obscure, and forms the main subject of this chapter. It is essential to the operation of some of the devices invented by Coanda, notably his mixing nozzles, and I would like to suggest that the term 'Coanda effect' be reserved for this phenomenon. Effect No.2 could if necessary be called after Chilowsky, Young or another early investigator, Lafay (86) and No.1, being a simple consequence of the inviscid-flow equations, deserves no more august name than the 'teapot effect', although Wille and Fernholz (103) mention the august names of Reynolds and Ackeret as early students of this effect.

In the two-dimensional wall jet $\partial U/\partial y$ is negative everywhere, except near the surface where it is positive and very large. Therefore the various curvature parameters related to $(\partial V/\partial x)/(\partial U/\partial y)$ are almost everywhere positive on a convex wall and negative on a concave wall: near the surface the sign is opposite but the parameter is small. Since the work of Newman (104) and Bradshaw and Gee (107) in about 1960, many basic research studies of wall jets on curved surfaces have been made, in addition to continuing work on blown flap schemes and other applications of the Coanda or teapot effects. Much work has also been done on the teapot effect for application to fluidic devices: little of this work is relevant to the present study because streamline curvature effects are not important in the teapot effect, and the complications of low Reynolds number and low aspect ratio make the interpretation of fluidic studies difficult. Wille and Fernholz (103), reporting on the first Euromech Colloquium on "The Coanda Effect", give 120 references to work up to 1965, but both the Colloquium and the report covered a wide range of work on curved laminar and turbulent shear layers in addition to the Coanda effect as defined above. Fernholz (189: 1965) reviews work on the Coanda effect proper. Newman's group at McGill University has made several contributions to knowledge of curved wall jets and free jets: Newman (190: 1969) reviews work up to that date, and the thesis by Guitton (7: 1970) contains an extensive review as well as original work, so that an exhaustive review is not necessary here.

Much of the available information about wall jets on curved surfaces consists of mean-velocity profile measurements in wall jets blowing round circular cylinders. Fekete (191) reports a detailed study including the effects of roughness: see also Ref.7. The ratio of nozzle height to cylinder radius has a negligible effect on the flow many nozzle heights downstream and most basic experimenters have chosen a sufficiently small ratio that a good approximation to self-preserving flow was attained while δ/R was still small enough for streamline curvature effects to be fairly small. However, large nozzle heights may be necessary or desirable in blown flap schemes: Fernholz (189) plots data from several sources covering the range $4 < R/h < 500$. Fernholz (192) has investigated the use of a spoiler in the outer part of the flow to achieve continued attachment at even smaller R/h , and Bradbury and Wood (193) have investigated the (unfavourable) effects of compressibility on the maximum deflection obtainable from a cylinder-flap combination with $R/h = 4$. Although h/R can be neglected as a parameter if it is small, the aspect ratio, (width of flow)/(distance from slot), can have an important effect on the apparent spreading rate because of secondary flows at the edges. The usual practice is to fit plane sidewalls at each side of the jet, preferably of such a height that the entrainment flow, as well as the turbulent region, is tolerably two-dimensional. However, strong secondary flows still occur in the streamwise corners, and, even if the aspect ratio is high enough for the regions of longitudinal vorticity (the true secondary flows) to occupy only a small fraction of the span, significant lateral convergence can be caused by growths of the displacement thickness of the shear layers on the side walls. This lateral convergence affects the apparent growth rate and also the position of separation of the wall jet from the curved surface. In the case of a circular cylinder, the separation point is at 226 ± 3 deg. from the jet origin if the Reynolds number is large and h/R and the effects of three-dimensionality are small (190), but widely differing separation points have been reported in the literature.

The growing wall jet on a cylindrical surface of constant curvature cannot be exactly self-preserving even if one neglects the effects of Reynolds number, h/R and three-dimensionality. The grossest manifestation of this lack of self-preservation is separation, which is usually explained in terms of the self-induced adverse pressure gradient that manifests itself as soon as the lines of constant U/U_{max} in the outer part of the flow acquire a radius of curvature significantly greater than the surface radius R [previous to this, the surface pressure is less than that at infinity by the nearly constant quantity $\int_0^\infty U^2 dn/R$, as follows approximately from Eq(10)]. The destabilizing effects of convex surface curvature lead to earlier separation because they reduce the velocity of the flow, by an increasing amount as the distance from the origin increases, and thus reduce its ability to withstand the inevitable pressure rise. The existing measurements near separation do not contribute to our knowledge of curvature effects: quite apart from any difficulties of interpretation of the measurements, it appears from flow-visualization studies like Fig.8 of Ref.190 that the streamlines near separation are almost straight except

close to the surface. Even far from separation the wall jet on a constant-radius surface is not a very convenient source of data for the effects of streamline curvature on the turbulence, because of departures from self-preservation. The history of the flow would affect the turbulence structure even in the absence of curvature effects, and the latter will themselves depend on the history of the curvature parameter via the processes crudely represented by Eq(37).

If the effects of Reynolds number on the surface shear stress are negligible, a self-preserving flow can be obtained if the surface radius of curvature is linearly proportional to distance from the origin: this gives constant δ/R . Giles, Hays and Sawyer (6, 111) and Guitton (7) have made measurements on logarithmic spiral surfaces ($R \propto s$, with s/R as large as unity) and despite difficulties with three-dimensional effects, fully discussed by Guitton, the discrepancies between the two sets of experiments (Fig.4) are no greater than the general scatter of previous measurements on plane wall jets. Both experiments included turbulence measurements, those of Guitton being the more detailed although confined to only two values of s/R .

Guitton correlated his own spiral data, and by implication the convex-spiral data of Giles et al., by

$$\frac{d\delta_{.5}}{ds} = 0.071 \left[1 + 11 \frac{\delta_{.5}}{R} \right] \quad (130)$$

for $\delta_{.5}/R \leq 0.3$

where $\delta_{.5}$ is the (larger) value of n at which $U/U_{\max} = 0.5$. Guitton's correlation for the wall jet on a convex circular cylinder at turning angles less than about 130 deg. ($\delta_{.5}/R < 0.17$) is

$$\frac{d\delta_{.5}}{ds} = 0.071 \left[1 + 12.8 \frac{\delta_{.5}}{R} - 14.1 \left(\frac{\delta_{.5}}{R} \right)^2 \right] \quad (131)$$

which he regards as a more plausible fit to the data than the alternative straight-line fit

$$\frac{d\delta_{.5}}{ds} = 0.069 \left[1 + 8.7 \frac{\delta_{.5}}{R} \right] \quad (132)$$

Giles et al. (6) do not give an analytic fit to their results but their curve through their convex spiral data has a negative second derivative while Newman (190) draws a curve with a positive second derivative through the spiral data of Giles et al. and some provisional data of Guitton's on spirals and circular cylinders. On balance there seems no justification for anything other than a linear fit for the spiral data, extending to significantly higher $\delta_{.5}/R$ than the quadratic fit to the circular cylinder data. Note that there is no inconsistency in correlating the growth rate on a circular cylinder as a function of $\delta_{.5}/R$ only; if h/R is small and the Reynolds number is large, the only length scales are R and s , so that $\delta_{.5}/R$ is a unique function of s/R . The difference between Eq(130) and Eq(131) is a measure of history effects both on the flow as a whole and on the curvature effects. Note that Newman's deduction (190) from his above-mentioned data fit common to spirals and cylinders, that history effects are negligible, is superseded by Guitton's later work. Sawyer (private communication) in work in progress on two-dimensional and axisymmetric wall jets over curved surfaces, including discontinuities in curvature, also finds significant history effects.

On a concave spiral, the growth rates measured by Giles et al. are larger (smaller stabilizing effects) than predicted by Eq(130) but the difference is within the discrepancies between the convex-surface data of Guitton and Giles et al., and may therefore be insignificant. However it should be emphasized that the data of Giles et al. seem to be of high quality (apart from three-dimensional effects in the downstream region of the most highly-curved spiral, pointed out by Guitton) so that they should be internally consistent to better accuracy than this. Straight-line fits to the concave-surface data of Giles et al. and to the data for the less highly curved surfaces are respectively

$$\frac{d\delta_{.5}}{ds} = 0.077 \left[1 + 10 \frac{\delta_{.5}}{R} \right], \quad (R < 0) \quad (133)$$

and

$$\frac{d\delta_{.5}}{ds} = 0.077 \left[1 + 13.4 \frac{\delta_{.5}}{R} \right], \quad (R > 0) \quad (134)$$

and the line

$$\frac{d\delta_{.5}}{ds} = 0.08 \left[1 + 12.5 \frac{\delta_{.5}}{R} \right] \quad (135)$$

plotted on Fig.4 is the best compromise fit for mild concave or convex curvature. Guitton also found smaller curvature effects for given $\delta_{.5}/R$ on a concave surface than on a convex surface but the difference is less than implied by Eqs (133) and (134). Spettel, Mathieu and Brison (8) reported measurements on a concave cylinder giving - to a linear approximation -

$$\frac{d\delta_{.5}}{ds} = 0.076 \left[1 + 9.5 \frac{\delta_{.5}}{R} \right] \quad (136)$$

in the region of $\delta_{.5}/R = 0.05$. This result agrees within likely experimental error with the concave-cylinder data quoted by Guitton and is close to the spiral-surface result, Eq(133), history effects being small for small $\delta_{.5}/R$ (strictly, for small $\delta_{.5}d^2\delta_{.5}/ds^2$).

It seems clear from the data of various experimenters that the shape of the wall jet velocity profile is little affected by surface curvature, except for a slight increase in the maximum velocity gradient in

the outer layer measured as a multiple of $U_{\max}/\delta_{.5}$. We can therefore use plane-wall profile data to discuss the growth-rate formulae and, for instance, Guitton's calculation that the flux Richardson number R_f at $y = \delta_{.5}$ is about $1.25\delta_{.5}/R$ should be valid over the whole range of $\delta_{.5}/R$ for which a local parameter is useful and shows that values of R_f of roughly 0.4 were reached in the convex spiral experiments plotted in Fig.4. This of course is well beyond the likely range of applicability of a linear F-factor analysis. R_f is roughly constant over the part of the "jet" layer where the shear stress is largest: near the positions of maximum velocity and of zero shear stress (which do not as a rule coincide) the behaviour of local curvature parameters is meaningless because the turbulent energy is supplied mainly by turbulent transport ("diffusion") rather than by local production. Even in the region of maximum shear stress in the jet layer, turbulent transport (which here corresponds to a loss of turbulent energy) is a significant fraction of local production or dissipation, and if the effects of streamline curvature are correlated by F-factors applied to the dissipation term the optimum values of α will contain hidden allowances for the failure of local-equilibrium approximation on which the F-factor analysis is based. Therefore we cannot expect the optimum values of α to be the same for a wall jet as for a boundary layer (where local equilibrium is a fair approximation). The simple argument that entrainment or spreading rate is proportional to the maximum shear stress in the jet layer, coupled with the assumption that the profile shape (in particular, $\partial U/\partial y$ at the point of maximum shear stress) is independent of curvature, shows that to a linear approximation the F-factor applied to the apparent mixing length has a value of α roughly equal to the coefficient of $\delta_{.5}/R$ in one of the linear growth-rate formulae. If we base the F-factor on $\frac{1}{2}R_f$ as parameter α is simply 1/1.25 times the above coefficient. Taking the coefficient as 12.5 from Eq(135) we get $\alpha \approx 10$, close to the "meteorological" value for an unstable flow. However, the mixing length is smaller than the dissipation length parameter L in the region of maximum shear stress because of the aforementioned losses by turbulent transport and the optimum value of α for use in a calculation method which applies the F-factor to L rather than ℓ will be different. The trial-and-error adjustment of α to force the wall-jet versions of the method of Ref.16 (45, 61) to agree with the results of Fig.4 for small convex curvature suggests $\alpha \approx 6$ (Appendix 2). However, this value depends significantly on the empirical modelling of the turbulent transport terms in the calculation method itself, which is uncertain even for a plane wall jet because of the lack of measurements of the triple velocity products that dominate the turbulent transport. Any improvement on the analysis, and of course any improvement on the F-factor concept, requires more turbulence measurements. Also, it must be remembered that the F-factor analysis is in spirit a small-perturbation analysis, restricted to say $0.5 < F < 1.5$, and its validity in highly-curved flows is suspect.

The most extensive turbulence measurements in a curved wall jet are Guitton's on convex spirals. He measured the shear stress, intensities and intermittency, the v -component flatness factor and the triple products uv^2 and $u\bar{w}^2$ for the cases $s/R = 0, 2/3$ and 1. Giles et al. measured $u^2, v^2, \bar{u}\bar{v}$ and the intermittency for $s/R = 0$ and 1, and in general their results agree well with Guitton's. Guitton allowed for the effects of high turbulence intensity on hot-wire response and his results seem internally consistent so that they can be taken as the best available. The trends of intensity and shear stress with curvature are in the expected sense. The trends of the intensity ratios and other structural parameters are interesting: \bar{v}^2/u^2 increases with increasing instability (increasing augmentation of radial motion) as is found in unstable buoyant flows, the value at $y = \delta_{.5}$ being 0.37 in a plane wall jet and 0.7 for the curved flows with very little further increase between $s/R = 2/3$ and $s/R = 1$. The ratios $\bar{u}\bar{v}/\bar{q}^2$ and $\bar{u}\bar{v}/(u^2\bar{v}^2)$ are virtually independent of curvature, and the variation of flatness factor $\bar{v}^4/(\bar{v}^2)^2$ simply reflects the behaviour of the intermittency, to be discussed below. The triple product uv^2 , plotted in the dimensionless form $uv^2/(\bar{u}^2\bar{v}^4)$, is significantly affected by curvature (Fig.27). In the plane wall jet it is negative for $y < 0.7\delta_{.5}$ while at $s/R = 1$ the negative region has almost disappeared, implying much smaller turbulent transport of positive uv into the wall layer (or much smaller transport of negative uv out of it, either statement implying a smaller effect of the wall boundary condition on the jet layer). The positive values of dimensionless uv^2 in the jet layer also increase with increasing curvature, and the increase would be larger still if the denominator contained \bar{v}^2 rather than $\sqrt{\bar{v}^4}$. The triple product $u\bar{w}^2$ shows similar but less pronounced behaviour, so that Guitton's explanation of the behaviour of uv^2 in terms of centrifugal "mixing length" arguments is evidently not the whole story. The main conclusion to be drawn from the measurements is that turbulent transport of uv is significantly but not grossly altered by curvature, except for the large effects near the surface. A correlation of the changes in terms of a bulk Richardson number (e.g. $\delta_{.5}/R$) should suffice for calculation methods: we return to this subject in Section 8.

Guitton's measurements (7) are the most significant evidence for the absence of "steady" longitudinal vortices from unstably-curved jets: he measured the spanwise variation of surface shear stress, using a Preston tube, and achieved a fairly uniform distribution after attention to the initial conditions of the jet. The great sensitivity of the flow to imperfections of the nozzle lip reported by Guitton and by Fekete (191) — which caused large spanwise variations — might possibly imply a predisposition to "steady" vortices, but Bradshaw and Gee (107) and other experimenters have noticed a similar sensitivity in wall jets on plane surfaces. Unfortunately there are no velocity correlation measurements, other than the early attempts of Bradshaw and Gee, to establish whether the large eddies develop unsteady longitudinal circulations as found in Johnston's rotating duct experiments (10). Guitton's intermittency measurements show that the value of $y/\delta_{.5}$ at which the intermittency is 0.5 moves towards the surface as the flow becomes more unstable. A plausible but not unique explanation is that (unsteady) large-eddy vortices exist and cause concentrated eruptions of turbulent fluid with a more widespread backflow [Fig.6 and the discussions of Patel's boundary layer measurements (Section 6) support this picture]. Caille (194) discussing bends in ventilation ducts, says that centrifugal instability in wall jets produces "high velocity gradients and longitudinal vortices", but offers no proof.

Limited turbulence measurements in wall jets on concave surfaces have been made by Guitton and by Spettel et al. A moderate decrease in turbulent intensity is observed, and again the v -component seems to be affected more than the u -component. The largest value of R_f near $y = \delta_{.5}$ found in the concave spiral measurements of Giles et al. was only about 0.04, so that collapse of the turbulence would not be expected in any part of the layer: larger negative values of s/R or $\delta_{.5}/R$ would be difficult to arrange in the laboratory and unlikely to occur in practice.

A final question concerns the applicability of the logarithmic inner law to wall jets. Some doubts

have been expressed in the literature, even in the case of plane jets: certainly the region in which the velocity profile follows the logarithmic law found in constant-pressure boundary layers is small, particularly at low Reynolds numbers, but the reason why the profile is convex upwards on log-linear axes is that the shear stress decreases rapidly with distance from the surface so that, according to the mixing length formula Eq(28) with $\ell = Ky$, $\partial U/\partial y$ also decreases. According to Huffman and Bradshaw (195), K remains near 0.41 even in strong shear stress gradients, but if the dimensionless parameter $-(\nu/\rho u_{\tau}^3)(\partial\tau/\partial y)_w$ is larger than about 0.001 the velocity jump across the viscous sublayer (which provides the constant of integration in the velocity profile obtained from the mixing length formula) is affected. In curved wall jets, as in boundary layers, R_f is very roughly $0.05 y/R$ near the surface and is therefore small throughout the inner part of the wall layer for all practicable values of $\delta_{.5}/R$ with the possible exception of flows close to separation. Therefore the inner layer profile should be deducible from the mixing length formula in both plane and curved wall jets, and curvature effects are probably negligible. Of course, to deduce the surface shear stress from a measured velocity profile we need an estimate of $\partial\tau/\partial y$ because the law of the wall now becomes (26)

$$\frac{U}{u_{\tau}} = f\left(\frac{u_{\tau}y}{\nu}, \frac{\nu}{\rho u_{\tau}^3} \frac{\partial\tau}{\partial y}\right) \quad (137)$$

but a rough estimate should suffice except in extreme cases. Therefore the doubts expressed by Guitton about the validity of the law of the wall in curved wall jets are not well founded and it can be used - with caution - in calculation methods and in data analysis.

Little basic information is available on three-dimensional curved wall jets (196) although more may become available as a result of work on the externally blown flap, in which the exhaust from an underwing engine is deflected by a trailing edge flap: heat transfer is of particular interest in this configuration.

Calculation methods for curved wall jets so far proposed in the literature (e.g. 6, 7, 111, 197, 198) involve either F-factor corrections to local mixing length or eddy viscosity (6, 111), or correlations of spreading rate with $\delta_{.5}/R$. Kind (197) used Guitton's fit (7) to Fekete's cylinder data (192) to produce a complicated analytical formula for entrainment rate as a function of δ/R : the linear approximation to this can be converted, using the principles and approximations of Section 3, to an F-factor with $\alpha \approx 3$, rather smaller than that deduced above from more recent data. As in the case of boundary layers, none of the alternative schemes offers any obvious fundamental advantage over the F-factor analysis and non-linear formulae based on local parameters should be viewed with suspicion. As far as I am aware, the calculations, by Morel's extension of the method of Ref.16, presented in Appendix 2 are the first application of a transport-equation method to curved wall jets, although the recent work of Sawyer involves an allowance for history effects. Hanjalic and Launder (34) have applied their transport-equation methods to wall jets on plane surfaces only.

8. CURVED FREE JETS AND MIXING LAYERS

In fully-developed curved jets one side is stable and the other unstable, so that any net effects on the growth rate are, more or less by definition, strictly beyond the scope of a linear correction formula like Eq(36) for small extra strain rates. However a linear variation is possible if one accepts different values of α in Eq(36) for stable and unstable cases. Studies of curved circular jets in a crosswind have not been sufficiently detailed to distinguish curvature effects from turbulence changes caused by gross distortion of the cross-section and the presence of a pair of contra-rotating vortices within the jet. There seems to be no information about turbulence behaviour in two-dimensional curved jets with a stream of equal total pressure on either side, despite the large amount of work done on jet flaps, but several experiments and analyses (e.g. Ref.110) have been performed on two-dimensional turbulent jets emerging from, and reattaching to, a solid surface. The turbulent intensity measurements of Matthews and Whitelaw (198) unfortunately begin downstream of reattachment. Another recent experiment - confined to mean flow measurements - is Ref.199. Wagnanski and Newman (200) have studied the emerging two-dimensional jet in an external stream but reported no turbulence measurements. Many experiments have been reported on the reattachment of a mixing layer bounding a separation bubble or cavity flow (see Ref.201 for a selective review) and several of these include turbulence measurements. Only recently have any serious turbulence measurements been made in a normally-impinging (circular) jet: Russell and Hatton's results (202) are reported as contour plots of turbulent energy $\frac{1}{2}(u^2 + v^2 + w^2)$, and show that the turbulent energy on a streamline originating from the maximum-energy of the free jet decreases by 20-30 per cent through the impingement region. In view of the fact that the flow turns through 90 deg. in a distance of the order of the jet width, this is a surprisingly small difference: unfortunately the measurements extend only to about three jet half-widths from the centre and the maximum turbulent energy is still falling at the end of the survey region, so that any lag effect cannot be assessed. The maximum shear stress (referred to the jet axis) decreases in magnitude by about 50 per cent through the impingement region, but as it changes sign as the flow deflects through 90 deg. it is not a very suitable measure of turbulent activity. The circular impinging jet experiences strong lateral (i.e. circumferential) divergence effects (see Section 3) which oppose the stabilizing effects of curvature and may account for the smallness of the decrease in turbulent energy through the impingement region.

The first extensive turbulence measurements in a curved mixing layer between two inviscid streams of unequal total pressure were made by Lumley and collaborators (see Ref.203 for a final report which refers to and corrects earlier publications). The flow developed in a tunnel of constant radius of curvature, the maximum ratio of shear-layer thickness to radius of curvature being about 0.2, about the same as in the spiral wall jet with $s/R = +2/3$ (Section 7). Both senses of curvature were investigated. Since δ/R varies with s this is not a self-preserving flow (the net advection of turbulent energy was positive in the unstable case but negative in the stable case) but detailed measurements were made at only one station in each case. The experiments were concentrated on the effects of curvature on the small-scale motion, seeking behaviour analogous to that of the "buoyant subrange" (the region of the wave-number spectrum of a buoyant flow in which shear production and dissipation of turbulent energy are negligible so that the

spectral density is determined by the energy transfer from lower wave numbers and the local transfer to or from potential energy). In fact, once difficulties in dissipation measurements had been overcome it was found that the spectrum followed the usual inertial subrange ("minus five-thirds") law in the relevant region: it is probably a general rule that the effects of streamline curvature are confined to the larger eddies, whose typical fluctuating rates of strain are of order $\partial U/\partial y$ and therefore not very large compared to the extra rate of strain U/R . The typical fluctuating rates of strain of smaller eddies increase steadily with increasing wave number, the root-mean-square rate-of-strain fluctuation of the turbulence as a whole being larger than $\partial U/\partial y$ by a factor roughly equal to the ratio of Reynolds shear stress to viscous shear stress, which is very large in all relevant cases. Lumley et al. (203) also measured overall energy balances: they differed significantly, but not spectacularly, between the stable and unstable cases. Turbulent transport ("diffusion") by triple velocity products was measured (204) and shows the expected transfer of energy from the high-intensity region towards the edges of the shear layer. The overall turbulent transport, obtained in Ref.203 as the difference of the measured advection, production and dissipation, purports to show a transfer of energy from the high-velocity edge of the shear layer to the low velocity edge in both the stable and unstable cases. Now this implies that the behaviour of the remaining contribution to the diffusion, namely that of the pressure-velocity correlation, is quite unlike that obtained by difference in a plane mixing layer (e.g. Ref.11). Curvature effects would be unlikely to produce changes in the same sense for stable and unstable curvature, and one is led to believe that even the revised dissipation measurements quoted in Ref.203 still contained some errors, specifically an underestimate of dissipation near the high-velocity edge.

Castro's experiment (11) on a flow [Fig.7(a)] which amounts to a two-dimensional normally-impinging jet with a potential core — otherwise a mixing layer deflected through 90 deg. — was set up especially to examine the effects of strong streamline curvature. The configuration, similar in principle to Lumley's guided mixing layer, appears to be unique in allowing a large rapid deflection without immediate change of species (the full-developed impinging jet changes, nominally, to a wall jet, but Castro's flow continues as a mixing layer until it finally grows to meet the solid surface). Thus the shear layer relaxes back to its original self-preserving form. The most striking feature of the results is that the relaxation is not monotonic. As seen in Fig.7(b) the turbulent energy decreases in the region of strong curvature, as expected, but then overshoots the plane-layer values (the plane layer values shown in Fig.7 were obtained in the same test rig in the absence of the impingement surface, so that relative values may be relied on whatever the absolute errors of measurement). Castro made extensive measurements of the terms in the turbulent energy equation, and also the terms in the transport equation for shear stress referred to the local direction of the shear layer, neglecting spatial transport by pressure fluctuations and obtaining the pressure-strain redistribution term in the shear stress transport equation by difference. The results (Fig.28) showed that the destruction terms (viscous dissipation or pressure-strain redistribution) actually decrease in the region of strong curvature, rather than increasing as happens in the case of mild curvature. The reason is that the secondary strain rate is so large that the generation terms themselves decrease by a large fraction — R_f (Fig.28) reaches 0.4 — and so the turbulent energy decreases at once. The dissipation length parameter, $L_f \equiv (\text{turbulent energy})^{3/2}/(\text{dissipation})$, does decrease in the region of strong curvature as in the case of small extra strain, but no simple combination of an F -factor and lag equation can fully explain the trajectory in the (R_f, L) plane. The reason for the overshoot phenomenon — found in all three normal stresses and the locally-oriented shear stress — is that the turbulent transport terms are greatly reduced in the regions of strong curvature, evidently because the large eddy structure collapses. A simple measure of the relative strength of the large eddies is shown in Fig.29. After the regions of strong curvature the turbulent transport terms increase rather slowly, evidently because the large eddy structure takes some time to renew itself; in some respects the turbulence downstream of the curved region resembles that in the later stages of transition, where intensities exceed those in the fully-developed flow.

A full presentation of Castro's results would be out of place in a general review. Further analysis is in progress, with the particular object of deriving rules for the behaviour of the turbulent transport terms. Fig.28 shows the eddy diffusivity of turbulent energy (defined on the figure). Quite apart from the usual singularities near the separate points where the intensity gradient and the triple products change sign, it is clear that eddy diffusivity equal to the plane-layer value multiplied by an empirical function of the bulk Richardson number or δ/R can not reproduce the measurements. Evidently the turbulent transport depends on a mixture of local and bulk parameters, with the probability of significant history effects, and it seems very likely that transport equations for triple products will be needed to predict such flows.

Two interesting qualitative features of Castro's results are (i) the intense irrotational motion near the high-velocity edge of the curved shear layer, for which the most obvious explanation is the presence of internal waves, and (ii) the finding that even in the region of maximum curvature the various possible definitions of the direction of the shear layer coincided within one or two degrees, the rate of change of total pressure along a streamline being determined mainly by the shear stress gradient normal to the shear-layer direction.

9. CLASSICAL VORTICES

We define a classical vortex as one formed by the complete or nearly-complete rolling up of a single vortex sheet or, exceptionally, two vortex sheets, in an otherwise uniform flow. The prototype is the trailing vortex behind one tip of a wing of high aspect ratio. We exclude vortices imbedded in flows with distributed axial vorticity (see Section 10) and, despite a good deal of experimental work, we have to exclude the early stages of rolling up of a vortex for lack of information about the turbulence. "Bathtub" vortices, formed by strong radial convergence of a weakly-swirling flow (95), necessarily have strong axial motion which may have large effects on the turbulence.

It has recently become clear that classical turbulent vortices have some very curious features

(i) A substantial fraction of the nominally-turbulent region is effectively laminar (Figs 5, 30). We shall refer to the quasi-laminar region as the "inner core" of the vortex, since the word "core" is used by some authors to describe the whole of the rolled-up region to distinguish it from the vortex sheet.

Many other types of swirling flow exhibit quasi-laminar inner cores.

(ii) The rate of growth of the vortex depends on Reynolds number even at scales typical of full-size aircraft.

(iii) According to an analysis by Govindaraju and Saffman (205) a turbulent vortex must develop a region in which the circulation is larger than at infinity, in order to conserve angular momentum despite the effects of viscous stresses in the irrotational (but not unstrained) flow outside the turbulent region, in which $W \propto 1/r$ (Fig.31).

The first feature is undoubtedly a result of the stabilizing effects of streamline curvature; the second is probably connected with the first and possibly with the third; and the third implies the existence of a region in which angular momentum decreases outwards, so that the effects of streamline curvature are expected to be destabilizing. We proceed to discuss these three features.

The most notable feature of a classical turbulent vortex, as of many swirling flows, is an inner core stabilized by rotation. To a good approximation the flow is "strain free" or "in solid-body rotation" (circumferential velocity proportional to radius, the behaviour of the axial velocity being passed over) the gradient Richardson number is 4 if $\partial W/\partial r$ is used in the denominator or ∞ if $(\partial W/\partial r - W/r)$ is used, and the flux Richardson number is 1; we cannot calculate $(L/K)/L_{mo}$ a priori, but to the extent that we can trust the local-equilibrium parameters in a strongly-curved flow it may be assumed that the turbulence is highly stabilized. This is confirmed by flow-visualization pictures such as Figs 5 and 30 which show an inner core for which "solid body" is almost a literal description, with a very sharp boundary between the outer turbulent flow and an apparently laminar region whose diameter is of the order of a tenth that of the vortex as a whole. Many other still photographs and movies (206-212) have been taken, notably during the current period of concern over the effect of trailing vortices on following aircraft, but it should be pointed out that the vortices in the flight experiments are often only a few seconds old and sometimes demonstrably not completely rolled up.

A noticeable feature of the inner cores is that smoke often collects near concentric cylindrical surfaces, molecular diffusion being small: these cylindrical striations probably arise from inhomogeneities in the vortex sheet feeding the vortex. It has occasionally been suggested that centrifugal effects on heavy smoke or dye particles distort the picture, but this is disproved by the experiments of White (213) and unpublished work by Dr. J.K. Harvey of Imperial College: they used dyes of various densities in water without apparent centrifugal effects.

As seen in Fig.30, large longitudinal velocities can occur in the core, in conditions where the longitudinal velocity in the fully-turbulent flow is negligibly small. This strong axial motion is probably a feature only of young vortices, especially those produced by the "bathtub" (95) mechanism in the popular Mabey-Squire vortex tube with radial entry (Fig.31, Ref.96). Brown (214) has recently pointed out that the axial velocity in the vortex close behind an aircraft is directed downstream relative to the aircraft, as a consequence of the low static pressure generated by the circumferential motion, while at larger distances, when the wing wake has rolled up more completely, the axial velocity is upstream relative to the aircraft, as a consequence of the momentum defect in the wake. The behaviour of the axial velocity therefore depends on the ratio of induced drag to profile drag. Further complications ensue when the engine exhausts interact with the vortices, and Brown's analysis is probably not very realistic for an aircraft with four engines mounted on the wings: when descending to land the net momentum defect in the wake is much smaller than the "drag" as usually defined, because the lift/drag ratio of an aircraft in landing configuration is much smaller than the reciprocal of the glide path slope (20 for a 3 deg. approach), while when climbing after takeoff there is a significant net thrust. Batchelor (215) has shown that strong interactions can occur between the circumferential and axial motions via the low static pressure near the axis, which is produced by the former and drives the latter. Muirhead emphasizes the role of axial flow in "bathtub" vortices (212). Harvey (216) found that acceleration of the wing producing the vortex (or, presumably, other types of pressure disturbance) could affect the vortex for many wing chords downstream. Although pressure gradients are undoubtedly largest near the axis, the concentration of axial motion in the laminarized core is significant: the purely viscous forces resisting axial motion in the core are likely to be smaller than the Reynolds stresses set up in the turbulent flow, leading to a "waveguide" phenomenon. Vortex breakdown appears to involve interaction between axial and circumferential motion, although much of the discussion in the literature has centred on the broad conservation properties rather than the detailed mechanism. Ref.217 is a careful review of the contending theories: see also Ref.218, in which it is pointed out that breakdown at a given swirl angle is more likely at low Reynolds numbers, implying that processes in the highly-stabilized inner core play a significant part in breakdown. Some of the current attempts to reduce the core vorticity of trailing vortices involve the stimulation of vortex breakdown.

A less spectacular feature of trailing vortices, which is almost certainly related to the behaviour of the inner core, and thus to the effects of streamline curvature, is the dependence of growth rate on Reynolds number even at Reynolds numbers typical of full-size aircraft (note that the Reynolds number Γ/v based on total circulation Γ is constant for a given vortex, although the circulation at the edge of a young vortex may be much less than the circulation round the wing). As will be seen below there is as yet no fully satisfactory theory to describe this effect, but a cautious qualitative hypothesis is that the local Reynolds number of the turbulence, based on turbulence intensity and length scale, is low over a large part of the vortex and not merely in the inner core. Crow (209, p.578) goes so far as to say that "the question remains open whether a simple vortex can sustain turbulence at all", i.e. that it may be maintained almost wholly by advection from upstream. R_i and R_f are not very meaningful in highly-curved flows but it is interesting to note that they do not necessarily reach maximum values on the axis. If we assume that the circumferential velocity distribution is the same as in a laminar line vortex,

$$W \propto \frac{1}{R} (1 - \exp(-R^2))$$

where $R = r/\sqrt{4\nu t}$, we find that R_f , based solely on the circumferential motion, rises from unity on the axis to 1.7 at the point of maximum W and continues to rise to the customary value of infinity at the outer edge where the angular momentum becomes constant. R_i of course becomes equal to infinity at the point of maximum W but remains positive thereafter. The laminar distribution is certainly not applicable

in detail and there is evidence that the circulation $2\pi W r$ does not rise monotonically with radius but overshoots the final value and decreases, leading to negative Richardson numbers in the outer part of the vortex. However it is certain that the turbulence is stabilized by streamline curvature at least as far out as the point of maximum circumferential velocity: although only the innermost part of the vortex is non-turbulent, the turbulence Reynolds number is probably low in most of the stabilized region. In Poppleton's experiments (219) at $\Gamma/\nu \approx 50,000$, a typical laboratory value, the Reynolds number based on $(\overline{w})^{1/2}$ and the radius of maximum W was only about 350. The result would be a significant interaction between \overline{w}_{\max} Reynolds stresses and viscous forces, similar in principle to the surprisingly large effect of viscosity on the outer part of a turbulent boundary layer at low Reynolds number: taking $(-\overline{u})_{\max}^{1/2} \delta/\nu$ as equivalent to the vortex Reynolds number just defined we infer $U_e \delta/\nu \approx 600$, where significant viscous effects are found.

The discussion above certainly demonstrates the dominant influence of streamline curvature on the behaviour of a turbulent vortex. It also nearly exhausts the consensus on the subject, because the phenomena mentioned have been elucidated only in the last few years (see Section 4).

The first theory of trailing vortex behaviour to agree with the main features of laboratory and flight experiments was that of Owen (220), who summarizes the experimental data available in 1970. The theory is based on a highly simplified model, with an annulus of fluid with significant Reynolds stress gradients separating the strain-free inner core from the irrotational induced velocity field. The inner core is not assumed to be truly laminar - this is a recent discovery - but the algebraic results are the same as if it were. Owen's detailed assumptions are heuristic and have been criticized by Saffman (221), but lead - with the insertion of two disposable constants - to good agreement with experiments over a wide range of Reynolds number. A detailed criticism of Saffman's, that Eq(4) of Owen's paper does not follow from Eq(1), is incorrect: the integration in question must be taken over a region that just includes the discontinuity in $\partial W/\partial r$ in Owen's simplified velocity profile. The most significant feature, missing from the earlier theory of Squire (222) and from some of the more elaborate models proposed recently, is that the vortex properties depend significantly on Reynolds number: Owen recognized that, because of the stabilizing effects of streamline curvature, the turbulence in the annular region is likely to be weak enough for viscous effects to be important. The final result of Owen's theory is a formula for the ratio of the "eddy viscosity" ν_T to the molecular viscosity ν

$$\frac{\nu_T}{\nu} = \Lambda^2 \left(\frac{\Gamma}{\nu} \right)^{1/2} \quad (138)$$

where Γ is the circulation at large radius and Λ is a constant of order unity which can absorb the effects of crudely assuming an eddy viscosity independent of radius. ν_T/ν varies from 10-100 in laboratory experiments to several thousand in flight tests: Owen's simplified theory does not explain why viscous effects are still important if ν_T/ν is very large and it seems unlikely that Eq(138) can hold for indefinitely large Reynolds numbers. The theory predicts that the ratio of annulus thickness to core diameter varies as $(\Gamma/\nu)^{1/4}$, but one cannot be certain of the identity or proportionality of Owen's core to the laminarized inner core of the flow-visualization photographs. More generally, the "cores" defined by different authors may not be simply related, and workers concerned mainly with the irrotational external flow or the vortex sheet behaviour tend to refer to the whole of the rolled-up region, laminarized and turbulent, as the "core". Definitions used include, in order of increasing radius,

- the laminarized region as seen in smoke photographs
- the region of substantially solid-body rotation
- the region between the surface and the point of maximum W
- the whole rolled-up region

Owen's analysis reveals another feature of vortices that is highly relevant to laboratory experiments and their interpretation. It is obvious - once pointed out - that the turbulence structure will not reach its final self-preserving state until the outer part of the turbulent region has made several revolutions at least. Owen showed that the age of the vortex in the flight experiments of Ref.223 was only about twenty times the current rotational period of the vortex core (the latter does of course increase with age, roughly as $t^{1/2}$) and the age of most of the laboratory vortices reviewed by Owen was less than one current period. The result is that the eddy-viscosity constant Λ in Owen's theory depends quite strongly on age and has barely reached its asymptotic value of 1.2 even in the flight experiments. This implies that a transport-equation calculation method is needed for complete vortex calculations: Owen's correlation for Λ is probably restricted to vortices from high-aspect-ratio wings.

Saffman (221) has recently produced an analysis which is totally different from Owen's but which also leads to a strong dependence on viscosity. He uses an adaptation of classical inner-and-outer similarity assumptions to derive a logarithmic law for the circulation at radii small compared to the overall radius of the vortex but large enough to include the region of maximum circumferential velocity. Rather different "mixing length" arguments, due to Hoffman and Joubert (224), can also be used to derive this logarithmic law. When the self-preserving forms for circulation and shear stress are substituted into the circumferential equation of motion with the viscous terms neglected, integration gives the circulation on the axis as of course zero, and Saffman explains the observed dependence of vortex growth on viscosity by saying "... the fluid can always use viscous effects to reduce the circulation to zero, and the experimental results indicate that this in fact happens. It appears that the fluid prefers to use viscous forces rather than constrain the inviscid dynamics to [make the above-mentioned weighted integral zero] exactly". The argument, if not the mathematics, is closely parallel to the invocation of viscous forces to prevent the energy spectrum of turbulence extending to infinite wave number (the equivalent of the weighted integral being the energy transfer). Now although viscous forces undoubtedly damp out the spectrum at high wave number, the spectral density at lower wave numbers does not depend on the actual value of the viscosity: it is at least possible that the circulation at the centre of a vortex could analogously be reduced to zero by viscous forces without dependence of the outer part of the circulation distribution on the actual value of the viscosity. Therefore although Saffman's argument is attractive and although a core dominated by viscous forces undoubtedly exists, the mechanism by which viscosity

affects the vortex development as a whole is still not clear.

Donaldson (225, 226) has extended his transport-equation calculation method to the case of trailing vortices. The empirical information used is very simple: various length scales are taken proportional to the vortex radius. The effects of streamline curvature are not explicitly allowed for except by the extra generation terms in the Reynolds-stress transport equations, so that the effect appears only as an f -factor and not an F -factor. However the general features of vortex behaviour are well predicted. The phenomenon of small growth rate in young vortices is if anything over-predicted. The growth rate is negligible for times less than $50 r_{\max}/W_{\max}$ where W_{\max} is the maximum circumferential velocity in the initial vortex and r the radius at which it occurs: this corresponds to a value of 100 for Owen's age parameter t/τ , a value reached only in flight experiments. It seems probable that Donaldson's chosen initial conditions were even further removed from self-preservation than those of real-life trailing vortices. Donaldson presents calculations at only one Reynolds number, $\Gamma/\nu \sim 6 \times 10^4$ where Γ is the circulation, so that the size of viscous effects is not clear. An interesting feature of the calculations is the prediction of an overshoot in circulation, which increases with the age of the vortex to a final value about 7 per cent of the nominal circulation; the radius of maximum circulation is about $3 r_{\max}$.

The overshoot in circulation — the third feature mentioned at the start of this Section — is important in determining curvature effects. The experimental evidence is scanty — it is very difficult to measure the circulation in the outer regions of the vortex because the circumferential velocity becomes very small — but the theoretical evidence provided by Donaldson's numerical calculations and Govindaraju and Saffman's analysis (205) is strong.

Govindaraju and Saffman's proof of the existence of an overshoot is simple mathematically but not very clear physically, and a commentary may be helpful. The proof rests on the fact that the viscous shear stress in the cross-sectional plane,

$$\nu \left(\frac{\partial W}{\partial r} - \frac{W}{r} \right)$$

goes to zero at large distances only as $1/r^2$ (since the circulation $\Gamma \equiv 2\pi W r$ is constant) while the Reynolds shear stress \overline{w} is assumed to go to zero much faster than this, as in non-swirling flows. The result is that while the Reynolds stress term disappears from the equation for the circulation defect integral

$$\int_0^{\infty} (\Gamma_0 - \Gamma) r \, dr$$

derived from the exact equation of motion, the viscous term does not. It follows that the dimensionless version of this integral,

$$J(x) \equiv \int_0^{\infty} \frac{\Gamma_0 - \Gamma}{\Gamma_0} \frac{r}{r_1} \frac{\partial r}{r_1} \quad (139)$$

where r_1 is a typical radius of the vortex core at distance x from the origin, varies as

$$J(x) = \frac{A}{r_1^2} + \frac{2\nu x}{U_e r_1^2} \quad (140)$$

where A is a constant of integration and x/U_e is the age of the vortex. In laminar flow, r_1^2 is of order $\nu x/U_e$ and J remains of order unity; but in turbulent flow r_1 is larger (though still proportional to x^2), the second term is small, and therefore J tends to a small constant value as A/r_1^2 decreases to zero with increasing x . Thus even if the initial distribution of circulation is monotonic like that in a laminar vortex, an overshoot must develop in the self-preserving profile far downstream so that the circulation-defect integral shall become small. (The paradox that a turbulent vortex with constant eddy viscosity would be effectively laminar for the purposes of the above analysis, and therefore would not develop an overshoot, is resolved by noting that in this case the Reynolds stresses would also go to zero as $1/r^2$ for large r , contrary to hypothesis.) Physically, the viscous stresses continue to reduce the circulation in the region outside the turbulence, which has a rate of shear strain equal to $2W/r \equiv \Gamma/(\pi r^2)$. Although the presence of a finite rate of shear strain doubtless encourages the growth of the turbulent regions and may lead to a less rapid decrease of Reynolds stress with increasing r than found in a non-swirling flow, the turbulent region does seem to be sharply bounded as usual (Fig.5) and the basic qualitative assumption of the analysis is plausible. The only reservations are that in real life the inhomogeneity of the outer boundary conditions (behind a wing of finite span or in a vortex tube of finite radius) may make the analysis less relevant.

According to Govindaraju and Saffman's theory and Donaldson's calculations the overshoot is noticeable only in fairly old vortices (even if the whole of the wing circulation has already rolled up into the vortex). Note that Owen's comment about the finite time needed to strain the turbulence into a self-preserving state is still applicable and may further delay the arrival at the asymptotic state. The youth and uncertain circulation of laboratory vortices add to the difficulty of detecting an overshoot experimentally; in the detailed experiments of Poppleton (219) there was certainly no overshoot at any radius less than $5 r_{\max}$. A very clear piece of evidence, which, however, raises more questions than it settles, is the overshoot in total pressure found by Earnshaw (227) in the incompletely rolled up vortex above a slender wing. An overshoot in circulation is implied, unless the overshoot is caused mainly by axial stresses, but the various explanations for the Earnshaw effect offered at the time were mostly applicable only to a vortex in process of rolling up (essentially a highly-curved mixing layer). One universally valid explanation was experimental error, but the only source of error that could not be checked was the effect of turbulence on the pitot tube and if this were the explanation it would imply very unusual behaviour of the turbulence. An overshoot in circulation generated in the rolling-up process would persist for some distance downstream and might be taken as evidence of overshoot in a fully rolled-up vortex. If the theoretical conclusion, that overshoot develops in rolled-up vortices only at rather large times, is correct, laboratory evidence for overshoot should be regarded with suspicion. To quote one example, perhaps unfairly, the measurements of Mason and Marchman (228), made at distances up to 30 chords behind a wing in a tunnel at $U_e c/\nu \approx 5 \times 10^5$, show an overshoot in circulation even though the

vortex is so young that its core has scarcely grown at all. Flight measurements merit caution for the rather different reason that the circulation distribution on an aircraft in approach configuration is far from smooth: the consequences for the initial rolling up of the vortex sheet are illustrated by Fig.8 of Ref.229, which shows hideous distortions with at least three incipient vortices on each side of the aircraft. Vortices from slender wings probably interact strongly because the ratio of core diameter to vortex spacing is not large, even close to the trailing edge. Therefore although the presence of an overshoot in circulation has been fairly convincingly demonstrated theoretically, it may be some time before we have experimental data reliable enough to serve as a basis for discussion of the quantitative effects of streamline curvature in the region of "unstable" angular momentum gradient.

The results of the earlier experiments on vortices in the laboratory and in flight are summarized by Owen (220). Recent experiments, mostly on vortices behind aircraft models in wind tunnels, include Refs 230-235. Apart from the fairly restricted measurements made by Chigier and Corsiglia (232) the main source of turbulence data is the work of Poppleton (219). He describes the work as "preliminary", saying that "the accuracy of some of the results was not as high as might be desired", but the general standards appear to compare very favourably with other recent work undertaken as part of the aircraft vortex wake programme. The most striking feature of the results is that all three components of turbulence intensity reach maximum values on the axis, and that the shear stresses appear to vary linearly across the axis with no trace of a stress-free laminarized core. A peak in u-component intensity on the axis was found in the 1957 experiment of Titchener and Taylor-Russell (236), and in the 1972 experiment of Chigier and Corsiglia (232). The only way of reconciling this result with the evidence of the smoke pictures is to suppose that the vortex core wanders about randomly, as has indeed been found in several experiments. Even a non-turbulent vortex would then show a maximum velocity fluctuation on or near the axis where the radial gradients of the velocity components are largest. The amplitude of disturbance of the core axis would have to be of the order of r_{max} to get a linear distribution of apparent shear stress if, as expected, the true shear stress is very small in a significant region of the core. In Poppleton's experiments r was about $0.01 x$, so that long-wavelength v-component fluctuations of at least $0.01 U_e$, or stronger fluctuations at shorter wavelength, would be needed to produce an amplitude roughly equal to r_{max} . Similar amplitudes would be needed to produce a displacement of the vortex by altering the lift of the aerofoil. It is probably unfair to blame wind tunnel turbulence entirely although it is reported (235) to have been responsible for some shortcomings of the results of Ref.232 and perhaps of other experiments: Poppleton (219) measured a v component r.m.s. level of about $0.01 U_e$ with the wing set at zero incidence, but the typical wavelengths were presumably small compared with the wing chord rather than of order x . However the maximum r.m.s. turbulence intensity in the vortex itself was as high as $0.025 U_e$ and it is plausible that the larger eddies in the truly-turbulent part of the vortex could cause large enough displacements of the core to produce the observed effects: the irrotational fluctuations generated by the annular regions of turbulence are likely to be a maximum on the axis. In addition, long-wavelength fluctuations in the axial velocity in the laminarized core, caused by disturbances at other positions on the axis, would be registered as "turbulence" by a hot wire: axial fluctuations of moderate wavelength might interact significantly with the mean circumferential motion in the manner described by Batchelor (215). Finally, mild precession of the vortex core may occasionally be induced. Judging by visual observations of delta-wing vortices in a smoke tunnel at Imperial College, quite strong precessional disturbances of the laminarized core can travel down the vortex, at roughly the free stream speed, maintaining their intensity for many core diameters. We can conclude that there are enough possible sources of disturbance to reconcile Poppleton's measurements with the flow-visualization pictures.

Unfortunately the key part of Poppleton's data, the measurement of $\overline{v'w'}$, exhibits considerable scatter. Pratte and Keffer (237) also found large scatter in $\overline{v'w'}$ measurements in a swirling jet: the extraction of $\overline{v'w'}$ from hot-wire readings is essentially ill-conditioned. Therefore, in the vortex as in the swirling jet, we have no shear-stress measurements reliable enough to indicate the effects of streamline curvature. Several authors (228, 230, 231, 238) have calculated the apparent eddy viscosity $\nu_{r\theta}$, in the cross-sectional plane, from mean-flow measurements but the confusion over validity of the mean-flow results makes it difficult to draw any general conclusion: Owen's theory is still the best correlation of results but the apparent eddy viscosity of the theory is not directly comparable with $\nu_{r\theta}$, and a more satisfactory theory, based on a detailed turbulence model such as Donaldson's must await better understanding of streamline curvature effects and of the behaviour of turbulence at low local Reynolds number.

This is not the place for a general discussion of trailing vortices. Ref.239 (186 pages, 124 references) is described by the author as "an initial step towards a more critical review". An entry to current research work, with emphasis on prediction, detection or reduction of aircraft trailing vortices, is given by Ref.209. Ref.240 is a collection of papers on all aspects of vortices but with very little attention to turbulence, and Ref.241 is a report on a specialist symposium.

10. SWIRLING SHEAR LAYERS

10.1 INTRODUCTION

This is a large category, including all flows whose mean streamlines are roughly helical [Fig.1(d)]: some have been discussed in previous sections. We start by establishing clear sub-categories (a precaution not always observed in previous discussions of swirling flows). In all cases we assume that W [the mean velocity component in the circumferential (θ) direction] is of the same order as U : if it is much smaller, the flow is only weakly swirling and any results for strongly-swirling flows will be applicable, while if W is much smaller than U the flow is better regarded as a slightly three-dimensional version of a curved flow in the r, θ plane. For a discussion of valid approximations, see Ref.242. We also assume that the resultant mean shear, $((\partial U/\partial r)^2 + (\partial W/\partial r)^2)^{1/2}$, is of the same order as $\partial U/\partial r$ so that we can refer to the latter as the "mean shear" in qualitative discussion. In effect we regard swirling flows as simple shear layers, with a simple shear of order $\partial U/\partial y$, perturbed by an extra rate of strain $e \equiv W/r$ analogous to the extra rate of strain $e = \partial v/\partial x = -U/r$ that appears in two-dimensional curved flows. Finally we call the thickness of the shear layer δ as usual, and distinguish the main types of swirling flow as

(i) thin annular swirling shear layers ($\delta \ll r$). As in two-dimensional curved thin shear layers with $\delta \ll r$, the direct effects of swirl on the turbulence will be small enough to represent by F-factors although three-dimensionality may introduce explicit extra terms in the equations of motion and thus complicate the calculations. The thin-shear-layer condition $\partial/\partial r \gg \partial/\partial x$ is obeyed but the radial pressure gradient may be significant (see Sections 2.2 and 2.3) for values of δ/r near the likely upper limits of validity of the F-factor approach. For purposes of analysing curvature effects these flows can be grouped with three-dimensional boundary layers (Section 5.3: note that axisymmetric flows of this type are analogous to flows over infinite swept wings). Experiments (133, 165-167) were discussed in Section 6 and will not be discussed further in this section.

(ii) slender swirling shear layers ($\delta \sim r$). This section includes annular shear layers too thick to qualify for class (i), and also the large number of axisymmetric or near-axisymmetric flows which are nominally turbulent on the axis. We call the simplification of the equations of motion that results from assuming $\partial/\partial r \gg \partial/\partial x$ (or more generally $\partial/\partial y, \partial/\partial z \gg \partial/\partial x$) the "slender-shear-layer" approximation. Isolated trailing vortices have already been discussed in Section 9, with particular reference to stabilization of the flow near the axis. The phenomenon of virtually complete suppression of turbulence near the axis necessarily appears in most of the slender flows to be discussed in the present section, because $W \propto r$ near the axis, leading to $Ri = 4$ (Section 9): in general the direct effects of streamline curvature will be too large to represent by simple F-factors. Moreover, in unstable swirling flows the large-eddy structure may be significantly modified by streamline curvature, leading to changes in turbulent transport that cannot easily be represented by local parameters. Therefore the Reynolds stress distribution will depend in a rather complicated way on the swirl velocity distribution and, in default of a unified treatment, different empirical information may be needed to describe different kinds of swirl distribution.

(iii) non-slender swirling shear layers ($\partial/\partial r \gg \partial/\partial x$). In swirling flows that are changing rapidly in the axial direction no simplification of the equations of motion is permissible, except, where appropriate, the simplification of axisymmetry, $\partial/\partial \theta = 0$ (precession of the central core has been observed in some nominally axisymmetric flows). In such flows, as in previous examples of strongly-curved flows, no quantitative analysis of direct curvature effects is possible at present because large changes in turbulence structure are implied, even by explicit terms introduced into the equations of motion by the various extra strain rates that occur. However it is qualitatively clear that curvature effects on the turbulence structure may play an important part in the flow development, especially by permitting easy axial motion of the fluid within a curvature-stabilized core. Fig.32 is a summary of the types of swirling flow to be discussed. It is customary to measure the strength of the swirl by the "swirl number", the ratio of the angular momentum integrated over the cross section to R times the axial momentum integrated over the cross section, where R is a typical radius of the flow. In jets the momentum integrals are conserved while R increases with x , whereas in pipes the angular momentum decreases while R remains constant: therefore the swirl number decreases with increasing x unless external forces are applied to maintain it. The swirl number gives no information about the distribution of W and is a far from adequate description of the swirl for present purposes.

The most popular type of swirl generator, whose most advanced version seems to be the "movable block" generator of Beér and Leuchel (243), is a fixed pipe with tangential injection of part or all of the mass flow. The swirl intensity and distribution depends on the ratio of the tangentially-injected flow to the total flow, the ratio of injection slot area to pipe diameter, the proximity of the end wall and the length-to-diameter ratio of the pipe: if the pipe is very long the swirl decays completely, and if it is short minor changes in geometry may have a large effect on the mean flow and turbulence at the exit. Precession of the core may occur at high swirl angles. Another type of swirl generator, capable of producing a fair approximation to solid-body rotation with uniform axial flow, is a rotating honeycomb or thick perforated disc, which may be regarded as a crude axial-flow turbomachine rotor. Traugott (100) obtained a low-turbulence flow close to solid-body rotation by using a well-designed rotor followed by several rotating screens: in Traugott's configuration the pressure drop through the screens was insufficient to remove the wakes of the rotor blades (coarse grids were inserted to do this at the cost of raising the turbulence level) but this is not a criticism of the basic idea. Solid-body rotation ($W \propto r$) can also be obtained at the exit of a long spinning pipe but the axial flow approximates to fully-developed pipe flow. A swirling flow with a nearly irrotational region ($W \propto 1/r$) surrounding a slender core can be produced by vanes in a radial contraction (Fig.31) but is less representative of real-life swirling flows. "Bathtub" vortices can be produced by radial inflow through a cylindrical rotating screen, which also gives $W \propto 1/r$ except near the axis where the core forms.

Current discussions of swirling flows and methods of calculating them (244-246) usually treat the effects of swirl in terms of the "anisotropy of eddy viscosity" or, in our present notation, differences between the quantities v_{rx} and $v_{r\theta}$ defined by

$$v_{rx} \equiv \frac{-\overline{uv}}{\partial u/\partial r} \quad \text{and} \quad v_{r\theta} \equiv \frac{-\overline{vw}}{r\partial(W/r)/\partial r} \quad (141)$$

We note once more the uncertainty of definition of the denominator of $v_{r\theta}$ - velocity gradient, vorticity gradient (as shown) or angular-momentum gradient? - and the certainty that the direct effects of curvature at the F-factor level will overwhelm the ambiguities of definition at f-factor level. The definition of $v_{r\theta}$ given here is the most common one in discussions of swirling duct flows. It offers the possibility that $v_{r\theta}$ is well-behaved in regions of solid body rotation where the numerator and denominator both go to zero, and the denominator is unlikely to go to zero elsewhere in simple swirling flows with $W \rightarrow 0$ as $r \rightarrow \infty$. These are of course operational advantages rather than a proof of physical relevance: W/r is not constant in an irrotational swirling flow ($W \propto 1/r$) although \overline{vw} is expected to be zero. Now unfortunately even plane three-dimensional flows will usually exhibit different eddy viscosities for the "streamwise" and "cross-stream" components of shear stress, because, although the transport equations for the two components are identical except for cyclic interchange of symbols, the mean pressure gradient and the boundary conditions will in general affect the streamwise and cross-stream motions in different ways. Even in thin attached boundary layers the angle between the resultant shear stress and the resultant velocity gradient (which would be zero if the eddy viscosity were isotropic) behaves in a very complicated

fashion (Section 5.3): the ability of calculation methods, even extensions of fairly sophisticated two-dimensional transport-equation methods, to predict the behaviour of this angle is by no means proved. Therefore correlations of the properties of plane three-dimensional flows by eddy-viscosity anisotropy factors are unlikely to be applicable to a wide range of flows. A purist objection to anisotropy factors is that eddy viscosity, like mixing length, is a local-equilibrium concept: local equilibrium implies that the turbulence is determined by the local rate-of-strain field, and in particular that the direction of the shear stress is the same as the direction of the velocity gradient, so that v_{rx} must equal $v_{r\theta}$. This by itself need not stop us using anisotropy factors for correlating data, any more than it stops us using eddy viscosity for correlating data in two-dimensional flows, but it lends weight to the practical objections outlined above.

It appears, therefore, that the anisotropy of eddy viscosity of three-dimensional flows is likely to be significant and ill-behaved even in plane thin shear layers (125, 247). Streamline curvature effects will further complicate the picture even if the shear layer remains thin or slender while attempts to describe non-thin swirling flows in terms of eddy-viscosity anisotropy factors are unlikely to lead to anything better than a broad-brush treatment and are most unlikely to tell us anything of permanent value about the direct effects of curvature on the turbulence. Swirling flows are an example of the frequent impossibility of deducing curvature effects by comparison with experiments on a non-curved but otherwise identical flow: their curvature and their three-dimensionality are inseparable. We must therefore fall back on "numerical experiment", examining predictions of swirling flows by calculation methods that give good results in the corresponding axisymmetric non-swirling flow and in three-dimensional plane flows: the discrepancy between prediction and experiment can be provisionally attributed to curvature effects, and minimised by application of F-factors or otherwise. This approach has not yet been tried with modern transport-equation methods except for the use of anisotropy factors for $v_{r\theta}$ in an eddy-viscosity transport equation for v_{rx} in Ref.245: these methods are at present mainly confined to two-dimensional (or non-swirling axisymmetric) flow, and more work is needed to develop a repertoire of methods for three-dimensional flows. Some attempts to modify simpler calculation methods for application to swirling flow will be referenced below. Two objections to using simpler local-equilibrium methods for the "numerical experiments" proposed above are that swirling flows, especially jets, are often highly turbulent with significant turbulent transport terms, and that equally often they have large mean transport terms because the flow changes rapidly in the axial direction. At present, therefore, all the theoretical attacks on swirling flows leave something to be desired: the paper by Koosinlin and Lockwood (246) gives a good idea of the current position.

We proceed to review the experimental work on swirling flows, excepting isolated vortices and thin annular shear layers. The most common types of swirling shear layer left in the category are swirling jets or plumes in nearly still air, and swirling pipe flows. In almost all cases the flow near the axis of rotation is stable and in a state close to solid-body rotation as far as the circumferential motion is concerned. Production of turbulent energy by the axial component of the mean shear, $\partial U/\partial r$, is small in this region because $\partial U/\partial r = 0$ on the axis. It therefore seems very probable that any swirling flow which changes fairly slowly in the x direction will have a laminar core as in a classical vortex. The stability further from the axis depends on the source of swirl, (i.e. the source of angular momentum) which determines the angular momentum gradient appearing in the relevant Richardson number, Eq(105). We emphasize yet again the unreliability of local-equilibrium curvature parameters, especially in highly-turbulent free shear layers. If swirl is introduced only at the source of the shear layer (i.e. at a jet nozzle or a pipe entry) the flow near the outer edge is unstable because the velocity falls rapidly to zero there, either in the undisturbed fluid or at a solid surface, so that there is a region in which the angular momentum decreases outward. Therefore the net effect of "pre-swirl" is usually to increase overall mixing rates, and by a larger fraction than would be expected merely on the basis of increased resultant velocity. Accordingly, swirling shear layers are commonly found in devices for augmenting or controlling mixing. Some idea of the magnitude of changes in mixing rate can be gained from Swithenbank and Chigier's (248) suggestion that pre-swirl could be used as the main method of control of combustion rate in a supersonic ramjet. Pre-swirl can also be used to shorten the noise-producing region of an exhaust jet (249) or to promote better mixing of the multiple exhaust streams of a by-pass turbojet. In view of the other data, the conclusion of Povinelli and Ehlers (250) that swirl (intensity not stated) had negligible effect on mixing downstream of a blunt-base fuel injector is difficult to understand. If swirl is introduced or maintained by rotation of the outer boundary or by entrainment of fluid with axial vorticity the turbulence is stable almost everywhere ("almost" being an acknowledgement of the possibility of an overshoot in circulation like that believed to exist in a turbulent line vortex).

The picture is complicated by the basically inviscid phenomenon of recirculation zones (Fig.32) near the axis of some strongly-swirling flows, where the static pressure is reduced so much by the swirl that fluid from further downstream is forced back along the axis. This is a deliberately vague description, designed to fit several versions of the phenomenon (245, 251-253). There is no reason to suppose that streamline curvature effects play an essential part, although the presence of a laminar core may be important in some cases, as will be seen below. Clearly the extra turbulence generated by recirculation may more than cancel any stabilizing effects of swirl, and we can neither extract useful information on curvature effects nor apply the foregoing rudimentary analysis to such complex flows. A good introduction is the 1964 paper by Gore and Ranz (251): for a review of current work, especially by the Sheffield group under Beér, see Chigier (129).

Any swirling flow with solid boundaries in the r,θ plane is likely to be significantly affected by fluid from the "Ekman" boundary layers that spiral inward on these boundaries under the influence of radial pressure gradient. Charwat and Schlesinger (254) have described the complicated flow pattern that occurs in the recirculating part of the wake of an axial cylinder in a swirling external flow. The ratio of the circumferential velocity to axial velocity at the cylinder radius was nearly 2.0. The recirculating flow supplies the Ekman boundary layer as well as the entrainment to the annular mixing layer, and the fluid leaving the Ekman boundary layer near the axis moves uniformly downstream, recirculation being confined to an annular zone. The effect of the extraction of fluid via the Ekman layer and the hypothetically laminar core is similar to that of suction through the base: the recirculation region is much shorter than in a non-swirling flow. A noteworthy feature of swirling base flows is that the angular velocity of the fluid in the free shear layer will tend to increase as it approaches the axis

(angular momentum being approximately conserved) and both the fluid which recirculates and that which escapes downstream may be swirling very strongly. Charwat and Schlesinger present some evidence that the flow downstream of the primary recirculating zone experienced what they call "vortex breakdown" but which appears to be the recirculation phenomenon found in strongly-swirling jets. Note that their flow is effectively the inner part of an annular swirling jet, a configuration popular in fuel injectors. It seems unlikely that detailed predictions of such a complicated flow will be possible in the near future, and although the photographs of Ref.254 show clear qualitative evidence of the stabilizing effects of rotation, particularly on the Ekman effluent, a consideration of the quantitative effects of streamline curvature would be premature. The same conclusions about the Ekman layer effects and the general complication of the flow apply to other confined vortices, typified by the Ranque-Hilsch vortex tube (a device for undermining faith in the second law of thermodynamics by separating an isothermal stream into one hot and one cold stream): an extensive review of this popular subject is given by Lewellen (255) and some interesting flow pictures by Johnston (256), Travers (257) and Yu (258) but no fresh information about curvature effects can be extracted. Badri Narayanan and Kangovi (259) have investigated the near-wake of a rotating axial cylinder in a purely axial external flow, in which case the Ekman flow is radially outwards and therefore less spectacular in its effects. The ratio of circumferential velocity to axial velocity was only 0.33 and although the (destabilizing) effects of rotation were noticeable as an increase in the spreading rate of the free shear layer and a reduction of about 30 per cent in the length of the recirculating region, no spectacular changes in the flow were observed.

10.2 SWIRLING WAKES AND JETS

The only experimental work on the swirling wake far downstream of a rotating body seems to be that of Liu (260). The velocity defect on the centre line decreased by about 20 per cent in the range $10 < x/R < 50$ as a result of rotation of a blunt-based body at a velocity ratio of 0.58, but the drag of the body was not measured and the results of Ref.(259) suggest that it may have increased considerably as a result of rotation, so that the change in velocity defect at constant drag would have been larger than 20 per cent. This implies significant effects of swirl on mixing rate in the earlier regions of the far wake.

Swirling jets and wakes have been classified by A.J. Reynolds (261) according to whether the ratio of a typical circumferential velocity W to a typical axial velocity U or velocity defect ΔU increases, decreases or remains constant as x increases. The only case in which the ratio increases is the axisymmetric swirling wake of a self-propelled body (zero drag but finite torque - not a practical situation although of course it applies to the usual idealization of a wingtip vortex of an aircraft of high aspect ratio). In the case of small swirl, implying negligible effect of the swirl on the axial motion, self-preservation and conservation of momentum and angular momentum requires $\Delta U \propto x^{-1/2}$, $W \propto x^{-3/4}$, $\delta \propto x^{1/4}$. Note that the wingtip vortex nominally has large swirl (negligible axial motion). In the case of the rotating body with finite drag, the small-swirl solution is $\Delta U \propto x^{-2/3}$, $W \propto x^{-1}$, $\delta \propto x^{1/3}$, and the relations for ΔU and δ have been verified by Liu for $x/R > 15$ (where the swirl was probably quite small and the turbulent motion maintained chiefly by the mean shear $\partial U/\partial r$ as in a non-swirling wake). In the case of the jet in still air, $U \propto x^{-1}$, $W \propto x^{-2}$, $\delta \propto x$. Now even if the small-swirl solution is not exactly valid it is certain that the ratio of typical velocities, W/U or $W/\Delta U$, will decrease steadily with distance from the origin of a swirling jet or wake. Therefore, particularly in the case of the swirling jet which is much more important than the swirling wake in practice, the major effects of swirl on mixing occur fairly close to the origin. Even in the case of small enough swirl for the axial flow to become approximately self-preserving, the swirl will have largely decayed before self-preservation is attained. It follows that the effects of swirl will interact with the effects of the initial conditions (262), specifically the profiles of axial and circumferential velocity just downstream of the jet nozzle or wake-producing body, which makes it most unfortunate that the majority of investigators of swirling jets have used rather arbitrary initial conditions not easily reproducible by others and sometimes not fully documented by the experimenters themselves.

From the point of view of reproducibility, the best swirling jet generator is a long rotating pipe giving a fully-developed pipe flow in solid-body rotation. This was used by Rose (263) in the first of the well-known experiments on the subject, published in 1962. Chigier and Chervinsky (264) quote work on annular swirling jets by Ullrich (1960). Rose shows that, for a pipe circumferential velocity of about 0.4 times the centre-line velocity of the pipe flow, the swirling jet at $x/d = 15$, where d is the pipe diameter, has almost twice the diameter of the non-swirling jet. However the turbulence intensity at $x/d = 15$ is about the same fraction of centre-line velocity in each case, indicating that the effects of swirl on the turbulence and on the mixing rate have already largely disappeared (the maximum swirl angle was about 9 deg. at $x/d = 15$). This is confirmed by measurements of mean-velocity decay at larger distances from the exit. Shortly after Rose's work, Lee (265) carried out a similar experiment and confirmed Rose's results.

In the years since Rose's paper a great deal of work has been done on swirling jets and associated flows. Nearly all theoretical work has been based either on assumptions of self-preservation or at least of negligible effect of swirl on the axial component of shear stress: the latter assumption is an extension, which can be seen in the present context to be unreliable, of the well-known "small-crossflow" assumption used in three-dimensional boundary layers. Since most engineers are interested in using swirl to promote mixing (inevitably in the non-self-preserving region) and since we are interested in the effect of swirl on turbulence structure this work is of little relevance: references are given, for instance, by Pratte and Keffer (237). Rubel (266) has correlated the eddy viscosity needed to predict the swirling jet measurements of Chervinsky (267) as a function of a simple Rossby number, equal to (axial velocity)/(swirl velocity). Rubel's correlation is non-linear but can be fitted quite closely by an eddy-viscosity factor

$$\left(1 + 7 \frac{W}{U}\right)$$

which can be related to an F-factor if one replaces W/U by a multiple of $(\partial W/\partial r)/(\partial U/\partial r)$, a reasonable approximation in the outer region of a swirling jet. The only other piece of theoretical work on swirling jets that implicitly includes an allowance for curvature effects on the turbulence is that of Schetz (268), who takes the value of his (supposedly isotropic) eddy viscosity from experiments on classical vortices.

Most other theoreticians have carried over empirical constants from the analogous non-swirling flow: for example Lee (269) uses an entrainment coefficient taken from experiments on non-swirling buoyant plumes and finds good agreement with his own experiments on plumes with swirl introduced at the source. In such a case it follows that the effect of swirl on mixing rate must have been negligible.

Experiments on swirling jets have been reported by several authors (237, 263-265, 270-272). Craya and Darrigol (271) report turbulence measurements, including some in a recirculating jet, but do not document their mean flow. The only detailed investigation of the turbulence, other than Rose's work, is that reported by Pratte and Keffer (237) also in the jet from a spinning pipe. The Reynolds number was only slightly higher than the minimum required for turbulent pipe flow, and the flow was apparently not fully developed at exit. The axial velocity profile measured one diameter downstream of the exit happened to be very close to a fully-developed jet profile, and as a result the mean flow appeared to be self-preserving at all the measurement stations although the turbulent quantities do not attain self-preservation until roughly $x/d = 12$. Measurements of all six independent Reynolds stresses were made, although the measurements of the shear stresses \overline{uv} , \overline{vw} and \overline{uw} are unfortunately rather scattered. The circumferential component of shear stress, $\overline{w\theta}$, appears to increase monotonically with distance downstream but since impossible non-zero values occur on the axis the measurement may not be trustworthy. A unique experiment on a pair of contra-rotating jets has also been reported by Keffer (273): the effects of streamline curvature on the turbulence had probably subsided before the jets interacted seriously.

Beér and his colleagues (notably Chervinsky and Chigier) at Ijmuiden and latterly at Sheffield, have concentrated on swirling flows for application to combustion systems. As well as the work on pre-swirling jets already referred to, they have studied jets and buoyant plumes which have no pre-swirl but which entrain swirling fluid from outside. A high level of swirl is maintained far downstream, in contrast to the pre-swirling jet. As pointed out by Emmons in the discussion following Ref.(272), the angular momentum in these flows increases with distance from the axis and, in the most common configuration, becomes nominally constant in the external swirling flow. There is at present no evidence of an overshoot in circulation like that believed to exist in trailing vortices. Therefore, again in contrast to the pre-swirling jet, there is probably no region of a constant-density externally-swirling flow in which the turbulence is intensified by the direct effects of swirl: of course the increase in resultant velocity tends to increase the turbulence level. Naturally, variable density is a feature of combustion systems and - see Eq(91) - the most common case of low density near the axis of a flame and high density in the external flow reinforces the stabilizing effect of a positive angular momentum gradient. Beér et al. (123) show photographs of a swirl-stabilized flame which is not only laminarized but laminated, with an annular structure like that seen in isolated vortex cores. In a cold helium/air flow, simulating a flame, the two components of Reynolds shear stress fell to zero in the core region, confirming that the flame itself was laminar. The Reynolds numbers of these laboratory flows - originally studied by Emmons and Ying (274) - are fairly small but much higher than the critical Reynolds number of a non-swirling flow. A large-scale version of the phenomenon is the "fire whirl", the effect on a large fire of entraining naturally-swirling air from the atmosphere. Swirling flames are an example of the class of flows in which a qualitative consideration of curvature effects is helpful in understanding the phenomena but which are rather too complicated to yield quantitative data for general use: turbulence measurements are difficult and numerical experiments may show up discrepancies other than those directly attributable to curvature effects.

10.3 SWIRLING PIPE FLOWS

Duct flows, like jets, can be classified according to whether the swirl is introduced at the start of the flow, to decay downstream, or maintained by helical vanes or by rotating the boundary. Note that rotating cylinder flows with no net axial motion were reviewed in Section 4 and thin annular boundary layers in Section 6.

Swirling flow in a stationary pipe, maintained by a "twisted tape" was investigated by Backshall and Landis (275). The so-called twisted tape was a helical partition of 27 deg. helix tip angle, extending across the full diameter and down the full length of the pipe, so that in effect the flow was that in a twisted duct of semi-circular cross section. Secondary flows analogous to the Ekman effect occur [see the earlier papers by Smithberg and Landis (276) and Seymour (277)] with convergence of fluid in the tape boundary layer towards the centre line of the pipe and a corresponding concentrated radial outflow into the main body of the fluid, in addition to quasi-inviscid secondary flow caused by skewing of the mean vorticity vector. Date (278) makes the useful point that these sources of secondary flow probably overwhelm the stress-driven secondary flows that would exist even in a straight semicircular pipe. Thorsen and Landis (279) discussed the further complication of large density gradients, and proposed correlations for heat transfer and friction factor involving a Grashof number based not on gravitational acceleration but on centrifugal acceleration. As commented in Section 5, "centrifugal buoyancy" effects are likely to be rather smaller than the curvature effects that appear even in constant-density flow. Backshall and Landis (275) concentrated on the flow near the circular wall of a pipe with a twisted tape, finding that the logarithmic law adequately correlated the resultant mean velocity profiles out to a distance from the wall of about 0.2 times the pipe radius a or 0.05 times the radius of curvature of the streamline. The value of R_f near the wall given by Eq(104) is about $-3y/a$, so that some curvature effects might be expected. Nearer the axis, where curvature effects are stabilizing but probably larger, departures from axisymmetry themselves affect the turbulence. Many other investigators have reported pressure drop and heat transfer in pipes with twisted tapes. The practical interest is in the increase in heat transfer to or from a given pipe with given mass flow: the status of empirical correlation formulae for pressure drop and heat transfer appears satisfactory (280) but our knowledge of the flow processes certainly is not. Date (278) reviews correlation formulae and presents interim calculation methods, which do not explicitly consider streamline curvature effects. For introductory reviews of the subject as a whole see the early paper by Kreith and Margolis (281) or the more recent paper by Lopina and Bergles (282). Ref.(280) is a general survey of heat-transfer augmentation by turbulence promoters. A very recent paper by Seban and Hunsbedt (283) treats the heat transfer in an annulus with a twisted "tape". Note that some investigators refer to the axial distance for 180 deg. (not 360 deg.) twist as the "pitch", and that the usual ambiguity between radius and diameter as a non-dimensionalizing factor also occurs: "helix tip angle" is unambiguous and meaningful.

There seems to be little detailed information on the decay of pre-swirl in a simple pipe flow: any device for generating strong swirl will cause large changes in the axial velocity profile, whose return to "full development" will be inseparable from the decay of the swirl, and the configuration is more attractive to the theoretician than the experimenter. The subject gradually merges into the study of classical isolated vortices in the Mabey-Squire type of vortex tube: it is frequently unclear whether experiments on "vortex flows" in tubes are supposed to relate to classical vortices surrounded by an irrotational flow ($W \propto 1/r$), to fully-turbulent pipe flow initially near a state of solid-body rotation ($W \propto r$), or to some unhappy compromise between the two. A fairly early paper of this type is Ref.97, which gives a short review of previous work. Unfortunately it is not possible to classify experiments by the swirl generator used: the use of a twisted tape or rotating grid implies a rough approximation to solid-body rotation, but a vortex tube with radial entry, of the type originally intended to generate a classical vortex with $W \propto 1/r$ outside the core, can be used by design or accident to produce almost any swirl distribution. Kreith and Sonju (285) made measurements of the decay of swirl in a pipe downstream of long twisted-tape swirl inducers with tip helix angles up to about 30 deg. The measurements are not sufficiently detailed to show how soon the flow becomes substantially axisymmetric. The main results for swirl decay were obtained using a "swirl meter", a flat plate at zero incidence, nearly spanning the pipe and free to rotate about a shaft on the axis. The rotational speed of the plate is an average, weighted in some unknown way, of W/r . The swirl so measured decreased to half its initial value by about 40 pipe diameters downstream of the end of the twisted tape, the decay rate decreasing as Reynolds number increased. Very good agreement was found with a theory which assumed a constant value of $v_{r\theta}$, independent of x and r and equal to about one-third of a representative average value of v_{rx} . While one can count this as further evidence for the anisotropy of eddy viscosity, the ostensible deduction from the constancy of $v_{r\theta}$ with x is that streamline curvature (which decreases with x) has no effect on the turbulence, even for an initial swirl angle as large as that in Backshall and Landis' experiment. Wolf, Lavan and Fejer (286) measured the swirl in a stationary pipe with a radial inlet, with vanes giving an approximation to free-vortex flow ($W \propto 1/r$). The swirl distribution soon took up the familiar form shown in Fig.32, but although the exponential decay of swirl substantiates Kreith and Sonju's assumption the value of v_{rx} deduced from the results is about half that found by Kreith and Sonju. This is as good a demonstration as one could wish of the sensitivity of swirling flow to the details of the swirl distribution, a sensitivity which may not be entirely attributable to the effects of streamline curvature but which is doubtless aggravated by those effects. It seems very improbable that the satisfactory logarithmic profiles of Ref.275, and the satisfactory decay predictions of Refs (285) and (286) with $v_{r\theta}$ independent of the decay of swirl, should really be taken as an indication of negligible curvature effects in pipe flow. Various other theoretical investigations (e.g. Refs 287, 288; see also Refs 245, 278) have used concepts generally similar to those of Kreith and Sonju, invariably with good agreement with experiment after choice of an empirical constant in the formula for $v_{r\theta}$ or its equivalent, and usually implying $v_{r\theta}$ much less than v_{rx} . There is a clear need for more experiments and for comparisons with more refined calculation methods to elucidate the effects of streamline curvature in swirling pipe flow. A recent paper is Ref.289. This paper seems to have suffered severely from typographical and linguistic difficulties but once more indicates $v_{r\theta} < v_{rx}$.

Rask and Scott (290) recently measured the decay of strong pre-swirl in an annular duct, which, like a pipe flow, is stable everywhere except near the outer boundary where W decreases rapidly. The mean flow exhibited inhomogeneities which they describe as having a spiral form like a spring of variable pitch: it seems very likely that these were helical vortices but it is not clear whether they were directly attributable to curvature effects on the turbulence or caused by an instability of the mean flow resulting from the rapid decrease in radial pressure gradient caused by the decay of the swirl. This latter effect is known to cause recirculation in strongly-swirling pipe flow: Gore and Ranz (251) classify it as a viscous effect because the swirl decays by viscous (or turbulent) action, in contrast to the recirculation that can occur close to a swirl generator, or at the exit of a pipe (i.e. the start of a jet) when the constraint of the wall on radial motion is removed. An intermediate explanation could be a form of precession of the swirling flow near the centre body analogous to that described by Syred and Beér (262) in a jet. Whatever the reason for Rask and Scott's results it is surprising that these departures from axisymmetry have been observed in an annular duct but not in a pipe where the flow near the axis is unconstrained: possibly separation or incipient separation from the centrebody is involved. Scott and Rask (291) have further analysed their swirling annular flow data to extract eddy viscosities. The results suffer from the difficulty first noticed by Wattendorf (82), that $\partial U/\partial r$ and \overline{uv} go to zero at different radii so that v_{rx} shows misleadingly large scatter even if negative values are rejected. Scott and Rask conclude that in general $v_{r\theta} < v_{rx}$, and they point out that quite low values of $v_{r\theta}$ appear near the inner wall: indeed $v_{r\theta}$ barely exceeds v in some conditions suggesting that the highly-stable flow near the inner wall has almost reverted to the laminar state.

White (213) investigated flow in a spinning pipe, fed from a swirl-vane vortex generator so that the entry flow was rotating at roughly the same speed as the pipe but did not have a fully-developed axial velocity profile. Cannon and Kays (143) investigated heat transfer in a spinning pipe with fully-developed (non-rotating) flow at entry. In these cases the effect of streamline curvature is everywhere stabilizing since W increases monotonically to the wall. In Cannon and Kays' experiment, a region of swirling relaminarized flow spread out from the wall into the non-rotating turbulent core. When the flow rate was increased, the speed of rotation of the pipe remaining constant, helical instability waves appeared at the laminar-turbulent interface. These may have been essentially similar to the streamwise vortices that appear in transition of a three-dimensional boundary layer even on a plane surface, but, as remarked in Section 5.6, the mechanism as described by the investigators could be a curved-flow analogue of the Kelvin-Helmholtz instability or overturning of a density interface in a gravitational field (144) with a region of large velocity gradient being overturned in a centrifugal field. White's flow-visualization pictures, taken near the pipe entry, show a stable but wandering core with some evidence of turbulent mixing at larger radii. At the highest rotational speed tested, the axial pressure gradient in fully-developed flow was only 0.6 of that in the stationary pipe at the same mass flow rate, indicating that turbulence was suppressed over most of the cross-section.

Several experimenters have reported on flow with an axial component between concentric rotating cylinders ("spinning", according to our chosen convention). Kaye and Elgar (292) plotted boundaries, in the Reynolds number-Taylor number plane, between laminar flow with and without vortices and turbulent flow

with and without vortices, for the (unstable) case of a rotating inner cylinder. The work was extended to heat transfer (with small temperature differences so that the velocity field was little affected) by Becker and Kaye (293): the measurements were not detailed enough to deduce the effects of curvature on the Reynolds analogy factor. Astill (294) further extended the work to the entry region, where the boundary layers on the rotating cylinders have a uniform non-swirling free stream as in the experiments of Parr (166), and Furuya (167). He comments that the change from turbulent flow without vortices to turbulent flow is "easily detected" by the appearance of sharp peaks in the hot wire trace. This suggests that even in the presence of axial flow the vortices between rotating cylinders are particularly strong, although in this case there is no direct circumferential "feedback" (Section 5.5) to maintain them. Perhaps the first of the possible constraining influences mentioned in Section 5.5 (that the number of vortices at any cross section must be an integer) is still powerful enough to sustain a simple, well-organized vortex structure. Gelhar and Monkmeier (295) who give a useful review of previous work, extended Kaye and Elgar's results to higher Reynolds numbers and found that helical vortices occurred if the Taylor number exceeded about 0.25 times the Reynolds number for a gap-to-mean radius ratio of 0.134, corresponding to a cylinder rotational speed of about 0.65 times the axial bulk velocity of the fluid, for Reynolds numbers based on bulk velocity and gap of about 1 to 3×10^4 . Both groups of experimenters found that, in the turbulent vortex regime, increasing the axial velocity decreased the mixing rate (Kaye and Elgar measured heat transfer, Gelhar and Monkmeier measured torque and in the latter experiment at least the Reynolds number was high enough for conventional transition effects to be absent). A plausible explanation is that increasing the axial velocity reduces the intensity of the vortices, which are likely to be more efficient in transporting heat or momentum than ordinary turbulent eddies. Nagib's discovery (74) of concentric sets of helical vortices of opposite pitch in the corresponding laminar flow is unlikely to be repeated in the more diffusive environment of turbulent flow (the multiple vortex system deduced by So and Mellor (160) from measurements in a curved turbulent boundary layer is kinematically impossible) but is a reminder that quite complicated transient motions might occur as modifications of the large eddy structure. Nagib's thesis is a helpful introduction to the problems of transition in swirling flows.

Humphreys, Morris and Barrow (296) measured heat transfer in the entry region of a pipe spinning about an axis parallel to itself (the application being to cooling passages in rotating machinery). Their results are correlated in terms of the acceleration ratio $h\Omega^2/g$ where h is the distance between the pipe axis and the axis of rotation. Although this parameter is frequently used in discussions of "centrifugal buoyancy" effects it is not a valid one because g does not enter the problem: the proper parameters are $\Omega d/\bar{U}$ and h/d , representing swirl effects and the relative importance of radial pressure gradient respectively [the ratio of the centrifugal pressure difference across a diameter to a typical dynamic pressure is of order $h\Omega^2/\bar{U}^2 \equiv (\Omega d/\bar{U})^2 \cdot (h/d)$]. In the entry region δ/d is an additional parameter. An additional parameter that appears when, as in the present case, significant density gradients occur is the 'centrifugal buoyancy' part of the Richardson number, e.g. Eq(91). However, Humphreys et al. found the effects of centrifugal buoyancy to be small, at least in the entry region, and attributed the increases in heat transfer (up to 50 percent at $h\Omega^2/g \approx 40$) to the fact that the entry flow was swirling with respect to the pipe as in Cannon and Kays' experiment. Unfortunately — though not surprisingly — no profile measurements were made in this rather complicated rig.

10.4 MISCELLANEOUS SWIRLING FLOWS

There are a few experiments on swirling flows that are not easy to classify. Koosinlin and Lockwood (297) made measurements in the boundary layer on a rotating cone in still air. In contrast to the rotating disc, in which the only extra rate of strain is lateral ($\partial v/\partial r$ in x, r, θ coordinates), the rotating cone suffers curvature/rotation effects as well as lateral divergence: the combination of the two extra strain rates presents a difficult problem. Also, the cone angle in Koosinlin and Lockwood's experiment (80 deg. included angle) was large enough to invalidate the Richardson number analysis for slowly-growing flows on rotating bodies leading to the first element of Eq(113) and to force reliance on the dubious arguments about the proper choice of axes in general three-dimensional flows following Eq(109). In view of the sparseness of the results (one profile each for U and W) no analysis can be attempted. Koosinlin and Lockwood also present results for an annular wall jet, blowing over the rotating cone from a nozzle at the apex: the net effect of rotation is to decrease the growth rate although Koosinlin and Lockwood (246) obtain quite good agreement between experiment and calculations by a method that does not explicitly allow for direct effects of curvature or rotation (or lateral divergence) on the turbulence.

Literature on swirling flows inside conical annular diffusers is reviewed by Hoadley and Hughes (298) and by Hughes (165). When the boundary layers become thick enough for the thin-shear-layer approximation to break down (implying curvature effects beyond the range of applicability of F -factors) significant interaction between boundary layers and potential flow may occur, and the main effect of swirl in suppressing separation, or transferring it from one wall to the other, may be exerted via changes in the inviscid flow rather than direct influence on the turbulence. The above-mentioned investigators also studied the effect of rotating the centrebody of an annular diffuser (a likely occurrence in a turbo-machine); separation from the hub was delayed over a certain range of rotational speeds.

Nakamura et al. (299) extended their own work (167) and that of Parr (166), on boundary layers on rotating cylinders in constant-pressure axial streams, to the case of thick "boundary layers" (δ/r as large as 0.45) and flow over axisymmetric steps ($h/\delta \sim 0.5$). Their mean velocity measurements are presented in some detail and should be useful for test cases. Without detailed comparisons with a calculation method known to give good results in thick "boundary layers" on non-rotating cylinders, the interaction between the effects of rotation and of large δ/r is difficult to distinguish; the rate of growth of the thickest rotating boundary layer appears to be nearly linear while the thinner boundary layers, rotating or non-rotating, grow more slowly than this, indicating that rotation effects increase strongly with δ/r at least up to $\delta/r \sim 0.45$. The step results show no unexpected features: the measurements were not detailed enough to detect the Ekman pumping effect mentioned earlier in the present Section.

Traugott's experiments (100) on turbulence generated by a rotating grid were described in Section 4,

and incidental results on curved boundary layers were obtained as a spin-off from the main measurements.

A configuration intermediate between the Ranque-Hilsch type of short vortex tube and the long pipe with decaying swirl is a long pipe fed from tangential nozzles near one closed end. Near the swirl generator a complicated flow can occur. The "swirl number" varies rapidly with streamwise distance because the axial momentum flux varies rapidly, so that even if a simple correlation on swirl number were admissible we could expect the flow to depend critically on geometry, while in practice the behaviour is likely to be more complicated than predicted by swirl-number correlations. For instance, King, Rothfus and Kermode (300) found a reversed-flow region near the axis, starting at the injector nozzle position and extending for a few tube diameters downstream. It is not clear how the reversed-flow region joined on to the presumed Ekman effluent jet travelling downstream along the axis, but precession and breakup of the jet near the plane of the injector nozzles would be expected. A more important question, in the context of studies of the decaying swirl far downstream, is whether the influence of the separated flow region propagates along a non-turbulent core. It is known that the cores of isolated vortices can transmit axial disturbances over long distances (216) and if the same is true of swirling pipe flows results for swirl decay inferred from experiments with a particular type of swirl generator may not be generally applicable.

This review of swirling flows makes it clear that although useful practical results and data correlations have been obtained, the subject is a confusing one and that our basic knowledge is accordingly confused. Much confusion could be avoided, however, by clearer classification of the different types of swirling flow and in particular by restricting the use of the words "vortex" and "vortex tube" to mean respectively the fully-rolled-up vortex, surrounded by irrotational fluid (Section 9) and the Ranque-Hilsch type of short vortex tube, relying on Ekman-layer pumping of fluid near an end wall. Fig.32 is a summary of the types of flow discussed above: at present each type must be considered separately and there is little prospect of a common treatment, because curvature effects on the turbulence structure are usually large. Fortunately, detailed predictions are not always required — in the case of pipes with twisted-tape swirl promoters, for instance, one requires only a correlation for heat transfer and pressure drop plus some qualitative understanding to aid optimum design. Qualitative understanding of curvature effects suggests that the development of any swirling flow may be quite sensitive to the initial swirl profile, specifically the extent of regions with a given sign of angular momentum gradient. Care should be taken to choose meaningful initial swirl distributions and to measure them accurately. On the theoretical side, formulation of transport-equation methods and comparison with mean-flow experiments is probably the only way of inferring curvature effects with adequate accuracy. The use of eddy-viscosity anisotropy factors is a much inferior approach and data correlations on this basis are unlikely to be widely applicable, although they have been useful in the past. For this reason the correlations of anisotropy factors quoted in the literature will not be reproduced here.

Two useful reviews are Ref.255, principally on the flow in Ranque-Hilsch vortex tubes and similar situations, and Ref.301, principally on the theoretical aspects of swirling flows in ducts: they contain about 350 and 220 references respectively, covering most aspects of swirling flows.

11. DISCUSSION AND CONCLUSIONS

11.1 PHENOMENA AND CALCULATION METHODS

An important class of "complex" turbulent flows [i.e. flows other than simple shear layers (p.4, Refs 1, 2)] consists of shear layers subjected to extra rates of strain, additional to the simple shear $\partial U/\partial y$. Most of the extra strain rates or body forces so far investigated (Fig.2 and Section 3) produce changes in Reynolds stress of the order of ten times the changes predicted by plausible extensions of calculation methods (Section 2.5) for simple shear layers. The reason is that the extra rates of strain have large effects on the higher-order structural parameters of the turbulence which are not reproduced by the empirical approximations to these parameters used in calculation methods. An obvious first step in allowing for these effects is to make the empirical approximations depend additionally on a dimensionless quantity representing the extra rate of strain. The simplest dimensionless quantity (p.16) is $e/(\partial U/\partial y)$, the local ratio of the extra strain rate to the simple shear, but this implies the assumption that $\partial U/\partial y$ is a suitable measure of the eddy frequency or fluctuating rate of strain and the turbulence quantity (Reynolds stress) $^{1/2}$ /(eddy length scale) is more realistic: the special case $(-\overline{uv})^{1/2}/L$ is equal to $\partial U/\partial y$ in the local-equilibrium approximation for a simple shear layer (p.13). Extra strain rates can be applied rather suddenly and their full effects on the turbulence structure are not felt for a time of the order of the lifetime of the eddies that carry the Reynolds stresses (pp 18-20), corresponding to a streamwise distance of roughly 10δ in the outer part of a boundary layer or 2δ in a mixing layer or jet. In many cases it is therefore necessary to allow for "history" effects in the correction factors for extra rates of strain, additional to, and more important than, any allowance for "history" effects in the basic calculation methods. This has not yet been done formally, but a simple lag equation for the effective value of e , Eq(37), produces significant improvements and is easy to apply to any type of calculation method.

In view of the dependence of the Reynolds stresses on the history of the extra strain rate, correction factors which are elaborate non-linear functions of the local parameters $e/(\partial U/\partial y)$ or $e/((-\overline{uv})^{1/2}/L)$ are probably not realistic, even if an "effective" value of e is used. Non-linear functions deduced from experiments on self-preserving or local-equilibrium flows are not likely to be valid in non-self-preserving flows. A further difficulty is that extra strain rates are likely to change the turbulent transport terms in the Reynolds-stress transport equations (Section 2.4) as well as the destruction/redistribution terms, and we have at present very few data on this effect. Without more data on extra strain rates in general it is probably unrealistic to use a correction factor more complicated than

$$F = 1 + \frac{\alpha e}{\partial U/\partial y} \quad (36)$$

where e is the effective value obtained from Eq(37) and α is a constant for a given type of shear layer and a given type of extra strain rate: at most, we can justify making α an empirical function of

y/δ , or changing the magnitude of α with the sign of e as in the Monin-Obukhov meteorological formula, Eq(119). Note that non-linear meteorological formulae are intended for the special case of the Earth's local-equilibrium inner layer, and note also that a more complicated parameter than $e/(\partial U/\partial y)$ may be needed in three-dimensional or compressible flows even though it is to be used in a linear formula. Following the usual spirit of linear formulae we restrict the application of Eq(36) to small extra strain rates (p.17), say $|e/(\partial U/\partial y)| < 0.05$ giving $0.5 < F < 1.5$ with $\alpha = 10$. Naturally this excludes a large number of cases one would like to be able to predict, in which large extra strain rates are applied to a shear layer. However Eq(37) has the property that the effective value of e at the end of a short region of extra rate of strain depends only on the total extra strain and not on the distribution of the extra rate of strain, which can therefore take large values for short periods without invalidating the linear analysis. Eq(37) is of course a simplification but it seems likely that a more refined lag equation would exhibit a similar response to "strain impulses". The linear analysis can therefore be applied to short regions of large extra strain rate and fails only for prolonged large extra strain rates or extremely strong strain impulses.

The simplest application of the correction factor F is to the length scale that necessarily appears in any calculation method, whether it be the apparent mixing length, a length factor in the apparent eddy viscosity, or a true eddy length scale like the dissipation length parameter L as in Eq(36), p.18. Since F is supposed to be limited to values close to unity we can write

$$\epsilon \equiv \frac{(-\overline{uv})^{3/2}}{L} = \frac{(-\overline{uv})^{3/2}}{L_0} \cdot \frac{1}{1 + \alpha e/(\partial U/\partial y)} \approx \frac{(-\overline{uv})^{3/2}}{L_0} \left(1 - \frac{\alpha e}{\partial U/\partial y} \right) \quad (142)$$

This has the advantage that in a flow subjected to several small extra strain rates (such as an axisymmetric compressible flow like that of Ref.54, which suffered from curvature, lateral dilatation and bulk compression) the different values of αe can simply be summed. This still applies if each αe is determined from a separate application of a lag equation like Eq(37), even if [as discussed after Eq(37), p.19] the lag is applied to e/U instead of e . A more dubious advantage is that computer calculations do not break down if $1 + \alpha e/(\partial U/\partial y)$ becomes zero: this avoids failures in unimportant regions near the edge of a shear layer where $\partial U/\partial y$ becomes small, but tempts one to use F -factors without considering their limits of validity. Eqs (37) and (142) have been implemented in the calculation method of Ref.16 as used for the numerical experiments in Appendix 2: further details are available from the author. In local equilibrium conditions L becomes equal to the apparent mixing length ℓ and F -factor modifications can therefore be made to the inner-layer logarithmic formula [Eq(43)] if it is used as a boundary condition for the calculation.

Examples of flows subjected to extra rates of strain were discussed in Sections 3.2 to 3.4: Ref.1 is a comprehensive bibliography of complex turbulent flows in general.

An important class of flows with extra strain rates are curved or rotating shear layers. Rotating flow systems are usually most conveniently analysed in rotating rectangular Cartesian coordinates but coordinate systems for curved shear layers and other distorted flows need more care. In two dimensions or on infinite swept wings (s,n) coordinates (Section 2.2) are appropriate: axisymmetric swirling flows can be analysed in (x,r) coordinates (Section 2.3). There are some physical uncertainties in the analysis of fully three-dimensional curved flows but here and in other cases of flows with complicated streamlines or complicated boundaries it may be necessary to use complicated coordinate systems to obtain numerical stability. The general tensor analysis of Appendix 1 is intended for use in such cases: it has not been necessary to use it in the present discussion of the physics of curvature effects. In the other limit of weak curvature effects the equations in the (s,n) system can be simplified, eventually reducing to those of the rectangular (x,y) system: it is hoped that Section 2.2. is an adequate list of the pitfalls awaiting practitioners of higher-order turbulent boundary layer theory.

The analogy between streamline curvature and buoyancy effects on turbulence, originally due to Prandtl (80, p.775), is no longer of great quantitative help in evaluating F -factors or other correction formulae, since meteorological formulae for the Earth's inner layer are at best only a rough approximation in other regions of laboratory shear layers and we now have at least some explicit data for the latter cases. However the algebraic analogy between the parameters for buoyancy and for curvature [Eqs (4,5) and (50) to (60): Sections 5.1 and 5.2: Table 2] is helpful in illuminating physical processes and resolving ambiguities in the case of curvature. Quantitative analyses for the stability of inviscid flows, analogous to classical treatments of buoyant fluids, are probably not very relevant to turbulence (p.38) although Orr-Sommerfeld solutions for curved or rotating turbulent flows, using an assumed eddy viscosity (pp.41-42) may be useful in comparative studies of the appearance of longitudinal vortices or other convection cells in unstable cases. The buoyancy/curvature analogy is qualitatively useful in discussions of instability vortices or the internal waves which probably appear in stably-curved turbulent flows (Sections 5.5 and 5.6). We note (pp.40-41) the difficulties in definition of vortices which arise from their gradual emergence from the large-eddy structure of the turbulence. Only disturbances from upstream or the effect of lateral boundaries can constrain the vortex pattern sufficiently for it to produce spanwise inhomogeneity of the mean flow. The behaviour of the turbulence will be little affected by the steadiness or otherwise of the vortex pattern: the distinction is man-made and can be eliminated by suitable averaging techniques. Probably the only case in which the distinction is material is that of a separating boundary layer: the reaction time of the external flow being presumably much longer than the typical time scale of unsteady vortices, the separation line (at which $d\delta/dx$ becomes of order unity) probably remains fairly straight if the vortices are unsteady, whereas strong spanwise variations of separation position may build up if the vortices are steady enough to produce spanwise periodicity of the mean flow.

The main dimensionless parameters for curved or rotating flows (Section 5.1) can be derived, following meteorological practice, either as the square of the ratio of the oscillation frequency of a displaced fluid element to a typical frequency of the turbulence or as the ratio of the extra production of radial-component turbulent intensity to the total production (R_i and R_f respectively). The extended Monin-Obukhov parameter, $(L/K)/L_{mo}$, is equal to (extra production)/(dissipation) and may be more useful in regions dominated by turbulent transport rather than production (if any local parameter is

useful in such circumstances). Although these parameters all reduce to $-2 e/(\partial U/\partial y)$ - with $e \equiv \partial V/\partial x \equiv -U/r$ - in the simplest case of constant-density two-dimensional local-equilibrium flow, they can be significantly different from this simple parameter in swirling, three-dimensional (Section 5.2) or compressible flows and all the evidence is that in these cases the "meteorological" parameters should be used in the F-factor instead of the rate-of-strain ratio. Since the difference in the case of adiabatic compressible flow is a factor $1 + (\gamma-1)M^2/2$ the point is of some importance in aeronautics. The meteorological parameters can be evaluated for more general cases of variable-density flow: the Richardson number with the centrifugal acceleration U^2/r replacing g is not a complete parameter for these cases.

Many of the experiments reported on curved or swirling shear layers were carried out in ignorance of the large size of curvature effects and are therefore outside the range of linear F-factor corrections. Unfortunately the turbulence data obtained in these experiments are not sufficient to help us extend the F-factor analysis in any rigorous fashion: for instance the only measurements of turbulent transport terms are the limited data of Guitton (7) in a wall jet, the measurements of Lumley and collaborators (204) in a mixing layer which seem to be inconsistent in some respects, and the recent work of Castro (11), also in a mixing layer. Therefore measurements of strongly-curved flows are not directly useful at present in formulating generally-applicable curvature corrections. Data for flows with mild curvature are not extensive enough to warrant correlations of α as functions of y/δ : the analysis of Parr's data by Cham and Head (127) suggesting a very large variation of α with y is not supported by any other analysis. The present position seems to be that fairly reliable values for α can be deduced for boundary layers and wall jets, the values appropriate to the dissipation length parameter used in the calculations of Appendix 2 by the method of Ref.16 being

Stable (convex) boundary layer:	$\alpha = 14$
Unstable (concave) boundary layer:	$\alpha = -9$
Stable (concave) wall jet:	$\alpha = 8$
Unstable (convex) wall jet:	$\alpha = 6$

The mixing-length data of Johnston and collaborators (158) in rotating ducts, and further analysis of the measurements of Wattendorf (82) and of Eskinazi and Yeh (98), agree at small distances from the wall with the above values of α for the boundary layer. Nearer the centre of the duct the mixing-length ratio ℓ/ℓ_0 on the stable side becomes a function [Eq(129) of the "bulk Richardson number" or "rotation number", h/R or $\Omega h/U$, rather than of a local parameter, at least when the bulk parameter is numerically large: here ℓ_0 is the mixing length at the same point in the plane flow (effectively a multiple of h). The behaviour of ℓ in the highly-unstable part of the duct flow where $Ur \sim \text{constant}$, so that $Ri \rightarrow 0$, $R_f \rightarrow \infty$, is less certain. Certainly for the rotating duct (Fig.6) and probably for the curved duct, this corresponds to dominance of the large eddy structure by longitudinal vortices ("steady" or otherwise) extending over a large fraction of the duct width: "steady" longitudinal vortices have also been observed in boundary layers. Therefore, limiting values of ℓ/ℓ_0 as functions of the "bulk Richardson number" δ/R can be expected in unstable cases also. Note that the length δ does not correspond exactly to the length $\frac{1}{2}h$: a precise trade-off could be obtained by considering the duct as two interacting boundary layers but this is not a universally accepted approach and it is better to await explicit data for the boundary layer. Note also that the relation between the behaviour of ℓ , just discussed, and the behaviour of L depends on the (unknown) behaviour of the turbulent transport terms. Eq(129) should not be applied directly to L or any other eddy length scale, although similar equations relating turbulence structural parameters to bulk curvature parameters should be valid as long as the equivalent of ℓ_0 in Eq(129) is simply related to bulk scales like h , δ or τ_w (the detailed distribution of ℓ_0 or its equivalent is obviously not relevant when the turbulence structure has been greatly altered by curvature effects).

The case of strongly-stable flows may not be as critical as the unstable case. Crudely speaking, if the turbulence is strongly suppressed the Reynolds stresses are negligible and any curvature-correction factor that predicts them to an order of magnitude is acceptable for calculation methods. The deductions from the calculations for So and Mellor's stable boundary layer in Appendix 2 suggest that the regular F-factor [applied in the form $L_0/L = 1 - \alpha e/(\partial U/\partial y)$ to avoid the singularity when $\alpha e/(\partial U/\partial y) = -1$] will predict the suppression of turbulence in a boundary layer fairly well as long as the value of L_0 is related to the sub-boundary-layer thickness rather than the width of the boundary layer before application of curvature. Johnston's correlation for the limiting value of ℓ/ℓ_0 or its equivalent should become useful in the future.

Therefore the best advice (based on the above discussion and on Appendix 2) that can be given to people wishing to calculate curved boundary layers or two-dimensional duct flows by the method of Ref.16 or similar methods is

* Use the F-factor in reciprocal form, Eq(142), with Eq(37) as a lag equation, and replace $e/(\partial U/\partial y)$ by half one of the "meteorological" parameters (Table 2) in three-dimensional or compressible flows or other difficult cases.

* Use the values of α given above, with $X = 10\delta$ in Eq(37).

* For the limiting value of L in the outer regions of unstable boundary layer take $L/\delta = f(\delta/R)$, L_0 being directly related to δ in the method of Ref.16. A highly provisional suggestion for the function f is $0.095 (1 + 30\delta/|R|)$, but since this is fairly close to the original (not reciprocal) local F-factor with the outer-layer approximation $\partial U/\partial y \sim 0.3 U/\delta$ the local F-factor could be used instead.

In the case of wall jets (Section 7) and possibly free jets (Section 8) without an external stream

* Use the F-factor, Eq(142); according to unpublished work by Sawyer, a lag equation is necessary in some cases, but X in Eq(37) is probably only about twice the shear-layer thickness or $3\delta.5$.

* For strongly-unstable flows use the growth-rate data of Ref.7 (Fig.4): no reliable comments can be made on limiting values of L because jet flows are dominated by turbulent transport processes and because the thin-shear-layer approximation used in the calculations of Appendix 2 is not valid in highly-unstable jets, the value of δ/R corresponding to a given Richardson number being higher than in boundary layers.

In the case of mixing layers or jets with an external stream little can be said. A wall jet beneath an external stream eventually reverts to a boundary layer so that the appropriate value of α for small curvature changes in some unknown manner from the wall-jet value to the boundary layer value. A free jet in an external stream eventually reverts to a small-deficit wake, for which we have no curvature data.

It is evident from the above that improvements in the proposed calculation rules could be made after a little more experimental work or even a little more numerical experiment or analysis of existing data. I have decided not to include advance details of the work being done by my colleagues and myself in what is supposed to be a general review, but we hope that its outcome will be a more solid data base and a clearer understanding of the effects of large curvature on turbulent transport.

At present it would be very risky to suggest general rules for calculating classical trailing vortices (Section 9) or other slender swirling flows (Section 10) which are nominally turbulent throughout their cross section. Again, the basic reason is our lack of information about turbulent transport terms. The core of a swirling flow is necessarily in solid-body rotation so that the Richardson number (Ri or R_f) is very large and turbulence is effectively suppressed unless the swirl is small: further from the axis turbulence is probably maintained in the face of strong stabilizing effects by turbulent transport from even larger radii. The apparent Reynolds number dependence of trailing vortices, even at full scale, suggests that a large fraction of the total volume of turbulent fluid is at low local Reynolds number, introducing further complications (note that there is no evidence that highly-stable boundary layers have extended regions of low local Reynolds number: the Reynolds shear stress at the edge of the sub-boundary-layer in So and Mellor's experiment (160) fell to zero as rapidly as in a conventional boundary layer). Laboratory data for swirling flows are plentiful, but no existing experiment is sufficiently systematic to show up Reynolds number effects attributable to stabilizing curvature rather than the usual influence of solid boundaries. A general criticism of past work on swirling jets and pipe flows is the failure to appreciate the delicate effect of swirl distribution on flow stability. In view of the difficulties encountered (219, 237, 302) in measurements of $\overline{v\omega}$ (the rate of radial transfer of circumferential momentum) it seems unlikely that reliable measurements of turbulent transport terms in the Reynolds stress transport equations (notably $\overline{v^2\omega}$) will be made in the near future but numerical experiments by transport-equation calculation methods may be fruitful.

Flows in curved or rotating pipes or low-aspect-ratio rectangular ducts, together with flows in pipes containing twisted tapes or other types of swirl generator, are dominated by secondary flows, and the effects of streamline curvature on the turbulence cannot be distinguished at present.

11.2 FUTURE RESEARCH WORK

The overt purpose of research work being to contribute to calculation methods, the previous sub-section can be re-interpreted as a suggested research programme to supply the information needed to improve calculations of curved flows. As always, the need is for experiments, and for experiments with a clearly-defined purpose preferably identifiable with the needs of calculation methods. The main needs seem to be

- * Data for boundary layers, and other shear layers, with curvature effects typical of aeronautical practice rather than the exaggerated effects studied in many previous experiments designed to investigate curvature effects. This is roughly a requirement that $0.5 < F < 1.5$ over most of the shear layer, and the results of the work should contribute to improvement of simple F-factor formulae. Three-dimensional or compressible flows particularly need attention, and our knowledge of heat transfer is mainly indirect or inferential (303). Turbulence data would of course be welcome but mean-flow data (including skin-friction measurements both for their intrinsic value and for checks on momentum conservation) can still be used as test cases for calculation methods. Tabulations of the mean-flow data used in the calculations of Appendix 2 are given in that Appendix.

- * Experiments on vortices and swirling flows that acknowledge the importance of curvature effects on turbulence. It seems likely that either great care or conditional-sampling techniques or both will be needed to investigate the stabilized inner cores of these flows, which appear to wander under the influence of longitudinally-propagating disturbances or the turbulent flow farther from the axis. Accurate measurements of all the Reynolds stress components in these three-dimensional flows will be difficult to obtain.

- * Measurements of the triple velocity products that dominate turbulent transport of Reynolds stresses in the radial direction. Reliable measurements in almost any situation would be welcome: data for uv^2 , in addition to Reynolds stress measurements, would enable the pressure-strain "redistribution" term in the \overline{uv} transport equations to be deduced if pressure transport were ignored. Pressure-fluctuation measurements within the turbulence would of course be desirable but although some apparently reliable data are available the technique is so difficult, particularly in laboratory flows, that significant contributions to curved flows are unlikely in the near future. Pressure transport seems to be small in most plane flows but may be large in stable curved flows bearing internal waves (11).

- * Basic investigations of the changes in large-eddy structure caused by streamline curvature, specifically the development of unsteady longitudinal vortices and their tendency, with increasing curvature effects, to become steady enough to contribute to mean longitudinal vorticity. The development of internal waves in stably-curved flows, still largely hypothetical, also merits study and can also be regarded as a consequence of curvature effects on the large eddies.

The demands made on calculation methods by the effects of curvature and other extra rates of strain are more severe versions of the demands made by plane flows. Empirical models of the turbulent transport of Reynolds stress must be extended, with the aid of experimental data, to curved flows: once more the large-eddy behaviour is the key, and correlations in terms of local parameters are not likely to be widely applicable. Transport equations for eddy length scales have only recently been developed for plane flows: since most of the terms in these equations are effectively unmeasurable and must be evaluated by numerical experimentation their extension to curved flows will not be easy. However a length-scale transport equation capable of reproducing mean transport (history effects) has been found to be necessary when extra

strain rates change rapidly, and turbulent transport of length scale (in the radial direction) presumably becomes important in the same circumstances as turbulent transport of Reynolds stress. Therefore, while local-equilibrium methods of mixing-length or eddy-viscosity type may be as adequate in mildly-curved flows ($0.5 < F < 1.5$) as in plane flows if assisted by an ordinary differential equation like Eq(37) for α , more highly curved flows may require partial differential transport equations for Reynolds stresses and at least one length scale. In the case of swirling flows, for instance, curvature effects are nearly always large near the axis, and calculation methods based on, say, eddy-viscosity anisotropy ratios are unlikely to attain aeronautical standards of accuracy except in a very narrow range of flows.

Much evidence of the importance of curvature effects has been reviewed in this AGARDograph, and the case for further research work seems plain. As well as being intrinsically important, streamline curvature merits study for the light it throws on the effects of extra strain rates in general. If existing calculation methods for simple shear layers are to be extended reliably to flows subjected to extra strain rate, or even if the rules for calculating curved flows set out in Section 11.1 are to be significantly improved, careful experiments and careful analysis of transport equations will be needed.

12. REFERENCES

1. Bradshaw, P. - Variations on a theme of Prandtl. AGARD Conf. Proc. 93, 1972, p.C-1. See also A bibliography of "complex" turbulent flows, Imperial College, Aero Dept., Rept 72-04, 1972.
2. Bradshaw, P. - Advances in turbulent shear flows. Von Karman Institute, Lecture Series 56, 1973.
3. Bradshaw, P. - Calculation of interacting turbulent shear layers. Duct flow. ASME J. Fluids Engg. (in press: see also ASME paper 72-WA/FE-25).
4. Dean, R.B. McEligot, D.M.
5. Thomann, H. - Effect of streamwise wall curvature on heat transfer in a turbulent boundary layer. J. Fluid Mech., vol.33, 1968, p.283.
6. Van Dyke, M.D. - Higher-order boundary-layer theory. Ann. Rev. Fluid Mech., vol.1, 1969, p.265.
7. Giles, J.A. Hays, A.P. Sawyer, R.A. - Turbulent wall jets on logarithmic spiral surfaces. Aero. Quart., vol.17, 1966, p.201.
8. Guitton, D.E. - Some contributions to the study of equilibrium and non-equilibrium turbulent wall jets over curved surfaces. McGill Univ., Mech. Engg. Dept., Ph.D. thesis, 1970.
9. Spettel, F. Mathieu, J. Brison, J.F. - Tensions de Reynolds et production d'énergie cinétique turbulente dans les jets pariétaux sur parois planes et concaves. J. de Méc., vol.11, 1972, p.403.
10. Huffaker, R.M. Jelalian, A.V. Keene, W.H. Sonnenschein, C.M. - Application of laser doppler systems to vortex measurement and detection. Aircraft Wake Turbulence and Its Detection (J.H. Olsen, A.Goldburg and M. Rogers, Eds.), New York, Plenum Press, 1971.
11. Johnston, J.P. Halleen, R.M. Lezius, D.K. - Effects of spanwise rotation on the structure of the two-dimensional fully developed turbulent channel flow. J. Fluid Mech., vol.56, 1972, p.533.
12. Castro, I.P. - A highly distorted turbulent free shear layer. Imperial College, Aero. Dept., Ph.D. thesis, 1973.
13. Stine, G.H. - Coanda effect. Aviation Week, 1 Jan 1973, p.64.
14. Von Karman, T. - Some aspects of the turbulence problem. Proc. 4th Int. Congr. Appl. Mech., Cambridge, 1934, p.54.
15. Rayleigh, J.W.S. - On the dynamics of revolving fluids. Proc. Roy. Soc. A, vol.93, 1916, p.148.
16. McLaren, T.I. Pierce, A.D. Fohl, T. - An investigation of internal gravity waves generated by a buoyantly rising fluid in a stratified medium. J. Fluid Mech., vol.57, 1973, p.229.
17. Murphy, B.L.
18. Bradshaw, P. Ferriss, D.H. - Applications of a general method of calculating turbulent shear layers. J. Basic Engg., vol.94D, 1972, p.345.
19. Rodi, W. - Basic equations for turbulent flow in cartesian and cylindrical coordinates. Imperial College, Mech. Engg. Dept., Rept. BL/TN/A/36, 1970.
20. Newman, B.G. - Some contributions to the study of the turbulent boundary layer near separation. Australian Dept. of Supply, Rept. ACA-53, 1951.
21. Bradshaw, P. Goodman, D.G. - The effect of turbulence on static-pressure tubes. A.R.C. R.&M. 3527, 1968.
22. Baum, E. - An interaction model of a supersonic laminar boundary layer on sharp and rounded backward facing steps. AIAA J., vol.6, 1968, p.440.
23. Alber, I.E. Lees, L. - Integral theory for supersonic turbulent base flows. AIAA J., vol.6, 1968, p.1343.
24. Wilcken, H. - Effect of curved surfaces on turbulent boundary layers. NASA TT F-11421, 1967 (translation of Ing.-Arch., vol.1, 1930, p.357).
25. Rosenhead, L.(Ed.) - Laminar Boundary Layers. Oxford, Clarendon Press, 1963.
26. Townsend, A.A. - The Structure of Turbulent Shear Flow. Cambridge, University Press, 1956.
27. Bradshaw, P. - The understanding and prediction of turbulent flow. Aero. J., vol.76, 1972, p.403.
28. Townsend, A.A. - Equilibrium layers and wall turbulence. J. Fluid Mech., vol.11, 1961, p.97.
29. Kline, S.J. - Proceedings, Computation of Turbulent Boundary Layers - 1968 AFOSR-IFP - Stanford Conference, Vol.1. Stanford Univ., Thermosciences Divn., 1969.
30. Morkovin, M.V. Sovran, G. Cockrell, D.G. (Eds.)
31. Donaldson, C. du P. - Calculation of turbulent shear flows for atmospheric and vortex motions. AIAA J., vol.10, 1972, p.4.
32. Reynolds, W.C. - Computation of turbulent flows - State-of-the-art, 1970. Stanford Univ., Thermosciences Divn., Rept. MD-27, 1970 and Chem. Engg. Progress, 1972.

30. Rotta, J.C. - Turbulent shear layer prediction on the basis of the transport equations for the Reynolds stresses. Sectional Lecture, 13th Int. Congr. Appl. Mech., Moscow, 1972 and DFVLR-AVA Ber.061-72 A17.
31. Patankar, S.V. Spalding, D.B. - Heat and Mass Transfer in Boundary Layers. London, Intertext, 1970.
32. Cebeci, T. - Analysis of Turbulent Boundary Layers. New York, Academic Press, 1973 (in press).
33. Nash, J.F. Patel, V.C. - Three-dimensional Turbulent Boundary Layers. Atlanta, SBC Technical Books, 1972.
34. Hanjalic, K. Launder, B.E. - A Reynolds-stress model of turbulence and its application to thin shear flows. *J. Fluid Mech.*, vol.52, 1972, p.609.
35. Rodi, W. - On the equation governing the rate of turbulent energy dissipation. Imperial College, Mech. Engg. Dept., TM/TN/A/14, 1971.
36. Daly, B.J. Harlow, F.H. - Transport equations in turbulence. *Phys. Fluids*, vol.13, 1970, p.2634.
37. Patel, V.C. - The effects of curvature on the turbulent boundary layer. A.R.C. R. & M. 3599, 1968.
38. Myring, D.F. - The effects of normal pressure gradients on the boundary layer momentum integral equation. RAE TR 68214, ARC 30858, 1968 (see also Myring and Young, *Aero. Quart.*, vol.19, 1968, p.105).
39. Howard, L.N. Gupta, A.S. - On the hydrodynamic and hydromagnetic stability of swirling flows. *J. Fluid Mech.*, vol.14, 1962, p.463.
40. Batchelor, G.K. Proudman, I. - The effect of rapid distortion on a fluid in turbulent motion. *Quart. J. Mech. Appl. Math.*, vol.7, 1954, p.83.
41. Crow, S.C. - Viscoelastic properties of fine-grained incompressible turbulence. *J. Fluid Mech.*, vol.33, 1968, p.1.
42. Lumley, J.L. - Towards a turbulent constitutive relation. *J. Fluid Mech.*, vol.41, 1970, p.413.
43. Tucker, H.J. - The distortion of turbulence by irrotational strain. McGill Univ., Mech. Engg. Dept., Rept. 70-7, 1970 (see also *J. Fluid Mech.*, vol.32, 1968, p.657).
44. Marechal, J. - Etude experimentale de la deformation plane d'une turbulence homogene. *J. de Mec.*, vol.11, 1972, p.263.
45. Morel, T. - Turbulent kinetic energy and free mixing. Paper presented at Langley Working Conference on Free Turbulent Shear Flows, 1972.
46. Green, J.E. Weeks, D.J. Brooman, J.W.F. - Prediction of turbulent boundary layers and wakes in compressible flow by a lag-entrainment method. RAE TR 72231, 1972.
47. Keffer, J.F. - The uniform distortion of a turbulent wake. *J. Fluid Mech.*, vol.22, 1965, p.135.
48. Keffer, J.F. - A note on the expansion of turbulent wakes. *J. Fluid Mech.*, vol.28, 1967, p.183.
49. Crabbe, R.S. - Measurements in a laterally strained turbulent boundary layer. McGill Univ., Mech. Engg. Dept., Rept. 71-2, 1971.
50. Townsend, A.A. - Entrainment and the structure of turbulent flow. *J. Fluid Mech.*, vol.41, 1970, p.13.
51. Cham, T.-S. Head, M.R. - Calculation of the turbulent boundary layer in a vortex diffuser. A.R.C. R. & M. 3646, 1970.
52. Gardow, E.B. - The three-dimensional turbulent boundary layer in a free vortex diffuser. M.I.T., Gas Turbine Lab., Rept. 42, 1958.
53. Head, M.R. Patel, V.C. - Improved entrainment method for calculating turbulent boundary layer development. A.R.C. R. & M. 3643, 1970.
54. Winter, K.G. Rotta, J.C. Smith, K.G. - Studies of the turbulent boundary layer on a waisted body of revolution in subsonic and supersonic flow. ARC R & M 3633, 1968.
55. Patel, V.C. Nakayama, A. Damian, R. - An experimental study of the thick turbulent boundary layer near the tail of a body of revolution. Iowa Inst. of Hydraulic Research, Rept. 142, 1972 (to appear in *J. Fluid Mech.*).
56. McMillan, O.J. Johnston, J.P. - Performance of low-aspect-ratio diffusers with fully developed turbulent inlet flows. Stanford Univ., Thermosciences Divn., Rept. PD-14, 1970.
57. Young, S.T.B. - Unpublished work at Imperial College: see Bradshaw, P. and Young, S.T.B. in RAE-DFVLR Seminar on non-hypersonic boundary layers (J.E. Green and E. Krause, eds.) ARC 33311, 1971.
58. Heskestad, G. - Hot-wire measurements in a plane turbulent jet. *J. Appl. Mech.*, vol.32, 1965, p.721.
59. Heskestad, G. - Hot-wire measurements in a radial turbulent jet. *J. Appl. Mech.*, vol.33, 1966, p.417.
60. Gartshore, I.S. - Two-dimensional turbulent wakes. *J. Fluid Mech.*, vol.30, 1967, p.547.
61. Morel, T. - Calculation of free turbulent mixing. Interaction approach. Illinois Institute of Technology, Mechanics Dept., Ph.D. Thesis, 1972.
62. Bradshaw, P. Ferriss, D.H. - Calculation of boundary layer development using the turbulent energy equation: compressible flow on adiabatic walls. *J. Fluid Mech.*, vol.46, 1971, p.83.
63. Zwarts, F. - Ph.D. Thesis, McGill University, 1970.
64. Bushnell, D.M. Alston, D.W. - Calculation of compressible adverse pressure gradient turbulent boundary layers. *AIAA J.*, vol.10, 1972, p.229.
65. Peake, D.J. Brakmann, G. Romeskie, J.M. - Comparisons between some high Reynolds number turbulent boundary layer experiments and various recent calculation procedures at Mach 4. AGARD Conf. Proc. 93, 1971.
66. Lewis, J.E. Gran, R.J. Kubota, T. - An experiment on adiabatic compressible turbulent boundary layer in adverse and favourable pressure gradients. *J. Fluid Mech.*, vol.51, 1972, p.657.
67. Bradshaw, P. - Anomalous effects of pressure gradient on supersonic turbulent boundary layers. Imperial College Aero Rept. 72-21, 1972.

68. Pasiuk, L. - Experimental Reynolds analogy factor for a compressible turbulent boundary layer with a pressure gradient. NOL TR 64-200, 1964.
 Hastings, G.M.
 Chatham, R.
69. Wilcox, D.C. - A turbulence model for high speed flows. Proc. 1972 Heat Transfer and Fluid Mech. Inst. (R.B. Landis and G.J. Hordemann, Eds.) 1972, p.231.
 Alber, I.E.
70. Bippes, H. - Dreidimensionale Störungen in der Grenzschicht an einer konkaven Wand. Acta Mechanica, vol.14, 1972, p.251.
 Görtler, H.
71. Coles, D.E. - Transition in circular Couette flow. J. Fluid Mech., vol.21, 1965, p.385.
72. Taylor, G.I. - Stability of a viscous liquid contained between two rotating cylinders. Phil. Trans. Roy. Soc. A, vol.223, 1923, p.289.
73. Coles, D.E. - Digital experiment in spiral turbulence. Phys. Fluids, vol.10, 1967, p.S120.
 Van Atta, C.W.
74. Nagib, H.M. - On instabilities and secondary motions in swirling flows through annuli. Illinois Institute of Technology, Mechanics Dept., Ph.D. Thesis, 1972.
75. Jeffreys, H. - Some cases of instability in fluid motion. Proc. Roy. Soc. A, vol.118, 1928, p.195.
76. Lezius, D. - The structure and stability of turbulent wall layers in rotating channel flow. Stanford Univ., Thermosciences Divn., Rept. MD-29, 1971.
 Johnston, J.P.
77. Görtler, H. - On the three-dimensional instability of laminar boundary layers on concave walls. NACA Tech. Memo. 1375 - translation of Math. Phys. Kl., Nachr. Ges. Wiss., Göttingen, vol.1, 1940, p.1.
78. Gregory, N. - The effect on transition of isolated surface excrescences in the boundary layer. ARC R & M 2779, 1950.
 Walker, W.S.
79. Johnston, J.P. - The effect of rotation on boundary layers in turbomachine rotors. Stanford Univ., Thermosciences Divn., Rept. MD-24, 1970 (to appear in NASA SP-304).
80. Prandtl, L. - Ludwig Prandtl Gesammelte Abhandlungen. (W. Tollmien, H. Schlichting and H. Görtler, Eds.) Springer, 1961.
81. Wendt, F. - Turbulente Strömungen zwischen zwei rotierenden konaxialen Zylindern. Ing.-Arch., vol.4, 1933, p.577.
82. Wattendorf, F.L. - A study of the effect of curvature on fully developed turbulent flow. Proc. Roy. Soc. A, vol.148, 1935, p.565.
83. Schmidbauer, H. - Turbulent friction layer on convex surfaces. NASA Tech. Memo 791 and ARC no.2608 - translations of Luftfahrtforsch., vol.13, 1936, p.160.
84. Taylor, G.I. - Distribution of velocity and temperature between concentric cylinders. Proc. Roy. Soc. A, vol.151, 1935, p.494.
85. Pai, S-I. - Turbulent flow between rotating cylinders. NACA TN 892, 1943.
86. Metral, A. - The Coanda effect. U.S. AEC-tr-3386 or British TIL/T4207, translations of French Pub. Sci. et Tech. du Min. de l'Air 218, 1948.
 Zerner, F.
87. Prandtl, L. - Essentials of Fluid Dynamics (Führer durch die Strömungslehre), London, Blackie, 1952.
88. Richardson, L.F. - The supply of energy from and to atmospheric eddies. Proc. Roy. Soc. A, vol.97, 1920, p.354.
89. Businger, J.A. - Flux-profile relationships in the atmospheric surface layer. J. Atmos. Sci., vol.28, 1971, p.181.
 Wyngaard, J.C.
 Izumi, Y.
 Bradley, E.F.
90. Schlichting, H. - Turbulenz bei Wärmeschichtung. Zeit. für Angew. Math. und Mech., vol.15, 1935, p.313.
91. Bradshaw, P. - The analogy between streamline curvature and buoyancy in turbulent shear flow. J. Fluid Mech., vol.36, 1969, p.177.
92. Thompson, B.G.J. - The calculation of shape-factor development in incompressible turbulent boundary layer with or without transpiration. AGARDograph 97, 1965, p.159.
93. Clauser, M. - The effect of curvature on the transition from laminar to turbulent boundary layer. NACA Tech. Note 613, 1937.
94. Kreith, F. - The influence of curvature on heat transfer to compressible fluids. Trans. ASME, vol.77, 1955, p.1247.
95. Einstein, H.A. - Steady vortex flow in a real fluid. Proc. 1951 Heat Transfer and Fluid Mech. Inst., Stanford, 1951, p.33.
 Li, H.
96. Mabey, D.G. - The formation and decay of vortices. Imperial College, Aero. Dept., D.I.C. thesis, 1953.
97. Keyes, J.J. - An experimental study of gas dynamics in high velocity vortex flow. Proc. 1960 Heat Transfer and Fluid Mech. Inst., Stanford, 1960.
98. Eskinazi, S. - An investigation on fully developed turbulent flows in a curved channel. J. Aero. Sci., vol.23, 1956, p.23.
 Yeh, H.
99. Yeh, H. - Boundary layer along annular walls in a swirling flow. Trans. ASME, vol.80, 1958, p.167.
100. Traugott, S.C. - Influence of solid-body rotation on screen-produced turbulence. NACA TN 4135, 1958.
101. Schubauer, G.B. - Investigation of separation of the turbulent boundary layer. NACA Rept. 1030, 1951.
 Klebanoff, P.S.
102. Tani, I. - Production of longitudinal vortices in the boundary layer along a concave wall. J. Geophys. Res., vol.67, 1962, p.3075.
103. Wille, R. - Report on the first European Mechanics Colloquium, on the Coanda effect. J. Fluid Mech., vol.23, 1965, p.801.
 Fernholz, H.
104. Newman, B.G. - The deflexion of plane jets by adjacent boundaries - Coanda effect. In Boundary Layer and Flow Control (G.V. Lachmann, Ed.) vol.1, London, Pergamon, 1961, p.232.
105. Fernholz, H. - Umlenkung von Freistrahlen an gekrümmten Wänden. Jahrbuch 1964 der WGLR, 1964, p.149.
106. Förthmann, E. - Über turbulente Strahlansbreitung. Ing.-Arch., vol.5, 1934, p.42 : translated as NACA TM789, 1936.
107. Bradshaw, P. - Turbulent wall jets with and without an external stream. ARC R. and M. 3252, 1960.
 Gee, M.T.

108. Von Glahn, U.H. - Use of the Coanda effect for obtaining jet deflection and lift with a single-plate deflection surface. NACA TN 4272, 1958.
109. Metral, A. - Sur un phénomène de deviation des veines fluides et ses applications. Proc. 5th Int. Congr. Appl. Mech., Cambridge, 1938.
110. Sawyer, R.A. - Two-dimensional reattaching jet flows including the effect of curvature on entrainment. J. Fluid Mech., vol.17, 1963, p.481.
111. Sawyer, R.A. - Two-dimensional turbulent jets with adjacent boundaries. Cambridge Univ., Engg. Dept., Ph.D. Thesis, 1962.
112. Stratford, B.S.
Jawor, Z.M.
Golesworthy, G.T.
113. Stratford, B.S.
Jawor, Z.M.
Smith, M.
114. Lumley, J.L.
Panofsky, H.A.
115. Turner, J.S.
116. Johnston, D.S.
117. Laderman, A.J.
Demetriades, A.
118. Wyngaard, J.C.
119. Gough, D.O.
Lynden-Bell, D.
120. Strittmatter, P.A.
Illingworth, G.
Freeman, K.C.
121. Synge, J.L.
122. Morkovin, M.V.
123. Beer, J.M.
Chigier, N.A.
Davies, T.W.
Bassindale, K.
124. Fahlbusch, H.
125. Bradshaw, P.
126. Johnston, J.P.
127. Cham, T.-S.
Head, M.R.
128. Kurzweg, U.H.
129. Chigier, N.A.
130. Tennekes, H.
131. Nicholl, C.I.H.
132. Cermak, J.E.
133. Mackrodt, P.A.
134. Favre, A.
Gaviglio, J.
135. Gupta, A.K.
Laufer, J.
Kaplan, R.E.
136. Zilitinkevich, S.S.
137. Sandmayr, G.
138. Smith, A.M.O.
139. McEligot, D.M.
Le Mone, M.A.
140. Angell, J.K.
141. Pao, Y.-H.
142. Stewart, R.W.
143. Cannon, J.N.
Kays, W.M.
144. Woods, J.D.
145. Greenspan, H.P.
146. Hines, C.O.
147. Mowbray, D.E.
Rarity, B.S.H.
- The mixing with ambient air of a cold airstream in a centrifugal field. ARC C.P. 687, 1962.
- The mixing between hot and cold airstreams in a centrifugal field. ARC CP 793, 1965.
- The Structure of Atmospheric Turbulence. Interscience, 1964.
- Buoyancy Effects in Fluids, Cambridge, University Press, 1973.
- Velocity and temperature fluctuation measurements in a turbulent boundary layer downstream of a stepwise discontinuity in wall temperature. J. Appl. Mech., vol.26, 1959, p.325.
- Measurements of the mean and turbulent flow in a cooled-wall boundary layer at Mach 9.37. AIAA paper 72-73, 1973.
- An experimental investigation of the small-scale structure of turbulence in a curved mixing layer. Penn. State Univ., Ph.D. Thesis, 1967.
- Vorticity expulsion by turbulence: astrophysical implications of an Alka-Seltzer experiment. J. Fluid Mech., vol.32, 1968, p.437.
- A note on the vorticity-expulsion hypothesis. J. Fluid Mech., vol.43, 1970, p.539.
- On the stability of a viscous liquid between two rotating co-axial cylinders. Proc. Roy. Soc. A, vol.167, 1938, p.250.
- Effect of compressibility on turbulent flows. In Mécanique de la Turbulence (A. Favre, Ed.). New York, Gordon and Breach, 1964.
- Laminarization of turbulent flames in rotating environments. Combustion and Flame, vol.16, 1971, p.39.
- Recovery factor in flow of cambered walls. Z. Flugwiss., vol.15, 1967, p.130.
- Calculation of three-dimensional turbulent boundary layers. J. Fluid Mech., vol.46, 1971, p.417.
- Measurements in a three-dimensional turbulent boundary layer induced by a swept, forward-facing step. J. Fluid Mech., vol.42, 1970, p.823.
- The turbulent boundary layer on a rotating cylinder in an axial stream. J. Fluid Mech., vol.42, 1970, p.1.
- A criterion for the stability of heterogeneous swirling flows. Zeit. für Angew. Math. und Phys., vol.20, 1969, p.141.
- Gasdynamics of swirling flows in combustion systems. Astro. Acta, vol.17, 1972, p.387.
- Free convection in the turbulent Ekman layer of the atmosphere. J. Atmos. Sci., vol.27, 1970, p.1027.
- Some dynamical effects of heat on a turbulent boundary layer. J. Fluid Mech., vol.40, 1970, p.361.
- Laboratory simulation of the atmospheric boundary layer. AIAA J., vol.9, 1971, p.1746.
- Spiralströmungen im zylindrischen Ringraum hinter Leitradern. Z. Flugwiss., vol.15, 1967, p.335.
- Turbulence et perturbations dans la couche limite d'une plaque plane. AGARD Rept. 278, 1960.
- Spatial structure in the viscous sub-layer. J. Fluid Mech., vol.50, 1971, p.493.
- Shear convection. Boundary-Layer Meteorology, vol.3, 1973, p.416.
- Über das Auftreten von Längswirbeln in turbulenten Grenzschichten an konkaven Wänden. DLR FB 66-41, 1966.
- On the growth of Taylor-Görtler vortices along highly concave walls. Quart. Appl. Math., vol.13, 1955, p.233.
- The structure and dynamics of horizontal roll vortices. Lecture presented at NCAR Colloquium on Dynamics of the Tropical Atmosphere, 1972.
- A comparison of circulations in transverse and longitudinal planes in an unstable planetary boundary layer. J. Atmos. Sci., vol.29, 1972, p.1252.
- Spectra of internal waves and turbulence in stratified fluids. Radio Sci., vol.4, 1969, p.1315.
- Turbulence and waves in a stratified atmosphere. Radio Sci., vol.4, 1969, p.1269.
- Heat transfer to a fluid flowing inside a pipe rotating about its longitudinal axis. J. Heat Transfer, vol.91, 1969, p.135.
- Wave-induced shear instability in the summer thermocline. J. Fluid Mech., vol.32, 1968, p.791.
- The Theory of Rotating Fluids. Cambridge, University Press, 1968.
- Gravity waves in the atmosphere. Nature, vol.239, 8th September 1972, p.73.
- A theoretical and experimental investigation of the phase configuration of internal waves of small amplitude in a density-stratified liquid. J. Fluid

- Mech., vol.28, pt.1, 1967, p.1.
148. Bretherton, F.P. - Waves and turbulence in stably stratified fluids. *Radio Sci.*, vol.4, pt.12, 1969, p.1279.
 149. Scorer, R.S. - Theory of waves in the lee of mountains. *Quart. J. Roy. Met. Soc.*, vol.75, 1949, p.41.
 150. Scorer, R.S. - Theory of lee waves Parts 2 and 3. *Quart. J. Roy. Met. Soc.*, vol.79, 1953, p.70 and vol.80, 1954, p.417.
 151. Phillips, O.M. - The maintenance of Reynolds stress in turbulent shear flow. *J. Fluid Mech.*, vol.27, pt.1, 1967, p.131.
 152. Pao, Y.-H. - Undulance and turbulence in stably-stratified media. In Clear Air Turbulence and Its Detection (J.H. Olsen, A. Goldberg and D.M. Rogers, Eds.), New York, Plenum Press, 1971.
 153. Reynolds, W.C. - The mechanics of an organized wave in turbulent shear flow. Parts I-III. *J. Fluid Mech.*, vol.41, 1970, p.241; vol.54, 1972, p.241; vol.54, 1972, p.263.
 154. Hussain, A.K.M.F. - Measurements of air motion in regions of clear air turbulence using high-power Doppler radar. *Nature*, vol.239, 29th September 1972, p.267.
 155. Browning, K.A. - Characteristics of Ekman boundary layer instabilities. *J. Fluid Mech.*, vol.44, 1970, p.79.
 156. Starr, J.R. - A technique for phase speed measurements in turbulent flow. *J. Fluid Mech.*, vol.42, 1970, p.689.
 157. Whyman, A.J. - An Introduction to Turbulence and Its Measurement. Oxford, Pergamon, 1971.
 158. Caldwell, D.R. - The suppression of shear-layer turbulence in rotating systems. *AGARD Conf. Proc.* 93, 1972.
 159. Van Atta, C.W. - A note on reverse transition. *J. Fluid Mech.*, vol.35, 1969, p.387.
 160. Stegen, G.R. - An experimental investigation of turbulent boundary layers along curved surfaces. *NASA CR-1940*, 1972.
 161. Bradshaw, P. - A critical review of existing methods of calculating the turbulent boundary layer. *ARC R. and M.* 3447, 1964.
 162. Johnstone, J.P. - Measurements of secondary flow in the boundary layers of a 180 degree channel. *ARC CP 1043*, 1968.
 163. Coles, D.E. - The turbulent boundary layer in a compressible fluid. *RAND Corp. Rept.* R-403-PR, 1962, and *ARC 24478*, 1963.
 164. Meroney, R.N. - Unpublished work, Imperial College, 1973.
 165. Hughes, D.W. - Swirling flow in an annular diffuser with a rotating centre-body. *Cambridge Univ., Ph.D. Thesis*, 1972.
 166. Parr, O. - Untersuchungen der dreidimensionalen Grenzschicht an rotierenden Drehkörpern bei axialer Strömung. *Ing.-Arch.*, vol.32, 1963, p.343.
 167. Furuya, Y. - Velocity profiles in the skewed boundary layers on some rotating bodies in axial flow. *J. Appl. Mech.*, vol.37, 1970, p.17.
 168. Nakamura, I. - On boundary layers in centrifugal compressors. *Creare, Inc.*, TN-95, 1970 (to appear in *NASA SP-304*).
 169. Dean, R.C. - Messungen in der ebenen turbulenten Grenzschicht im rotierenden System. *DLR FB 68-07*, 1968.
 170. Anders, U. - Prediction of velocity profiles for turbulent boundary layers on the blading of radial impellers. *Proc. 4th Conf. on Fluid Machinery* (L. Kisbocskói and A. Szabó, Eds.), Budapest, Akadémiai Kiadó, 1972, p.771.
 171. Litvai, E. - Strömung in gekrümmten Rohren. *Zeit. für Angew. Math. und Mech.*, vol.14, 1934, p.257.
 172. Adler, M. - Friction factors for turbulent flow in curved pipes. *J. Basic Engg.*, vol.81, 1959, p.123.
 173. Itō, H. - Study on forced convective heat transfer in curved pipes (Second report, turbulent region). *Int. J. Heat and Mass Transfer*, vol.10, 1967, p.37.
 174. Mori, Y. - Fluid flow in radial rotating tubes. *Proc. 9th Int. Congr. Appl. Mech.*, vol.2, 1957, p.341.
 175. Nakayama, W. - Development of turbulence during the buildup of a boundary layer at a concave wall. *Phys. Fluids*, vol.10, 1967, p.S108.
 176. Trefethen, L. - Turbulent transfer in rotary flows of an incompressible fluid. *Fluid Mech. - Soviet Research*, vol.1, 1972, p.121.
 177. Tillman, W. - Effect of streamwise wall curvature on compressible turbulent boundary layers. *Phys. Fluids*, vol.10, 1967, p.S174.
 178. Koosinlin, M.L. - The prediction of turbulent boundary layers on rotating axially-symmetrical bodies. *Imperial College, Mech Engg. Dept.*, Rept. BL/TN/A/46, 1971.
 179. Lockwood, F.C. - Procedure for predicting the influence of longitudinal curvature on boundary-layer flows. *ASME paper 71-WA/FE-37*, 1971.
 180. Rastogi, A.K. - Curvature and transition effects in turbulent boundary layers. *AIAA J.*, vol.9, 1971, p.1868.
 181. Whitelaw, J.H. - On the two-dimensional boundary layers as they appear on turbomachine blades. *AGARDograph 164*, 1972, p.1.
 182. Cebeci, T. - Calculation of turbulent boundary layers and wall jets over curved surfaces. *AIAA Journal*, vol.11, 1973, p.517.
 183. Papailiou, K. - Supersonic turbulent boundary layer growth over cooled walls in adverse pressure gradient. *Wright-Patterson AFB Rept.* ASD TDR 62-87, 1962.
 184. Satta, A. - The effect of adverse pressure gradients on the characteristics of turbulent boundary layers in supersonic streams. *J. Aero/Space Sci.*, vol.29, 1962, p.1.
 185. Nurzia, F. - Wind tunnel investigation of turbulent boundary layers on axially symmetric bodies at supersonic speeds. *Douglas Aircraft Co. Rept.* LB-31425, AD-435111, 1964.
 186. Dvorak, F.
 187. Kepler, C.E.
 188. O'Brien, R.L.
 189. McLafferty, G.H.
 190. Barber, R.E.
 191. Clutter, D.W.
 192. Kaups, K.

186. Young, C.H. - Hypersonic transitional and turbulent flow studies on a lifting entry vehicle. J. Spacecraft & Rockets, vol.9, 1972, p.883.
Reda, D.C.
Roberge, A.M.
187. Zakkay, V. - An experimental study of vortex generation in a turbulent boundary layer undergoing adverse pressure gradient. NASA CR-2037, 1972.
Calarese, W.
188. Lighthill, M.J. - Note on the deflection of jets by insertion of curved surfaces and on the design of bends in wind tunnels. ARC R. & M. 2105, 1945.
189. Fernholz, H.-H. - Zur Umlenkung von Freistrahlen an konvex gekrümmten Wänden (Coanda-Effekt). Habilitationsschrift, Tech. Univ. Berlin, 1965, and DLR FB 66-21, 1966. Translated as Canadian NRC-TT-1504, 1971.
190. Newman, B.G. - The prediction of turbulent jets and wall jets. Canadian Aero. & Space J., vol.15, 1969, p.287.
191. Fekete, G.I. - Coanda flow of a two-dimensional wall jet on the outside of a circular cylinder. McGill Univ., Mech. Engg. Research Labs. Rept. 63-11, 1963.
192. Fernholz, H.-H. - Aerodynamische Hysterese, Steurschneiden- und Reynoldszahl-Einfluss bei der Strömungsumlenkung und Ablosen an stark gekrümmten Wänden (Coanda-Effekt). Zeit. Flugwiss., vol.15, 1967, p.136.
193. Bradbury, L.J.S. - An exploratory investigation into the deflection of thick jets by the Coanda effect. RAE TR 65235, ARC 27586, 1965.
Wood, M.N.
194. Caille, C. - The even distribution of air emerging at right angles from a duct. Sulzer Tech. Rev., vol.1, 1956, p.28.
195. Huffman, G.D. - A note on von Karman's constant in low Reynolds number turbulent flows. J. Fluid Mech., vol.53, 1972, p.45.
Bradshaw, P.
196. Patankar, U.M. - Three-dimensional curved wall jets. J. Basic Engg., vol.94, 1972, p.339.
Sridhar, K.
197. Kind, R.J. - A calculation method for circulation control by tangential blowing around a bluff trailing edge. Aero. Quart., vol.19, 1968, p.205.
198. Matthews, L. - Plane-jet flow over a backward-facing step. Imperial College, Mech. Engg. Dept., Rept. EHT/TN/A/27, 1971.
Whitelaw, J.H.
199. Schwartzbach, C. - An experimental investigation of curved two-dimensional turbulent jets. AGARD Conf. Proc. 93, 1972.
200. Wagnanski, I. - The reattachment of an inclined two-dimensional jet to a flat surface in streaming flow. CASI Transactions, vol.1, 1968, p.3.
Newman, B.G.
201. Bradshaw, P. - The reattachment and relaxation of a turbulent shear layer. J. Fluid Mech., vol.52, 1972, p.113.
Wong, F.Y.F.
202. Russell, P.J. - Turbulent flow characteristics of an impinging jet. Proc. Inst. Mech. Engrs., vol.186, 1972, p.635.
Hatton, A.P.
203. Wyngaard, J.C. - Structure of turbulence in a curved mixing layer. Phys. Fluids, vol.11, 1968, p.1251.
Tennekes, H.
Lumley, J.L.
Margolis, D.P.
204. Rapp, A.F. - Turbulent and pressure transport in a curved mixing layer. Phys. Fluids, vol.10, 1967, p.1347.
Margolis, D.P.
205. Govindaraju, S.P. - Flow in a turbulent trailing vortex. Phys. Fluids, vol.14, 1971, p.2074.
Saffman, P.G.
206. Küchemann, D. - Vortex motions - some illustrations. RAE TM Aero 1229, 1970.
Maskell, E.C.
207. Fennell, L.J. - Vortex breakdown - some observations in flight on the HP 115 aircraft. RAE TR 71177, 1971.
208. Olsen, J.H. - Aircraft Wake Turbulence and Its Detection. New York, Plenum Press, 1971.
Goldburg, A.
Rogers, M. (Eds.)
209. Poppleton, E.D. - Exploratory measurements of the flow in the wing tip vortices of a Lockheed Hercules. Sydney Univ., Aero. Dept., Rept. ATN-7104, 1971 and STAR N72-28277.
210. Adams, G.N. - Some observations of vortex core structure. Canad. Aero. and Space J., vol.18, 1972, p.159.
Gilmore, D.C.
211. Oon, E.H. - Decay of trailing vortices. ARC CP 1238, 1973.
212. Muirhead, V.U. - Compressible vortex flow. AIAA paper 73-106, 1973.
213. White, A. - Flow of a fluid in an axially rotating pipe. J. Mech. Engg. Sci., vol.6, 1964, p.47.
214. Brown, C.E. - Aerodynamics of wake vortices. AIAA J., vol.11, 1973, p.531.
215. Batchelor, G.K. - Axial flow in trailing line vortices. J. Fluid Mech., vol.20, 1964, p.645.
216. Harvey, J.K. - Observation of a mechanism causing a trailing vortex to break up. Imperial College, Aero. Dept., Rept. 70-08, ARC 32607, 1970.
Fackrell, J.E.
217. Hall, M.G. - Vortex breakdown. Prog. Aerosp. Sci., vol.12, 1972.
218. Sarpkaya, T. - On stationary and travelling vortex breakdown. J. Fluid Mech., vol.45, 1971, p.545 (see also AIAA J., vol.9, 1971, p.1217).
219. Poppleton, E.D. - A preliminary experimental investigation of the structure of a turbulent trailing vortex. McGill Univ., Mech. Engg. Res. Labs., TN 71-1, 1971.
220. Owen, P.R. - The decay of a turbulent trailing vortex. Aero. Quart., vol.21, 1970, p.69.
221. Saffman, P.G. - Structure of turbulent line vortices. Unpublished paper, Caltech., 1973 and ASTIA document AD-753131.
222. Squire, H.B. - The growth of a vortex in turbulent flow. Aero. Quart., vol.16, 1965, p.302.
223. Rose, R. - Aircraft vortex wakes and their effect on aircraft. ARC CP 795, 1963.
Dee, F.W.
224. Hoffman, E.R. - Turbulent line vortices. J. Fluid Mech., vol.16, 1963, p.395.
Joubert, P.N.
225. Donaldson, C. du P. - Decay of an isolated vortex. Aircraft Wake Turbulence and Its Detection (J.H. Olsen, A. Goldburg and M. Rogers, Eds.), New York, Plenum Press, 1971 (see also Ref.28).
Sullivan, R.D.
226. Donaldson, C. du P. - The relationship between eddy transport and second-order closure models for stratified media and for vortices. ARAP, Inc., Rept. 180 (paper presented at

- Langley Working Conference on Free Turbulent Shear Flows), 1972.
227. Earnshaw, P.B. - An increment in total head in the neighbourhood of a leading edge vortex. RAE TR 66218, 1966.
 228. Mason, W.H. - Far-field structure of aircraft wake turbulence. *J. Aircraft*, vol.10, 1973, p.86.
 229. Hackett, J.E. - Vortex wakes behind high-lift wings. *J. Aircraft*, vol.8, 1971, p.334.
 230. Ragsdale, R.G. - A mixing length correlation of turbulent vortex data. ASME paper 61-WA-244, 1961.
 231. McCormick, B.W. - Structure of trailing vortices. *J. Aircraft*, vol.5, 1968, p.260.
 232. Tangler, J.L. - Wind-tunnel studies of wing wake turbulence. *J. Aircraft*, vol.9, 1972, p.820.
 233. Sherrieb, H.E. - Flight test studies of the formation and dissipation of trailing vortices. *J. Aircraft*, vol.10, 1973, p.14.
 234. Chigier, N.A. - Wind tunnel simulation of full scale vortices. NASA CR-2180, 1973.
 235. Corsiglia, V.R. - Prediction of far flow field in trailing vortices. AIAA paper 72-989, 1972.
 236. Chevalier, H. - Experiments on the growth of vortices in turbulent flow. ARC CP 316, 1957.
 237. Rorke, J.B. - The swirling turbulent jet. *J. Basic Engg.*, vol.94, 1972, p.739.
 238. Moffitt, R.C. - A flight evaluation of methods for predicting vortex wake effects on trailing aircraft. NASA TN D-6904, 1972.
 239. Sheaffer, Y.S. - Aircraft trailing vortices. A survey of the problem. Carleton Univ., Divn. of Aerothermodynamics, Rept. ME/A72-1, 1972.
 240. Chigier, N.A. - Report on the IUTAM symposium on concentrated vortex motions in fluids. *J. Fluid Mech.*, vol.21, 1965, p.1.
 241. Titchener, I.M. - On the dynamics of turbulent vortical flow. *Zeit. für Angew. Math. und Physik*, vol.12, 1961, p.149.
 242. Taylor-Russell, A.J. - Combustion Aerodynamics. Barking, Applied Science Publishers, 1972.
 243. Reynolds, A.J. - Nonisotropic turbulent stress distribution in swirling flows from mean value distributions. *Int. J. Heat and Mass Transfer*, vol.14, 1971, p.573.
 244. Beer, J.M. - Turbulent swirling flows with recirculation. Imperial College, Mech. Engg. Dept., Ph.D. Thesis, 1972.
 245. Chigier, N.A. - The prediction of axisymmetrical turbulent swirling boundary layers. Imperial College, Mech. Engg. Dept., Rept. HTS/73/1, 1973.
 246. Roberts, L.W. - Measurements of three-dimensional turbulent boundary layers. Cambridge Univ., Engg. Dept., Ph.D. Thesis, 1971.
 247. Koosinlin, M.L. - Vortex mixing for supersonic combustion. Proc. 12th Symposium (International) on Combustion, Poitiers, 1969, p.1153.
 248. Lockwood, F.C. - Preliminary note on a mixing nozzle-ejector shroud combination for jet noise reduction. NPL Aero Rept. 1116, 1964.
 249. Vermeulen, A. - Swirling base injection for supersonic combustion ramjets. AIAA J., vol.10, 1972, p.1243.
 250. Swithenbank, J. - Backflows in rotating fluids moving axially through expanding cross sections. *J.A.I.Ch.E.*, vol.10, 1964, p.83.
 251. Chigier, N.A. - Turbulence measurements in swirling recirculating flows. Proc. Symposium on Internal Flows, Salford Univ., 1971, p.B27.
 252. Bradshaw, P. - Velocity and static pressure distributions in swirling air jets issuing from annular and divergent nozzles. *J. Basic Engg.*, vol.80, 1964, p.788.
 253. Povinelli, L.A. - The structure of blunt base wakes in swirling flow. *Astro. Acta*, vol.17, 1972, p.375.
 254. Ehlers, R.C. - A review of confined vortex flows. NASA CR-1772, 1972.
 255. Gore, R.W. - Stability of rotating stratified fluids. AIAA J., vol.10, 1972, p.1372.
 256. Ranz, W.E. - Experimental investigation of flow patterns in radial-outflow vortexes using a rotating-peripheral-wall water vortex tube. NASA CR-991, 1968.
 257. Syred, N. - Experiments on a shrouded, parallel disk system with rotation and coolant throughflow. *Int. J. Heat and Mass Transfer*, vol.16, 1973, p.311.
 258. Beér, J.M. - Base flow behind rotating axisymmetric bodies. Indian Inst. of Sci., Dept. of Aero. Engg., Rept. 71FM5, 1971.
 259. Chigier, N.A. - Wake of an axially symmetrical body with spinning. Proc. 9th Int. Symposium on Space Technology and Science, Tokyo, 1971, p.373.
 260. Beér, J.M. - Similarity in swirling wakes and jets. *J. Fluid Mech.*, vol.14, 1962, p.241.
 261. Charwat, A.F. - The damping of precessing vortex cores by combustion in swirl generators. *Astro. Acta.*, vol.17, 1972, p.783.
 262. Schlesinger, M.E. - A swirling round turbulent jet. *J. Appl. Mech.*, vol.29, 1962, p.616.
 263. Lewellen, W.S. - Experimental investigation of swirling vortex motion in jets. *J. Appl. Mech.*, vol.34, 1967, p.443.
 264. Johnston, S.C. - Axisymmetric turbulent swirling jet. *J. Appl. Mech.*, vol.32, 1965, p.258.
 265. Travers, A. - Some effects of swirl on turbulent mixing and combustion. NASA CR-1956, 1972.
 266. Yu, J.P. - Turbulent swirling jet diffusion flames. AIAA J., vol.7, 1969, p.1877.
 267. Sparrow, E.M. - Approximate analysis of a turbulent, swirling jet in a co-flowing stream. DFVLR FB 71-80, 1971.
 268. Eckert, E.R.G.
 269. Badri Narayanan, M.A.
 270. Kangovi, S.
 271. Liu, C.-Y.
 272. Reynolds, A.J.
 273. Syred, N.
 274. Beér, J.M.
 275. Rose, W.G.
 276. Chigier, N.A.
 277. Chervinsky, A.
 278. Lee, S-C.
 279. Rubel, A.
 280. Chervinsky, A.
 281. Schetz, J.A.

269. Lee, S.-C. - Axisymmetrical turbulent swirling natural convection plume. *J. Appl. Mech.*, vol.33, 1966, p.647 and p.656.
270. Kerr, N.M. - Swirl. Part I: effect on axisymmetrical turbulent jets. *J. Inst. Fuel*, vol.38, 1965, p.519.
271. Fraser, D. - Turbulent swirling jet. *Phys. Fluids*, vol.10, 1967, p.5197.
272. Craya, A. - Aerodynamic study of turbulent burning free jets with swirl. Proc. 11th Symposium (International) on Combustion, 1967, p.489.
273. Chigier, N.A. - A counter-rotating pair of turbulent jets. Univ. of Toronto, Mech. Engg. Dept., Unpublished Report, 1972 (NRC grant A-2746).
274. Pratte, B.D. - The fire whirl. Proc. 11th Symposium (International) on Combustion, 1967, p.475.
275. Emmons, H.W. - The boundary layer velocity distribution in turbulent swirling pipe flow. *J. Basic Engg.*, vol.91, 1969, p.728.
276. Ying, S.-C. - Friction and forced-convection heat transfer characteristics in tubes with twisted tape swirl generators. *J. Heat Transf.*, vol.86, 1964, p.39.
277. Backshall, R.G. - Fluid flow through tubes containing twisted tapes. *Engineer*, vol.222, 1966, p.634.
278. Landis, F. - Prediction of friction and heat transfer in tubes containing twisted tapes. Imperial College, Mech. Engg. Dept., Ph.D. Thesis, 1973.
279. Smithberg, E. - Friction and heat transfer characteristics in turbulent swirl flow subjected to large transverse temperature gradients. *J. Heat Transf.*, vol.90, 1968, p.87.
280. Landis, F. - Survey and evaluation of techniques to augment convective heat and mass transfer. *Prog. in Heat and Mass Transfer*, vol.1, 1969.
281. Bergles, A.E. - Heat transfer and friction in turbulent vortex flow. *Appl. Sci. Res. A*, vol.8, 1959, p.459.
282. Kreith, F. - Heat transfer and pressure drop in tape-generated swirl flow of single-phase water. *J. Heat Transfer*, vol.91, 1969, p.434.
283. Margolis, D. - Friction and heat transfer in the swirl flow of water in an annulus. *Int. J. Heat and Mass Transfer*, vol.16, 1973, p.303.
284. Lopina, R.F. - Analysis of the flow and energy separation in a turbulent vortex. *Int. J. Heat and Mass Transfer*, vol.3, 1960, p.173.
285. Bergles, A.E. - The decay of a turbulent swirl in a pipe. *J. Fluid Mech.*, vol.22, 1965, p.257.
286. Seban, R.A. - Measurements of the decay of swirl in turbulent flow. *AIAA J.*, vol.7, 1969, p.971.
287. Hunsbedt, A. - Universal velocity similarity in fully turbulent rotating flows. *J. Appl. Mech.*, vol.34, 1967, p.437.
288. Deissler, R.G. - Analytical investigations of incompressible turbulent swirling flow in stationary ducts. *J. Appl. Mech.*, vol.36, 1969, p.15 (see also NASA CR-1169, 1968).
289. Perlmutter, M. - Decay of swirl in a straight pipe flow. *Hungarian Acad. Sci., Proc. 4th Conf. on Fluid Machinery, Budapest, Akadémiai Kiado, 1972.*
290. Kreith, F. - Decay of turbulent swirl in an annular duct. Univ. Minnesota, Dept. Mech. Engg. HTL TR 89, 1970.
291. Sonju, O.K. - Experimental turbulent viscosities for swirling flow in a stationary annulus. Univ. Minnesota, Dept. Mech. Engg. HTL TR 94, 1971.
292. Wolf, L. - Modes of adiabatic and diabatic fluid flow in an annulus with an inner cylinder rotating. *Trans. ASME*, vol.80, 1958, p.753.
293. Lavan, Z. - Measurements of diabatic flow in an annulus with an inner rotating cylinder. *J. Heat Transfer*, vol.84, 1962, p.97.
294. Fejer, A.A. - Studies of the developing flow between concentric cylinders with the inner cylinder rotating. *J. Heat Transfer*, vol.86, 1964, p.383.
295. Kinney, R.B. - Turbulent helical flow in an annulus. *Proc. ASCE, J. Engg. Mech. Divn.*, vol.94, EMI, 1968, p.295.
296. Rochino, A. - Convection heat transfer in the entry region of a tube which revolves about an axis parallel to itself. *Int. J. Heat and Mass Transf.*, vol.10, 1967, p.333.
297. Saito, S. - Turbulent mean velocity measurements on a rotating cone. Imperial College, Mech. Engg. Dept., Rept. BL/TN/A/55, 1972.
298. Saito, K. - Swirling flow in an annular diffuser. *Gas Turbine Consultative Cttee. Rept.* 680, 1970.
299. Aoki, S. - The thick turbulent boundary layers on rotating cylinders in axial flow. Proc. 2nd Int. JSME Symposium on Fluid Machinery and Fluidics, Tokyo, 1972, p.41.
300. Rask, D.R. - Static pressure and velocity profiles in swirling incompressible tube flow. *J.A.I.Ch.E.*, vol.15, 1969, p.837.
301. Scott, C.J. - Survey of some aspects of swirling flows. Aerospace Research Labs., USAF, Rept. ARL 71-0244, 1971.
302. Kaye, J. - Eksperimentalnoe issledovanie turbulentnogo zakruchennogo techeniya v tsilindricheskoi trube. *Izv. Sibirskogo Otdeleniya Akad. Nauk SSSR, Ser. Tekh. Nauk*, no.13, 1972, p.3 (see Int. Aerospace Abstracts, A73-21601, 1973).
303. Becker, K.M. - Convection heat transfer in rotating systems. *Advances in Heat Transfer*, vol.5, 1968, p.129.
304. Kaye, J. - The boundary layer in three-dimensional flow. I. Derivation of the equations for flow along a general curved surface. *Phil. Mag.*, Ser.7, vol.42, 1951, p.239.
305. Astill, K.N. - The turbulent boundary layer on a rotating nose-body. *Aero. Quart.*, vol.22, 1971, p.389.
305. Cham, T.S. - Head, M.R.

306. Miloh, T. - Orthogonal coordinate systems for three-dimensional boundary layers, with particular reference to ship forms. *J. Ship Res.*, vol.17, 1973, p.50.
307. Patel, V.C. - An integral prediction method for three-dimensional turbulent boundary layers in incompressible flow. RAE Tech. Rept. 70147, ARC 32647, 1970.
308. Myring, D.F. - Numerical methods in fluid dynamics. AGARD Lecture Series 57, 1973.
309. Krause, E. - Imperial College, Chem. Engg. Dept., Ph.D. Thesis, 1973.
310. Markatos, M.C. - Approximation of the surface metric tensor by means of bicubic spline interpolation. RAE Tech. Rept. 72185, 1972.
311. Smith, P.D. - Vectors, Tensors and the Equations of Fluid Mechanics. Englewood Cliffs, Prentice Hall, 1967.
312. Gaffney, P.L. - Tensor Analysis and Continuum Mechanics. Berlin, Springer, 1972.
313. Aris, R. - Interpretation of viscous terms in the turbulent energy equation. *J. Aero. Sci.*, vol.20, 1953, p.111.
314. Harlow, F.H. - Turbulent transport equations. *Phys. Fluids*, vol.10, 1967, p.2323.
315. Nakayama, P.I. - Proceedings, Computations of Turbulent Boundary Layers - 1968 AFOSR-IFP-Stanford Conference, Vol.2. Stanford Univ., Thermosciences Divn., 1969.
316. Coles, D.E. - An experimental flow with zero skin friction throughout its region of pressure rise. *J. Fluid Mech.*, vol.5, 1959, p.1.
- Hirst, E.A. - Stratford, B.S.

ACKNOWLEDGEMENTS

It will be clear from the foregoing that I am indebted to librarians near and far, particularly Mrs. S.D. Bradshaw of the Aeronautical Research Council and Miss A.M. Pindelska of the Department of Aeronautics, Imperial College. Permission to reproduce copyright material was kindly given by the Editors of the *Journal of Fluid Mechanics* and Prof. H. Thomann (Fig.3) and Prof. J.P. Johnston (Fig.6). Permission to reproduce photographs was given by Dr R.M. Huffaker (Fig.5) and Dr E.D. Poppleton (Fig.30). I am grateful to the Von Karman Institute for inviting me to give part of a lecture course, part of the notes for which were a first draft of part of this monograph. Many people have helped me with comments on the draft, access to unpublished work, or general discussions of the subject: in particular I would like to mention Prof. J.M. Beér, Dr I.P. Castro, Prof. H. Fernholz, Dr M.R. Head, Prof. J.H. Horlock, Dr B.E. Launder, Dr F.C. Lockwood, Prof. P.A. Libby, Prof. J.P. Johnston, Prof. R.N. Meroney, Prof. H.M. Nagib, Prof. V.C. Patel, Prof. P.G. Saffman and Mr S.T.B. Young. Dr. T. Morel provided programs and running instructions for the free-shear-layer versions of the calculation method, and Mr S.T.B. Young carried out the calculations of Appendix 2 on the CDC 6400 of the Imperial College Computer Centre. The monograph having been typed by Miss J. Pratt, it may confidently be stated that any remaining errors are my own. Finally I am grateful to Prof. A.D. Young, the Editor, for his advice and encouragement.

APPENDIX 1

SPECIAL COORDINATE SYSTEMS

This Appendix begins with a discussion of coordinate systems, followed by an introduction to general tensor analysis, needed in transforming the equations of motion to arbitrary coordinate systems. Readers not concerned with coordinate transformations may start reading at Section A 1.3, and apply the following rules

(i) interpret symbols u and x with superior or inferior indices (e.g. u_i , x^i) as standing for any one of the velocity components or coordinates (e.g. u_i means u or v or w consistently throughout an equation). This is ordinary tensor notation,

(ii) take $g_{ij} u^i$ to mean u_j ,

(iii) take $u^i_{,j}$ to mean $\partial u_i / \partial x_j$,

(iv) after applying (ii) and (iii), sum over all three values of an index that is repeated in a single term ($\partial u_i / \partial x_i \equiv \partial u / \partial x + \partial v / \partial y + \partial w / \partial z$),

(v) in Eqs (A1.17) to (A1.21) take U_i as the instantaneous velocity, later denoted by $U_i + u_i$.

A1.1 CHOICE OF COORDINATE SYSTEM

Curved or swirling flows are best analysed in coordinate systems other than the familiar Cartesian system with three straight, mutually perpendicular axes: two examples used in the main text are (s, n, z) coordinates, where s is a simply-curved reference line and n and z its normals, and (x, r, θ) cylindrical polar coordinates. By using a slight modification of the usual "Cartesian" tensor notation we can write the exact equations of motion so that their form in any given coordinate system can be deduced fairly easily. Several standard textbooks (e.g. Refs 23, 33) give the Navier-Stokes or boundary-layer equations in conventional notation but incorporating scale factors to allow their evaluation in any orthogonal coordinate system. An orthogonal system is one in which the length of an infinitesimal line element depends only on the squares of increments in the coordinates and not on the products of different increments: for instance the square of the length of an infinitesimal line element in two-dimensional rectilinear coordinates (x, y) inclined at angle ϕ is

$$dS^2 = dx^2 + dy^2 + 2 dx dy \cos \phi \quad (A1.1)$$

so that the coordinates are orthogonal if $\phi = \pi/2$ and non-orthogonal otherwise.

There is only one coordinate system that is everywhere orthogonal and has as one of its coordinate surfaces the surface of a given simply-connected body. The coordinate surfaces belonging to the other two sets must intersect the body surface in the lines of principal curvature. If the body is not simply-connected (if for instance it is doughnut-shaped or if there are two separate bodies) there is in general no such coordinate system at all. As pointed out by Howarth (Ref.304) an infinite number of coordinate systems can be found which are orthogonal at the surface of a simply-connected body: for the purposes of calculating the boundary layer on the body using the thin-shear-layer approximation the non-orthogonality at points distant from the surface can be neglected. The most popular coordinate system for three-dimensional boundary layer calculations uses the streamlines of the potential flow just outside the boundary layer as one set of coordinate lines, the other sets being the curved lines in the surface that are everywhere normal to the streamlines and the straight lines normal to the surface. This system has the general advantage that the direction of flow in the boundary layer is usually not too different from the external streamline direction so that integration of the parabolic boundary layer equations in the streamline direction is usually numerically stable (it has a particular advantage in methods which treat the velocity component in the external streamline direction as having some of the properties of the streamwise velocity in a two-dimensional boundary layer). Its disadvantages, however, are being gradually realized. Because of convergence and divergence of the streamlines, the size and shape of a unit rectangle in the surface may vary greatly from place to place: in this respect, the streamline coordinate system is likely to be generally worse than the everywhere-orthogonal system. Also, it is better if possible to avoid a coordinate system that alters whenever the incidence of the body alters or whenever the displacement effect of the boundary layer alters significantly. Two interesting compromises for bodies like hulls or fuselages are the approach of Cham and Head (305) who formulate their equations in a system based on body geometry and then transform to streamline coordinates, and the body-oriented coordinate system of Miloh and Patel (306) consisting of the intersections with the body of cross-sectional planes normal to the axis together with the curved lines in the surface orthogonal to the lines of intersection.

Some work has been done on coordinate systems for three-dimensional boundary layer calculation which are non-orthogonal even in the body surface. Both Myring (307) and Krause (308) point out that a convenient rectilinear system for swept wings consists of the generators and the intersections of the wing surface with planes parallel to the direction of flight. In this and other systems for boundary layer calculation the most convenient choice for the third set of coordinate lines is the set of straight lines normal to the surface.

The concept implicit in the above discussion is that of the streamlined body, with little effect of the thin turbulent region on the external inviscid flow. In this case the latter can be calculated separately, perhaps in a different coordinate system or even by means of a transformation that predicts the velocity distribution only at the surface and not in the interior of the fluid. In complex turbulent flows such as those described elsewhere in this monograph the thin-shear-layer approximation may be violated in some parts of the fluid and the thin portions of free shear layers are unlikely to lie in the coordinate surfaces of any coordinate system based on the body shape. Now the essential difficulty in numerical solutions of the steady Navier Stokes equations at high Reynolds numbers is that the viscous or turbulent stress gradients, although comparable in general with the total acceleration, may be small

compared to the individual terms in the acceleration $U_{\rho} \partial U_i / \partial x_{\rho}$. Therefore the truncation errors in the finite-difference representation of the individual acceleration terms may be comparable with the actual size of the viscous terms, leading to inaccuracy if the errors have a stabilizing effect (like the "pseudoviscosity" of upwind differences and similar schemes) and to instability if they do not. The three ways of avoiding this difficulty are

- (i) to use so small a mesh size that the Reynolds number based on mesh width and local velocity is of order unity (in turbulent flow the relevant viscosity is, roughly speaking, the eddy viscosity);
- (ii) to use a highly accurate difference scheme [to all appearances this is likely to take almost as much computer time as (i)];
- (iii) to choose coordinate axes aligned with the direction of the velocity — i.e. the direction of any thin shear layer — so that, for each value of i , $U_{\rho} \partial U_i / \partial x_{\rho}$ has one predominant term: then, provided that the truncation errors in the acceleration and the pressure gradient nearly cancel, which can be arranged by using the same finite-difference approximation for the two, adequate accuracy can be obtained. This is close to the procedure used naturally by choosing conventional thin-shear-layer axes or by making the stream function one of the coordinates, and is the only one of the three likely to be acceptable at practical Reynolds numbers.

Now at high Reynolds numbers viscous or turbulent stresses will be significant only in fairly thin shear layers, so we need not use streamline coordinates everywhere. However, to calculate the interactions between the shear layers and the external stream that occur in many complex turbulent flows we are likely to need a coordinate system that is adjusted — possibly by iteration during the calculation — to minimise truncation errors. In general the most convenient system is likely to be non-orthogonal, at least in some parts of the field. The equations of motion and their finite-difference analogues will contain extra factors (functions of the metric tensor) depending on the coordinate system, but the manipulation of these by the numerical analyst and by the computer itself need not be an order of magnitude more complicated than in the case of orthogonal systems. Indeed, orthogonal systems with complicated boundary surfaces may be more difficult to process numerically than a geometrically-simple non-orthogonal system: the calculation of an orthogonal system surrounding a two-dimensional body is exactly equivalent to calculating the streamlines and equipotentials of inviscid flow about that body, and Markatos (309) found that the computer time required to set up a coordinate system orthogonal to an analytically-specified wavy surface exceeded the time taken to calculate the viscous flow on one side of the surface. Both Miloh and Patel (306) and Smith and Gaffney (310) have discussed the numerical approximation of the extra factors in surface coordinate systems for three-dimensional boundary layer calculation: Smith and Gaffney's results are directly applicable to two-dimensional Navier-Stokes problems. The fully three-dimensional case has not yet been tackled but, at least in the case of turbulent flow, our lack of physical knowledge prevents us treating a fully three-dimensional flow with any confidence.

A1.2 GENERAL TENSOR ANALYSIS

An essential tool in the discussion of coordinate systems which are not specified beforehand is general tensor analysis. The subject is usually regarded with some horror by non-mathematicians, but it is merely a convenient system of notation and a set of rules for transforming familiar equations into unfamiliar coordinates. Those unimpressed with the elegance of the derivations can simply take the rules on trust.

There seems to be no textbook in which the mathematics of general tensors is explained in the most appropriate way for analysis of the equations of fluid motion [the nearest approach being the book by Aris (311) in which fluid motion is used to illuminate general tensor analysis rather than the other way around]: the following self-contained account has therefore been prepared. It is intended to be more rigorous than the use of general tensors by recent authors who are really concerned only with orthogonal coordinates. As Flügge points out in the preface to Ref.312, general tensor analysis, "like other sharp tools, can be very beneficial and very dangerous, depending on how it is used".

The equation numbers of the main results (e.g. A1.6) are underlined>.

Consider a coordinate system x^i ($i = 1, 2$ or 3) where we write the index i above the symbol for future convenience. The transformation to another coordinate system \bar{x}^j ($j = 1, 2, 3$) can be written with complete generality as

$$d\bar{x}^j = \frac{\partial \bar{x}^j}{\partial x^i} dx^i \quad (\text{A1.2})$$

where the derivative is evaluated at the local value of x^i , and the whole expression is summed over the three values of i . More generally, if a^i is any vector other than a position vector x^i , it transforms to

$$\bar{a}^j = \frac{\partial \bar{x}^j}{\partial x^i} a^i \quad (\text{A1.3})$$

Quantities that transform in this way are called "contravariant". Quantities that transform according to the rule

$$\bar{a}_j = \frac{\partial x^i}{\partial \bar{x}^j} a_i \quad (\text{A1.4})$$

with both i -indices in the numerator, are called "covariant", and written with the index below the symbol. Coordinates necessarily transform according to the first rule, Eq(A1.3), and are therefore always contravariant. Higher-order tensors can have mixed indices, e.g. b^i_{jk} : this example counts as covariant, by a majority of the indices. The tensor summation convention applies only if the repeated index appears once in the covariant and once in the contravariant position. A tensor with equal numbers of covariant and contravariant indices is a scalar. In non-orthogonal systems the order of the indices matters: b_{jk} and b_{kj} are in general different. The derivative operator $\partial/\partial x^i$ has its index in the denominator

and counts as covariant. Velocities, $\partial x^i / \partial t$, and accelerations, $\partial^2 x^i / \partial t^2$, are time derivatives of position vectors and are therefore contravariant. Since accelerations in fluid flow depend on stress gradients, the latter must also be contravariant; therefore the stress tensor must be a second-order tensor with two contravariant indices, so that its gradients, with two contravariant indices and one covariant, are contravariant by majority. A mild paradox is that since work is a scalar equal to force times distance, force (and therefore acceleration) ought apparently to be covariant: however scalar "dot" products contain special factors to ensure that the final result is a scalar irrespective of the variance of the tensors concerned [see the last element of Eq(A1.6) for example] and force and acceleration can therefore be taken to be contravariant.

Consider as the fundamental coordinate system the rectangular Cartesian coordinates X^i . By Pythagoras' theorem the distance dS between two points with coordinates X^i and $X^i + dX^i$ is given by

$$dS^2 = (dX^{(1)})^2 + (dX^{(2)})^2 + (dX^{(3)})^2 \quad (A1.5)$$

We enclose numerical contravariant indices in parentheses to avoid confusion with exponents. Using Eq(A1.3), the length of the line element in any transformed coordinates x^i (obviously the same length) is given by

$$\begin{aligned} dS^2 &= \sum_{k=1}^3 \left(\frac{\partial X^k}{\partial x^i} dx^i \cdot \frac{\partial X^k}{\partial x^j} dx^j \right) \\ &\equiv g_{ij} dx^i dx^j \end{aligned} \quad (A1.6)$$

where the right hand side is summed over i and j [$g_{11}(dx^{(1)})^2 + g_{12} dx^{(1)} dx^{(2)} \dots$] and where the identity defines a tensor g_{ij} (chosen covariant so that dS^2 is a pure scalar) called the "metric tensor". It is clear from the definition that it is convenient to take $g_{ij} = g_{ji}$ in any coordinate system: in Eq(A1.1), $g_{12} = g_{21} = \cos \phi$, not $2 \cos \phi$. A contravariant metric tensor can be consistently defined by

$$g_{ij} g^{jk} = \delta_i^k \quad (A1.7)$$

where $\delta_i^k = 1$ if $i = k$ and is zero otherwise. In orthogonal coordinates g_{ij} is by definition zero unless $i = j$ [compare Eqs (A1.1) and (A1.6)]. A covariant index can be converted into a contravariant one by the relation

$$a^j = g^{ij} a_i \quad (A1.8)$$

and vice versa: the same operation can be performed successively on the indices of a higher-order tensor but if non-orthogonal coordinate systems are to be used we must distinguish between tensors like p_j^i , equal to $g^{li} p_{lj}$, and p_j^i , equal to $g^{li} p_{jl}$, because in general $p_{lj} \neq p_{jl}$ in non-orthogonal systems. Therefore although some authors preach or practice the arbitrary raising and lowering of indices, it is safer to keep to the natural variances that follow from the essential contravariance of coordinates in the way expounded at the end of the previous paragraph.

Especially when dealing with complicated or non-orthogonal coordinate systems, it is convenient to generalize the usual rules of differentiation so that derivatives of g_{ij} are automatically included: the new operation is called "covariant differentiation". Covariant differentiation of a contravariant vector (or majority-contravariant tensor) a^i with respect to x^j is given by

$$a^i_{,j} = \frac{\partial a^i}{\partial x^j} + \left\{ \begin{matrix} i & j \\ k & \end{matrix} \right\} a^k \quad (A1.9)$$

Flügge (312) and others use the notation a^i/j . Covariant differentiation of a covariant vector a_j is given by

$$a_{i,j} = \frac{\partial a_i}{\partial x^j} - \left\{ \begin{matrix} i & j \\ k & \end{matrix} \right\} a_k \quad (A1.10)$$

where the "Christoffel symbol of the second kind" is given by

$$\left\{ \begin{matrix} i & j \\ k & \end{matrix} \right\} = \frac{1}{2} g^{ip} \left(\frac{\partial g_{pj}}{\partial x^k} + \frac{\partial g_{pk}}{\partial x^j} - \frac{\partial g_{jk}}{\partial x^p} \right) \quad (A1.11)$$

It is covariant with respect to j and k and contravariant with respect to i , and therefore covariant by majority. The result of these rules is that we need not explicitly consider the effect of coordinate transformations on derivatives: in particular, $g_{ij,l}$ and $g^{ij}_{,l}$ are zero. The symbol becomes much simpler if the coordinates are orthogonal when Eq(A1.7) shows that $g_{ii} g^{ii} = 1$ (no summation). Defining the "scale factors" h_i by $g_{ii} = h_i^2$ we get, for orthogonal coordinates,

$$\begin{aligned} \left\{ \begin{matrix} i & j \\ k & \end{matrix} \right\} &= 0 \text{ if } i, j, k \text{ are all different} \\ &= \frac{1}{h_l} \frac{\partial h_l}{\partial x^m} \text{ if } i = j = k = l = m \\ &\quad \text{or } i = j = l, k = m \\ &\quad \text{or } i = k = l, j = m \\ &= -\frac{h_l}{h_m^2} \frac{\partial h_l}{\partial x^m} \text{ if } j = k = l, i = m \end{aligned} \quad (A1.12)$$

Some simplification is possible whenever one or more of the g_{ij} is zero or constant, as is likely to be the case in most practical coordinate systems.

Some coordinate systems do not all have dimensions of length. For example, in the (x,r,θ) system θ is an angle, and as a result $\partial\theta/\partial t$ is not the velocity component in the θ direction. We therefore have to distinguish between the quantities that appear in the equations of motion written in general tensor notation, and their "physical components" in a given coordinate system. It is always most convenient to write the general equations so that they represent the physical components in a Cartesian system: the only apparent differences from the ordinary Cartesian equations are the appearance of co- and contra-variant tensors and of the metric tensors g_{ij} or g^{ij} . In order to recover physical components in any other system we need to apply further factors so that, for instance, the θ -component velocity appears correctly as $r\partial\theta/\partial t$. The rules are that the physical j -component of a contravariant vector a^i , written $a(j)$, is

$$a(j) = (g_{jj})^{\frac{1}{2}} a^j \equiv h_j a^j \quad (\text{no summation}) \quad (\text{A1.13})$$

which also defines h_j , one of the three "scale factors". To obtain the physical j -component of a covariant vector we first raise the index and then apply Eq(A1.9), getting

$$a(j) = (g_{jj})^{\frac{1}{2}} g^{ij} a_i = h_j g^{ij} a_i \quad (\text{no summation}) \quad (\text{A1.14})$$

In the special case of orthogonal coordinates, g^{ij} is zero unless $j = i$, so that

$$a(j) = (g_{jj})^{\frac{1}{2}} g^{jj} a_j = a_j/h_j \quad (\text{A1.15})$$

since $g^{jj} = 1/g_{jj}$. Physical components of tensors are extracted by application of the vector rules to each index in turn. We do not need to apply these rules to the metric tensor, which is not a physical quantity in a given coordinate system but a relation between two coordinate systems. The physical component of the derivative of a quantity a^i written with a necessary change of the covariant index as $a(i,m)$ and including the physical component of ∂x^ℓ , is $h_i h_m g^{\ell m} a^i_{,\ell}$. Converting $a^i_{,\ell}$ back to a conventional derivative by Eq(A1.9) and expressing it in terms of the physical components of its elements, we get

$$a(i,m) = h_i h_m g^{\ell m} \left[\frac{\partial}{\partial x_\ell} \left(\frac{a(i)}{h_i} \right) + \left\{ \begin{matrix} i & \\ n & \ell \end{matrix} \right\} \frac{a(n)}{h_n} \right] \quad (\text{A1.16})$$

where the derivative of h_i must be evaluated explicitly. We see that the insertion of the Christoffel symbol and the conversion a^i to physical components both introduce derivatives of metric quantities: when dealing only with orthogonal coordinates where the Christoffel symbols reduce to functions of the scale factors h_i both processes can be considered together (in fact, in the example above the derivative of h_i cancels with part of the Christoffel symbol) but in non-orthogonal systems they are distinct.

The complete procedure for deriving the differential equations which represent the conservation principles of physics in any chosen coordinate system is therefore

- (i) write the equations for Cartesian coordinates in general tensor notation with the correct variance, replacing partial derivatives by the " $_{,\ell}$ " operator and ignoring derivatives of metric tensors;
- (ii) work out the metric tensor g_{ij} (A1.6) and the scale factors $h_i \equiv \sqrt{g_{ii}}$ for the chosen coordinate system, and evaluate the Christoffel symbols (A1.11);
- (iii) convert the " $_{,\ell}$ " operators back to $\partial/\partial x_\ell$ by using (A1.9) and (A1.10);
- (iv) recover the physical components of vectors and tensors by using Eqs (A1.13), (A1.14) and (A1.16);
- (v) substitute for the metrics, scale factors and Christoffel symbols from step (ii);

Step (i) is performed below, once for all. Steps (iii) and (iv) could be performed once for all but specialization from the general form to any of the particular coordinate systems likely to be used in practice would be rather more complicated than applying the rules given above and taking advantage of the zero elements of g_{ij} . Steps (ii) and (v) would be done by hand if the coordinate system were specified algebraically and by computer if it were specified numerically.

A1.3 THE EQUATIONS OF FLUID FLOW

We now apply these rules and definitions to the principles of conservation of mass and momentum for an incompressible fluid with viscous stress proportional to rate of strain [see (311), Ch.8]. To begin with, we use U^i for the instantaneous (mean plus fluctuating) velocity.

The mass-conservation (continuity) equation is

$$U^{\ell}_{,\ell} = 0 \quad (\text{A1.17})$$

The contravariant rate of strain is related to the covariant rate of strain

$$e_{qr} \equiv \frac{1}{2}(U_{q,r} + U_{r,q}) \quad (\text{A1.18})$$

by

$$e^{i\ell} = g^{qi} g^{r\ell} e_{qr} \quad (\text{A1.19})$$

and is therefore

$$e^{i\ell} = \frac{1}{2}(g^{r\ell} U_{,r}^i + g^{qi} U_{,q}^\ell) \quad (\text{A1.20})$$

The viscous stress gradients in the x^i -component Navier Stokes equation can be written as $2\nu e^{i\ell}$ and we see that the contribution of the second term in Eq(A1.20) to this vanishes by continuity, leaving $\nu g^{r\ell} U_{,r\ell}^i$ which can be shown to be a self-consistent definition of $\nu \nabla^2 U^i$ in general tensors.

The x^i -component Navier-Stokes equation becomes

$$\frac{\partial U^i}{\partial t} + U^\ell U_{,\ell}^i = -g^{i\ell} \frac{p_{,\ell}}{\rho} + \nu g^{r\ell} U_{,r\ell}^i + F^i \quad (\text{A1.21})$$

where F^i is any body force per unit mass. All the quantities in Eqs (A1.17), (A1.20) and (A1.21) have the proper variance as outlined at the beginning of this section, and the difficulty over the order of indices in mixed tensors does not appear.

Adding the zero quantity $U^i U_{,\ell}^\ell$ to the left of Eq(A1.21) allows us to write its second term as $(U^\ell U^i)_{,\ell}$ so that the extra Reynolds stress gradients that appear in turbulent flow are obviously $-(u^\ell u^i)_{,\ell}$, where we now return to the convention that large and small letters denote mean and fluctuation respectively.

In rotating axes the Coriolis "body force" $2\Omega \times \underline{U}$ must be added to the right hand side of Eq(A1.21). Since the body force or acceleration must be contravariant we take it as

$$F^i \equiv 2 \epsilon^{i\ell m} \Omega_\ell (U_m + u_m) \quad (\text{A1.22})$$

where $\epsilon^{i\ell m}$ is +1 if i, ℓ, m are in cyclic order 123123, -1 if they are in anticyclic order 321321, and zero if i, ℓ and m are not all different. Ω_ℓ represents a vector normal to the plane of rotation and is therefore (311, p.176) covariant. U_m is a velocity component normal to the angular velocity vector (i.e. a time derivative of a normal vector, $\partial n_m / \partial t$) and must therefore be taken covariant as well. The index can be raised for compatibility with the other velocities but this should be done at the end of any further tensor manipulation.

The mean-momentum equation for incompressible turbulent flow in the presence of a Coriolis "body force" caused by rotating the axes at angular velocity Ω is then

$$\frac{DU^i}{Dt} \equiv U^\ell U_{,\ell}^i \equiv (U^\ell U^i)_{,\ell} = -g^{i\ell} \frac{\bar{p}_{,\ell}}{\bar{\rho}} - \overline{(u^\ell u^i)_{,\ell}} + \nu g^{r\ell} U_{,r\ell}^i + 2\epsilon^{i\ell m} \Omega_\ell U_m \quad (\text{A1.23})$$

where $\epsilon^{i\ell m}$ is defined after Eq(A1.22). In Cartesian coordinates $g^{i\ell} \bar{p}_{,\ell}$ can be read as $\bar{p}_{,i}$ and $\overline{\nu g^{r\ell} U_{,r\ell}^i}$ as $\overline{\nu U_{,\ell\ell}^i}$. In compressible flow, using mass-averaged quantities such that $\bar{\rho} \bar{U}^i = \bar{\rho} U^i + \rho' u^i$ where $\bar{\rho}$ and ρ' are the mean and fluctuating parts of the density ρ , and defining the mass-weighted fluctuation \tilde{u}^i by $U^i + u^i = \bar{U}^i + \tilde{u}^i$ so that \tilde{u}^i has a non-zero mean value, we have

$$(\bar{\rho} \tilde{u}^i)_{,\ell} = -g^{i\ell} \bar{p}_{,\ell} - \overline{\rho \tilde{u}^i} + \text{complicated viscous terms} \quad (\text{A1.23a})$$

The Reynolds-stress transport equation for $\overline{u^i u^j}$ is obtained, as explained in Section 2, by multiplying the instantaneous u^i -component momentum equation by u^j and adding the u^j -component equation multiplied by u^i . With some use of Eq(A1.17) we get

$$\begin{aligned} \frac{D(\overline{u^i u^j})}{Dt} &\equiv U^\ell (\overline{u^i u^j})_{,\ell} = \\ &- (\overline{u^i u^\ell} U_{,\ell}^j + \overline{u^j u^\ell} U_{,\ell}^i) \\ &+ \overline{p'(g^{i\ell} u_{,\ell}^j + g^{j\ell} u_{,\ell}^i) / \bar{\rho}} \\ &- (g^{i\ell} (\overline{p' u^j})_{,\ell} + g^{j\ell} (\overline{p' u^i})_{,\ell}) / \bar{\rho} - \overline{(u^i u^j u^\ell)_{,\ell}} \\ &+ \nu g^{r\ell} (\overline{u^i u^j}_{,r\ell} + \overline{u^j u^i}_{,r\ell}) \\ &+ 2\Omega_\ell (\epsilon^{i\ell m} \overline{u^j u_m} + \epsilon^{j\ell m} \overline{u^i u_m}) \end{aligned} \quad (\text{A1.24})$$

The six lines represent respectively mean transport, generation, redistribution by pressure fluctuations, turbulent transport, viscous transport and destruction, and redistribution due to rotation of the axes with respect to the stress tensor. Fig.9 summarizes the terms.

The viscous terms can be decomposed into

$$\nu g^{r\ell} (\overline{u^i u^j})_{,r\ell} - 2\nu g^{r\ell} \overline{u_{,r}^i u_{,\ell}^j}$$

The first term, which can be written as $\nabla \cdot \nabla^2(\overline{u^i u^j})$, clearly contains spatial gradients of turbulence quantities, so that its integral over the flow volume is zero: therefore it is a viscous transport term. The second term, which we have simplified by using $g^{lr} = g^{rl}$, may be called the viscous destruction term.

The turbulent energy equation for $\frac{1}{2} \overline{u^i u^i}$ is $\frac{1}{2} g_{ji}$ times Eq(A1.19), where the metric tensor lowers the j index to make each term a scalar, like $\frac{1}{2} \overline{u_i u^i}$ itself. Note that the individual normal stresses are still contravariant. The Coriolis terms in the turbulent energy equation are zero: mathematically, this is because of the symmetry of the stress tensor and the anti-symmetry of ϵ^{ilm} ; physically, rotation of the axes does not affect scalar quantities. The viscous destruction or "dissipation" term, ϵ , is the rate at which the rates of strain do work against viscous stresses and therefore is $\frac{1}{2} \overline{v e^{i\ell} e_{i\ell}}$, where e is as defined in Eqs (A1.13) and (A1.15) but includes only the fluctuating velocity components. As shown by Corrsin (313) this differs from the so-called destruction term as decomposed above by a further spatial-gradient term:

$$\epsilon \equiv \frac{1}{2} \overline{v e^{i\ell} e_{i\ell}} = \nu g_{ji} g^{rl} \overline{u^i_{,r} u^j_{,\ell}} - \overline{v(u^i u^j)_{,ij}} \tag{A1.25}$$

However both contributions to the viscous transport are small except at very low local Reynolds numbers, and the complete viscous term in any of the $\overline{u^i u^j}$ equations is usually approximated by the so-called destruction term

$$- 2 \nu g^{rl} \overline{u^i_{,r} u^j_{,\ell}}$$

A "destruction transport equation" for this term can be obtained by differentiating the u^i -component Navier Stokes equation with respect to x^r and multiplying by $g^{rl} u^j_{,\ell}$, adding $g^{rl} u^i_{,r}$ times the x^ℓ derivative of the u^j -component Navier Stokes equation and taking the mean to get

$D g^{rl} \overline{u^i_{,r} u^j_{,\ell}} / Dt$. This automatically includes Corrsin's viscous transport term in the turbulent energy equation: our knowledge of the behaviour of the destruction transport equations is so fragmentary that this inclusion does not affect our decisions about closure schemes. The other part of the viscous transport, $\nabla \cdot \nabla^2 \overline{u^i u^j}$, can be represented exactly if the $\overline{u^i u^j}$ are known, although it may not be realistic to bother with it. The destruction transport equation for the case $i = j$ is given in Cartesian coordinates by Harlow and Nakayama (314) and discussed in Refs (25, 34, 35): the general tensor form of any given equation should be clear from Eq(A1.21).

A1.4 TWO SPECIAL COORDINATE SYSTEMS

We now consider the special (s,n) and (x,r,θ) coordinate systems for which the mean-momentum and continuity equations are given in Section 2. There is of course no need to use general tensor analysis to derive equations in these well-known systems, but as an example we derive the continuity equation in x,r,θ coordinates, with velocity components U,V,W.

Since $ds^2 = (dx)^2 + (dr)^2 + r^2(d\theta)^2$ we have $g_{11} = g_{22} = 1$, $g_{33} = r^2$, and $h_1 = h_2 = 1$, $h_3 = r$ as the square roots of the g elements. Consider Eq(A1.16) with $a^i_{,\ell}$ equal to $U^i_{,\ell}$, so that the metric factor outside the brackets becomes $h_\ell h_m g^{\ell m}$: in any orthogonal system this is zero unless $\ell = m$ when it becomes $h_\ell^2 g^{\ell\ell} = g_{\ell\ell} g^{\ell\ell} = 1$, using Eq(A1.7) and the definition of h_j implied in Eq(A1.13). Therefore

$$0 = U^i_{,\ell} = \frac{\partial U}{\partial x} + \frac{\partial V}{\partial r} + \frac{\partial}{\partial \theta} \left(\frac{W}{r} \right) + \left\{ \begin{matrix} \ell & \ell \\ n & \ell \end{matrix} \right\} \frac{U(n)}{h_n} \tag{A1.26}$$

Eq(A1.12) gives the Christoffel symbol as $\frac{1}{h_\ell} \frac{\partial h_\ell}{\partial x^n}$ which is zero unless $\ell = 3$, $n = 2$ when it is $1/r$. Thus the continuity equation becomes

$$\frac{\partial U}{\partial x} + \frac{\partial V}{\partial r} + \frac{1}{r} \frac{\partial W}{\partial \theta} + \frac{V}{r} = 0 \tag{A1.27}$$

The turbulent energy equation, for $\frac{1}{2} \overline{q^2} \equiv \frac{1}{2} (\overline{u^2} + \overline{v^2} + \overline{w^2})$ in (s,n) coordinates, given by Castro (11) is

$$\begin{aligned} \frac{D(\frac{1}{2} \overline{q^2})}{Dt} &\equiv \left[U \frac{\partial}{\partial s} + \left(1 + \frac{n}{R} \right) \frac{\partial}{\partial n} \right] (\frac{1}{2} \overline{q^2}) \\ &= - \overline{u^2} \left(\frac{\partial U}{\partial s} + \frac{V}{R} \right) - \left(1 + \frac{n}{R} \right) \overline{v^2} \frac{\partial V}{\partial n} - \overline{uv} \left[\left(1 + \frac{n}{R} \right) \frac{\partial U}{\partial n} + \frac{\partial V}{\partial s} - \frac{U}{R} \right] \\ &\quad - \frac{\partial}{\partial s} \left(\frac{\overline{p'u}}{\rho} + \frac{1}{2} \overline{q^2 u} \right) - \frac{\partial}{\partial n} \left[\left(1 + \frac{n}{R} \right) \left(\frac{\overline{p'v}}{\rho} + \frac{1}{2} \overline{q^2 v} \right) \right] \\ &\quad - \epsilon \end{aligned} \tag{A1.28}$$

where the four lines represent respectively advection, production, diffusion and dissipation: we neglect viscous diffusion of turbulent energy, which is negligible except in the viscous sublayer where x,y

coordinates can be used. The individual equations for $\overline{u^2}$, $\overline{v^2}$ and $\overline{w^2}$ are given (in slightly different notation) by So and Mellor (160) and can be deduced from the equations given by Rodi (17).

The shear stress equation, also given by Castro (11) and (apparently with minor inconsistencies) by So and Mellor (160) is

$$\begin{aligned} \frac{D(-\overline{uv})}{Dt} &\equiv \left[U \frac{\partial}{\partial s} + \left(1 + \frac{n}{R} \right) v \frac{\partial}{\partial n} \right] (-\overline{uv}) \\ &= \overline{u^2} \left(\frac{\partial v}{\partial s} - \frac{U}{R} \right) + \left(1 + \frac{n}{R} \right) \overline{v^2} \frac{\partial U}{\partial n} - \frac{U}{R} (\overline{u^2} - \overline{v^2}) \\ &\quad - \frac{\overline{p'}}{\rho} \left(\frac{\partial v}{\partial s} + \left(1 + \frac{n}{R} \right) \frac{\partial u}{\partial n} \right) \\ &\quad + \frac{\partial}{\partial s} \left(\frac{\overline{p'v}}{\rho} + \overline{u^2v} \right) + \left(1 + \frac{n}{R} \right) \frac{\partial}{\partial n} \left(\frac{\overline{p'u}}{\rho} + \overline{uv^2} \right) + \left(2 \frac{\overline{uv^2} - \overline{u^3}}{R} \right) \end{aligned} \quad (A1.29)$$

where the four lines represent mean transport, generation, redistribution (usually destruction) by pressure fluctuations, and turbulent transport by pressure and velocity fluctuations: we have neglected the viscous term entirely because it is negligible except in and fairly near the viscous sublayer and possibly in some other flows at low local Reynolds number. The last group in the generation term represents the effect of rotation of axes. If the axes are rotated by a small angle θ the shear stress in the new axes is, to first order, $-\overline{uv} + \theta(\overline{u^2} - \overline{v^2})$; in the present case the axes rotate at an angular velocity $d\theta/dt = (-U/R)$ so an extra contribution to $D(\overline{uv})/Dt$ arises. The last group in the transport term arises from the irregular shape of the control volume, as does part of the last group in the diffusion term of the turbulent energy equation.

The turbulent energy equation in (x, r, θ) coordinates with velocity components U, V and W respectively, is given by Rodi (17) as

$$\begin{aligned} &\left[U \frac{\partial}{\partial x} + v \frac{\partial}{\partial r} + \frac{W}{r} \frac{\partial}{\partial \theta} \right] (\frac{1}{2} \overline{q^2}) \\ &= - \overline{u_i u_j} \frac{\partial U_i}{\partial x_j} - \frac{v}{r} \overline{u^2} + \frac{W}{r} \overline{vw} \\ &\quad - \frac{\partial}{\partial x} \left(\frac{\overline{p'u}}{\rho} + \frac{1}{2} \overline{q^2} u \right) - \frac{1}{r} \frac{\partial}{\partial r} \left\{ r \left(\frac{\overline{p'v}}{\rho} + \frac{1}{2} \overline{q^2} v \right) \right\} - \frac{1}{r} \frac{\partial}{\partial \theta} \left(\frac{\overline{p'w}}{\rho} + \frac{1}{2} \overline{q^2} w \right) \\ &\quad - \epsilon \end{aligned} \quad (A1.30)$$

where the terms are in the same order as in Eq(A1.21) and $\overline{u_i u_j} \partial U_i / \partial x_j$ is the sum of the nine terms obtained by taking u_i or u_j as u, v or w ; the components of x_j are taken as x, r and $r\theta$. All terms in θ are zero in axisymmetric flow: terms in W are zero only in axisymmetric non-swirling flow.

The shear stress equations, for $-\overline{uv}$ and $-\overline{vw}$ respectively, are

$$\begin{aligned} &\left[U \frac{\partial}{\partial x} + v \frac{\partial}{\partial r} + \frac{W}{r} \frac{\partial}{\partial \theta} \right] (-\overline{uv}) \\ &= \overline{u^2} \frac{\partial v}{\partial x} + \overline{uv} \left(\frac{\partial U}{\partial x} + \frac{\partial v}{\partial y} \right) + \overline{v^2} \frac{\partial U}{\partial y} + \frac{\overline{uw}}{r} \frac{\partial v}{\partial \theta} + \frac{\overline{vw}}{r} \frac{\partial U}{\partial \theta} \\ &\quad - \frac{\overline{p'}}{\rho} \left(\frac{\partial v}{\partial x} + \frac{\partial u}{\partial r} \right) \\ &\quad + \frac{\partial}{\partial x} \left(\frac{\overline{p'v}}{\rho} + \overline{uv^2} \right) + \frac{\partial}{\partial r} \left(\frac{\overline{p'u}}{\rho} \right) + \frac{1}{r} \frac{\partial}{\partial r} (r \overline{uv^2}) + \frac{1}{r} \frac{\partial}{\partial \theta} (\overline{uvw}) - \frac{\overline{uw^2}}{r} \end{aligned} \quad (A1.31)$$

and

$$\begin{aligned} &\left[U \frac{\partial}{\partial x} + v \frac{\partial}{\partial r} + \frac{W}{r} \frac{\partial}{\partial \theta} \right] (-\overline{vw}) \\ &= \overline{uw} \frac{\partial v}{\partial x} + \overline{vw} \frac{\partial v}{\partial r} + \overline{w^2} \left(\frac{\partial v}{\partial \theta} - \frac{W}{r} \right) + \overline{uv} \frac{\partial W}{\partial x} + \overline{v^2} \frac{\partial W}{\partial r} + \frac{\overline{vw}}{r} \frac{\partial W}{\partial \theta} + \frac{V}{r} \overline{vw} - \frac{W}{r} (\overline{w^2} - \overline{v^2}) - \end{aligned}$$

$$\begin{aligned}
& - \frac{p'}{\rho} \left(\frac{\partial w}{\partial r} + \frac{1}{r} \frac{\partial v}{\partial \theta} \right) \\
& + \frac{\partial}{\partial x} (\overline{uvw}) + \frac{\partial}{\partial r} \left(\frac{\overline{p'w}}{\rho} + \overline{v^2w} \right) + \frac{1}{r} \frac{\partial}{\partial \theta} \left(\frac{\overline{p'v}}{\rho} + \overline{vw^2} \right) + 2 \frac{\overline{v^2w}}{r} - \frac{\overline{w^3}}{r}
\end{aligned} \tag{A1.32}$$

Eqs (A1.28) and (A1.29) are special cases of Eqs (A1.30) and (A1.32) with $r\theta \rightarrow s$, $r \rightarrow n + R$ and x derivatives neglected in the latter equations. Rodi (17) gives the equations for the other Reynolds stresses in (x, r, θ) coordinates. Note that the division of the terms into mean transport, generation, etc. is not simple. Strictly, the quantities on the left of the transport equations should be reducible, by adding multiples of the continuity equation, to quantities whose volume integrals are all zero. Here we have grouped the terms according to their mathematical form rather than their physical meaning: Rodi groups the rotation-of-axis terms, discussed above, with the mean transport terms, and makes several other non-obvious groupings without explanation.

APPENDIX 2

NUMERICAL EXPERIMENTS

This Appendix contains details of the calculations by the method of Ref.16 referred to elsewhere in the text: see Tables 3 and 4 for a summary of the test cases. In all cases the thin-shear-layer approximation was used, the normal pressure gradient being neglected, and the values quoted for the integral thicknesses δ^* and θ were obtained from the plane-flow definitions rather than the curved-flow definitions of Refs 37, 38 or 183. The errors introduced by these two simplifications tend to cancel, since the calculations of U/U_e approximate to U_r/U_{re} . Of course, these are f-factor effects (pp.17-18) and are small compared to F-factor effects, except in the case of severe curvature where changes due to f-factor effects become of order unity. The input data used for most of the calculations are tabulated at the end of the Appendix and may be useful for calculations by other methods: no great precision is claimed and some discrepancies in the original data may have gone unnoticed. Data for Schubauer and Klebanoff's aerofoil (101: Fig.26) are tabulated by Coles and Hirst (315).

It should be pointed out that many of the test cases have very strong curvature, beyond the reach of F-factors. Calculations are included partly to demonstrate the limits of the F-factor analysis and partly to demonstrate the large differences between the experimental data and calculations with no curvature correction. In the compressible flows with curvature-induced pressure gradient, bulk compression/dilatation effects are larger than curvature effects, but again the calculations with no allowance for extra rate of strain disagree strongly with experiment. The experiment of Stratford (316: see also 315) on a separating boundary layer probably exhibited strong curvature effects but the aspect ratio of the tunnel was so small that secondary flows in the corners probably had a large effect: the flow was far from two-dimensional. The axisymmetric diffuser experiments of Fraser tabulated in Ref.315 appear not to suffer significantly from the extra strain effects of lateral divergence or of convex longitudinal curvature, but since these effects are of opposite sign they may merely have tended to cancel. For different reasons, therefore, the experiments of Stratford and of Fraser are not useful as test cases.

Meroney's measurements (164) on surfaces with $\delta/R \sim 0.01-0.02$ are the first since Schmidbauer's to provide a test of the F-factor correction for curvatures typical of aerofoils and turbomachines without the complications of compressibility. The results shown in Fig.25(a) are from a first series of runs: the concave-surface data are those taken on the centre-line of the tunnel which happens to be near the line of maximum surface shear stress and minimum boundary-layer thickness (i.e. the line of maximum inflow in the longitudinal vortex system). The amplitude of c_f variation at $x = 39$ in, about 40 initial boundary-layer thicknesses from the start of curvature, is about ± 10 per cent with a spanwise wavelength of about 1.2δ . At this position, the flux Richardson number at $y/\delta = 0.5$ is numerically about 0.07 on both the concave and the convex surface, so that the F factors are just within the range $0.5 < F < 1.5$ set as an arbitrary limit: at larger y larger values of R_f are found [Fig.25(b)] but the dissipation term to which the F-factor is applied becomes fairly small compared to the turbulent transport terms, and in any case the velocity gradient is small so that errors in calculating it have little effect on the overall profile. Agreement between experimental values of the integral parameters [Fig.25(a)] and calculations, using Eq(37) with $X = 10\delta$ and Eq(119) with $\beta = 7$ (convex) and $\beta = 4.5$ (concave), seems satisfactory. It is hoped that the final results of the experiment, which is still in progress, may suggest improved values of β (or α) or even improved forms of F-factor.

In the experiments of So and Mellor (160) the ratios of boundary-layer thickness to radius of curvature were as high as 0.08 on a convex surface and 0.13 on a concave surface (higher values were attained in a boundary layer separating from a convex wall but we have not done calculations for this case). These high values are beyond the reach of linear F-factors. The non-linear F-factor-like correction applied to the eddy viscosity by So and Mellor contains an empirical constant adjusted to suit their convex-surface data. They take

$$-\overline{uv} = \nu_{T,p} \frac{\partial U}{\partial y} (1 - S)^2 \left(1 - 4.05 \frac{(1+S)}{(1-S)^2} \right)^{3/2} \quad (A2.1)$$

where $S \equiv (U/R)/(\partial U/\partial y)$ as in Eq.(86) and $\nu_{T,p}$ is the empirical eddy viscosity value used in plane flow. The linearized version of this correction factor corresponds to an F-factor with α equal to 8 when applied to eddy viscosity or about 16 when applied to mixing length or dissipation length parameter, compared with the value of 14 suggested above for an F-factor applied to L on a convex (stable) surface. Therefore So and Mellor's factor would give results fairly close to Eq(36), with $\alpha = 14$, for cases of mild curvature. It does not contain any lag allowance and, being based on local parameters, is automatically suspect in highly-curved flows where turbulent transport terms are important: however, the fit to So and Mellor's own results is very good.

Calculations by the method of Ref.16 of the integral parameters are shown in Fig.22 (a) and (b). An initial set of calculations on the convex surface was done with the conventional boundary-layer thickness (the distance from the surface at which $U = 0.995 U_e$) as a scaling length for L , but it was then realised that the "correct" thickness to use is that of the turbulent sub-boundary-layer, the total thickness of the mean velocity profile being immaterial because its outer part is not turbulent. (So and Mellor's use of δ^* for scaling is also unrealistic in this case.) Fig.22(c) shows a comparison between measured and calculated shear stress at the last station shown on Fig.18(a), for the two choices of scaling length. Agreement is quite good for the general profile shape and the thickness of the sub-boundary layer, underlining the statement on p.70 that any correction factor that predicts strong suppression of turbulence in highly-stable cases will give good agreement with experiment. Note, however, that the magnitude of c_f is not well predicted.

On the concave surface, longitudinal vortices form. So and Mellor regard the law of the wall as untrustworthy on a concave surface apparently because the velocity at the edge of the inner layer falls below the logarithmic line instead of rising above it as is more usual: however their quoted values of c_f , obtained from "Clauser plots" using the law of the wall, seem plausible and in reasonable agreement with calculations (though not with the hot wire measurements). So and Mellor measured velocity profiles at

only two streamwise positions: integral thicknesses at the crest and trough of the periodic spanwise variation are shown in Fig.22(b) for comparison with calculations.

Although extensive data tabulations are given in So and Mellor's report some difficulties were experienced in extracting initial and boundary conditions for a calculation because of gaps or inconsistencies: therefore the tabulated data given here should not be taken as definitive.

Young's experiment on a "curvature impulse" in a 30 deg bend with $\delta/R \approx +0.2$ or -0.1 is still in progress. The calculations shown in Fig.23 for flow on and downstream of the concave surface agree satisfactorily with experiment although, as in Meroney's experiment, mapping of the longitudinal vortex pattern is not yet complete. The need for a lag equation to modify the F-factor is evident.

As mentioned in the Introduction, Thomann's experiment at $M = 2.5$ (4) is the only one at any speed to investigate plane, concave and convex surfaces with nominally identical starting conditions and negligible pressure gradient. Unfortunately only surface heat transfer was measured and the starting conditions are uncertain. In the calculations we have assumed that the momentum thickness at $x/L = 1$ was as calculated by Thomann using Walz' method, and that the Stanton number (based on the difference between wall temperature and recovery temperature) was everywhere equal to $1.16 c_f/2$, an accepted ratio for flat surfaces. A further difficulty is that the method of Ref.16 is fully operational only for adiabatic walls: in the calculations we have taken the temperature profile to be given by the adiabatic Crocco law

$$T_w/T = 1 + r \left(\frac{\gamma-1}{2} \right) M^2 \quad (A2.2)$$

with the recovery factor r taken as 0.52 to get the right wall temperature ($T_w/T_o \approx 0.7$), which underestimates the temperature within the boundary layer. This combination of uncertainties and approximation results in the agreement with experiment being rather poor even for the plane surface [Fig.27(a), curve ①]. St (or c_f) is overestimated: Thomann's measurements on the plane surface [the circles in Fig.27(a)] seem slightly erratic, and decrease with x more rapidly than expected, but allowance for the small adverse pressure gradient reported by Thomann scarcely changed the calculations.

The curved-surface calculations were all done with the lag equation, Eq(37), with a "time constant" of 10δ . Although this "time constant" is certainly an over-estimate near the surface, the calculations seem to underestimate the lag in the response of heat transfer to a change in curvature. Now the main sources of data used to confirm the applicability of the traditional "time constant" of 10δ to Eq(37) were the retarded-accelerated boundary layer of Lewis et al. (66) at $M_e \approx 4$ (Fig.11) and the low-speed curvature-impulse data of Young (57: Fig.23). Although it is clear from these comparisons that the simple lag equation, Eq(37), does not give perfect agreement with experiment, it can be concluded that the "time constant" does not change very greatly with Mach number, and this agrees with the empirical finding that velocity profile shapes do not change greatly with Mach number so that the typical value of $\partial U/\partial y$ used in making the "time constant" $\frac{1}{2}q^2/(-\bar{u} \partial U/\partial y)$ should not change greatly with Mach number. However, wall cooling leads to fuller velocity profiles, smaller typical values of $\partial U/\partial y$ and thus larger "time constants": Morkovin's hypothesis of the insensitivity of turbulence structure to small density fluctuations should guarantee the insensitivity of $\bar{u}v/q^2$ to Mach number and heat transfer in the ranges in question. We have not explored the effects of varying the "time constant", in view of the other uncertainties in the calculation but it appears that a value of not more than 15δ would optimise agreement with experiment. The difference between this and the traditional value of 10δ can be plausibly attributed to heat transfer: therefore the value of 10δ should be used in adiabatic flows where the velocity profile shape is closely the same as at low speeds.

Once it is granted that the "time constant" used in the calculations is rather too small it follows that the calculations with the low-speed values of α in Eq(36) — curves ② and ③ in Fig.27(a) — underestimate the effects of curvature (compare the experimental and theoretical values at the last measurement station). However curves ④ and ⑤, including the compressibility correction $1 + (\gamma-1)M^2/2$ for an adiabatic wall from Eq(93), seem to be significant overestimates. This discrepancy too can be explained away, in principle, by the effects of heat transfer: it can be seen from the first-order form of Richardson number, quoted following Eq(97), that cooling the wall, which reduces the numerical value of the (negative) temperature gradient $\partial T/\partial r$, reduces the compressibility correction. In Thomann's experiment T_w/T_e was about 1.5, compared to 2.2 on an adiabatic wall at the same Mach number, so that the compressibility correction would be significantly reduced.

In summary, Thomann's experiment is at least not in demonstrable conflict with the values of α and of the "time constant" suggested above. It would be very desirable to have c_f measurements for an adiabatic wall with about the same δ/R ; boundary layer profiles are of course desirable but an adequate value of initial momentum thickness could be obtained by integrating the c_f distribution from the leading edge or transition point.

Sturek and Danberg's measurements [Fig.27(b)] were made on a concave surface with $|\delta/R| \approx 0.03$. Surface shear stress was measured with a Preston tube, but the resulting Van-Driest-transformed logarithmic profiles in the curved region have a rather higher intercept than the accepted value of 5 [adequately fitted, for instance, by the $M_e = 4$ data of Lewis et al. (66)]. The tops of the bars on the experimental points for c_f in Fig.27(b) represent values derived from the accepted (transformed) logarithmic law. Values of δ^* and θ are those evaluated by the experimenters from "ideal" conditions, the compressible analogue of the "potential wall velocity" as defined by So and Mellor and others: these values agree quite well with those calculated by the method of Ref.16 neglecting normal pressure gradients, and the latter agree with the eddy-viscosity calculations of Cebeci (private communication). The run of boundary layer is only about 15 times the initial δ and the initial conditions significantly affect the results. The total pressure on a given streamline changes appreciably only near the wall so that θ and H are scarcely affected by allowances for the effects of curvature and bulk compression/dilatation on the shear stress. The calculated maximum shear stress at the last measurement station increases by about 35 per cent when both allowances are made: the flow experiences a "strain impulse" (p.19) which has not produced very large changes in turbulence structure by $x = 21$ in, so that in principle a linear F-factor with a lag equation should be capable of describing the flow up to this point. However the present lag equation, Eq(37), is certainly not

adequate because the variation of response time with distance from the surface is not represented. This fact, and the uncertainty of the starting conditions and c_f measurements, makes it impossible to deduce more from the calculations than the evident need for allowances for extra rates of strain. Kepler and O'Brien's experiment [Fig.27(c)] on a concave surface with 24 deg. turning angle had $|\delta/R| \approx 0.06$ at the start of curvature, with a very strong adverse pressure gradient. A persuasive argument for the importance of extra strain effects is that a calculation with no allowance for them predicts separation of the boundary layer, which did not occur in the experiment: with an allowance for bulk compression, c_f falls no lower than half its original value while a further allowance for curvature raises c_f slightly further. Surface shear stress was not measured and the values of δ^* and θ depend on the definitions chosen: the disagreement between calculations using the plane-layer definitions and the experimental values using a "free stream" velocity varying with y according to the inviscid flow equation is large. Fig.27(c) shows the very large disagreement between calculated and experimental velocity profiles after only 12 deg. of turning, i.e. a distance of about 3.5 δ from the start of curvature (U_e is the nominal velocity at the boundary layer edge in the case of the experiments, and the velocity corresponding to the wall static pressure in the case of the calculations). Now the total pressure profiles plotted against stream function would (in the absence of experimental and numerical errors) coincide almost exactly except near the wall because the pressure gradients greatly exceed the Reynolds stress gradients. Very little can be learned about turbulence from an experiment such as this, in which not even the surface shear stress was measured.

Full calculations have not been done for two more supersonic flows, McLafferty and Barber's two-dimensional concave-surface boundary layer (184) and Clutter and Kaups' axisymmetric bodies (185). Both sets of data are nominally useful although McLafferty and Barber's flow cannot be checked for two-dimensionality because of the lack of c_f measurements. A calculation of McLafferty and Barber's flow without allowance for curvature and bulk compression went to separation; again the implication is that extra strain rates have a large effect on the turbulence. McLafferty and Barber noted a lag in the response of the flow to the wall curvature: it is not possible to distinguish curvature lag effects from ordinary history. Clutter and Kaups' measurements are ideal for a test case except for the small ratio of cross-sectional radius of curvature to boundary layer thickness, the rapid lateral divergence and of course the effects of bulk compression; the flow is not unlike that over the rear of Winter's waisted body (54) for which calculations by a method with nearly the same physical input as the present one have been reported by Green et al. (46).

Clearly, better confidence in the corrections for bulk compression and lateral divergence is needed before curvature effects in supersonic flows can be fully elucidated. Thomann's measurements give modest support to the present suggested values for "time constant" X , empirical "constant" α or β , and Mach number dependence of the Richardson number.

The wall jet calculations do not correspond exactly to any experiment and are not reproduced here. For convenience the runs were done with a finite free stream velocity, one-tenth of the maximum velocity on the initial profile which was that of a fully-developed wall jet. The thickness $\delta_{.5}$, defined as the value of y at which the velocity is half the maximum U_{max} , is surprisingly insensitive to U_e/U_{max} as long as the latter does not exceed about one-third. With $R = \pm 10x$ to simulate the logarithmic spiral flow, but without any allowance for normal pressure gradients or extra terms in the (s,n) equation, the values of $d\delta_{.5}/dx$ were 0.085 on a convex surface and 0.065 on a concave surface using Eq(119) with $\beta = 7$ in stabilized regions and $\beta = 4$ in destabilized regions. On a flat surface the calculated $d\delta_{.5}/dx$ was 0.075, agreeing adequately well with experiment. Comparison of the calculated spreading rates for these values of β with the data of Fig.4 suggests that the optimum values of β are 4 in stabilized regions and 3 in destabilized regions ($\alpha = 8$ and 6 respectively). Strictly the original values of β should be used in the wall region on the argument that it is nearer a boundary layer than a jet, but curvature effects on the turbulence in the wall region are negligible. Eq(37) was not used in these calculations: as written, Eq(37) would have an effect even in self-preserving flows but the "time constant" X of jet flows is probably very small and its effects would be noticeable only in cases of sudden change of curvature.

A significant feature of the wall jet calculations was the relative size of the percentage changes in L , mixing length ℓ and eddy viscosity ν_T . The change in $L/\delta_{.5}$ between convex and concave cases was 15 per cent, the change in ℓ/δ was 8.5 per cent and the change in $\nu_T/(U_{max} \delta_{.5})$ was 26 per cent. The departure from the usual rule that ν_T changes twice as much as ℓ and L , valid in boundary layers, is evidently due to variations in profile shape between the different cases. These variations may be exaggerated by deficiencies in the calculation method but are probably real in part (as mentioned on p.54, the dimensionless velocity gradient increases with increasing convex curvature and this is the sense required to explain the comparison between ν_T and ℓ). The implication is that values of α obtained by optimising the behaviour of Eq(36) applied to L would be double those obtained from the application of Eq(36) to ℓ . Another boundary-layer rule, that entrainment velocity is proportional to maximum shear stress, is not very well obeyed: τ_{max} varies more than $\sqrt{\delta_{.5}}$ which is proportional to entrainment velocity if wall stress is neglected. This supports the inference in Section 3 that the size of α in jet flows is underestimated by assuming entrainment proportional to shear stress.

Further analysis of the data and calculations presented in this Appendix will be reported separately.

Some of the sets of input data for the calculations are tabulated below. For full details of input for the method of Ref.16 see NPL Aero Rept. 1269 (1968) and IC Aero Rept. 71-24 (1971). Where no profiles of initial U/U_e ("U") and $\tau/\rho_e U_e^2$ ("TAU") are given, these were generated from the input values of momentum thickness θ , Reynolds number $U_e \theta/\nu$ and $c_f/2$, using the "synthetic starting profile" option: this employs the Coles velocity profile family, with an assumed mixing-length distribution to generate the shear stress profile. The sequence of data input, ignoring the first card indicating the number of cases which is always one as shown here, is

(i) I array (control parameters and counts of points). Only I(5), the number of free-stream velocity and curvature ordinates, and I(6), the number of points on the initial profile, are relevant in general.

TABLE 1 CONDITIONS FOR 10 PER CENT CHANGE IN SHEAR STRESS

* boundary layers or duct flows with a streamline radius of curvature less than about 200-300 times the shear-layer thickness
* wall jets or free jets with a streamline radius of curvature less than about 100 times the shear-layer thickness
* flows in high-aspect-ratio ducts rotating about the major axis at an angular velocity greater than about 0.005 U/h
* boundary layers on axisymmetric bodies, or flow in circular ducts, which rotate about the axis at an angular velocity greater than about 0.003 U/δ
* very large changes occur in any flow with solid-body rotation superimposed on an axial flow.

TABLE 2 REFERENCE TABLE OF BUOYANCY/CURVATURE PARAMETERS
For use in Eq(117) or its first-order version, Eq(36) with $\alpha = 2\beta$

Flow	Ri or ω_{BV}^2	R_f	Recommended* approximation
2-dimensional curved layer	Eq(72)	Eq(79)	Eq(73) or (84)
Rotation about z axis	89	89	89 (last form)
Compressible flow or heat transfer	90	95	98
Coplanar rotation and curvature	99	-	100
Swirling flow [†]	-	102	-
Axisymmetric swirling flow [†]	-	103	108
Infinite swept wing [†]	-	103	109
Compound curvature ^{†§}	-	-	109
Spinning cylinder in axial flow	114	113	115

* $|\overline{uv}|^{1/2}/L$ generally preferable to $\partial U/\partial r$ if different.

† Assume effect of F-factor is on shear stress component in direction of streamline.

§ Take axes to maximise U/r.

Check text for notation used and range of applicability.

TABLE 3 EXPERIMENTS ON LOW-SPEED BOUNDARY LAYERS AND DUCT FLOWS

Date	Author	Ref.	Maximum δ/R	Pressure Gradient	c_f	$\tau(y)$	Turbulence
- boundary layers on two-dimensional curved surfaces -							
1930	Wilcken	22	- 0.2	$\sim z$	from τ	from U	-
1936	Schmidbauer	83	+ 0.04	$f \rightarrow a$	from U ?	-	-
1937	Clauser	93	$\pm .015$	z	-	-	(u^1 only)
1950	Schubauer & Klebanoff	101	+ 0.02	a	log law	Hot wire results suspect	
1962	Tani	102		$\sim z$		-	-
1968	Patel B.L.	37, 162	± 0.06	$\sim z$	-	-	-
	Patel cyl.	37	+ 0.03	f	fn (R_0, H)	-	-
1972	So & Mellor	160	$\pm .13$	z, a	from τ	Hot wire measurements	
1973	Meroney	164	$\pm .01$	$\sim z$	surface tube	" "	"
1973	Young	57	+0.2, -0.1	$\sim z$	" "	" "	"
- curved or rotating ducts -							
1935	Wattendorf	82	± 0.05	-	surface tube	from p.g.	-
1956	Eskinazi & Yeh	98	± 0.05	-	from p.g.	from p.g.	
1967-1972	Johnston & co-workers	10	± 0.1	-	log law	from p.g.	flow viz.
- boundary layers in swirling flow, or in axial flow over rotating cylinders -							
1963	Parr	166	+ 0.1*	z	-	-	-
1967	Mackrodt	133	-	$\sim z$	-	-	-
1971	Hughes	165	range	z, a	-	from U	-
1972	Nakamura	167, 299	+ 0.2*	z, a, f	-	-	-
- curved rotating duct -							
1968	Anders	169	$\pm ?$	a	surface tube	-	-
1972	Litvai	170	$\pm ?$	a	-	-	-

Key: a = adverse, f = favourable, z = nominally zero. For rotating ducts δ/R becomes $\frac{1}{2}h\Omega/\bar{U}$. For rotating bodies in axial flow and for the curved rotating duct, both curvature and rotation are important. *Figure given is $\delta/(\text{cross-section radius})$.

TABLE 4 EXPERIMENTS ON HIGH-SPEED BOUNDARY LAYERS

Date	Author	Ref.	Maximum δ/R	Pressure Gradient	Mach no.	Remarks
1962	Kepler & O'Brien	183	-0.06	a	3 \rightarrow 2	
1962	McLafferty & Barber	184	-0.04	a	3 \rightarrow 2	Low $Re_0, \approx 2500$ for most detailed case
1964	Clutter & Kaups	185	$-\infty, -0.02$	a	1.6, 2.6, 3.3, 4.5	Bodies of revolution with flares - strongly divergent axisymmetric
1968	Thomann	4	± 0.02	z	2.5	Heat transfer measurements only
1968	Winter, Rotta & Smith		-	a, f	0.6, 1.4, 2.0	Waisted body of revolution: c_f from surface tube may be unreliable
1971	Sturek & Danberg	*	-0.03	a	3.5 \rightarrow 3	c_f from Preston tube

For Key see Table 3.

Several other experiments have been reported, but in insufficient detail to be useful as test cases. Of the "two-dimensional" cases above, only Sturek and Danberg measured c_f ; Thomann measured St but not temperature profiles. Therefore there is no proper check on two-dimensionality except in Sturek and Danberg's flow which appeared to be slightly converging; other flows may be three-dimensional in either sense.

* Sturek, W.B. and Danberg, J.E., AIAA paper 71-162 and Univ. of Delaware DMAE Rept. 141, 1971.

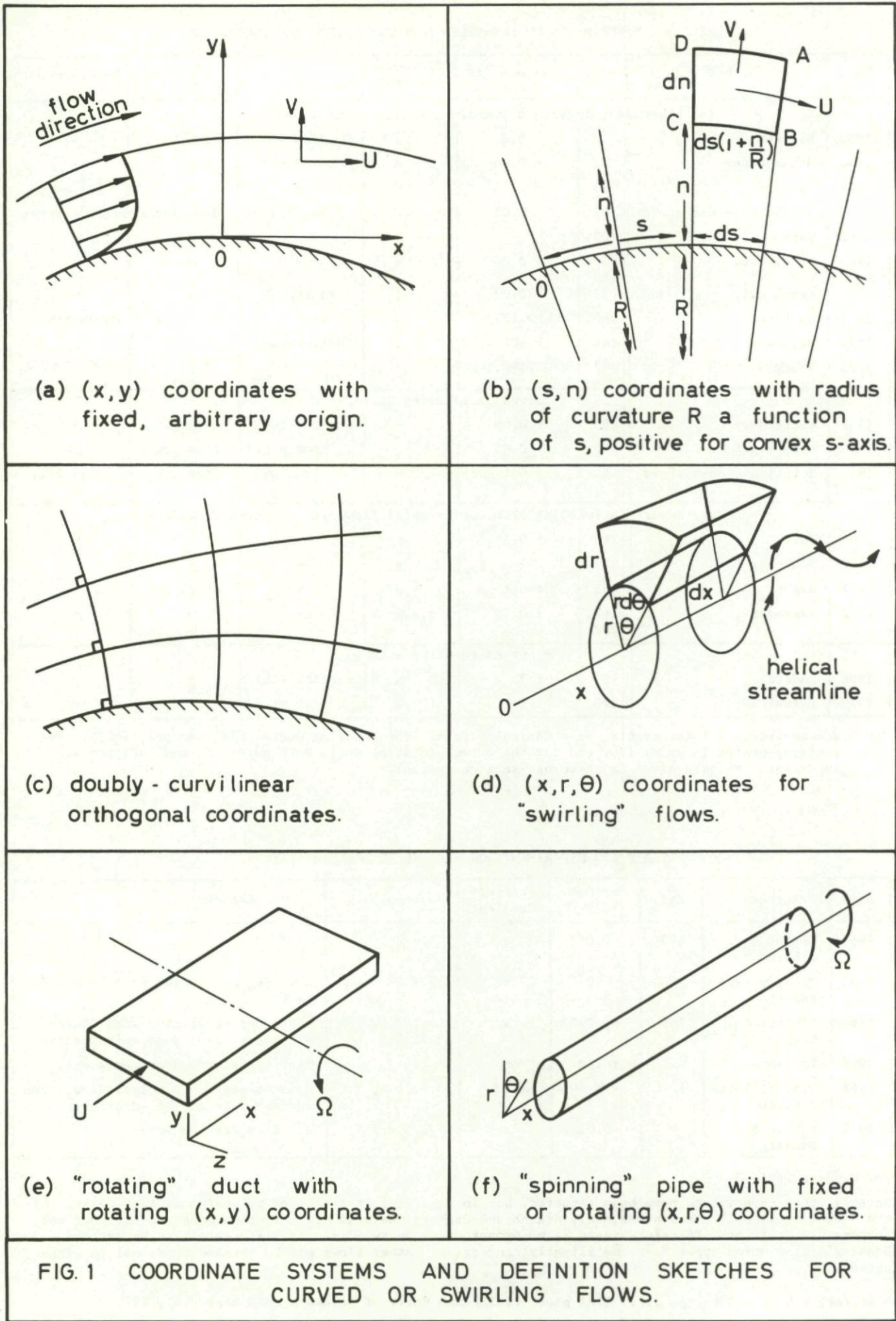


FIG. 1 COORDINATE SYSTEMS AND DEFINITION SKETCHES FOR CURVED OR SWIRLING FLOWS.

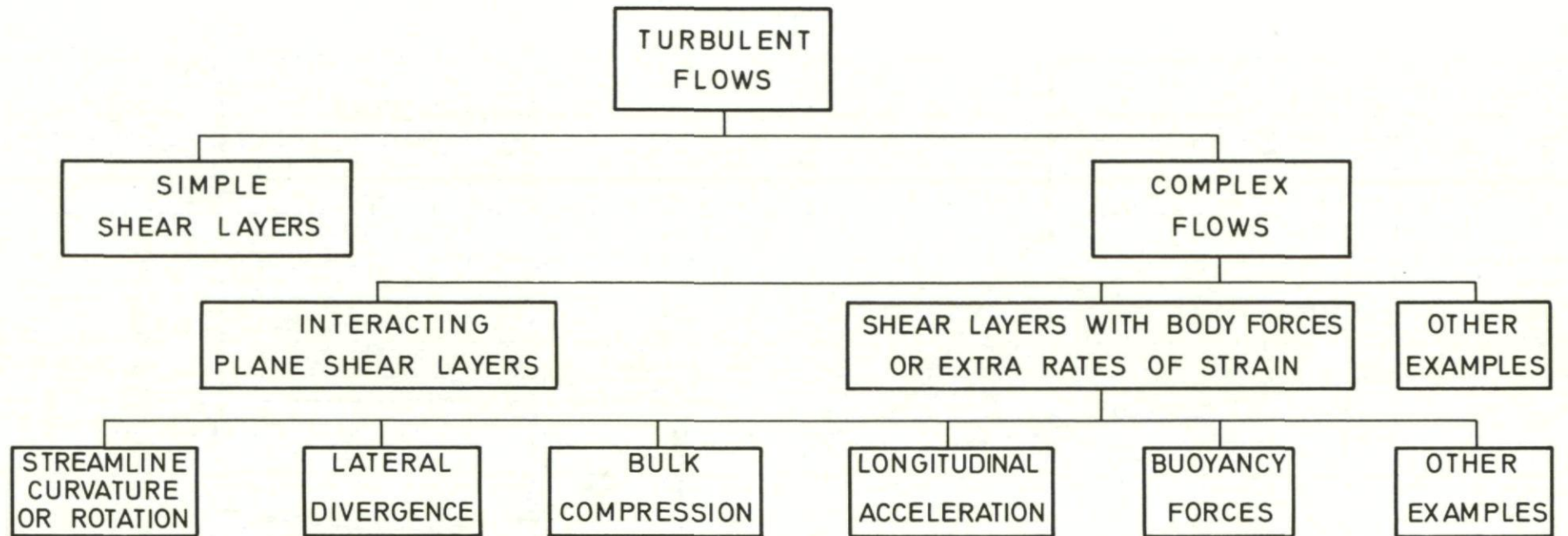


FIG. 2 SUGGESTED CLASSIFICATION OF TURBULENT FLOWS.

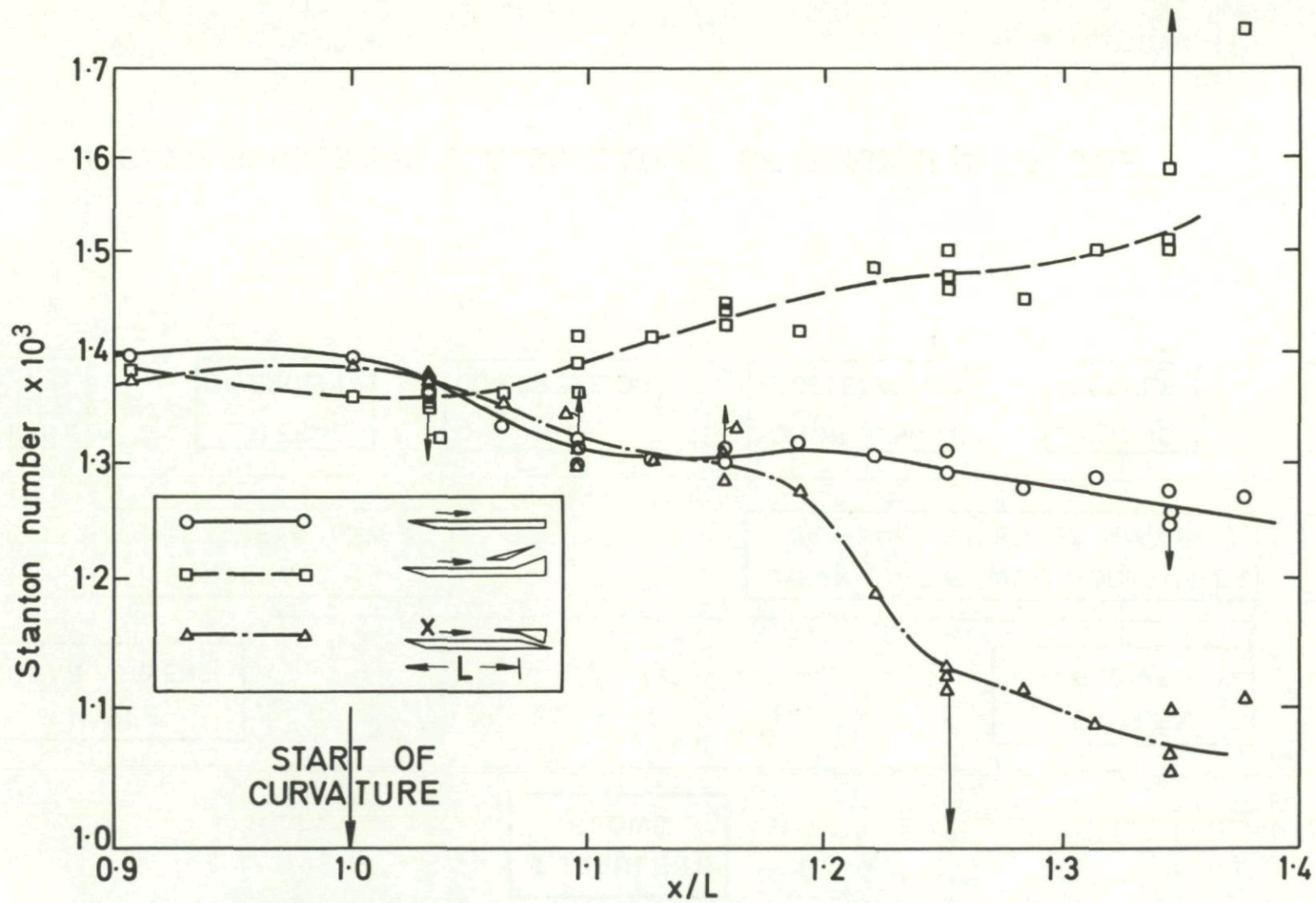
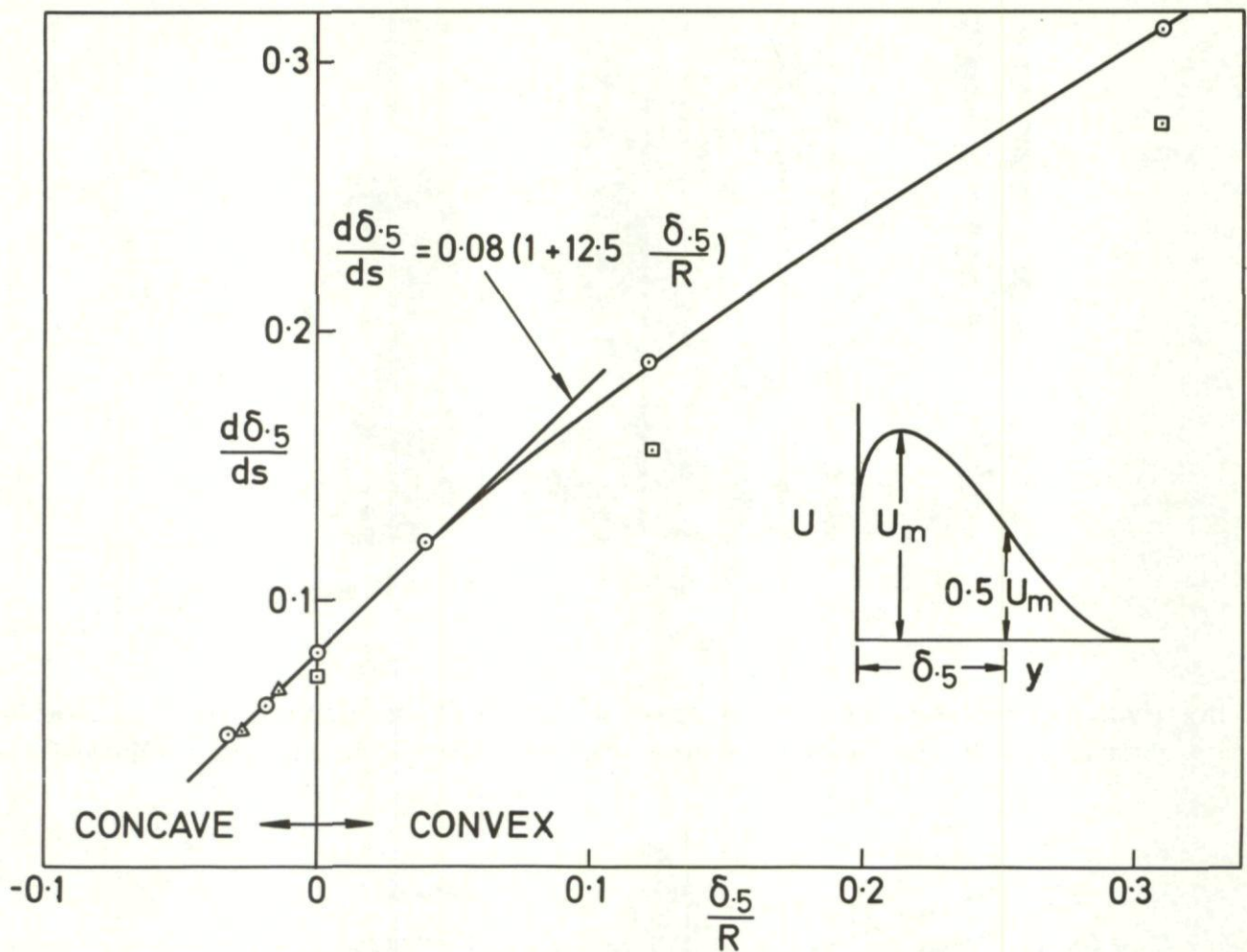
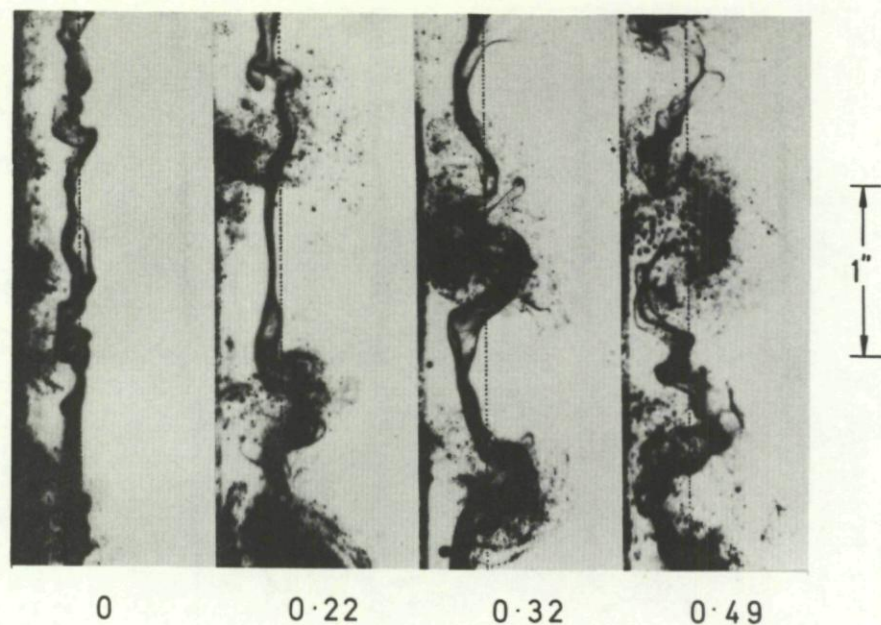
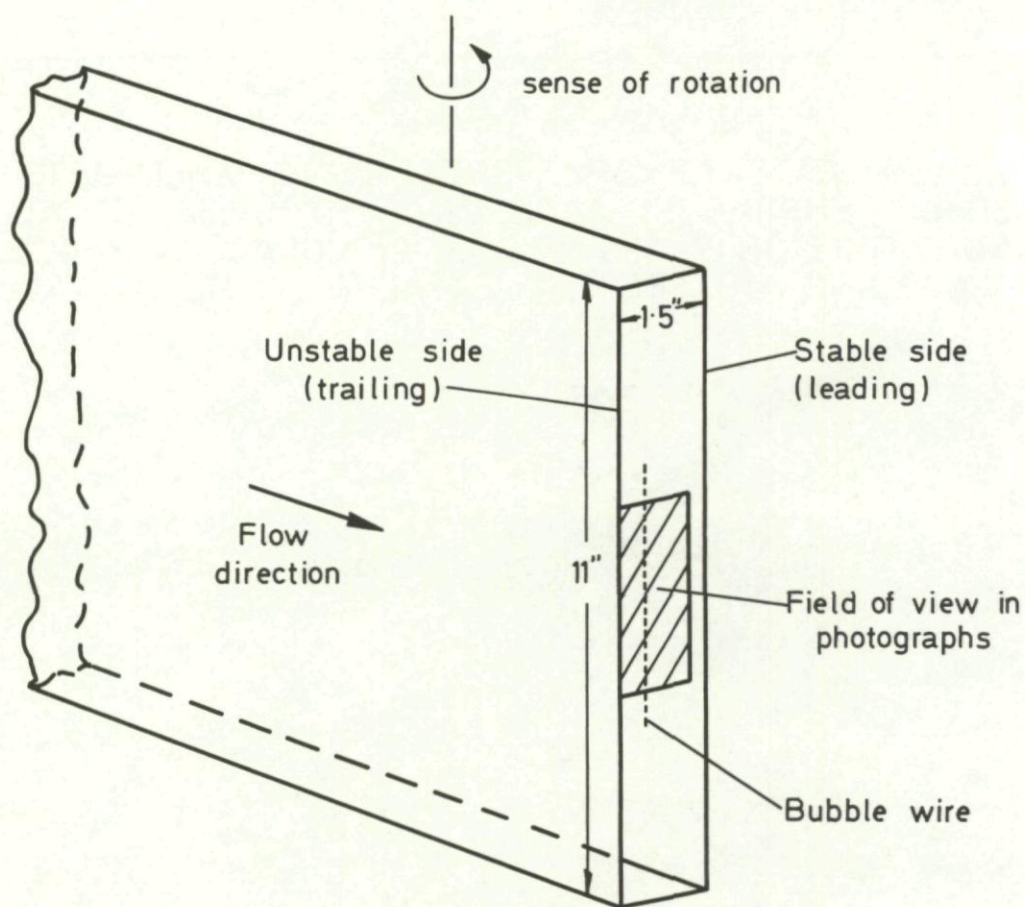


FIG. 3 STANTON NUMBER (DIMENSIONLESS SURFACE HEAT TRANSFER COEFFICIENT) IN CONSTANT-PRESSURE SUPERSONIC BOUNDARY LAYER ON CONCAVE, PLANE AND CONVEX WALLS (AFTER THOMANN (4)).



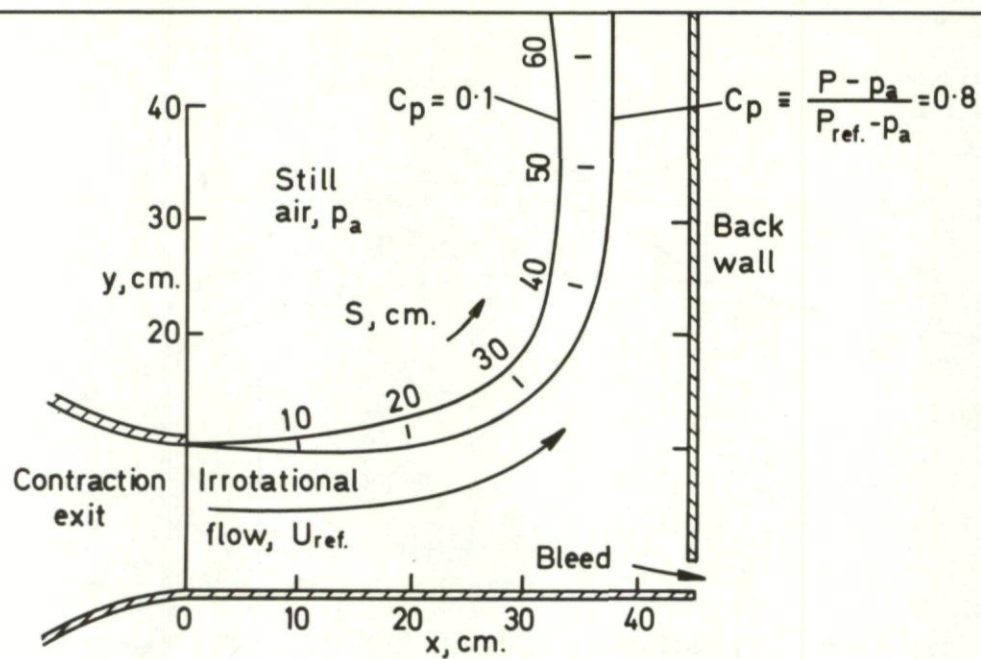


(a) Hydrogen bubble pictures: values of $\Omega h/\bar{U}$ shown. Dotted line indicates position of bubble wire. Larger bubbles have erupted from sublayer.



(b) Duct configuration showing field of view.

FIG. 6 LONGITUDINAL VORTICES IN ROTATING DUCT FLOW
(JOHNSTON ET AL (10)).



(a) Arrangement of test rig.

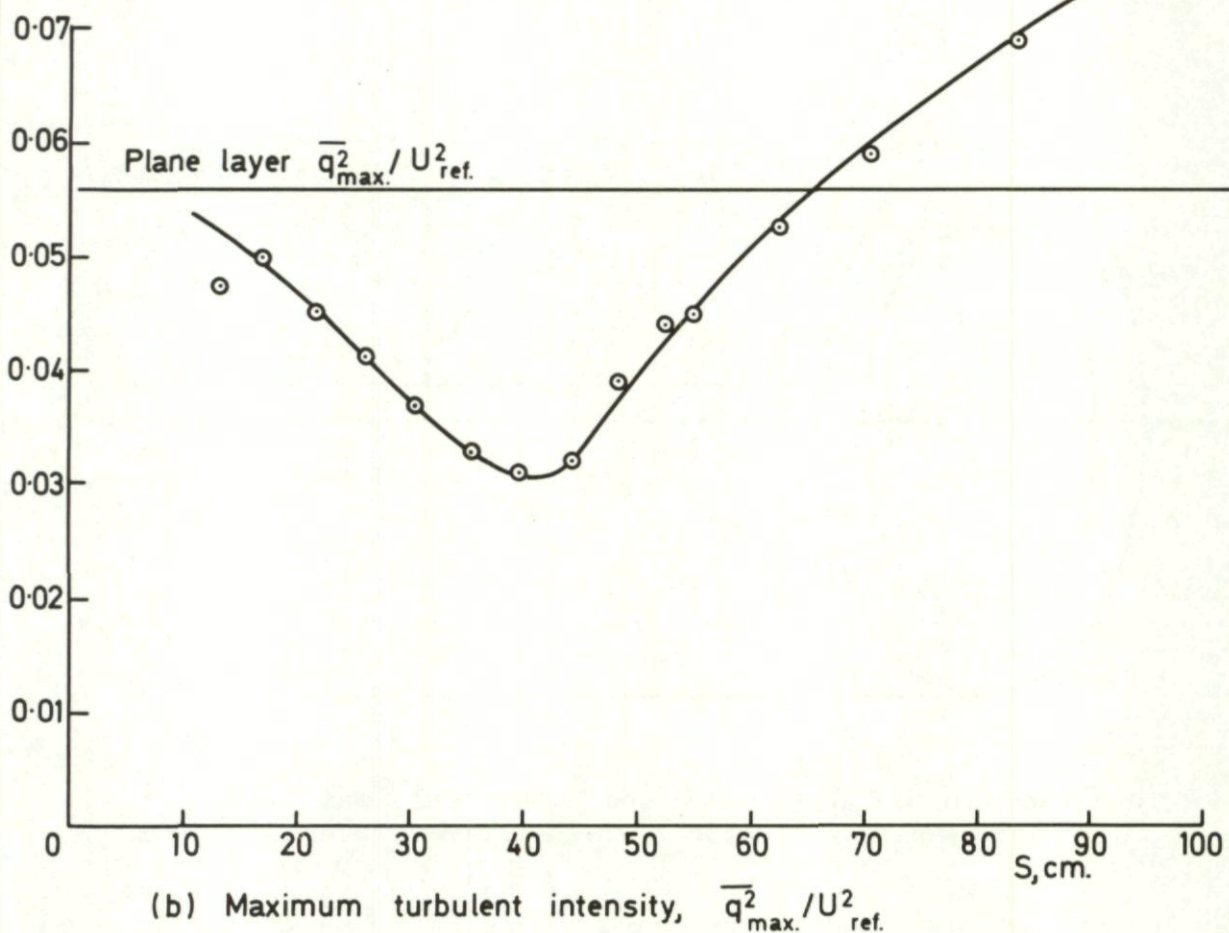
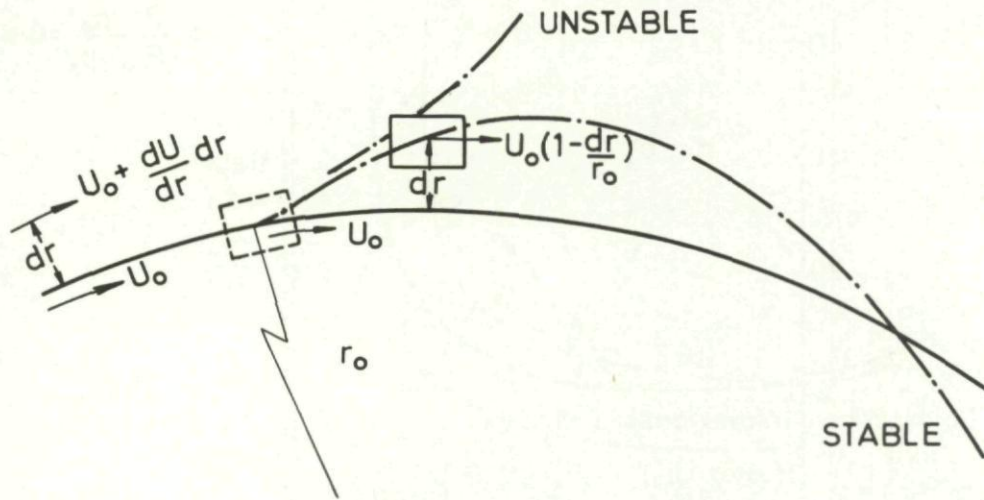
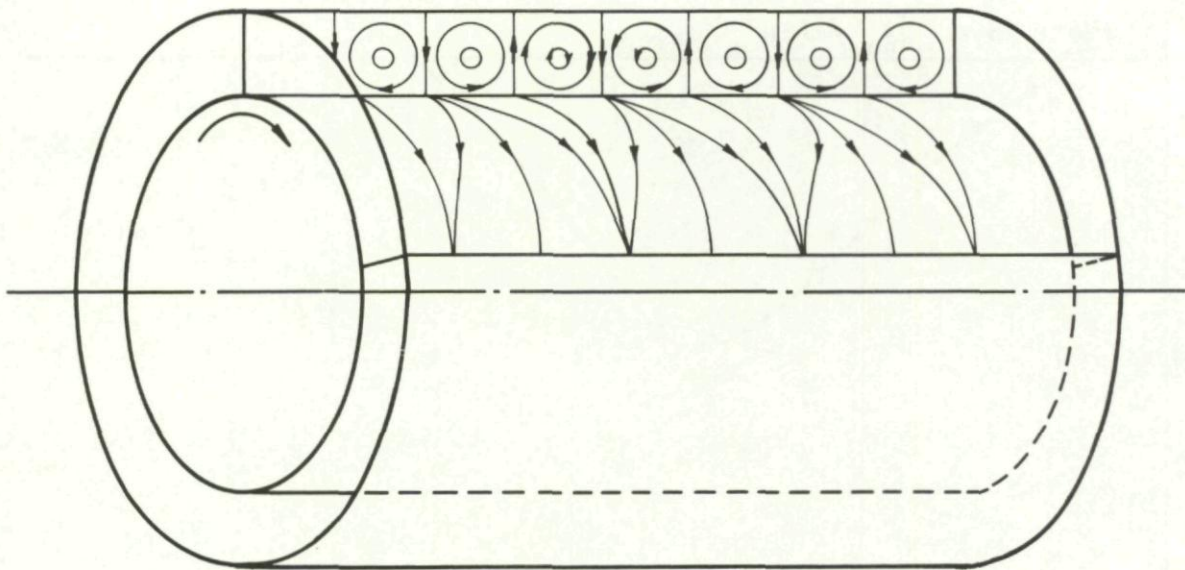


FIG. 7 REDUCTION AND OVERSHOOT OF TURBULENT INTENSITY IN STABLY-CURVED MIXING LAYER (11).

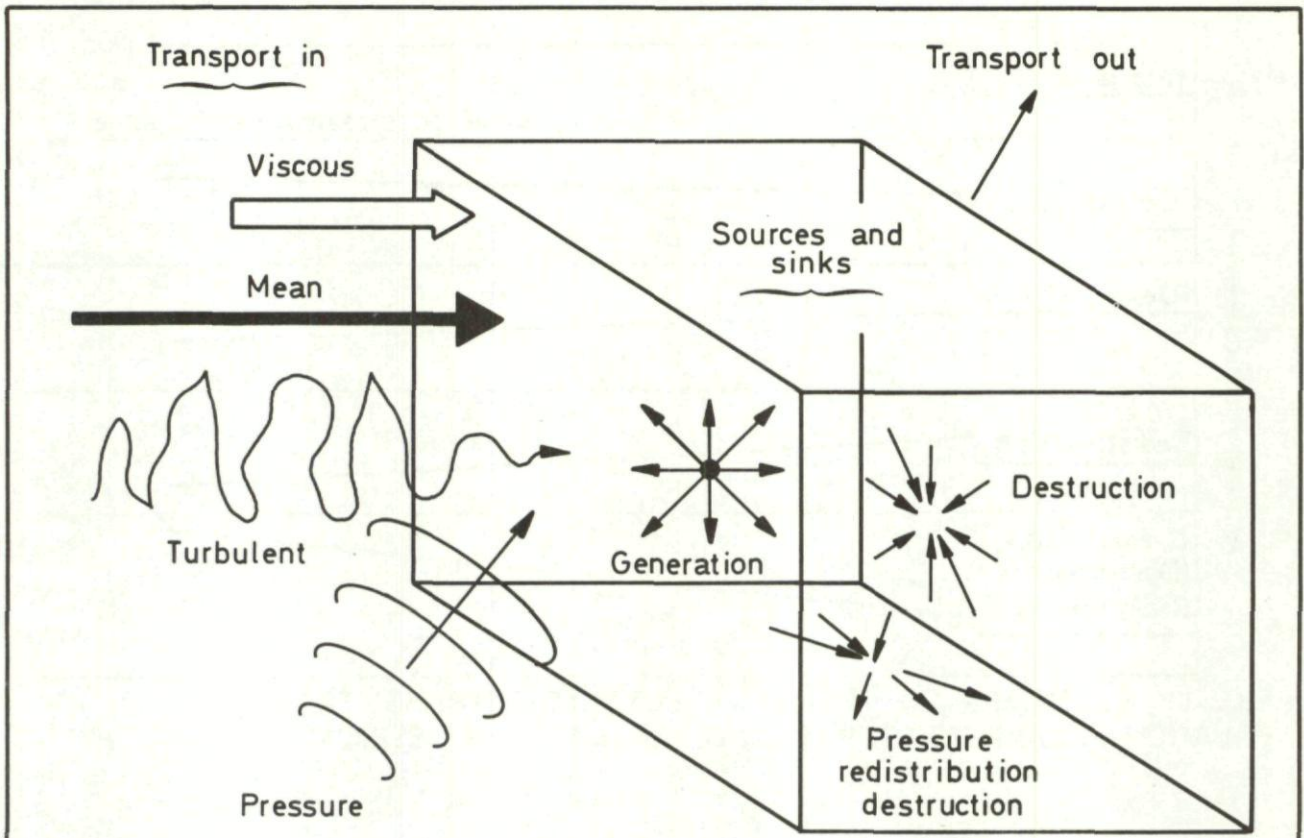


(a) Motion of displaced element in a curved flow.

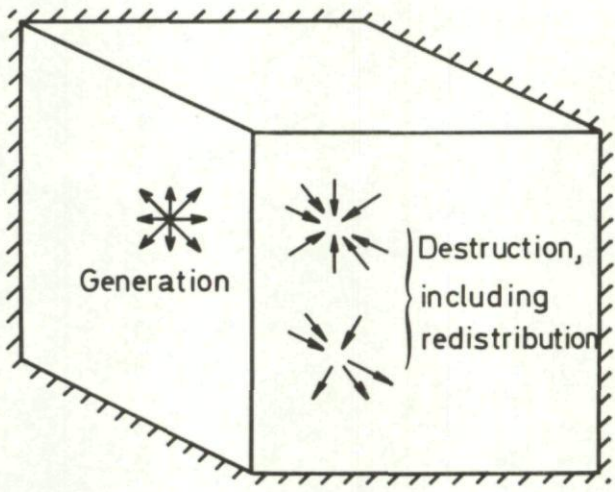


(b) Cross-sectional "streamlines" and streamlines near surface in contra-rotating toroidal vortices between circular cylinders.

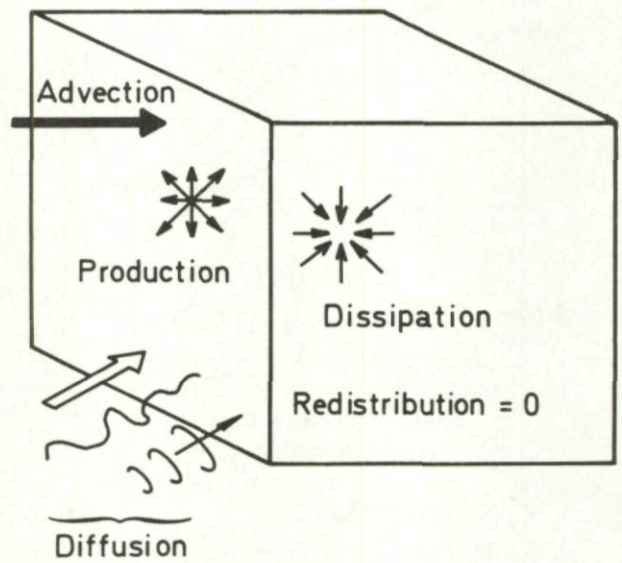
FIG. 8 IDEALIZED AND REAL EXAMPLES OF UNSTABLE CURVED FLOWS.



(a) Processes represented by transport equations for turbulence quantities.



(b) Local equilibrium.



(c) Nomenclature for turbulent energy equation.

FIG. 9 TRANSPORT EQUATIONS.

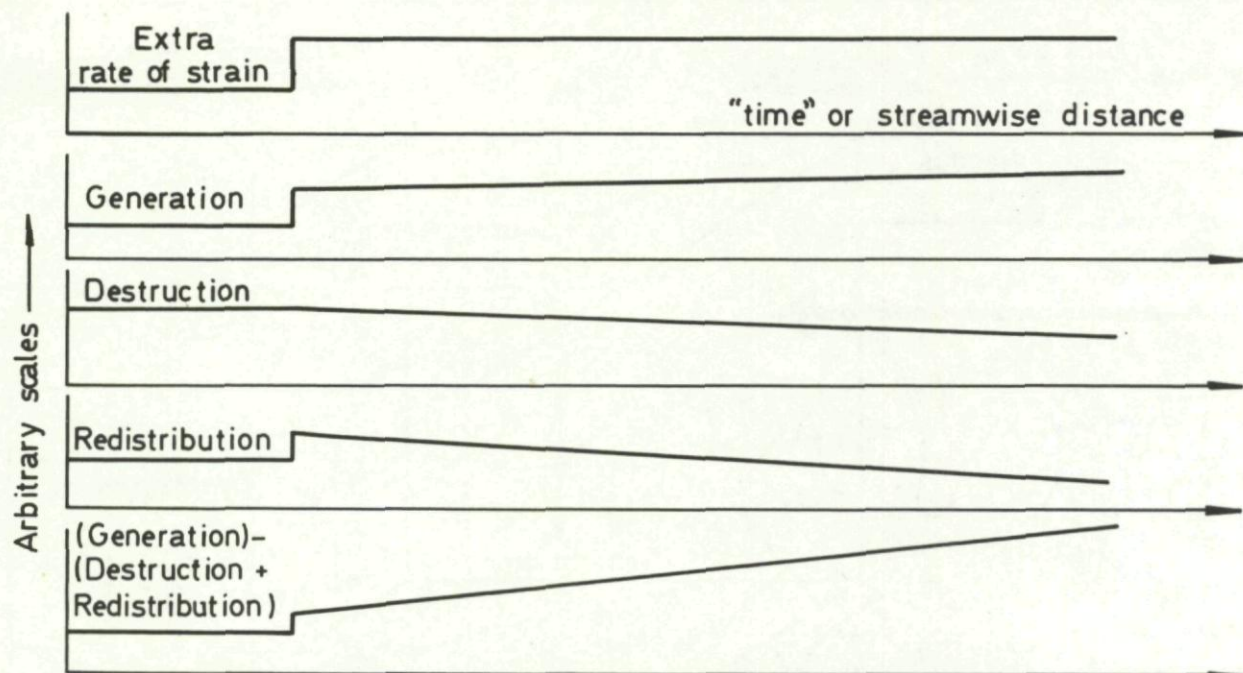


FIG. 10 RESPONSE OF TERMS IN REYNOLDS-STRESS TRANSPORT EQUATION (FIG. 9) TO STEP CHANGE IN RATE OF STRAIN.

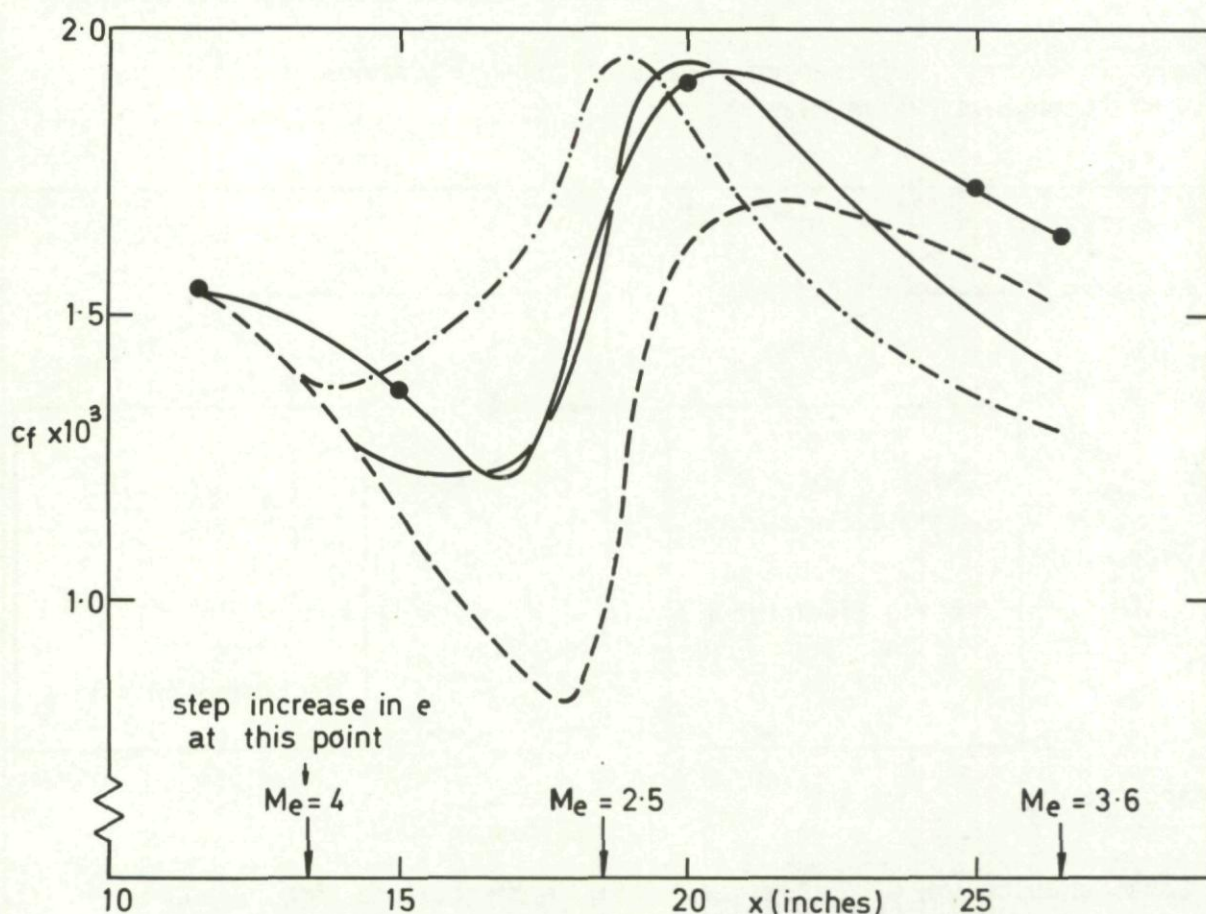


FIG. 11 RETARDED-ACCELERATED SUPERSONIC BOUNDARY LAYER (66)
 —●—, MEAN LINE THROUGH MEASUREMENTS. ---, CALCULATION (16)
 WITHOUT DILATATION CORRECTION. - · - ·, CALCULATION USING EQ (36)
 WITH $e = -\text{div } \underline{U}$, $\alpha = 10$. —, CALCULATION USING EQ (36) AND EQ (37)
 WITH "TIME CONSTANT" OF 10δ .

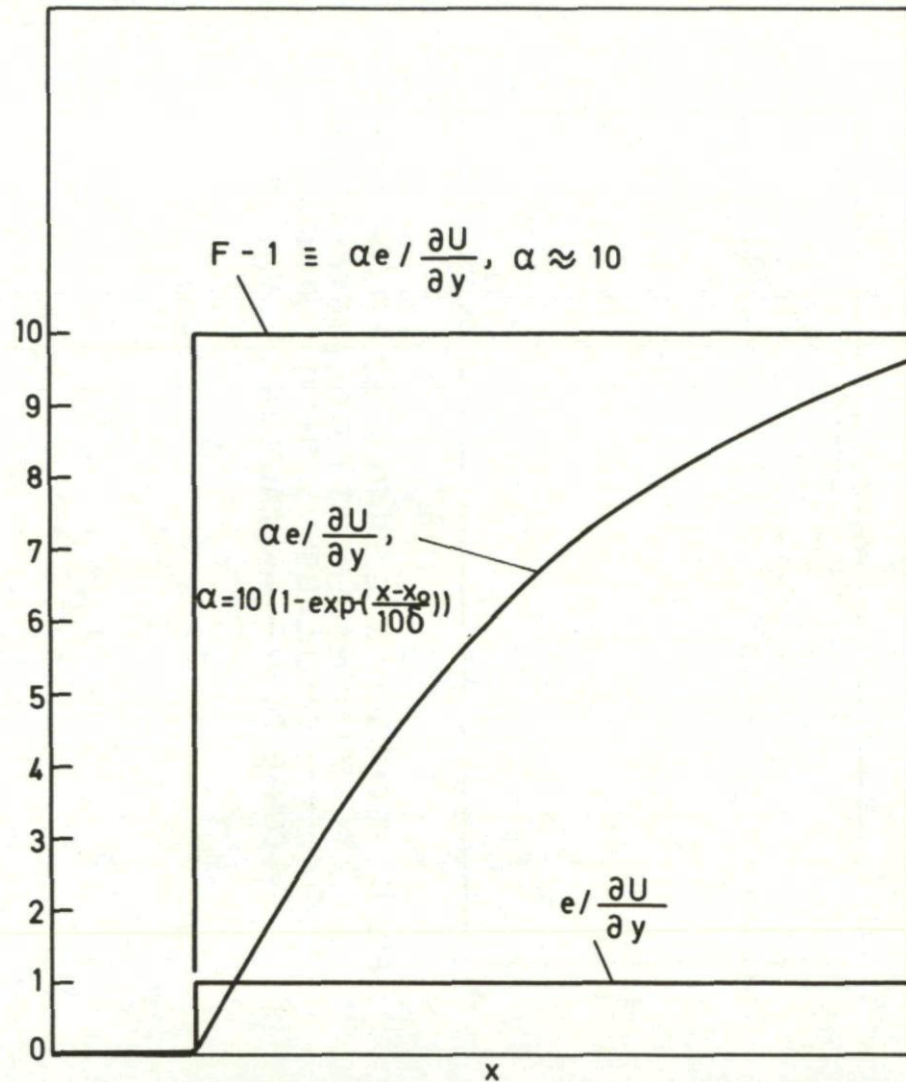


FIG. 12 RESPONSE OF F-FACTOR AND LAGGED F-FACTOR TO A STEP CHANGE IN EXTRA STRAIN RATE e .

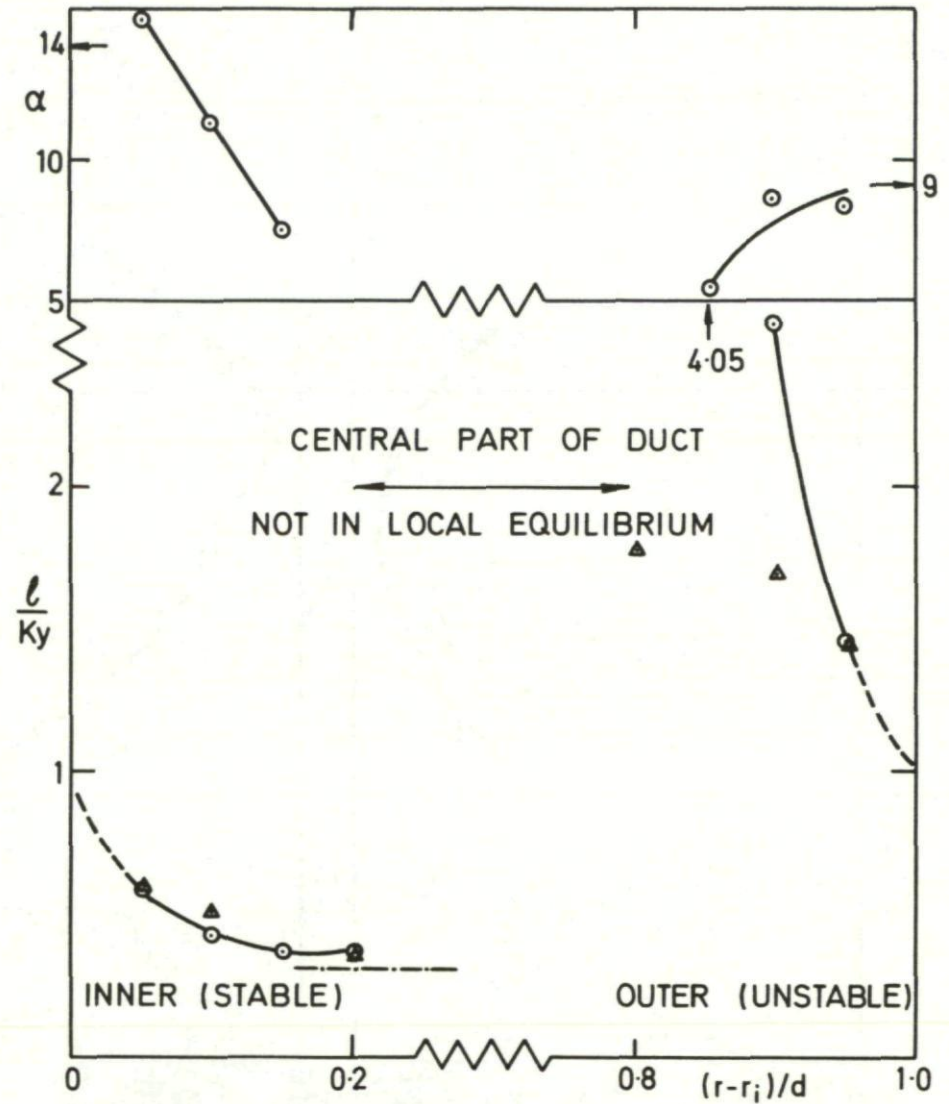


FIG. 13 MIXING LENGTH AND " α " FACTOR NEAR THE WALLS OF A CURVED DUCT: DATA OF ESKINAZI AND YEH (\odot) AND WATTENDORF (\blacktriangle). LIMITING VALUES OF α FROM BUOYANCY ANALOGY SHOWN \rightarrow ; LIMITING ℓ/Ky FROM EQ (129) SHOWN \dashrightarrow .

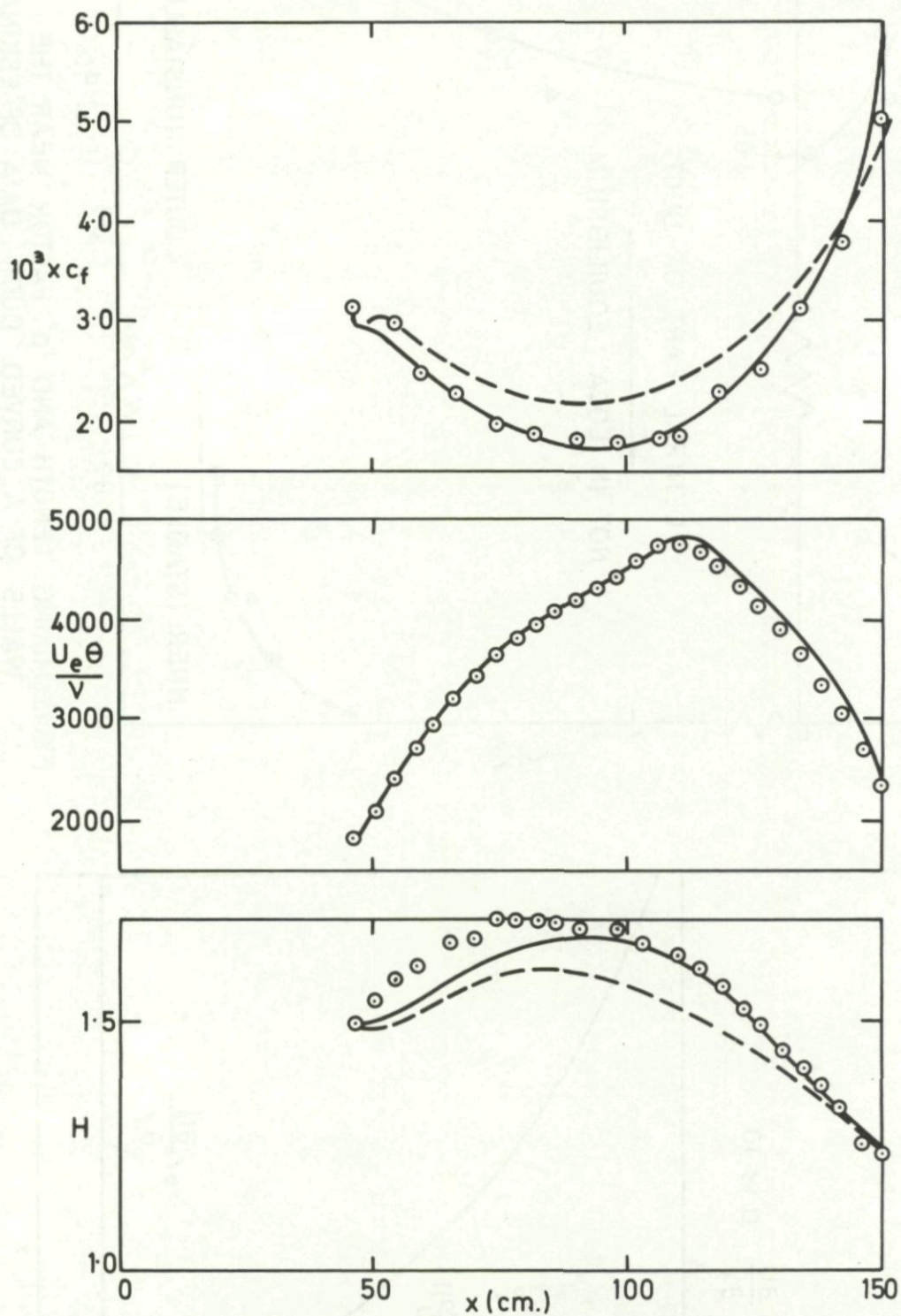
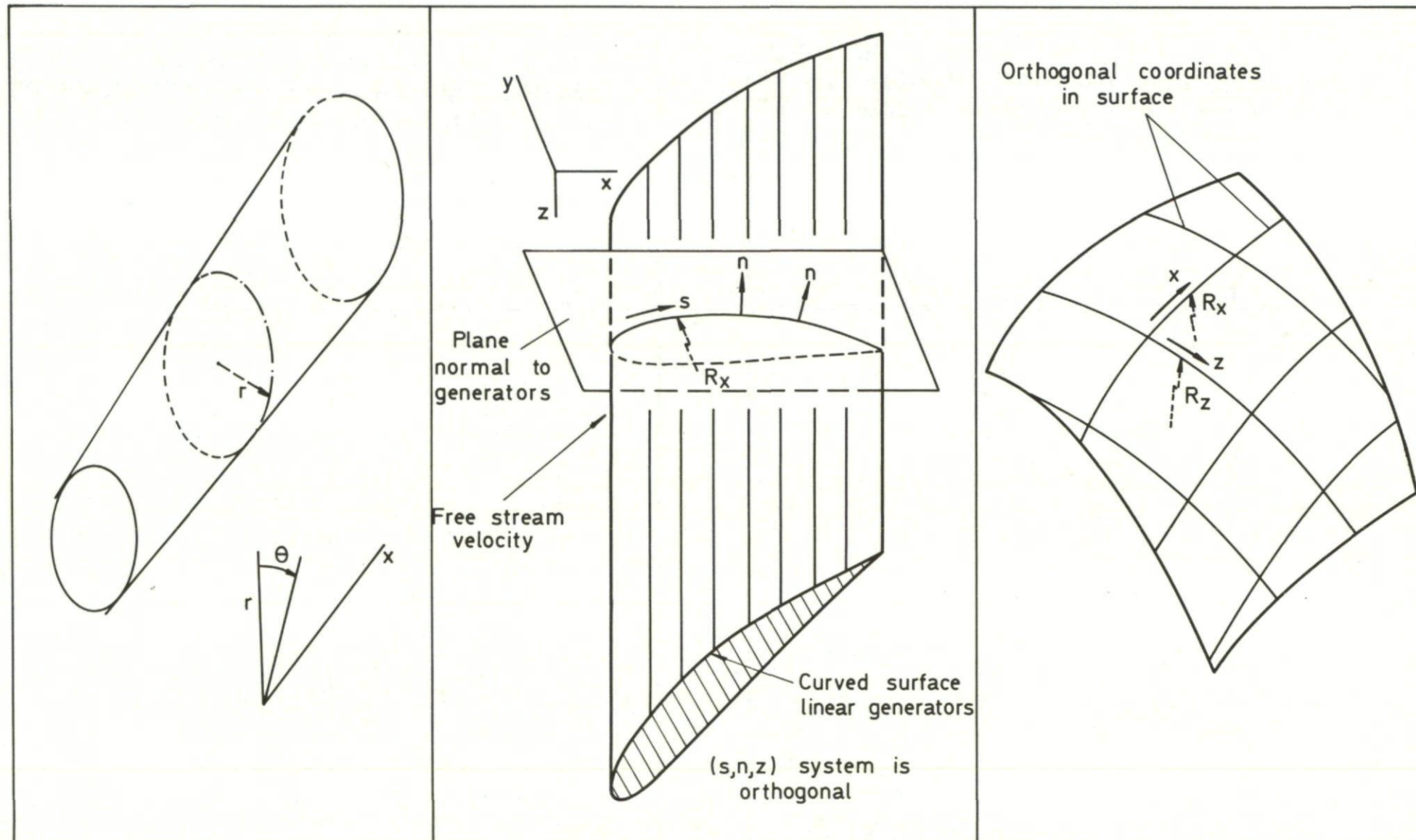


FIG. 14 RETARDED-ACCELERATED BOUNDARY LAYER OF SCHMIDBAUER (83: FIG. 6). \circ : EXPERIMENT
 ---: CALCULATION WITHOUT CURVATURE CORRECTION. —: CALCULATION WITH $\alpha = 14$.



(a) Slowly-growing axis-symmetric swirling flow.

(b) Boundary layer on "infinite" swept wing.

(c) Boundary layer with compound curvature.

FIG. 15 THREE - DIMENSIONAL CURVED FLOWS.

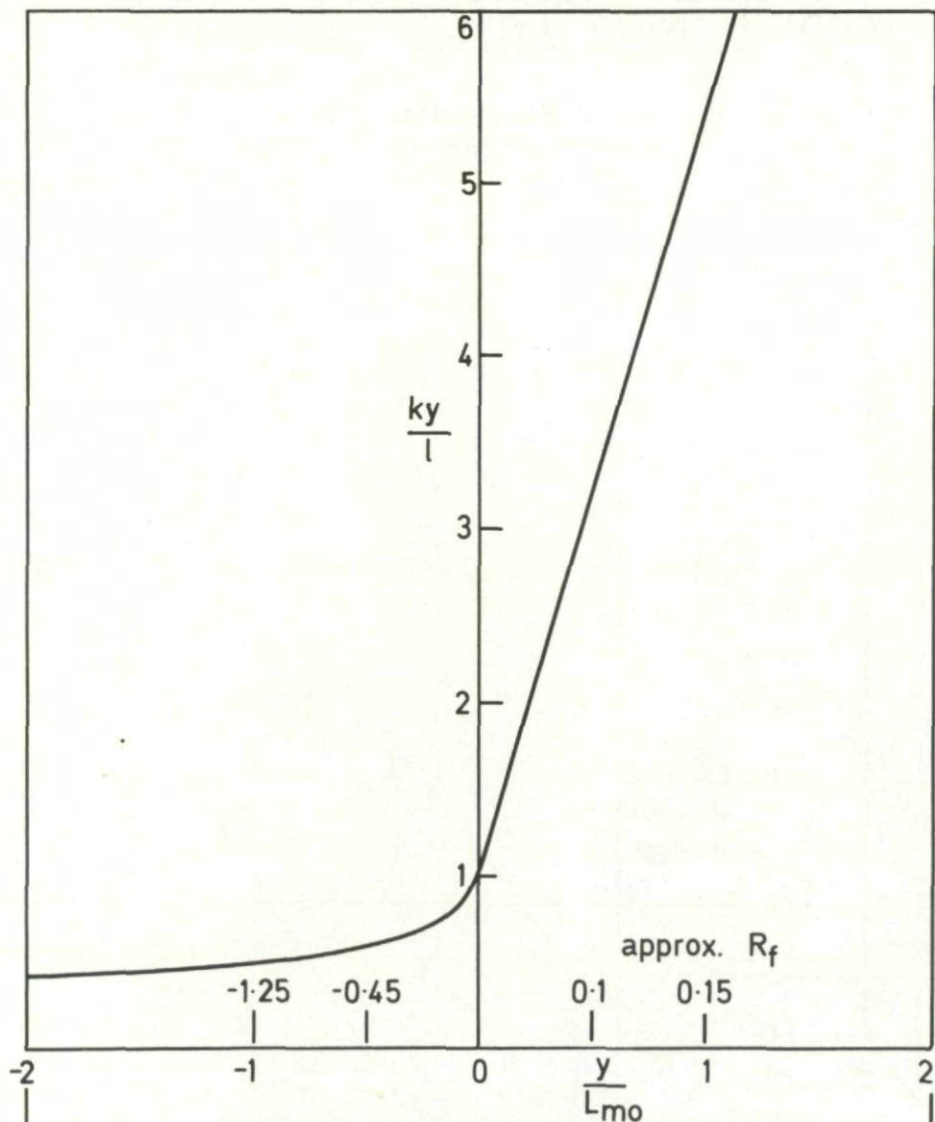


FIG. 16 VARIATION OF APPARENT MIXING LENGTH WITH BUOYANCY PARAMETER IN ATMOSPHERIC INNER LAYER. (CONSENSUS OF SEVERAL AUTHORS.)

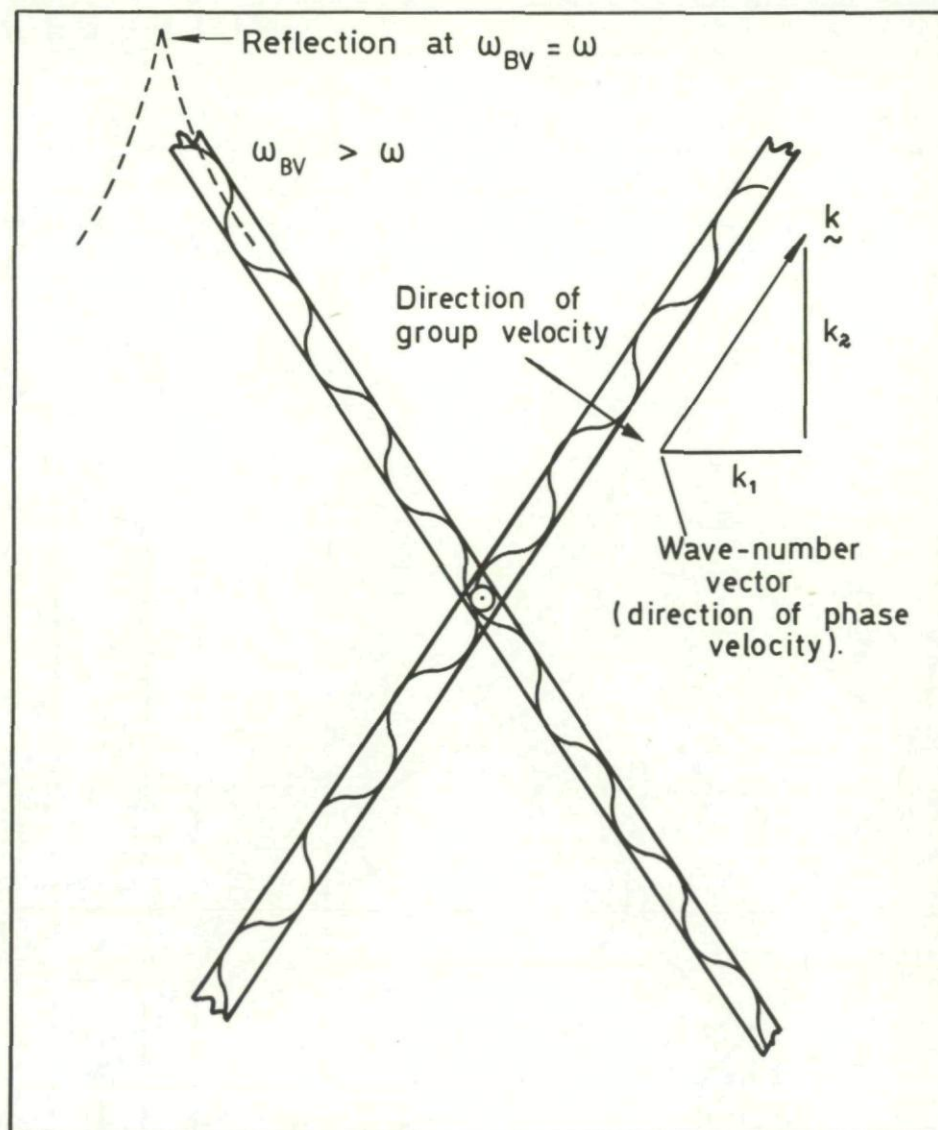
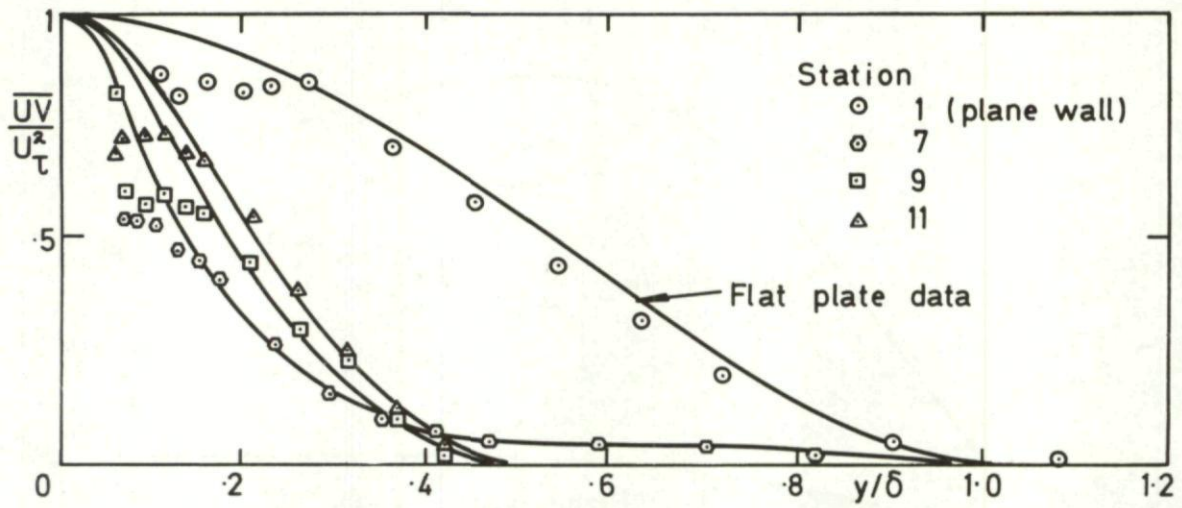
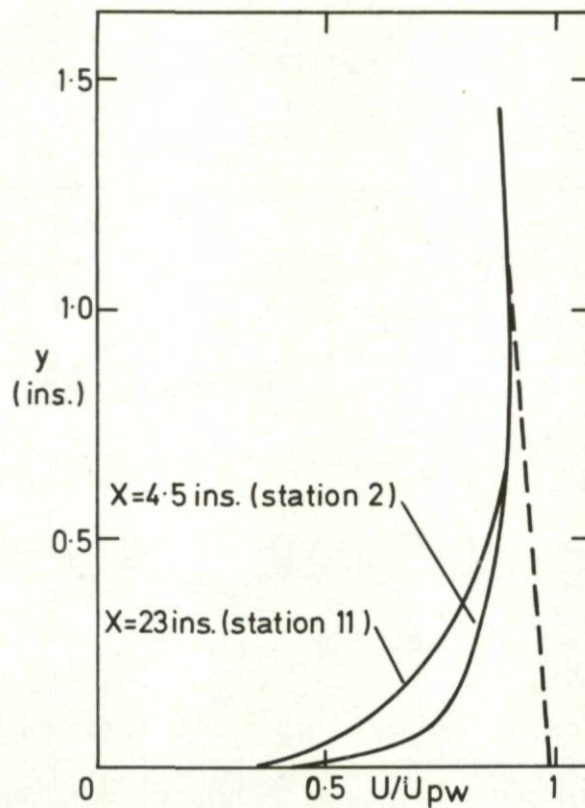


FIG. 17 GENERAL CONFIGURATION OF INTERNAL WAVES FROM A POINT SOURCE IN A STABLY-STRATIFIED FLUID.



(a) Distribution of shearing stress for constant pressure flow along convex wall, $\delta/R \approx 0.08$.



(b) Growth of internal boundary layer on convex wall. X measured from start of curvature: $R \approx 12.8$ inches.

FIG. 18 COLLAPSE OF TURBULENCE IN OUTER REGION OF HIGHLY-STABLE BOUNDARY LAYER (160).

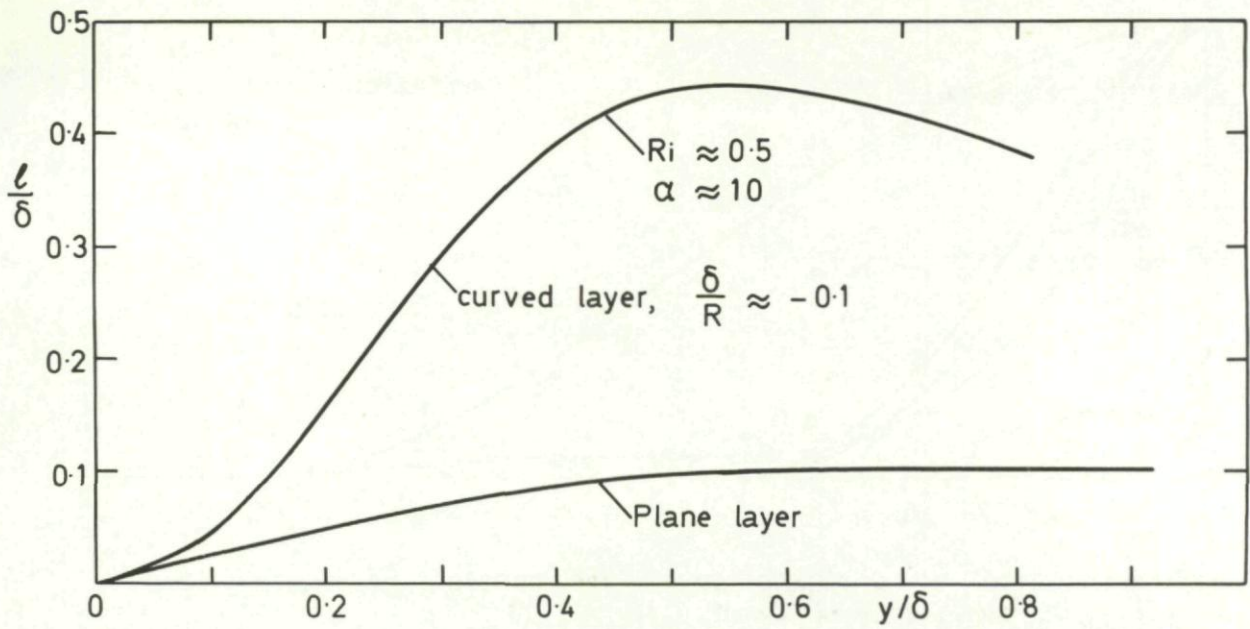


FIG. 19 MIXING LENGTH AND "α" FACTOR IN A HIGHLY CURVED BOUNDARY LAYER : DATA OF WILCKEN (22)

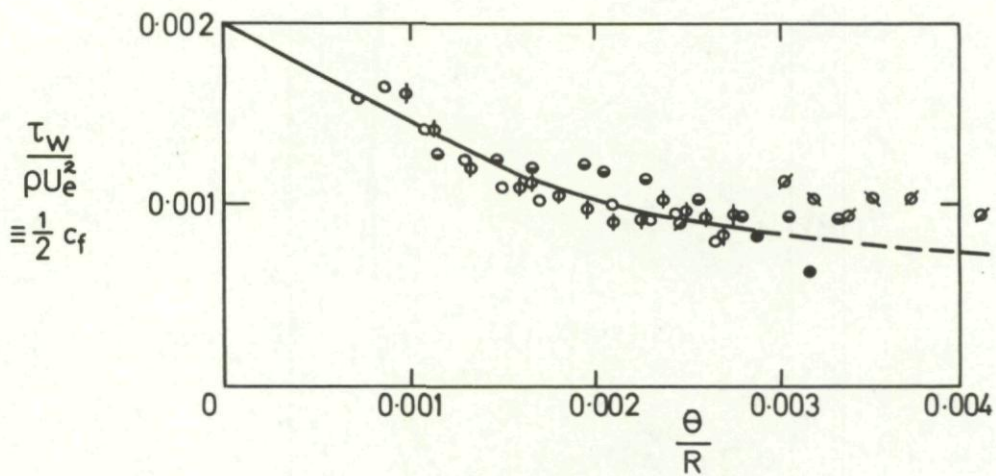


FIG. 20 DEPENDENCE OF SKIN FRICTION COEFFICIENT ON CURVATURE ACCORDING TO SCHMIDBAUER (83: FIG. 4) THE GENERAL TREND IS CORRECT BUT THE VARIATION APPEARS TO BE OVERESTIMATED.

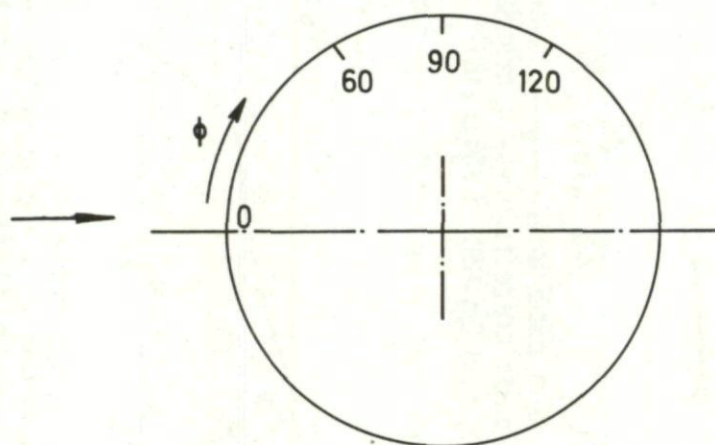
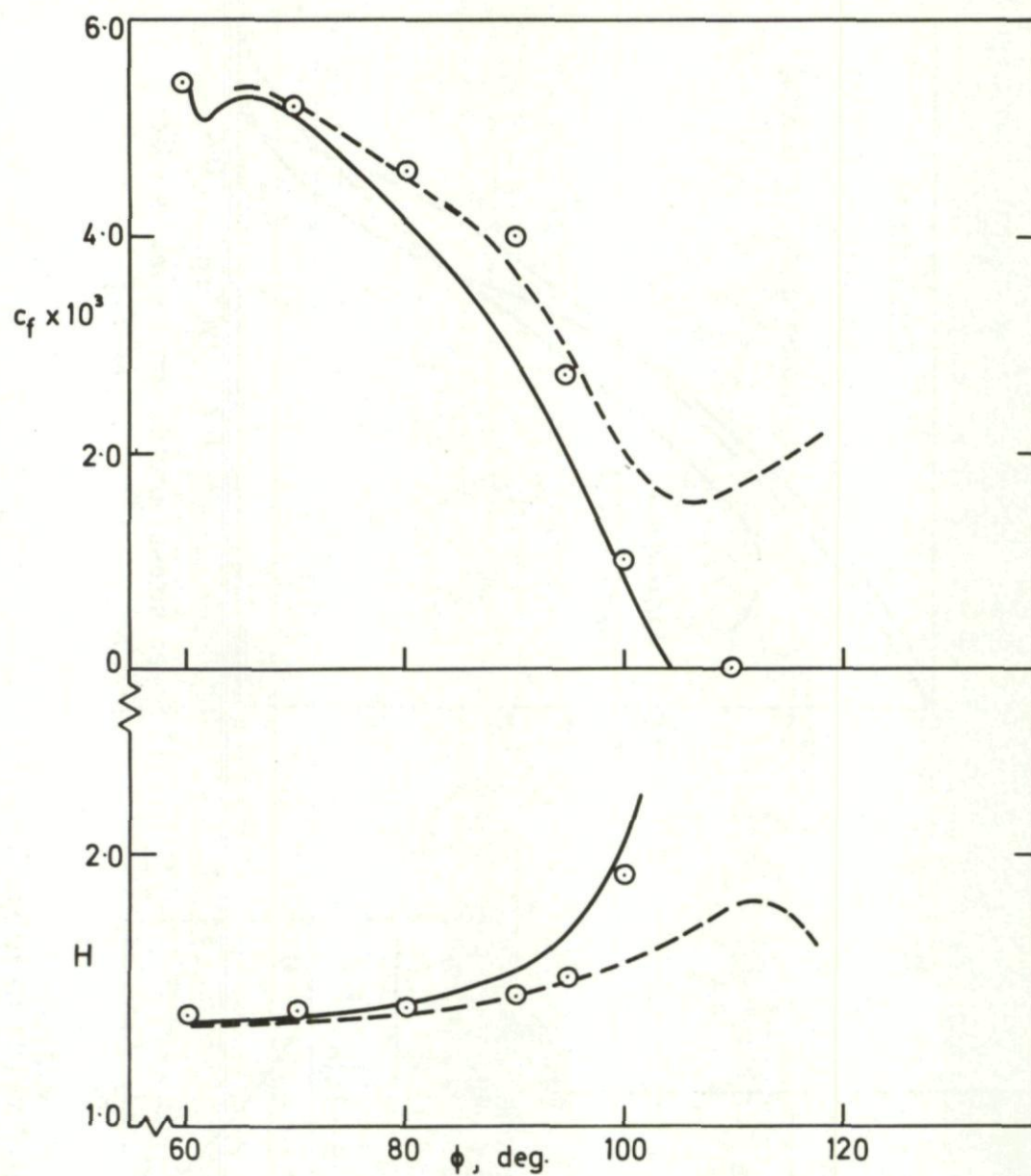
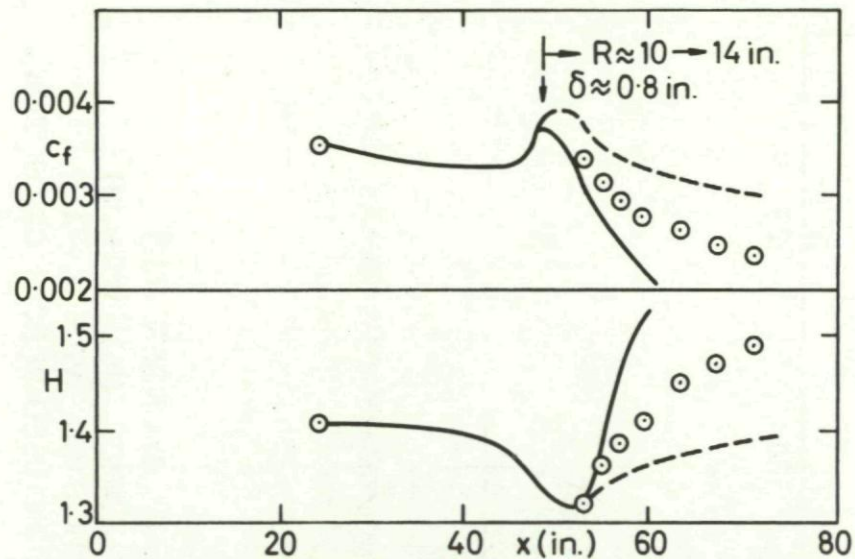
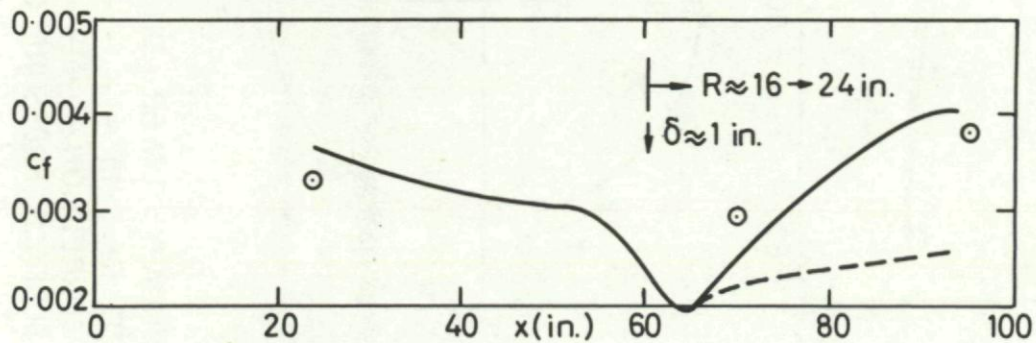


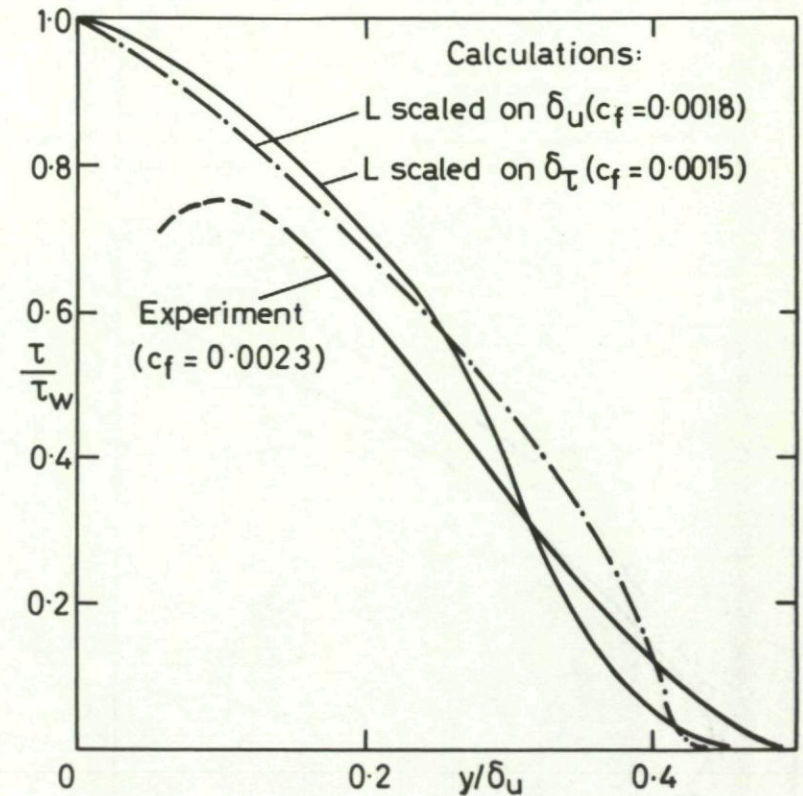
FIG. 21 BOUNDARY LAYER ON CIRCULAR CYLINDER (37).
 ○ EXPERIMENT, $Re=5 \times 10^5$. — — — —, CALCULATION (16) WITHOUT CURVATURE CORRECTION. — — — —, CALCULATION WITH $\alpha = 14$.
 MEASURED SURFACE PRESSURE DISTRIBUTION USED IN BOTH CALCULATIONS.



(a) Convex surface. \circ , experiment. ---, calculation without curvature correction. —, calculation with Eq (37), $X = 10\delta$, and Eq (119), $\beta = 7$ ($\alpha = 14$).



(b) Concave surface. \circ , experiment. ---, calculation without curvature correction. —, calculation with Eq (37), $X = 10\delta$, and Eq (119), $\beta = 4$ ($\alpha = 8$). At $x = 96$, $\theta_{\max} = 227$, $\theta_{\min} = -113$.



(c) Shear stress profile on convex surface station 11 ($x = 71$ in.): see Fig. 18 (a).

FIG. 22 EXPERIMENTS OF SO AND MELLOR (160) ON CONCAVE AND CONVEX SURFACES. (SEE ALSO FIG. 18).

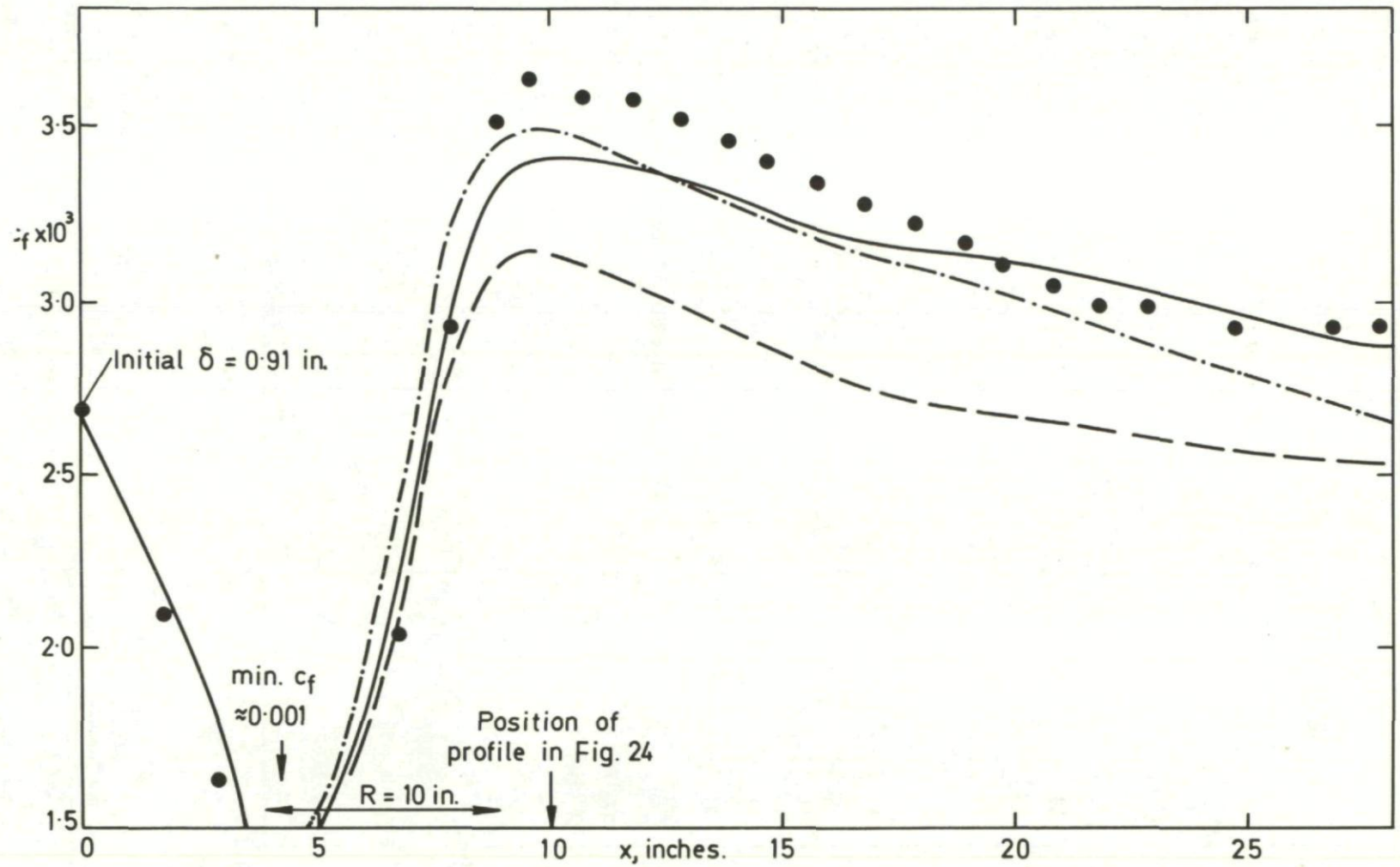


FIG. 23 BOUNDARY LAYER WITH "CONCAVE CURVATURE IMPULSE" (DURATION ABOUT 10δ) DATA OF YOUNG (57): FOR CONFIGURATION SEE FIG. 24. ●, EXPERIMENT.— — —, CALCULATION (16) WITHOUT CURVATURE CORRECTION.— · — ·, CALCULATION USING EQ.(117) WITH $\alpha = 9$. — — —, CALCULATION USING EQ.(117) AND EQ.(37) WITH "TIME CONSTANT" OF 10δ .

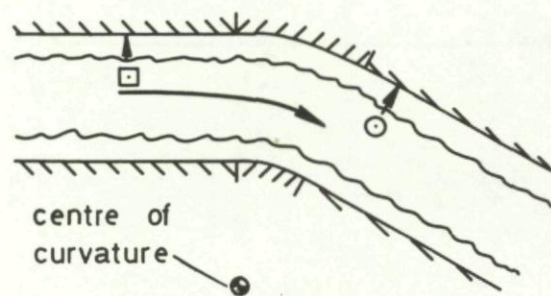
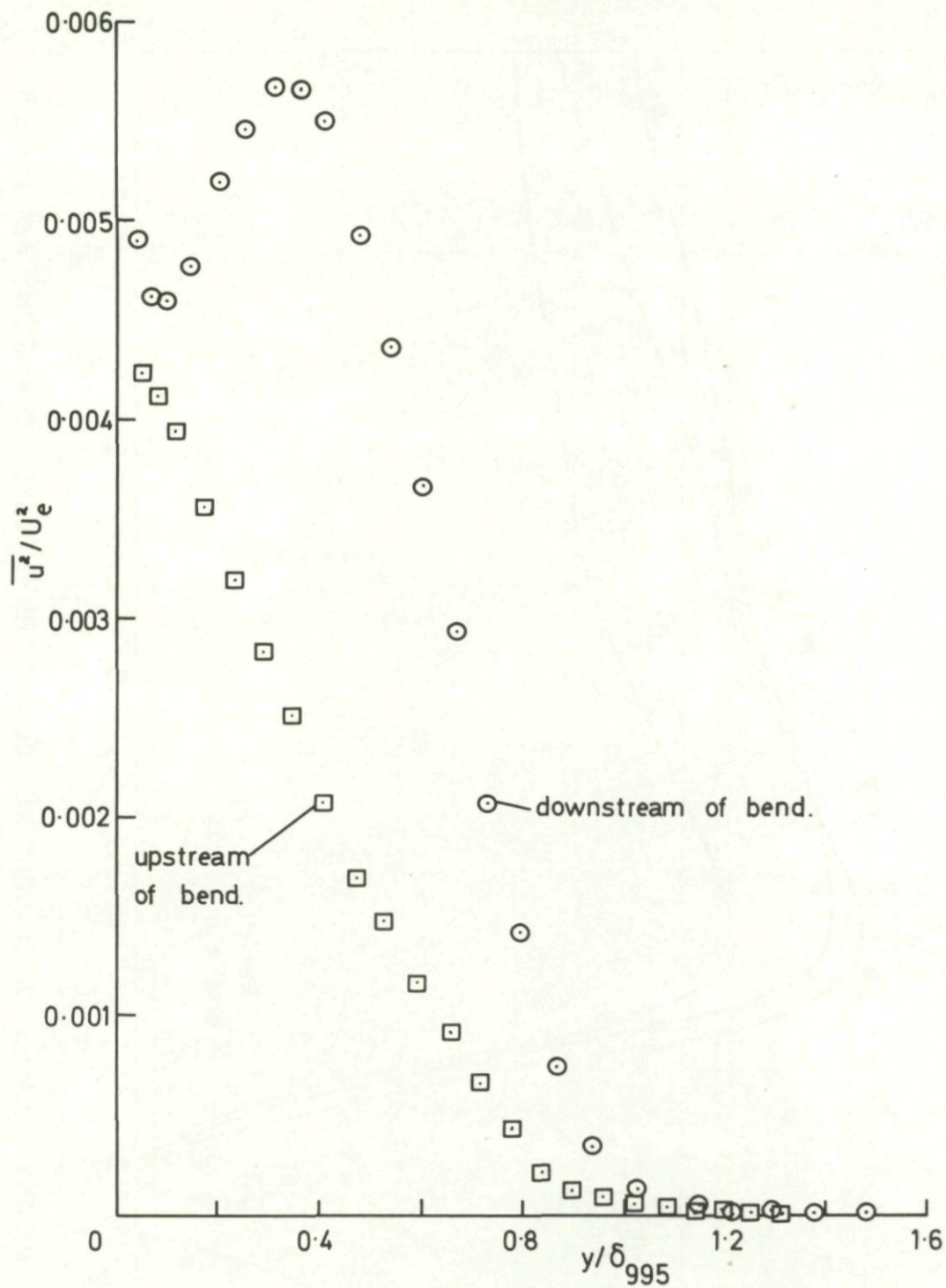
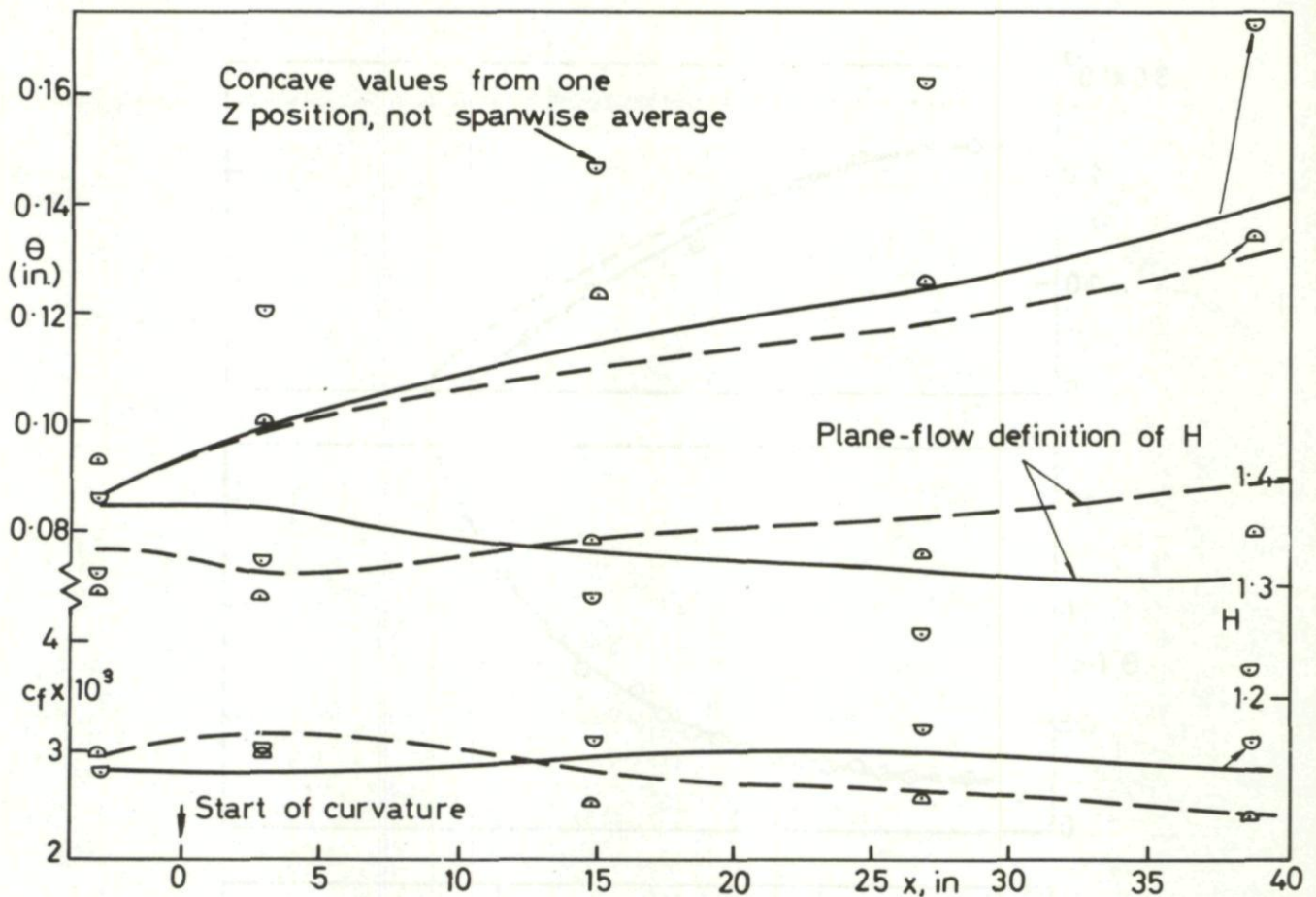
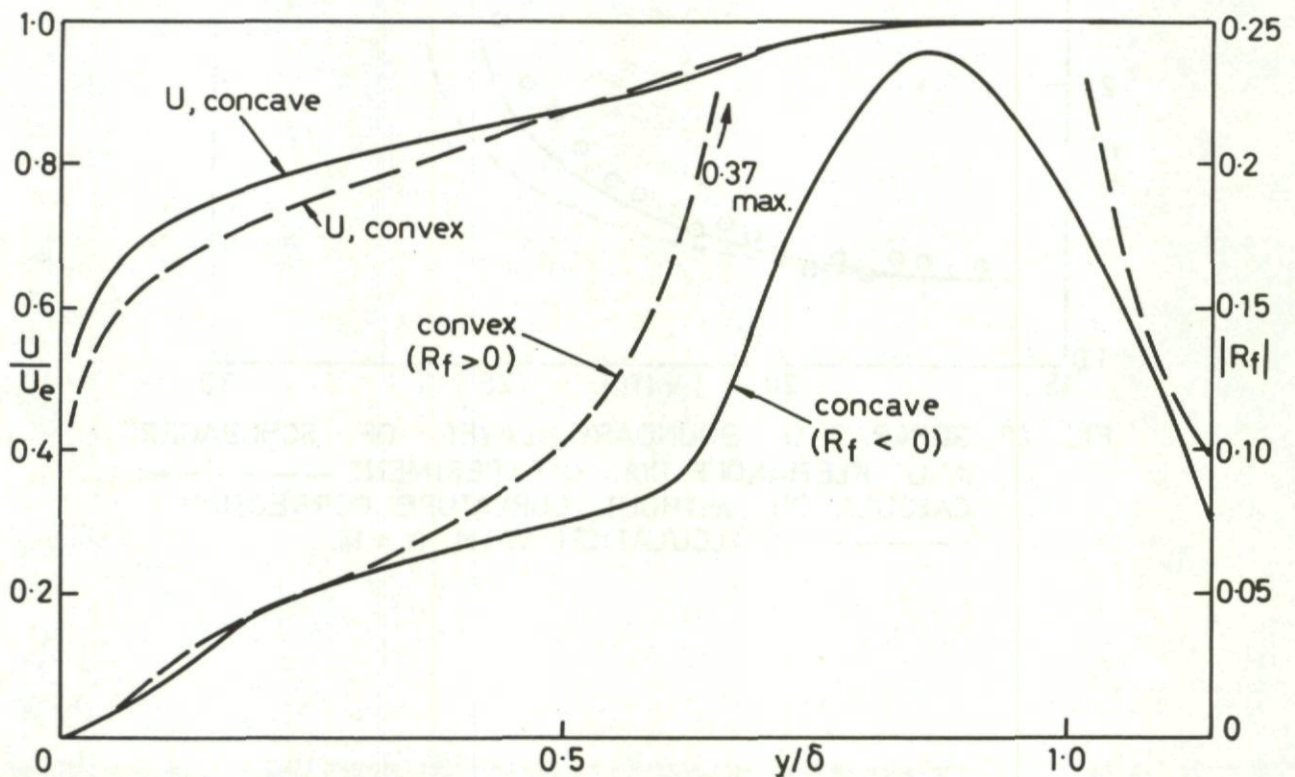


FIG. 24 u -COMPONENT INTENSITY IN UNSTABLY-CURVED BOUNDARY LAYER, $\delta/R = -0.1$ (57): SEE FIG. 23.



(a) Provisional results for integral parameters



(b) Calculated velocity and flux Richardson number at $x = 42$ in.

FIG. 25 EXPERIMENTS OF MERONEY (164) ON CONCAVE AND CONVEX SURFACES. \triangle (CONVEX) AND \circ (CONCAVE), EXPERIMENT. —, CALCULATION USING EQ (37) WITH $X=10\delta$ AND EQ(119) WITH $\beta=7(\alpha=14)$ CONVEX, $\beta=4(\alpha=8)$ CONCAVE.

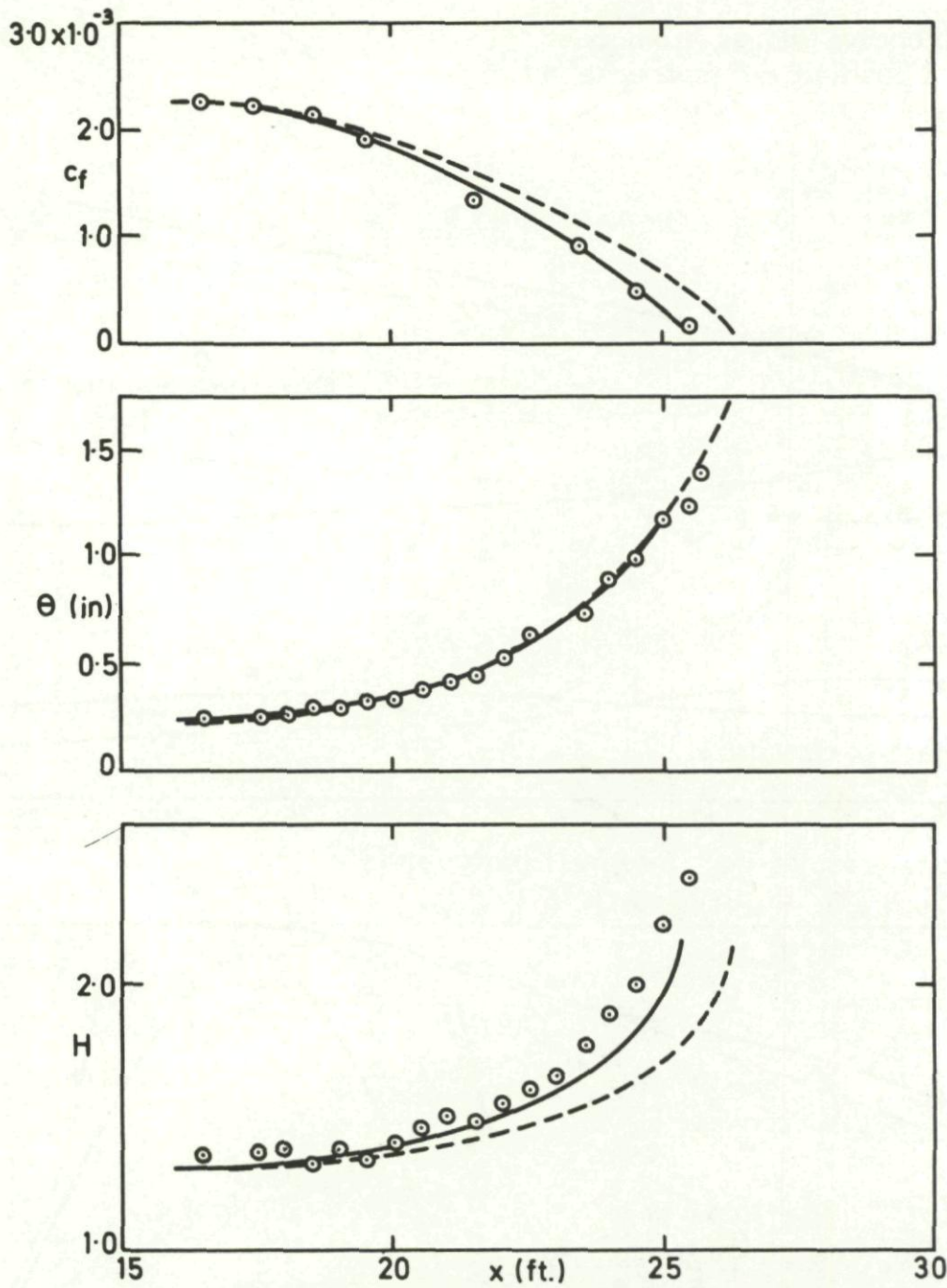
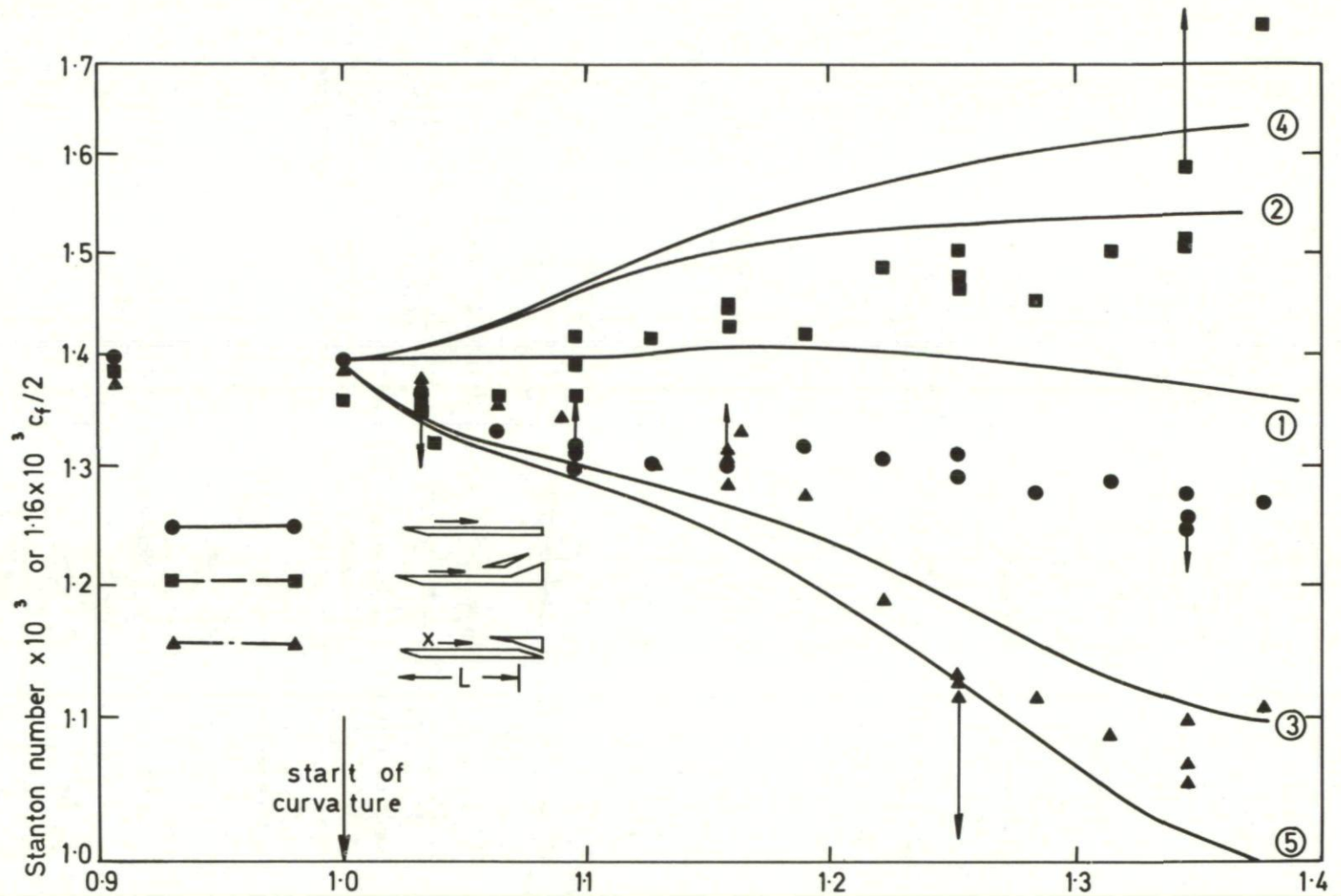
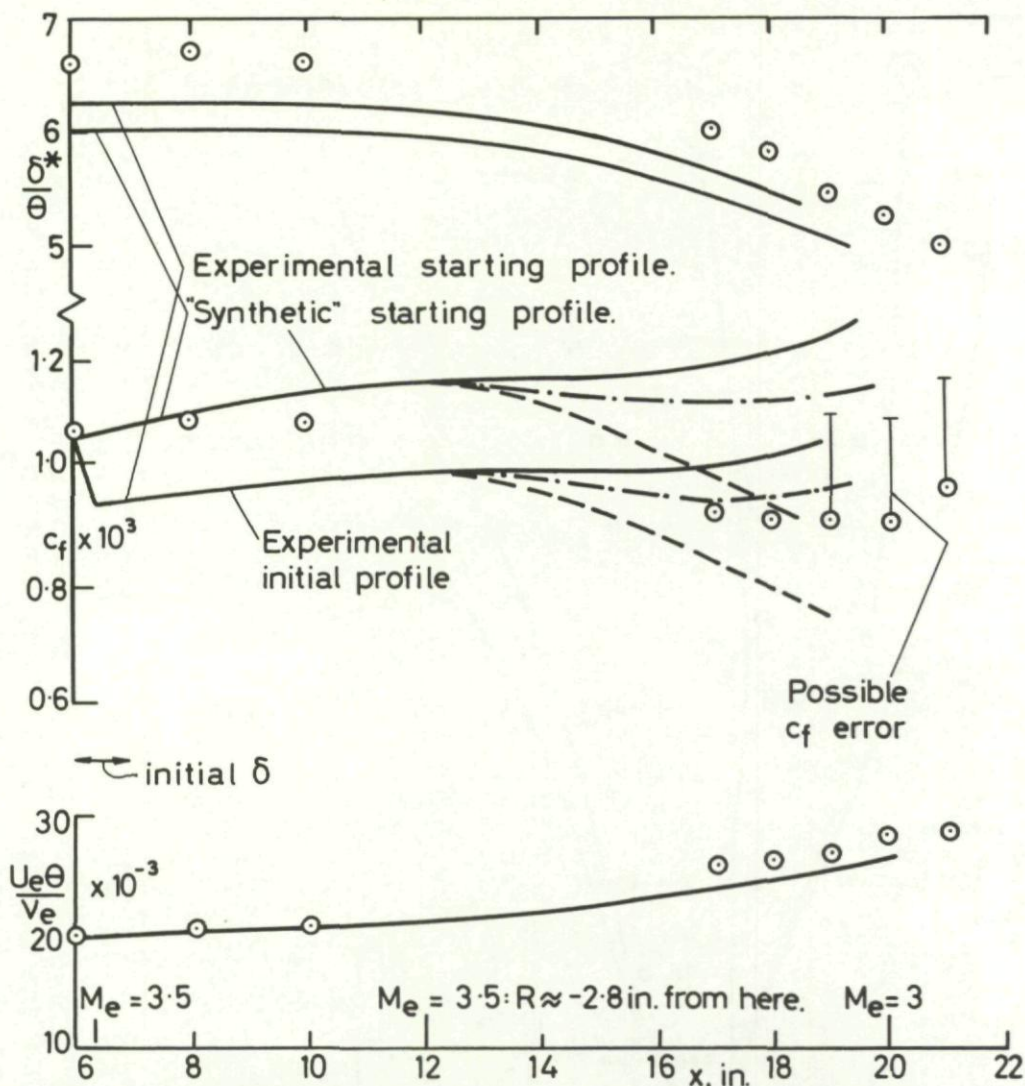


FIG. 26 SEPARATING BOUNDARY LAYER OF SCHUBAUER AND KLEBANOFF (101). \circ : EXPERIMENT. -----: CALCULATION WITHOUT CURVATURE CORRECTION. ———: CALCULATION WITH $\alpha = 14$.

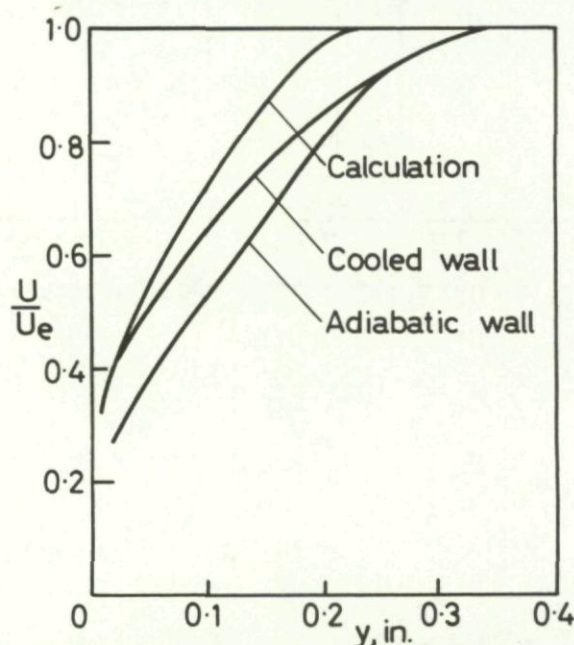


(a) Heat-transfer measurements of Thomann (4) at $M_e \approx 2.5$. Symbols-experiment (see fig. 3). Lines-calculations. ① Plane surface. ② Concave, $\alpha = 9$. ③ Convex, $\alpha = 14$. ④ Concave, $\alpha = 9$ ($1+0.2 M^2$). ⑤ Convex, $\alpha = 14$ ($1+0.2 M^2$), all with "time constant" of 105.

FIG. 27 DEMONSTRATION CALCULATIONS FOR COMPRESSIBLE CURVED FLOWS BY METHOD OF REF. 16 (SEE APPENDIX 2): $1+0.2 M^2$ IS COMPRESSIBILITY FACTOR IN Ri.



(b) Concave-surface measurements of Sturek and Danberg. \circ , experiment. — — — calculation without extra strain allowances. — · —, calculation with bulk compression allowance, $\alpha=10$. —, calculation with compression and curvature allowance.



(c) Concave-surface measurements of Kepler and O'Brien. Profiles at 1.2 in. from start of curvature. Calculated profiles corrected for bulk compression and curvature, and for bulk compression only, are identical.

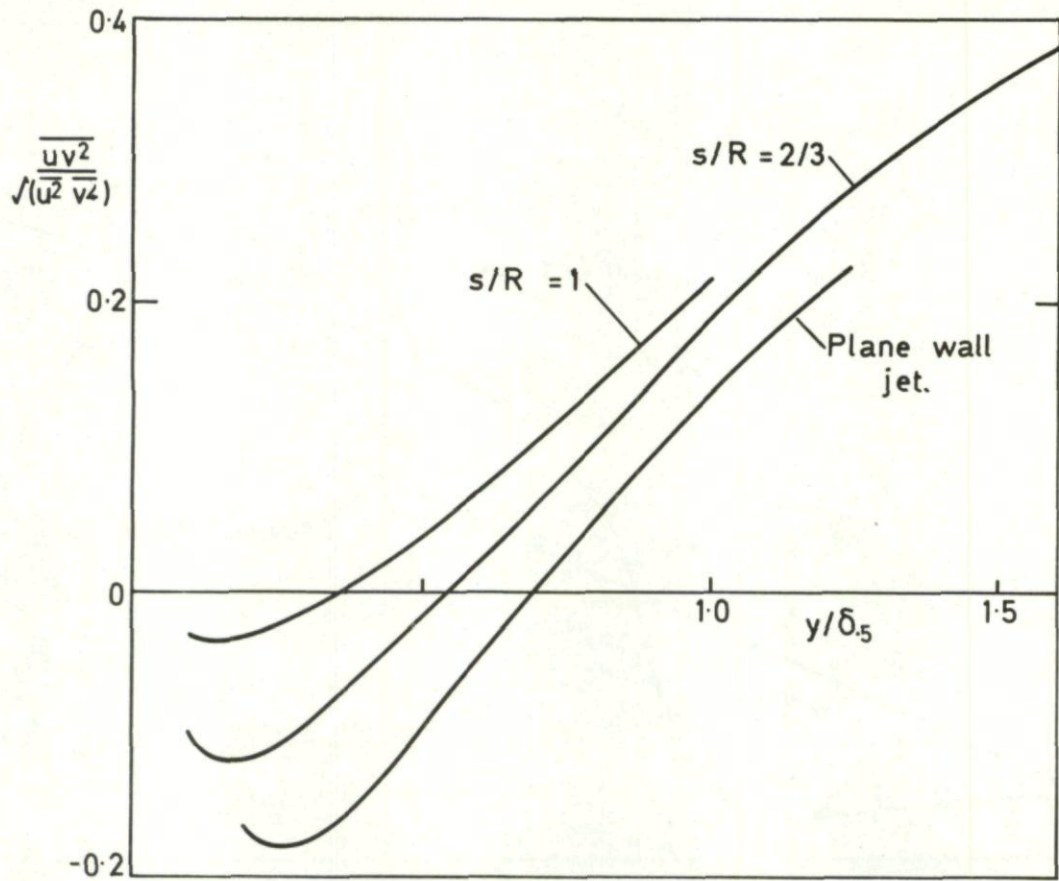
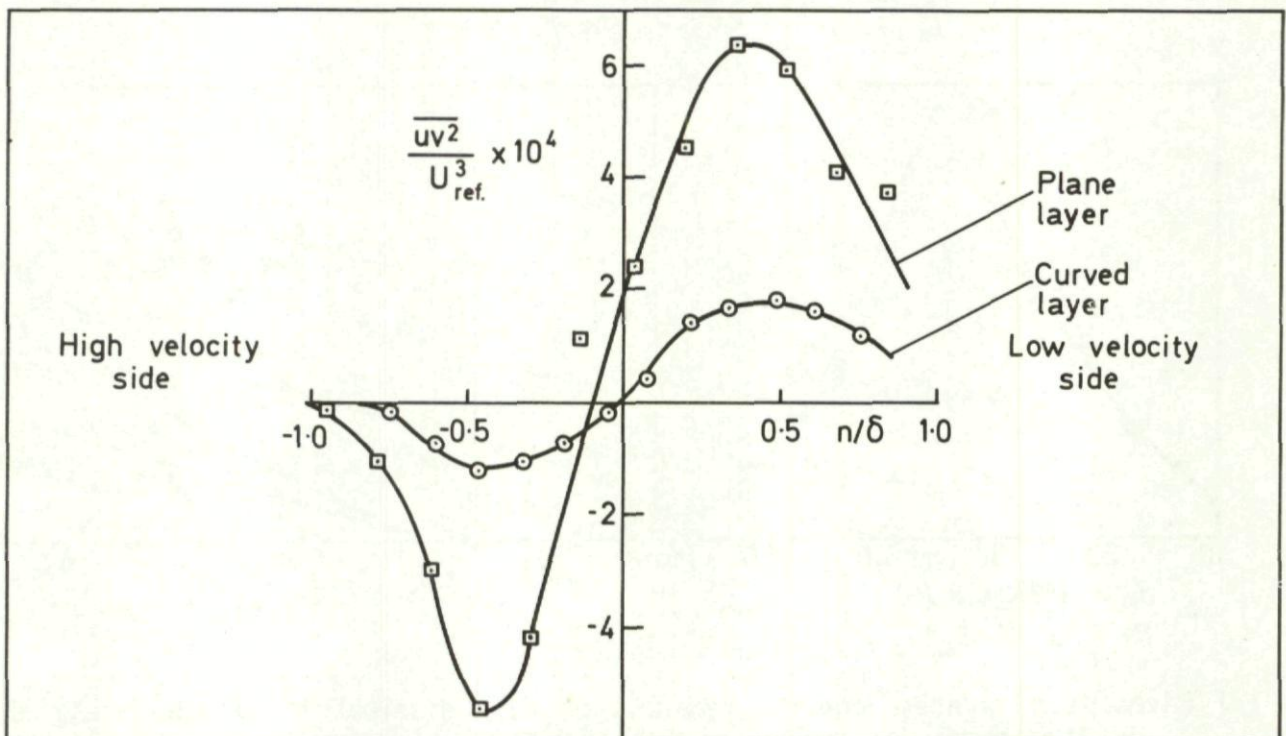
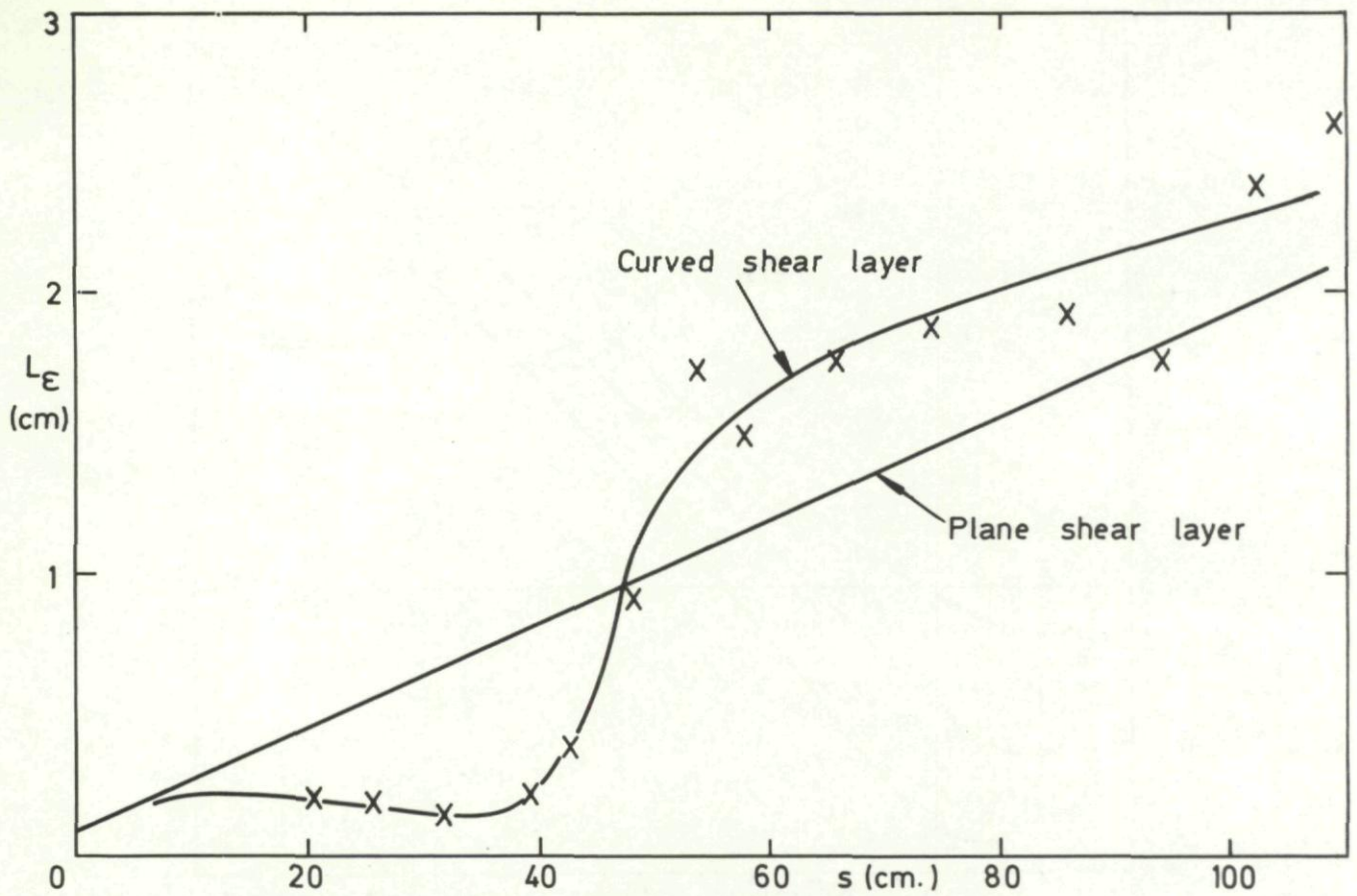


FIG. 28 TRIPLE PRODUCT REPRESENTING TRANSPORT OF \overline{uv} . DATA OF GUITTON (7) FOR WALL JETS ON SPIRAL SURFACES.

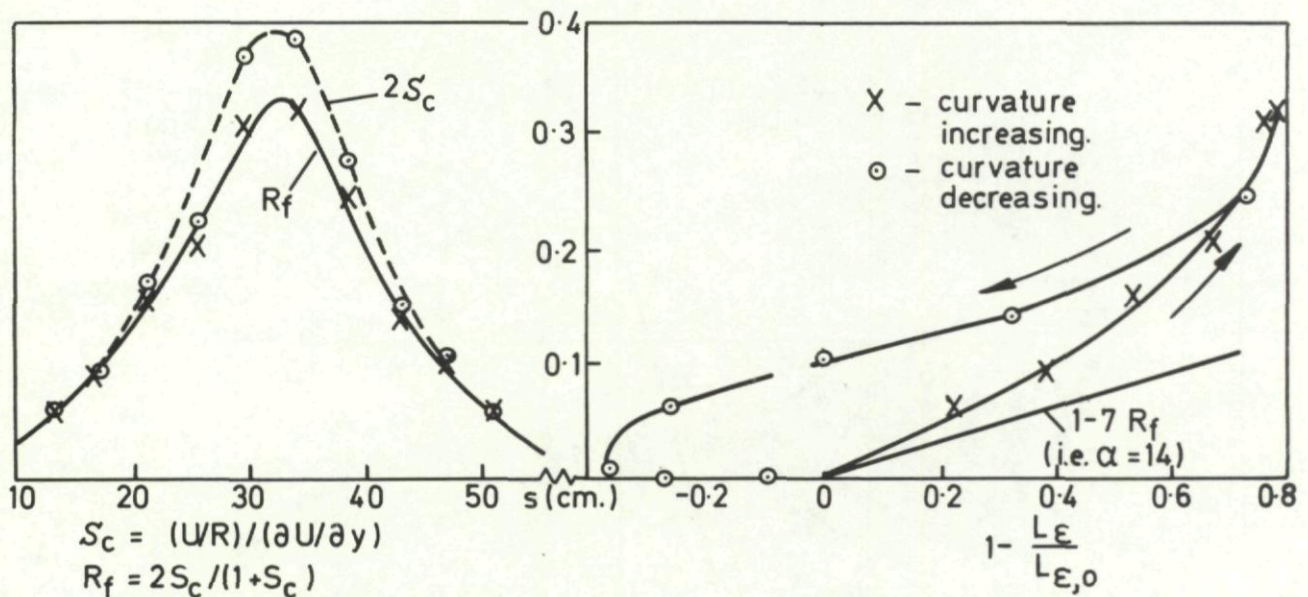


(a) Triple product representing transport of \overline{uv} in (S,n) coordinates. $s=34\text{cm}$; " δ " is distance between $c_p = 0.81$ and $c_p = 0.0625$ ($U/U_{ref.} = 0.9, 0.25$ in plane layer); n origin is point of maximum intensity.

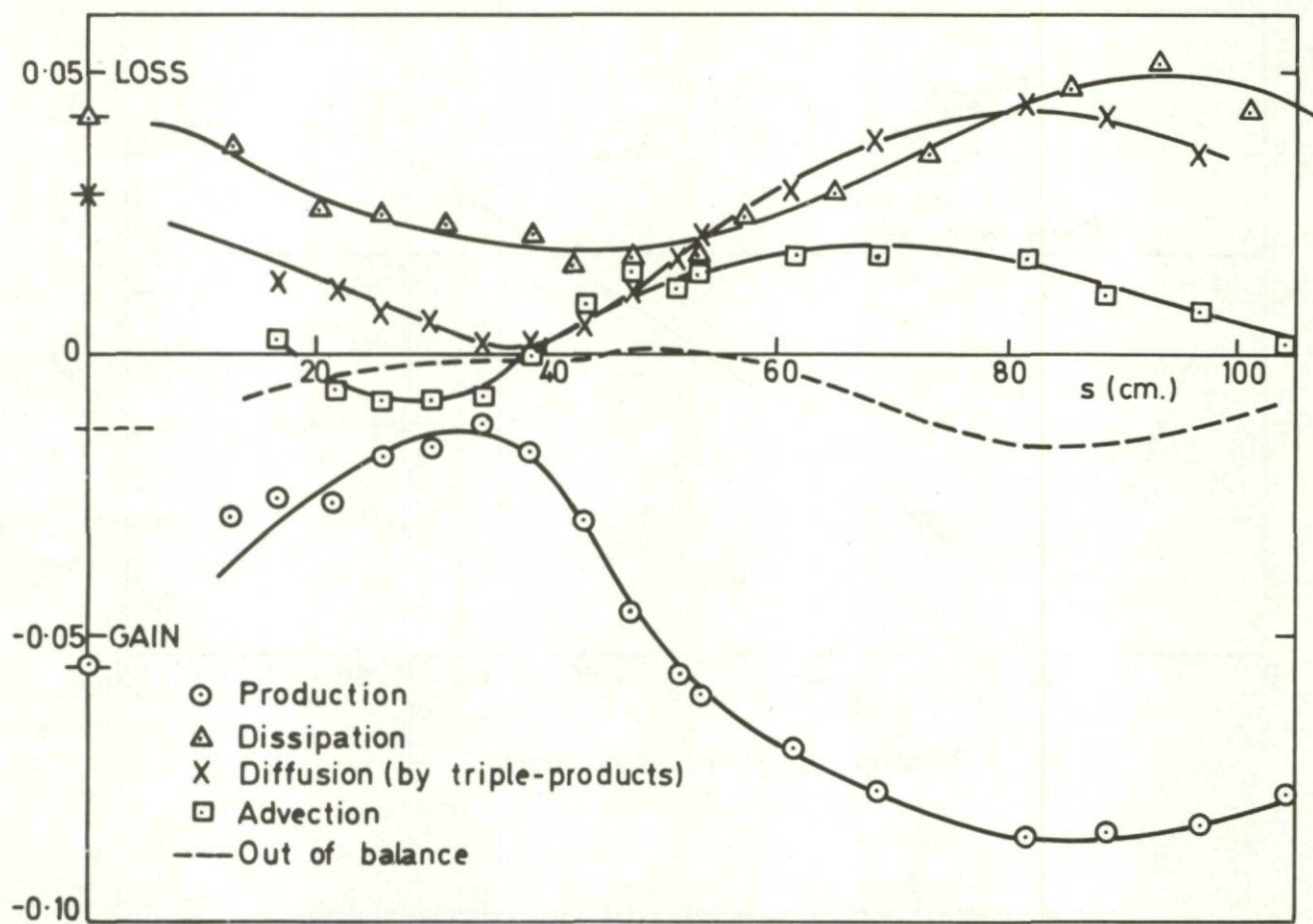
FIG. 29 STABLY-CURVED MIXING LAYER (11). FOR CONFIGURATION see FIG. 7(a).



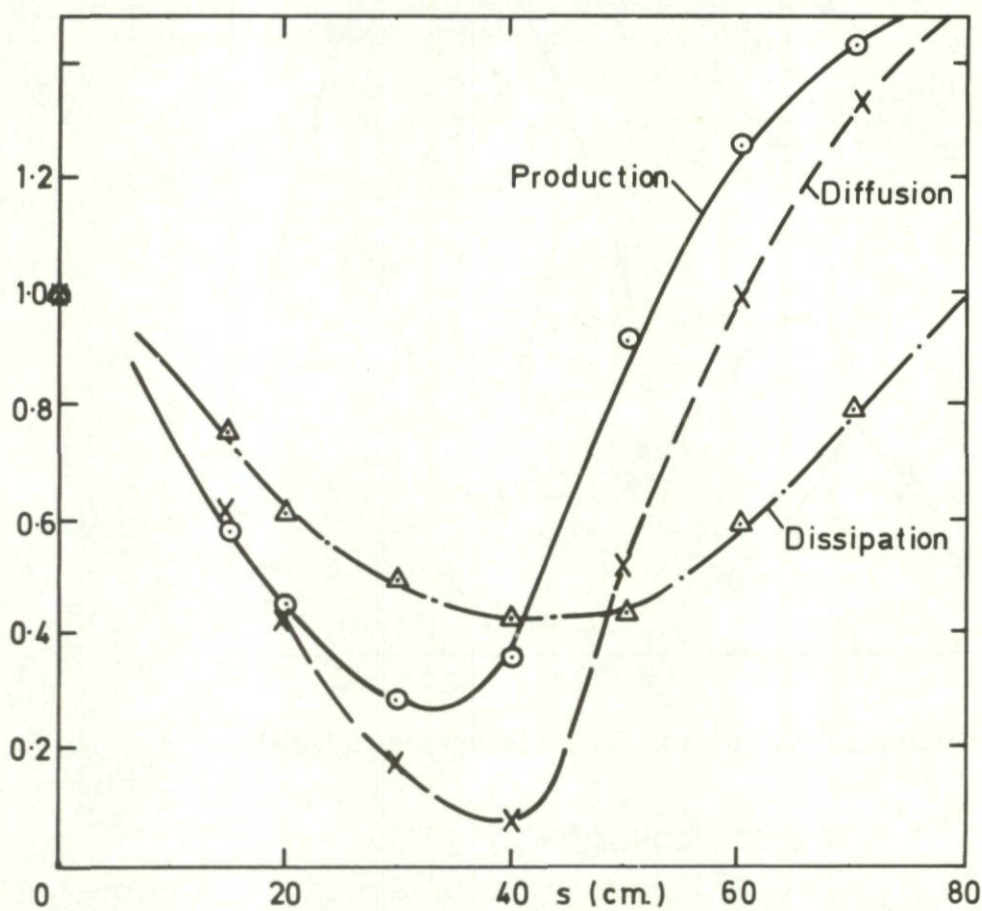
(b) Dissipation length parameter, $L_\epsilon \equiv (\overline{q^2})^{3/2}/\epsilon$



(c) Richardson number and its relation to the dissipation length scale in the region of maximum intensity.

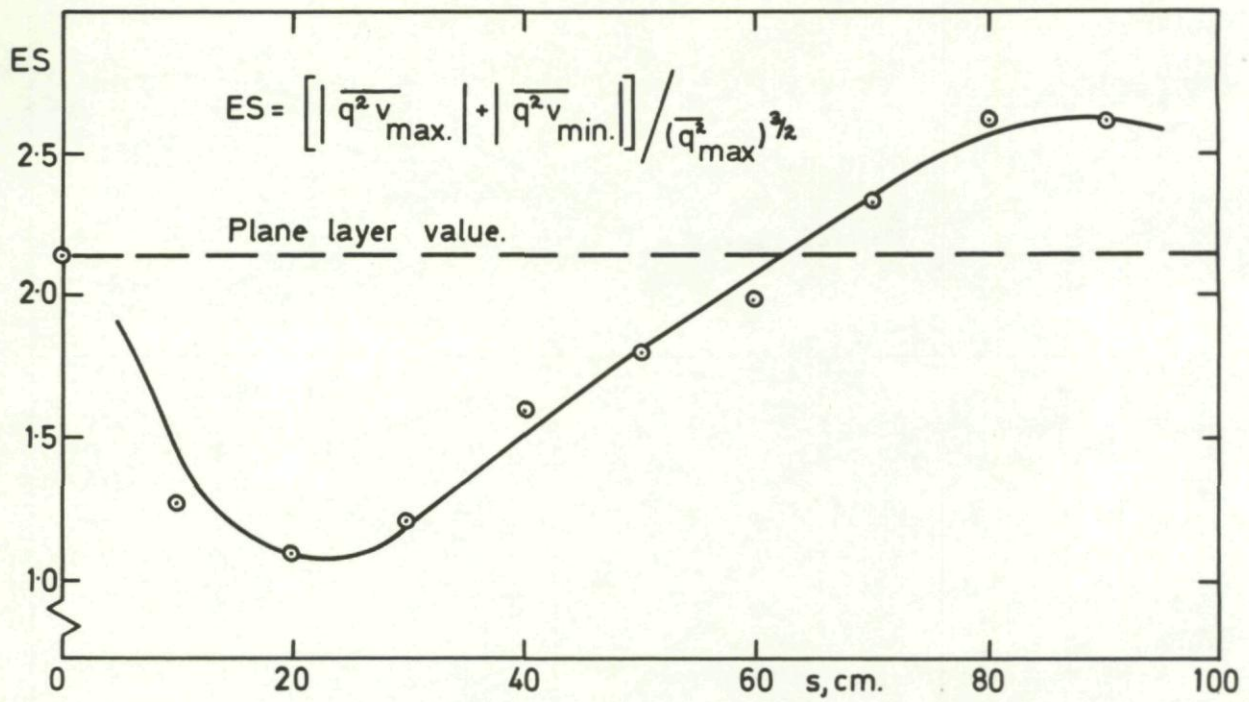


(d) Energy balance around line of maximum intensity.

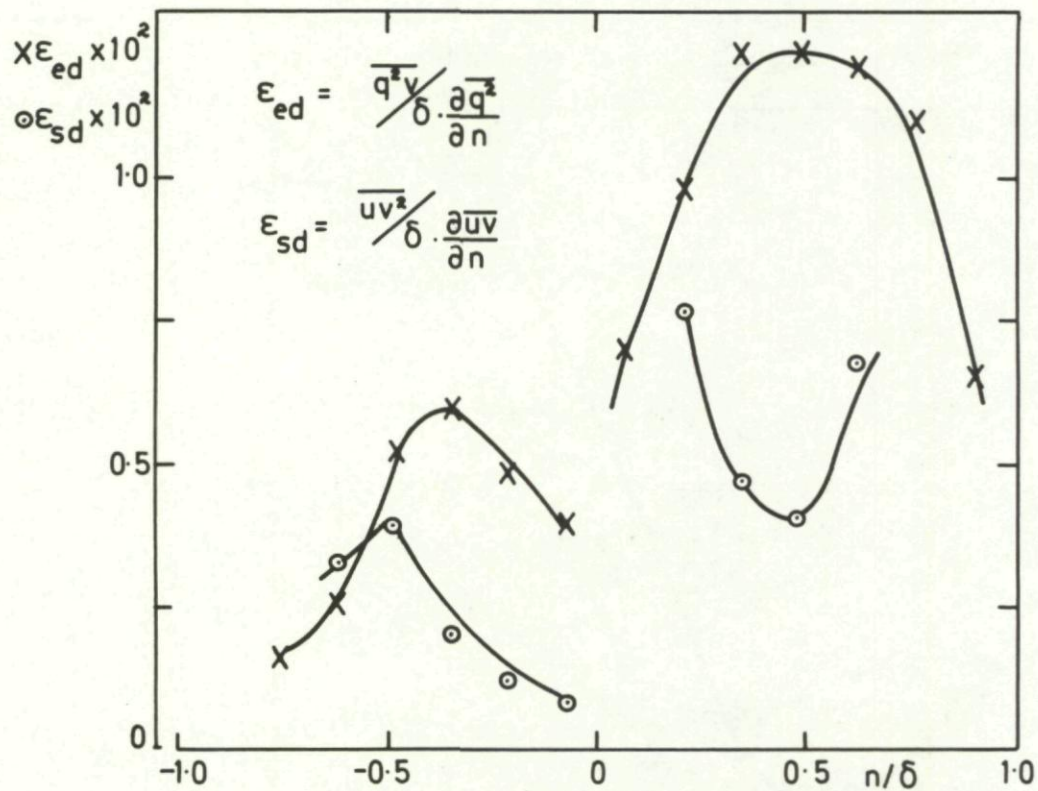


(e) Relative reduction in terms of fig. 29(d)

FIG. 29 (CONTINUED).



(f) Relative large-eddy strength.



(g) "Eddy diffusivities" of $\overline{q^2}$ and \overline{uv} . $s=34\text{cm}$. (see fig. 29(a)).

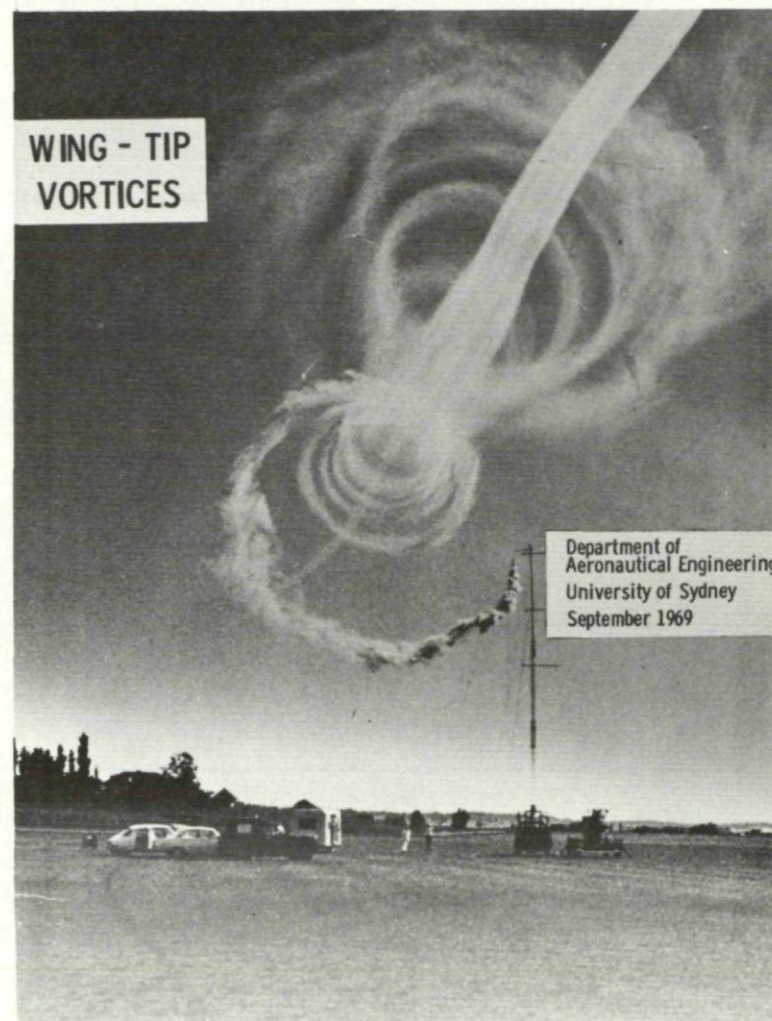
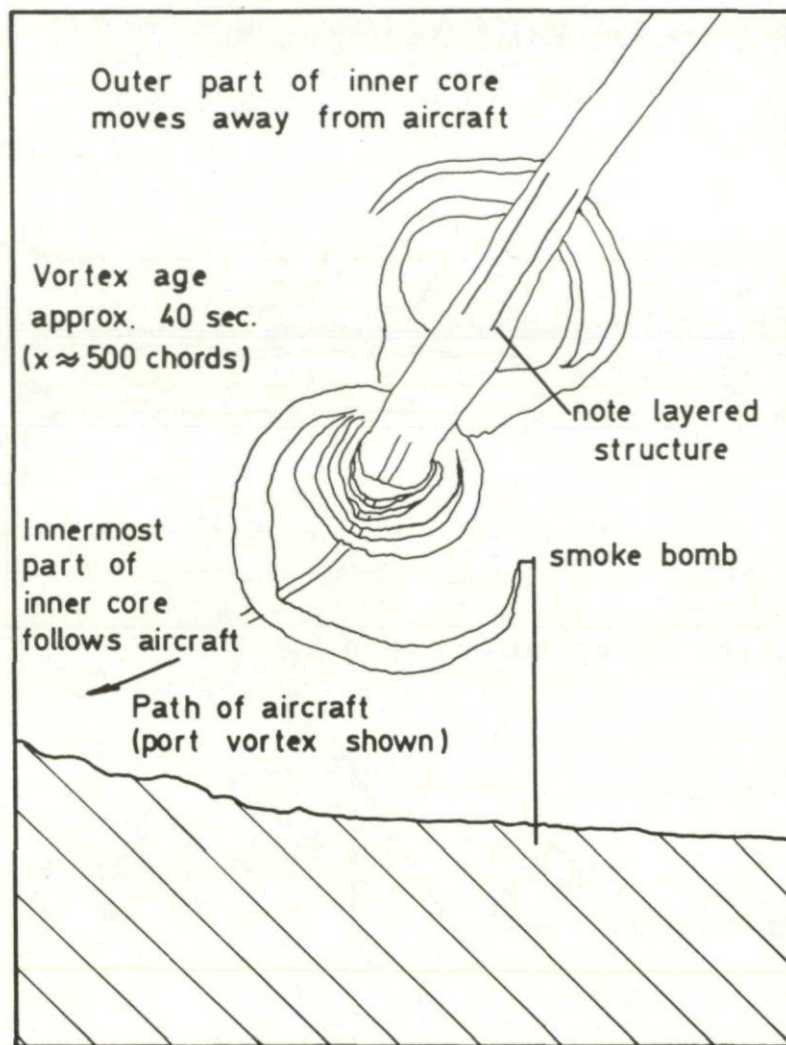
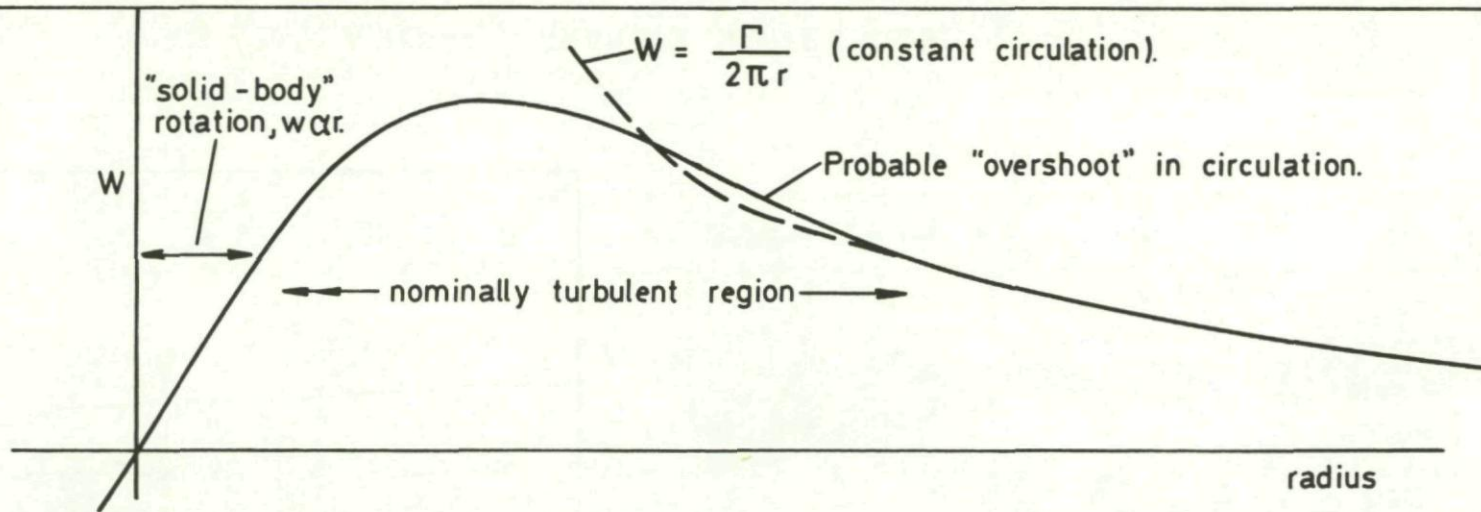
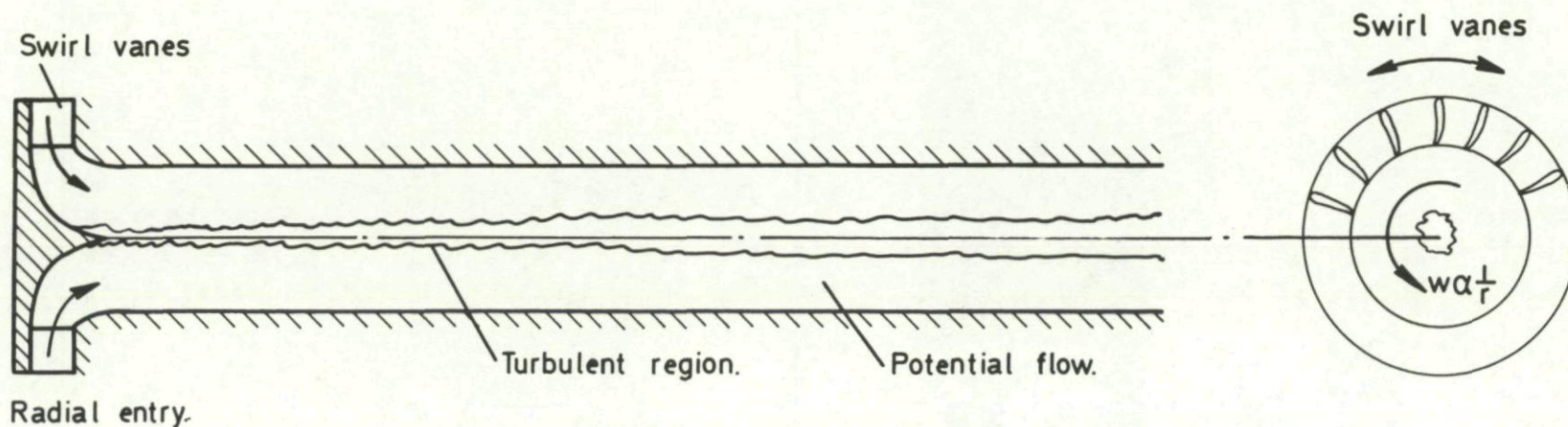


FIG. 30 AIRCRAFT TRAILING VORTEX (209).



(a) Typical distribution of circumferential velocity.



(b) Mabey-Squire (96) tube for generating classical vortices.

FIG. 31 CLASSICAL (TRAILING) VORTICES.

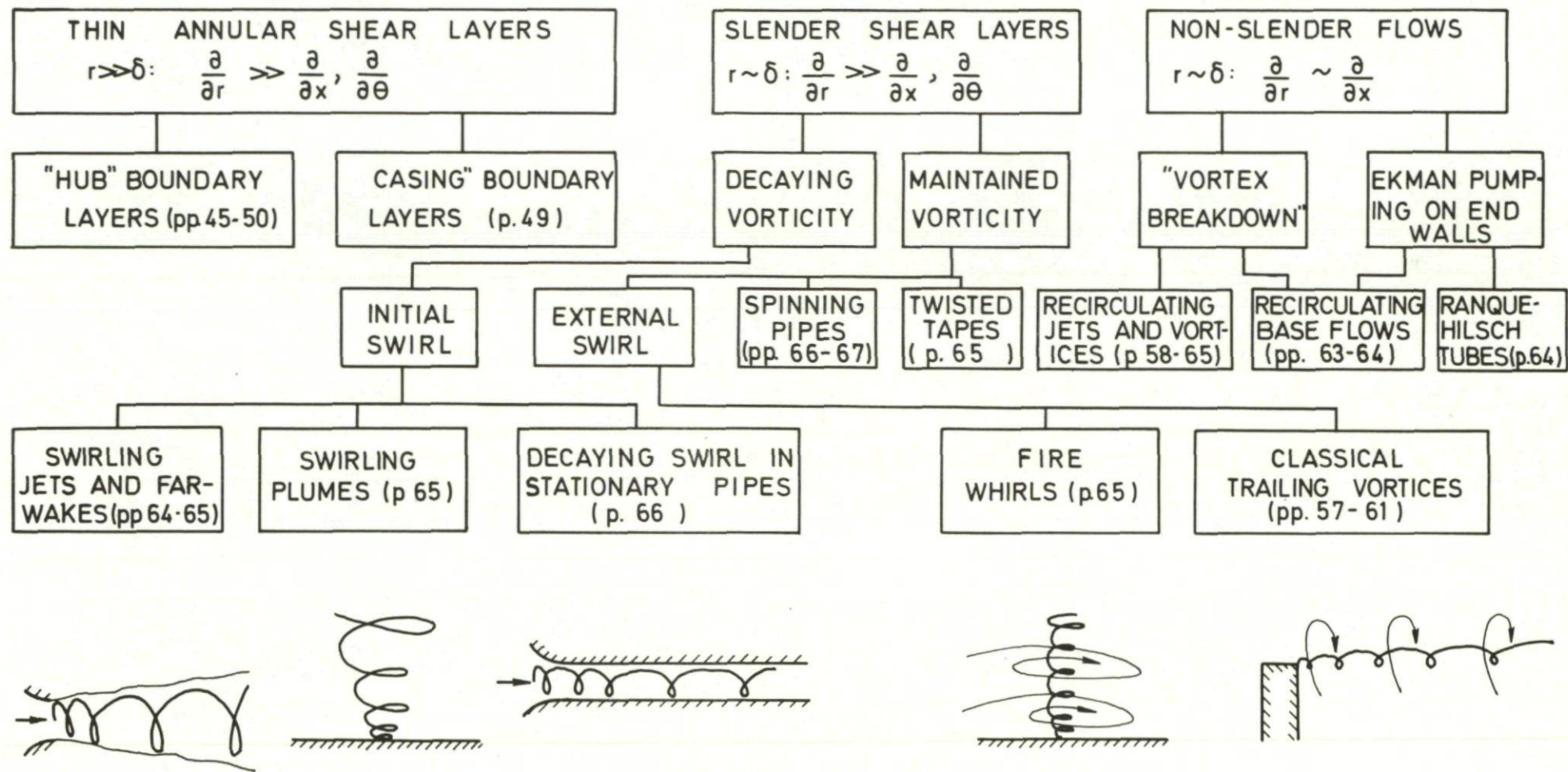
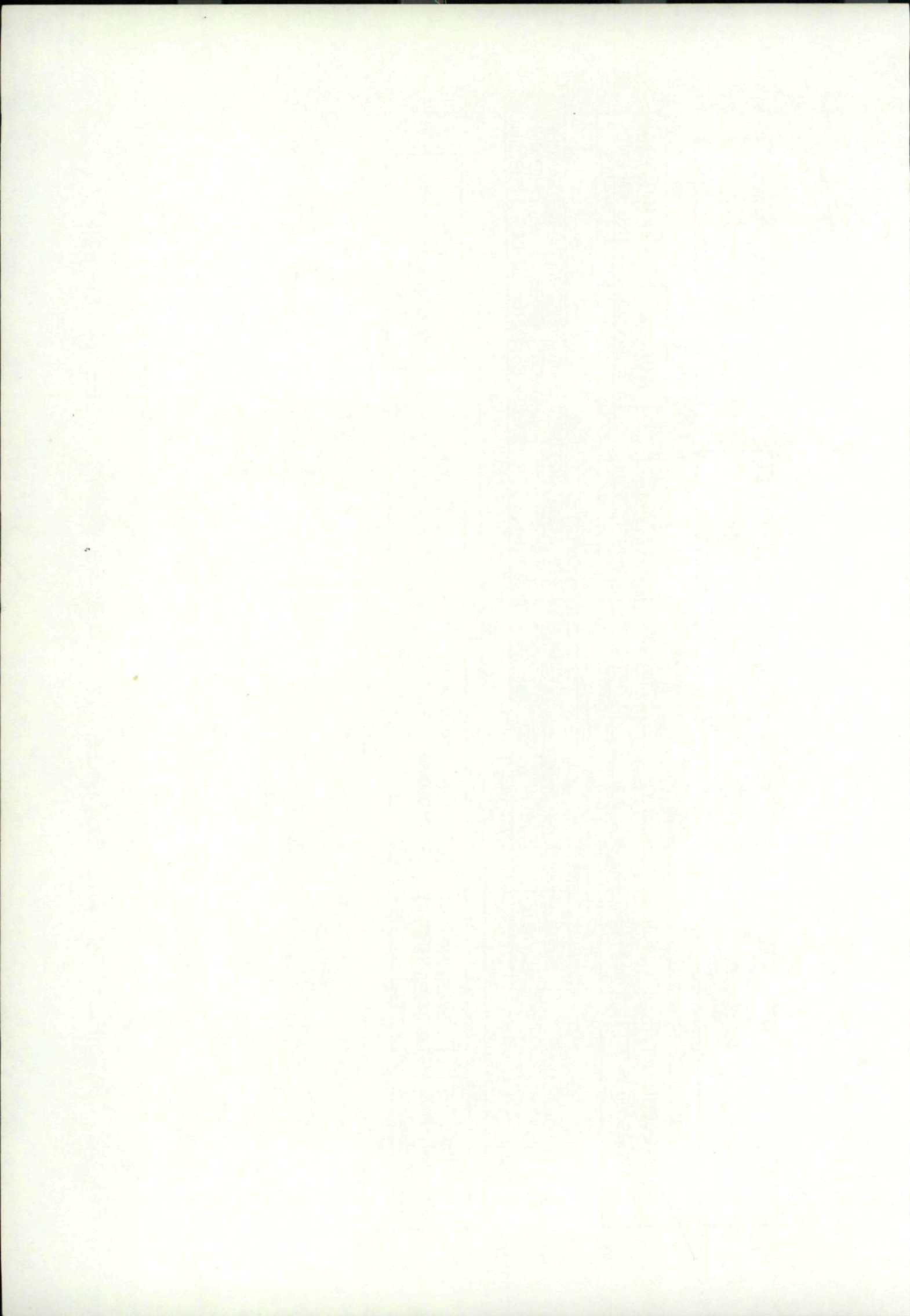
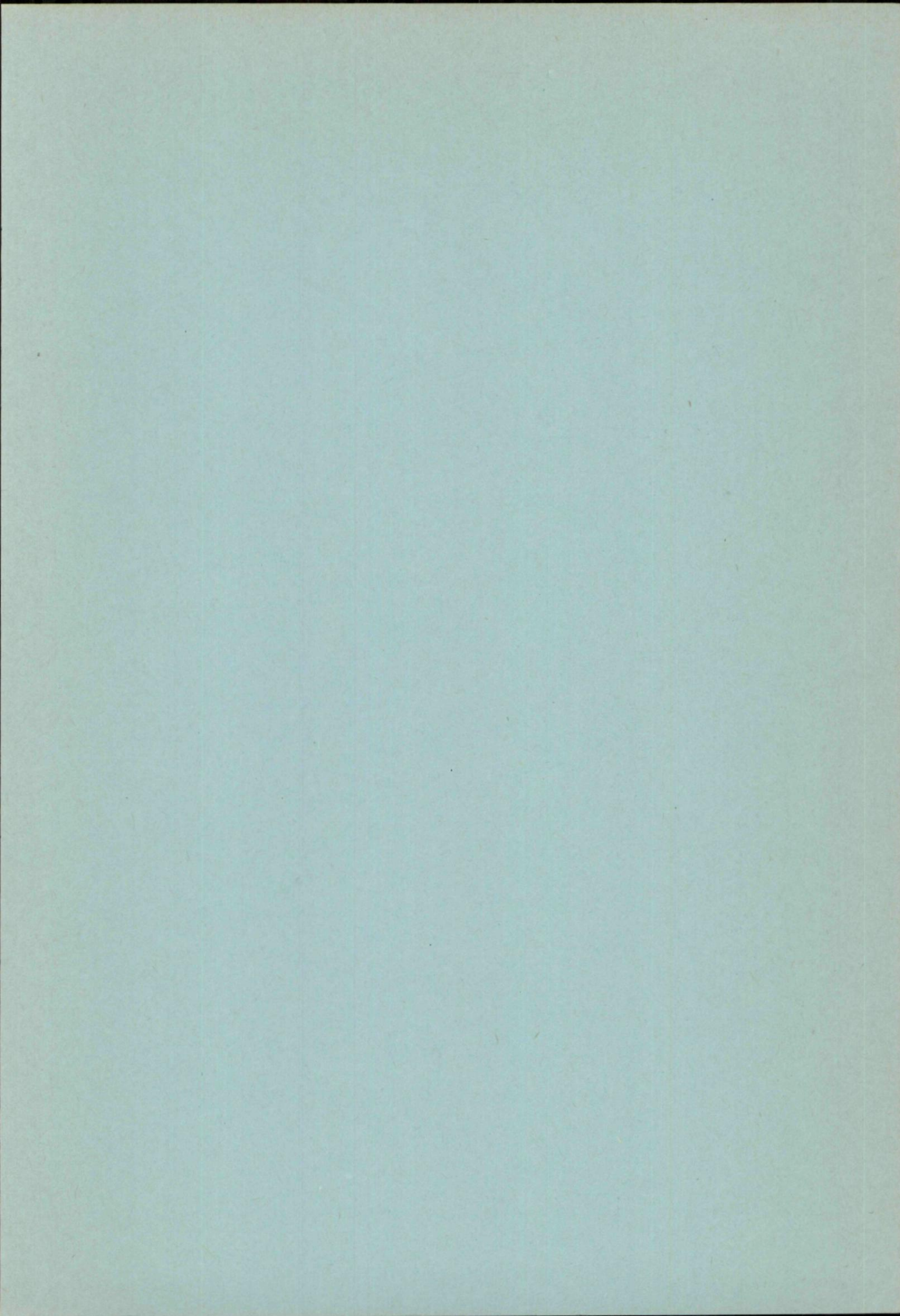


FIG. 32 CLASSIFICATION AND EXAMPLES OF SWIRLING FLOWS (SEE pp. 61-62)





NATIONAL DISTRIBUTION CENTRES FOR UNCLASSIFIED AGARD PUBLICATIONS

Unclassified AGARD publications are distributed to NATO Member Nations through the unclassified National Distribution Centres listed below

BELGIUM

Coordonnateur AGARD – VSL
Etat-Major de la Force Aérienne
Casernes Prince Baudouin
Place Dailly, 1030 Bruxelles

CANADA

Director of Scientific Information Services
Defence Research Board
Department of National Defence – 'A' Building
Ottawa, Ontario

DENMARK

Danish Defence Research Board
Østerbrogades Kaserne
Copenhagen Ø

FRANCE

O.N.E.R.A. (Direction)
29, Avenue de la Division Leclerc
92, Châtillon-sous-Bagneux

GERMANY

Zentralstelle für Luftfahrtokumentation
und Information
Maria-Theresia Str. 21
8 München 27

GREECE

Hellenic Armed Forces Command
D Branch, Athens

ICELAND

Director of Aviation
c/o Flugrad
Reykjavik

ITALY

Aeronautica Militare
Ufficio del Delegato Nazionale all'AGARD
3, Piazzale Adenauer
Roma/EUR

LUXEMBOURG

Obtainable through BELGIUM

NETHERLANDS

Netherlands Delegation to AGARD
National Aerospace Laboratory, NLR
P.O. Box 126
Delft

NORWAY

Norwegian Defense Research Establishment
Main Library,
P.O. Box 25
N-2007 Kjeller

PORTUGAL

Direccao do Servico de Material
da Forca Aerea
Rua de Escola Politecnica 42
Lisboa
Attn of AGARD National Delegate

TURKEY

Turkish General Staff (ARGE)
Ankara

UNITED KINGDOM

Defence Research Information Centre
Station Square House
St. Mary Cray
Orpington, Kent BR5 3RE

UNITED STATES

National Aeronautics and Space Administration (NASA)
Langley Field, Virginia 23365
Attn: Report Distribution and Storage Unit

* * *

If copies of the original publication are not available at these centres, the following may be purchased from:

Microfiche or Photocopy

National Technical
Information Service (NTIS)
5285 Port Royal Road
Springfield
Virginia 22151, USA

Microfiche

ESRO/ELDO Space
Documentation Service
European Space
Research Organization
114, Avenue Charles de Gaulle
92200, Neuilly sur Seine, France

Microfiche

Technology Reports
Centre (DTI)
Station Square House
St. Mary Cray
Orpington, Kent BR5 3RE
England

The request for microfiche or photocopy of an AGARD document should include the AGARD serial number, title, author or editor, and publication date. Requests to NTIS should include the NASA accession report number.

Full bibliographical references and abstracts of the newly issued AGARD publications are given in the following bi-monthly abstract journals with indexes:

Scientific and Technical Aerospace Reports (STAR)
published by NASA,
Scientific and Technical Information Facility,
P.O. Box 33, College Park,
Maryland 20740, USA

United States Government Research and Development
Report Index (USGDRI), published by the
Clearinghouse for Federal Scientific and Technical
Information, Springfield, Virginia 22151, USA

